ISSN 0370–8691

NATIONAL ACADEMY OF SCIENCES OF THE REPUBLIC OF ARMENIA

Communications of the Byurakan Astrophysical Observatory

2

Erevan 2020

Introduction

Editorial board*

Astronomical surveys are the main source for discovery of astronomical objects and accumulation of observational data for further analysis, interpretation, and achieving scientific results. In 1940s-1950s Palomar Observatory Sky Survey (POSS, at present digitized as DSS1) gave more data that it was collected during the whole epoch of astronomical observations before. Similarly, Markarian Survey (or the First Byurakan Survey, FBS) was the first large-area spectroscopic survey resulting at low-dispersion spectra of 20,000,000 objects. Later on, many all-sky or large-area surveys appeared (POSS2 (DSS2), SDSS, etc.). Sloan Digital Sky Survey (SDSS) so far has provided the largest database (both photometric and spectroscopic) and SDSS-based virtual sky may be explored for new discoveries. CALIFA gives a new large set of spectra. Gaia and LSST are the next source for vast amount of information. Modern multiwavelength surveys include GOODS, COSMOS, GAMA, and others. The large amount of data requires new approaches to data reduction, management and analysis. We now deal with Big Data. Powerful computer technologies are required, including clusters and grids. Virtual Observatories (VOs) have been created to coordinate astronomers' and computer scientists' actions and help in accomplishment of complex research programs using all the accumulated data. International Virtual Observatory Alliance (IVOA) unifies 20 VO projects for joint efforts toward handling of Big Data and creation of an environment for more efficient research. The International Council of Scientific Unions (ICSU) has created World Data System (WDS) to unify data coming from different science fields for further possibility of exchange and new science projects.

Benyamin Markarian (1913-1985) was the first to conduct and accomplish a large-area (17,000 sq. deg.) spectroscopic survey in 1965 to search for active galaxies. Markarian survey is until now the largest objective-prism spectroscopic survey, it was the first systematic search for active galaxies using a new method of UV-excess, it resulted in the discovery of 1515 UVX galaxies (Markarian galaxies), including many AGN and Starbursts, first classification of Seyferts into Sy1 and Sy2, and definition of Starburst galaxies. BAO is famous for other surveys as well: Arakelian and Kazarian galaxies, Shahbazian compact groups, Parsamian cometary nebulae and other objects also are well known. This gives good grounds for holding international symposia at the Byurakan observatory to discuss large astronomical surveys and the prospects they provide for solving many problems of modern astrophysics.

The first meeting dedicated to the topic "Astronomical Surveys and Big Data" was successfully held in 2015. In September 2020, the second international symposium "Astronomical Surveys and Big Data 2" dedicated to this topic was held. The organizers brought together astronomers and computer scientists who are actively involved in working with astronomical surveys, catalogs, archives, databases and VOs. The meeting will contribute to the following:

- Review and discuss large astronomical surveys to summarize observational data obtained in astronomy;
- Give tribute to Markarian Survey and other important surveys;
- Review and discuss astronomical catalogues, databases and archives;
- Learn about major current and upcoming surveys (including PanSTARRS, Gaia, and LSST);
- Learn and discuss how large observational data sets are changing astronomy;

*combao@aras.am

- Introduce tools and techniques for working with large data sets (including access, analysis, and visualization);
- Discuss the future of astronomical research by joint efforts of astronomers and computer scientists.

This issue of "Communications of BAO" includes the proceedings presented international symposium "Astronomical Surveys and Big Data 2". All the papers passed relevant peer-review

Surveys for active galaxies: discovery and studies

A. M. Mickaelian[*], H. V. Abrahamyan, G. M. Paronyan, G. A. Mikayelyan, and M. V. Gyulzadyan

NAS RA Byurakan Astrophysical Observatory (BAO), Byurakan 0213, Aragatzotn Province, Armenia

Abstract

We present surveys and related studies of active galaxies carried out at the Byurakan Astrophysical Observatory (BAO). This was one of the main research subjects at BAO during many years, since mid-1950s, when Viktor Ambartsumian suggested the hypothesis of the activity of the galactic nuclei. A number of surveys and searches for Active Galactic Nuclei (AGN) and other active galaxies were accomplished during 1960s-1980s. Since mid-1990s, our research group carried out new surveys and studies of active galaxies based on the First Byurakan Survey (FBS or Markarian Survey) and then a number of others. Here we also present the recent results of studies on active galaxies (both AGN and Starbursts) by the Extragalactic group of the Byurakan Astrophysical Observatory (BAO) Research Department "Astronomical Surveys". These studies are characterized by multiwavelength approach to statistical analysis of large amount of data obtained in different wavelengths; from X-ray to radio. A fine classification scheme for active galaxies has also been suggested.

Keywords: *active galaxies, AGN, Starburst Galaxies, quasars, Seyfert galaxies, LINERs, composite spectrum objects, HII, IRAS galaxies, variable sources*

Introduction

The Byurakan Astrophysical Observatory has always been famous for surveys for active galaxies. Such search works started just after Viktor Ambartsumian's hypothesis on Active Galactic Nuclei (AGN) in mid-1950s. Here we give a list of the most important surveys carried out in 1960s-2000s.

Byurakan Surveys for Active Galaxies

- **First Byurakan Survey (FBS) – Markarian Survey**, *1515* UVX galaxies
  B. E. Markarian, V. A. Lipovetsky, J. A. Stepanian, 1965-1980: 1515 UV-excess (UVX) galaxies, Markarian galaxies (Markarian et al., 1989, Mazzarella & Balzano, 1986)

- *High surface brightness galaxies, 621* **Arakelian galaxies**; Arakelian (1975)

- **Second Byurakan Survey (SBS)**
  B. E. Markarian, J. A. Stepanian, V. A. Lipovetsky, L. K. Erastova, V. H. Chavushian, 1978-91: UVX and emission line gals., QSOs (∼3600 objects, incl. 1800 gals; 600 QSOs, 170 Sy, 12 BLL); Markarian et al. (1987)

- **Shahbazian's compact groups of compact galaxies;** Baier et al. (1974)

- **Kazarian survey:** 706 UVX (Kazarian) galaxies; Kazarian et al. (2010)

- **Second Part of the FBS: Blue Stellar Objects (FBS BSOs)**, 1103 objects
  H. V. Abrahamian, A. M. Mickaelian, 1987-1996: QSOs and Seyferts

[*]aregmick@yahoo.com

DOI: 10.52526/25792776-2020.67.2-149

- *Optical identification and study of* **IRAS sources**, *1278* **BIG objects**
  A. M. Mickaelian et al., 1995-2004: ULIRGs, AGN and SB
- *Optical identification and study of* **ROSAT sources**; *4253* **ROSAT AGN**
  A. M. Mickaelian et al., 2002-2006: AGN and SB

Recent results of the Extragalactic group of BAO Research Department "Astronomical Surveys" are related to multiwavelength studies of active galaxies using large amount of data from X-ray, UV, optical, IR and radio ranges, with heavy use of cross-correlations, classifications on activity types using our observations and SDSS spectra (Ahumada et al., 2020), building diagnostic diagrams, Spectral Energy Distributions (SEDs), etc. Results on HRC/BHRC sample objects (optical identifications of ROSAT X-ray sources), studies of Markarian galaxies in UV and multiwavelength SEDs, abundance and star formation determinations in Mrk galaxies from SDSS spectra, revised optical classification of "LINERs", study and classification of SDSS spectra for Byurakan-IRAS Galaxies (BIG objects), summary of observations and study of Byurakan-IRAS Galaxies, discovery of new bright ULIRGs from the IRAS PSC/FSC Combined Catalogue (Abrahamyan et al., 2015) and their spectral classification using SDSS spectra, radio variable sources at 1400 MHz and their optical variability, classification of BZCAT objects having uncertain types (BZU objects), and optical variability of blazars are given in individual sections.

Markarian galaxies in UV and multiwavelength studies (Mickaelian et al., 2018b). The UV properties of 1152 Markarian galaxies have been investigated based on GALEX data. These objects have been investigated also in other available wavelengths using multi-wavelength data from X-ray to radio. Using our classification for activity types for 779 Markarian galaxies based on SDSS spectroscopy, we have investigated these objects on the GALEX (Bianchi et al., 2011), 2MASS and WISE (Cutri et al., 2013) color-magnitude and color-color diagrams by the location of objects of different activity types and have revealed a number of loci. UV contours overplotted on the optical images revealed additional structures, particularly spiral arms of a number of Markarian galaxies. UV (FUV and NUV) and optical absolute magnitudes and luminosities have been calculated showing graduate transition from AGN to Composites, HIIs and Absorption line galaxies from (average M) -17.56m to -15.20m in FUV, from -18.07m to -15.71m in NUV and from AGN to Composites, Absorption line galaxies and HII from -21.14m to -19.42m in optical wavelengths and from (average L) 7×10^9 to 4×10^8 in FUV, from 1×10^{10} to 5×10^8 in NUV and from AGN to Composites, Absorption line galaxies and HII from 7×10^{10} to 1×10^{10} in optical wavelengths.

Abundance and Star Formation Determinations in Mrk galaxies from SDSS Spectra (Gyulzadyan et al., 2018). We analyze the oxygen and nitrogen abundance and specific star formation rates (sSFR) in Markarian galaxies from Sloan Digital Sky Survey (SDSS) spectra. The Data Release 7 (DR7) of SDSS contains photometric data for more there 1000 and spectral information for more than 700 Markarian objects. The Mrk sample has played a central role in the task of distinguishing between the astrophysical different types of phenomena that occur in AGNs. In the course of the Markarian survey, more than 200 Seyfert galaxies, and hundreds of starbursts, blue compact, and H II galaxies were discovered. The Markarian survey remains perhaps the best-known source of such objects in the local universe. We have measured their line fluxes and derived the O and N abundances using recent calibrations. We have compared the oxygen and nitrogen abundances derived from global emission-line Sloan Digital Sky Survey (SDSS) spectra of galaxies using (1) the Te method and (2) two recent strong-line calibrations: the ON and NS calibrations. The behaviour of the [N/H] ratio in under abundant regions gives strong support to a partially primary origin of nitrogen. The star formation rate (SFR) is one of the main parameters used to analyze the evolution of galaxies through time. In the local Universe, the Hα luminosity derived from IFS observations can be used to measure SFR, at least in statistically significant, optically-selected galaxy samples, once stellar continuum absorption and dust attenuation effects are accounted for.

Activity Types of Galaxies Selected from HRC/BHRC Sample (Paronyan et al., 2018, 2019, 2020). In this study we carry out detailed spectral classification of 371 (173+198) AGN candidates from the Joint HRC/BHRC sample, which is a combination of HRC (Hamburg-ROSAT Catalogue, Zickgraf et al. (2003)) and BHRC (Byurakan-Hamburg-ROSAT Catalogue). These objects were revealed as optical counterparts for ROSAT X-ray sources (Voges et al., 1999, 2000); however, spectra for 371 of them are given in SDSS without definite spectral classification. We studied these 371 objects using the SDSS spectra and revealed the detailed activity types for them. Three diagnostic diagrams and direct examination of the spectra were used to obtain more confident classification. We also identified these sources in other wavelength ranges and calculated some of their parameters. In Figure 1 we give examples of SDSS DR15 spectra for some classified HRC-BHRC objects.

Revised optical classification of "LINERs" (Abrahamyan et al., 2018b). This work is dedicated to reclassification of LINERs. For our investigation we use the catalogue Véron-Cetty & Véron 13th edition (Véron-Cetty & Véron, 2010). In this catalogue 926 LINERs are included. Cross-correlation of these sources with SDSS DR14 gives 176 objects which have spectra in SDSS. Having medium-resolution spectra from SDSS we have done reclassification of these sources. As a result, 54% of these sources have changed their classification.

Study and Classification of SDSS Spectra for Byurakan-IRAS Galaxies (Mickaelian et al., 2018a). The sample of Byurakan-IRAS galaxies (BIG) has been created based on optical identifications of IRAS Point Source Catalog (PSC; IRAS (1988)) at high galactic latitudes. As a result, 1178 galaxies have been identified. 172 of them have been observed spectroscopically with Byurakan Astrophysical Observatory (BAO, Armenia) 2.6 m, Special Astrophysical Observatory (SAO, Russia) 6m and Observatoire de Haute Provence (OHP, France) 1.93 m telescopes. Later on, spectra were obtained for more 83 BIG objects in Sloan Digital Sky Survey (SDSS). We have extracted and studied these spectra, classified them and measured spectral features. Diagnostic diagrams have been built to distinguish starbursts (SB), LINERs and Seyfert galaxies. Cross-correlations were made for these objects with multiwavelength (MW) catalogues and their physical properties were studied. Among these 83 objects, 55 HII, 8 Seyfert galaxies, 2 LINERs, 4 other AGN, 6 composite spectrum objects, and 8 other emission-line galaxies have been revealed. Three of these objects are Ultra-Luminous InfraRed Galaxies (ULIRG).

Observations and study of Byurakan-IRAS Galaxies were summarized (Mikayelyan et al., 2019b). A general analysis of optical spectroscopic data on 257 Byurakan-IRAS Galaxies (BIG objects) obtained with the BAO 2.6m, SAO 6m, OHP 1.93m telescopes and taken from SDSS spectroscopic database was carried out. 149 star-formation regions (SB) galaxies, 42 galaxies with active nuclei (AGN), and 28 galaxies with a composite spectrum were identified. The spectra of 21 galaxies show signs of emission, but without the possibility of more precise determination of their activity type (we assign them as Em), 13 galaxies appear to have star formation rates that do not exceed normal (we assign them as HII), and 3 are absorption galaxies (we assign them as Abs). We give in Table 1 the distribution of 257 BIG objects by activity types.

Table 1. The distribution of 257 BIG objects by activity types.

Activity type	**Number of objects**	**%**	**Activity type**	**Number of objects**	**%**
HII	149	58.0	AGN	13	5.1
Composite	22	8.6	Em	21	8.2
HII / LINER	4	1.5	Norm	13	5.1
HII / Sy	2	0.8	Abs	3	1.1
LINER	12	4.6	Unknown	1	0.4
Sy	17	6.6	**All**	**257**	**100.0**

Discovery of new bright ULIRGs from the IRAS PSC/FSC Combined Catalogue (Mikayelyan et al., 2018). High-luminosity IR galaxies (LIRGs, ULIRGs, and HLIRGs) are important for studies related to star-formation processes in the early Universe, as their luminosity allows to detect them at large distances. High IR indicates active star-formation and often starburst processes, which is typical to HII (starburst, SB) and AGN. An interesting question is whether the starburst triggers AGN or vice versa or there is no direct impact. Considering that very often such objects manifest double and multiple structure, it is also interesting to investigate the interrelationship between the SB, nuclear activity and interactions or merging. We have analyzed the IRAS PSC/FSC Combined Catalogue for search for new bright ULIRGs. By means of the SDSS DR14 data, namely redshifts for those objects having spectroscopy, we have calculated the IR luminosities and have found 114 very high-luminosity IR galaxies; 107 ULIRGs and 7 HLIRGs. Among them, 48 new ULIRGs and 7 new HLIRGs have been discovered. These objects have been studied by SDSS color-color, luminosity-redshift and other diagrams. Further studies will include the content of the sample for activity types and other available data.

Spectral Classification of ULIRGs from IRAS PSC/FSC Combined Catalogue (Mikayelyan et al., 2019a). High-luminosity IR galaxies (LIRGs, ULIRGs, and HLIRGs) are important for studies related to star-formation processes in the early Universe, as their luminosity allows to detect them at large distances. High IR indicates active star-formation and often starburst processes, which is typical to HII (starburst, SB). In many cases high IR indicates an Active Galactic Nuclei (AGN). An interesting question is whether the starburst triggers AGN or vice versa or there is no direct impact. Considering that very often such objects manifest double and multiple structure, it is also interesting to investigate the interrelationship between the SB, nuclear activity and interactions or merging. As a result of cross-correlation of the IRAS PSC/FSC Combined catalogue with SDSS DR14, 114 ULIRGs were separated and classified by the activity types. 1 BLL, 2 quasars, 29 Seyferts of types 1.0-1.8, 5 Seyferts of type 2, 14 LINERS, 36 HII, 14 objects with a composite spectrum (Composite) were identified. Among the type 1 Seyfert galaxies there are many objects with narrow lines.

Radio variable sources at 1400 MHz and their optical variability (Abrahamyan et al., 2018a). In the present study we have cross-correlated NVSS (Condon et al., 1998) and FIRST (Helfand et al., 2015) radio catalogues having radio flux measurements at the same 1.4 GHz frequency. This way we benefit from repeated observations from both catalogues, as they give more accurate positions and fluxes and more important, reveal large differences between the two measured fluxes, thus allowing to establish radio variability. As a result, 79,382 radio variables have been revealed, including 6301 with flux differences at 1.4 GHz larger than 15 mJy, 1917 with flux differences > 45 mJy and 260 with flux differences > 200 mJy. By using a special technique (Mickaelian & Sinamyan, 2010, Mickaelian et al., 2011), 2425 optically variable objects out of 6301 radio sources have been revealed. 2425 radio sources with both high radio and optical variability into four categories have been divided. 1206 (19%) out of 6301 radio sources have activity types from available catalogues and 619 (25.5%) out of 2425 radio sources with at the same time radio and optical variability have activity types from available catalogues. In addition, 279 radio sources out of 2425 have high variability in optical range. We have established their activity types when available. The IR fluxes and colors for the 6301 variable radio sources have been studied. Color-color diagrams show that most of the "unknown" sources are galaxies. The activity types for 110 (42%) out of 260 extremely high variable radio sources also have been retrieved. We give in Table 2 the distribution of the activity types of 6301 radio sources having radio variability.

Classification of BZCAT objects having uncertain types (Abrahamyan et al., 2019a) was aimed at understanding some optical properties of blazars having uncertain types (BZU) in BZCAT Catalogue v5 (Massaro et al., 2015). Cross-correlation with SDSS revealed 43 BZU objects that have spectra in SDSS out of the total 227 BZU ones. We have carried out spectral re-classification for these 43 blazar candidates for activity types. As a result, 37 (86%) objects out of 43 changed their previous type.

Optical variability of blazars (Abrahamyan et al., 2019b). The analysis of blazars' parameters from BZCAT leads to a conclusion that they do not have the same properties. The preliminary criterion to include an object in the catalog was the strong radio emission; however, two type of radio sources were selected: BL Lacertae (BLL) objects and Flat Spectrum Radio Quasars (FSRQ). As

Table 2. Activity types of 6301 radio sources having radio variability.

No.	Activity Type	Numbers
1	Blazar (BZB, BZG, BZQ, BZU)	308
2	QSO	639
3	Sy 1.0 / Sy 1	19
4	Sy 1.2	2
5	Sy 1.5	6
6	Sy 1.9	2
7	Sy 2.0 / Sy 2	9
8	AGN	97
9	Starburst	1
10	FSS (Flat-Spectrum radio source)	87
11	USS (Ultra-Steep-Spectrum radio source)	36
	Known (total)	**1206 (19%)**
	Unknown	**5095 (81%)**
	Total	**6301 (100%)**

a number of properties are typical of blazars (strong radio emission, optical variability, continuum optical spectra, polarization, high luminosity, etc.), using the optical data, we investigate them to clarify which property plays the most significant role in their classification as blazars. We found that 60% of blazars have optical variability. We use a technique developed based on POSS1 and POSS2 photometry and group the variability into extreme, strong, medium, and low classes. In the optical range, 51 blazars have powerful variability (extreme variables), and 126 are high variables. In addition, 63% of blazars have detected radiation in X-ray and 28% have detected radiation in gamma rays. We give the average statistical characteristics of blazars based on our analysis and calculations.

Fine Analysis of Emission-Line Spectra and Classification of Active Galaxies. Using the SDSS spectroscopy, we have carried out fine optical spectral classification for activity types for 710 AGN candidates. These objects come from a larger sample of some 2500 candidate AGN using pre-selection by our various samples. More than 800 QSOs have been identified and classified, including 710 QSOs, Seyferts and Composites. The fine classification shows that many QSOs show the same features as Seyferts, i. e. subtypes between S1 and S2 (S1.2, S1.5, S1.8 and S1.9). We have introduced subtypes for the QSOs: QSO1.2, QSO1.5, QSO1.8, QSO1.9, though the last subtype does not appear in SDSS wavelength range due to mostly highly redshifted HVT (the main line for identification of the 1.9 subtype). We also have classified many objects as Composites, spectra having composite characteristics between Sy and LINERs, Sy and HII or LINERs and HII; in some cases all three characteristics appear together resulting as Sy/LINER/HII subtype (Mickaelian et al., 2020). We have used the following works for deriving our fine classification of active galaxies: Heckman (1980), Hoffmeister (1929), Khachikian & Weedman (1974), Oke & Gunn (1974), Osterbrock (1981), Osterbrock & Pogge (1985), Schmidt (1963), Schmitt (1968), Seyfert (1943), Strittmatter et al. (1972), Terlevich (1997, 2000), Thuan & Martin (1981), Véron et al. (1997), Weedman (1977).

Summary

A number of interesting results have been obtained in the field of multiwavelength studies of active galaxies, including X-ray, IR and radio sources identified with AGN and Starbursts. Among the important results one could mention:

- Study of SDSS spectra of 371 optical identifications of HRC/BHRC Sample ROSAT X-ray sources (Paronyan et al., 2018, 2019, 2020). These sources were also identified in other wavelength ranges and some of their parameters were calculated.

- The UV properties of 1152 Markarian galaxies were investigated based on GALEX data (Mickaelian et al., 2018b). Using our classification for activity types for 779 Markarian galaxies based on SDSS spectroscopy, we have investigated these objects on the GALEX, 2MASS and WISE color-magnitude and color-color diagrams by the location of objects of different activity types and have revealed a number of concentrations.

- Abundance and Star Formation Determinations in more than 700 Markarian galaxies from SDSS Spectra (Gyulzadyan et al., 2018). We have measured their line fluxes and derived the O and N abundances using recent calibrations. The behavior of the [N/H] ratio in under-abundant regions gives strong support to a partially primary origin of nitrogen.

- Revised optical classification of objects classified as "LINERs" in the Catalogue Véron-Cetty & Véron 13th edition (Abrahamyan et al., 2018b), where 926 LINERs are included. We found 176 objects having spectra in SDSS DR14. The re-classification of these objects led to 54% of them to change their activity types.

- Study and classification of SDSS spectra for Byurakan-IRAS Galaxies (Mickaelian et al., 2018a). To the previously observed 172 BIG objects (with BAO, SAO and OHP telescopes) 83 BIG objects were added having spectra in SDSS. Among them, 55 HII, 8 Seyfert galaxies, 2 LINERs, 4 other AGN, 6 composite spectrum objects, and 8 other emission-line galaxies have been revealed. Three of these objects are ULIRGs. The observations and study of 257 Byurakan-IRAS Galaxies were summarized in Mikayelyan et al. (2019b).

- Discovery of new bright ULIRGs from the IRAS PSC/FSC Combined Catalogue (Mikayelyan et al., 2018). By means of the SDSS DR14 data, namely redshifts for those objects having spectroscopy, we have calculated the IR luminosities and have found 114 very high-luminosity IR galaxies; 107 ULIRGs and 7 HLIRGs. Among them, 48 new ULIRGs and 7 new HLIRGs have been discovered. Spectral classification of these ULIRGs were carried out (Mikayelyan et al., 2019a). 1 BLL, 2 quasars, 29 Seyferts of types 1.0-1.8 (including narrow-line), 5 Seyferts of type 2, 14 LINERS, 36 HII, 14 objects with a composite spectrum (Composite) were identified.

- Radio variable sources at 1400 MHz were studied and their optical variability waa revealed (Abrahamyan et al., 2018a). As a result, 79,382 radio variables have been revealed, including 6301 with flux differences at 1.4 GHz larger than 15 mJy. By using a special technique (Mickaelian & Sinamyan, 2010, Mickaelian et al., 2011), 2425 optically variable objects out of 6301 radio sources have been revealed.

- Classification of BZCAT objects having uncertain types was carried out (Abrahamyan et al., 2019a). 43 BZU objects were found to have SDSS spectra and as a result, 37 (86%) objects changed their previous type.

- Optical variability of blazars was studied (Abrahamyan et al., 2019b). We found that 60% of blazars have optical variability. In the optical range, 51 blazars have powerful variability (extreme variables), and 126 are high variables. In addition, 63% of blazars have detected radiation in X-ray and 28% have detected radiation in gamma rays.

We give in Table 3 a Summary of Projects on Search and Studies of Active Galaxies by our group during 1990s-2010s.

Table 3: Summary of Projects on Search and Studies of Active Galaxies.

Project	**Years**	**Objectives**	**Objects**	**References**
FBS QSOs/Seyferts	1986-2001	Bright QSOs and Seyferts	1,103	Mickaelian (2000a, 2003, 2004a, 2008), Mickaelian et al. (1999, 2001b, 2002a)
IRAS BIG sample	1994-2010	AGN, SB, ULIRGs	1,178	Mickaelian (1995, 1997, 2000b, 2001a,b, 2002), Mickaelian & Gigoyan (1998a,b), Mickaelian & Sargsyan (2004a,b), Mickaelian et al. (1997)
IRAS BIG spectroscopy	1997-2019	AGN, SB, ULIRGs	257	Mickaelian (2003, 2004b), Balaian et al. (2001), Mickaelian & Sargsyan (2010), Sargsyan & Mickaelian (2006), Mickaelian et al. (1998, 2001a, 2002b, 2003, 2018a, 2019)
ROSAT BSC/FSC sources	2002-2006	Search for new AGN	6,003	Véron-Cetty et al. (2004), Mickaelian et al. (2006)
Bright AGN	2001-pres.	Statistical analysis	~10,000	
Mrk galaxies	2010-pres.	Spectral and MW studies	1,515	Mickaelian et al. (2013, 2018b), Gyulzadyan et al. (2018)
IRAS PSC/FSC extragalactic sample	2011-pres.	Large IR galaxies sample	145,902	Hovhannisyan et al. (2011), Abrahamyan et al. (2015)
IRAS PSC/FSC ULIRGs	2018-2019	IRAS PSC/FSC ULIRGs	114	Mikayelyan et al. (2018, 2019a)
Spitzer ULIRGs	2003-2010	High IR/opt flux ratio galaxies	32	Sargsyan et al. (2008)
SB/AGN Spitzer spectra	2011	SB/AGN Spitzer spectra	301	Sargsyan et al. (2011)
HRC/BHRC AGN	2010-pres.	AGN content in X-ray	4,253	Mickaelian et al. (2016), Paronyan et al. (2018, 2019, 2020)
NVSS-FIRST variability, etc.	2013-pres.	Study of radio variability	6,301	Abrahamyan et al. (2018a)
Radio AGN	2020	Contents of radio AGN	1,864	Abrahamyan et al. (2020)
LINERs	2018	Physical properties of LINERs		Abrahamyan et al. (2018b)
ROSAT-NVSS sources	2013-pres.	Search for new AGN, statistics	9,193	Paronyan et al. (2014)
MW study of Blazars	2014-pres.	New Blazars, definition	3,561	Abrahamyan et al. (2019a,b)
Fine analysis of emission-line spectra	2001-2007	Physical properties of AGN	90	Kazarian & Mickaelian (2007)
SBS QSOs in WISE	2017	QSOs	450	Erastova & Mickaelian (2017)
DFBS AGN	2002-pres.	New bright active galaxies	~10,000	
Fine classification of active galaxies	2006-pres.	Accurate types and subtypes	~10,000	Mickaelian et al. (2020)

References

Abrahamyan H. V., Mickaelian A. M., Knyazyan A. V., 2015, A&C, 10, 99

Abrahamyan H. V., Mickaelian A. M., Paronyan G. M., Mikayelyan G. A., Gyulzadyan M. V., 2018a, A&C, 25, 176

Abrahamyan H. V., Mickaelian A. M., Mikayelyan G. A., Paronyan G. M., 2018b, ComBAO, 65, 1

Abrahamyan H. V., Mickaelian A. M., Paronyan G. M., Mikayelyan G. A., Gyulzadyan M. V., 2019a, ComBAO, 66, 1

Abrahamyan H. V., Mickaelian A. M., Paronyan G. M., Mikayelyan G. A., 2019b, AN, 340, 437

Abrahamyan H. V., Mickaelian A. M., Paronyan G. M., Mikayelyan G. A., 2020, Ap, 63, 322

Ahumada R., Allende Prieto C., Almeida A., et al 2020, ApJS, 249, 3

Arakelian M. A., 1975, ComBAO, 47, 3

Baier F. W., Petrosyan M. B., Tiersch H., Shakhbazyan R. K., 1974, Ap, 10, 327

Balaian S. K., Akopian S. A., Mickaelian A. M., Burenkov A. N., 2001, AstL, 27, 284

Bianchi L., Herald J., Efremova B., Girardi L., Zabot A., Marigo P., Conti A., Shiao B., 2011, Ap&SS, 335, 161

Bird A. J., et al., 2010, ApJS, 186, 1

Condon J. J., Cotton W. D., Greisen E. W., Yin Q. F., Perley R. A., Taylor G. B., Broderick J. J., 1998, AJ, 115, 1693

Cutri R. M., Wright E. L., Conrow T., et al 2013, VizieR Online Data Catalog: AllWISE Data Release, VizieR On-line Data Catalog: II/328. Originally published in: IPAC/Caltech

Erastova L. K., Mickaelian A. M., 2017, AApTr, 30, 261

Gyulzadyan M. V., Mickaelian A. M., Abrahamyan H. H., Mikayelyan G. A., Paronyan G. M., 2018, ComBAO, 65, 392

Heckman T. M., 1980, A&A, 87, 152

Helfand D. J., White R. L., Becker R. H., 2015, ApJ, 801, 26

Hoffmeister C., 1929, AN, 236, 233

Hovhannisyan A., Sargsyan L. A., Mickaelian A. M., Weedman D. W., 2011, Ap, 54, 147

IRAS 1988, Joint IRAS Science W.G., IRAS Catalog of Point Sources, Version 2.0

Kazarian M. A., Mickaelian A. M., 2007, Ap, 50, 127

Kazarian M. A., Adibekyan V. Z., McLean B., Allen R. J., Petrosian A. R., 2010, Ap, 53, 57

Khachikian E. Y., Weedman D. W., 1974, ApJ, 192, 581

Markarian B. E., Stepanian J. A., Erastova L. K., 1987, IAU S121, p. 25

Markarian B. E., Lipovetsky V. A., Stepanian J. A., Erastova L. K., Shapovalova A. I., 1989, ComSAO, 62, 5

Massaro E., Maselli A., Leto C., Marchegiani P., Perri M., Giommi P., Piranomonte S., 2015, Ap&SS, 357, 75

Mazzarella J. M., Balzano V. A., 1986, ApJS, 62, 751

Mickaelian A. M., 1995, Ap, 38, 349

Mickaelian A. M., 1997, Ap, 40, 1

Mickaelian A. M., 2000a, AApTr, 18, 557

Mickaelian A. M., 2000b, Ap, 43, 309

Mickaelian A. M., 2001a, Ap, 44, 33

Mickaelian A. M., 2001b, Ap, 44, 185

Mickaelian A. M., 2002, Ap, 45, 288

Mickaelian A., 2003, AApTr, 22, 753

Mickaelian A. M., 2004a, BalA, 13, 655

Mickaelian A. M., 2004b, Ap, 47, 361

Mickaelian A. M., 2008, AJ, 136, 946

Mickaelian A. M., 2017, ComBAO, 64, 15

Mickaelian A. M., Gigoyan K. S., 1998a, Ap, 41, 161

Mickaelian A. M., Gigoyan K. S., 1998b, Ap, 41, 232

Mickaelian A. M., Sargsyan L. A., 2004a, Ap, 47, 91

Mickaelian A. M., Sargsyan L. A., 2004b, Ap, 47, 213

Mickaelian A. M., Sargsyan L. A., 2010, Ap, 53, 483

Mickaelian A. M., Sinamyan P. K., 2010, MNRAS, 407, 681

Mickaelian A. M., Gigoyan K. S., Russeil D., 1997, Ap, 40, 379

Mickaelian A. M., Akopian S. A., Balaian S. K., Burenkov A. N., 1998, AstL, 24, 635

Mickaelian A. M., Gonçales A. C., Véron-Cetty M. P., Véron P., 1999, Ap, 42, 1

Mickaelian A. M., Balayan S. K., Hakopian S. A., 2001a, AApTr, 20, 315

Mickaelian A. M., Gonçalves A. C., Véron-Cetty M. P., Véron P., 2001b, Ap, 44, 14

Mickaelian A. M., Abrahamian H. V., Guibert J., Chesnel R., 2002a, Ap, 45, 73

Mickaelian A. M., Hakopian S. A., Balayan S. K., Dodonov S. N., Afanasiev V. L., Burenkov A. N., Moiseev A. V., 2002b, BulSAO, 53, 144

Mickaelian A. M., Hovhannisyan L. R., Sargsyan L. A., 2003, Ap, 46, 177

Mickaelian A. M., Hovhannisyan L. R., Engels D., Hagen H. J., Voges W., 2006, A&A, 449, 425

Mickaelian A. M., Mikayelyan G. A., Sinamyan P. K., 2011, MNRAS, 415, 1061

Mickaelian A. M., Abrahamyan H. V., Paronyan G. M., Harutyunyan G. S., 2013, AN, 334, 887

Mickaelian A. M., Paronyan G. M., Harutyunyan G. S., Abrahamyan H. V., Gyulzadyan M. V., 2016, AApTr, 29, 333

Mickaelian A. M., Harutyunyan G. S., Sarkissian A., 2018a, AstL, 44, 351

Mickaelian A. M., Abrahamyan H. V., Gyulzadyan M. V., Paronyan G. M., Mikayelyan G. A., 2018b, Ap&SS, 363, 237

Mickaelian A. M., Abrahamyan H. V., Paronyan G. M., Mikayelyan G. A., Gyulzadyan M. V., 2019, ComBAO, 66, 173

Mickaelian A. M., Abrahamyan H. V., Paronyan G. M., Mikayelyan G. A., 2020, Frontiers in Astronomy and Space Sciences

Mikayelyan G. A., Mickaelian A. M., Abrahamyan H. V., Paronyan G. M., 2018, ComBAO, 65, 13

Mikayelyan G. A., Mickaelian A. M., Abrahamyan H. V., Paronyan G. M., Gyulzadyan M. V., 2019a, Ap, 62, 452

Mikayelyan G. A., Mickaelian A. M., Abrahamyan H. V., Paronyan G. M., Gyulzadyan M. V., 2019b, ComBAO, 66, 31

Moshir M., Copan G., Conrow T., et al 1989, IRAS Faint Source Catalog, Version 2.0, NASA

Oke J. B., Gunn J. E., 1974, ApJL, 189, L5

Osterbrock D. E., 1981, ApJ, 249, 462

Osterbrock D. E., Pogge R. W., 1985, ApJ, 297, 166

Paronyan G. M., Abrahamyan H. V., Harutyunyan G. S., Mickaelian A. M., 2014, in Mickaelian A. M., Sanders D. B., eds, Vol. 304, Multiwavelength AGN Surveys and Studies. pp 164–165, doi:10.1017/S1743921314003652

Paronyan G. M., Mickaelian A. M., Abrahamyan H. V., Mikayelyan G. A., 2018, ComBAO, 65, 412

Paronyan G. M., Mickaelian A. M., Harutyunyan G. S., Abrahamyan H. V., Mikayelyan G. A., 2019, Ap, 62, 147

Paronyan G. M., Mickaelian A. M., Abrahamyan H. V., Mikayelyan G. A., 2020, Ap, 63, 166

Sargsyan L. A., Mickaelian A. M., 2006, Ap, 49, 19

Sargsyan L., Mickaelian A., Weedman D., Houck J., 2008, ApJ, 683, 114

Sargsyan L., Weedman D., Lebouteiller V., Houck J., Barry D., Hovhannisyan A., Mickaelian A., 2011, ApJ, 730, 19

Schmidt M., 1963, Nature, 197, 1040

Schmitt J. L., 1968, Nature, 218, 663

Seyfert C. K., 1943, ApJ, 97, 28

Strittmatter P. A., Serkowski K., Carswell R., Stein W. A., Merrill K. M., Burbidge E. M., 1972, ApJ, 175, L7

Terlevich R., 1997, RMAA, 6, 1

Terlevich R., 2000, In: Advanced Lectures on the Starburst-AGN Connection, Eds. Aretxaga, I.; Mújica, R.; Kunth, D., World Scientific, p. 279

Thuan T. X., Martin G. E., 1981, ApJ, 247, 823

Véron-Cetty M. P., Véron P., 2010, A&A, 518, A10

Véron-Cetty M. P., et al., 2004, A&A, 414, 487

Véron P., Gonçales A. C., Véron-Cetty M. P., 1997, A&A, 319, 52

Voges W., et al., 1999, A&A, 349, 389

Voges W., Aschenbach B., Boller T., et al 2000, MPE, Garching. The ROSAT Faint Source Catalogue

Weedman D. W., 1977, Vistas in Astronomy, 21, 55

Zickgraf F. J., Engels D., Hagen H. J., Reimers D., Voges W., 2003, A&A, 406, 535

Big Data in Astronomy: Surveys, Catalogs, Databases and Archives

A. M. Mickaelian*

NAS RA Byurakan Astrophysical Observatory (BAO), Byurakan 0213, Aragatzotn Province, Armenia

Abstract

We present the modern situation in astronomy, where Big Data coming from the Universe put new tasks for catalogizing, storage, archiving, analysis and usage of the scientific information. The two major characteristics of modern astronomy are multiwavelength (MW) studies (from γ-ray to radio, as well as multi-messenger studies, using also neutrinos, gravitational waves, etc.) and Big Data (including data acquisition, storage and analysis). Present astronomical databases and archives contain billions of objects observed in various wavelengths, both Galactic and extragalactic, and the vast amount of data on them allows new studies and discoveries. Astronomers deal with big numbers. Surveys are the main source for discovery of astronomical objects and accumulation of observational data for further analysis, interpretation, and achieving scientific results. We review the main characteristics of astronomical surveys, we compare photographic and digital eras of astronomical studies (including the development of wide-field observations), we give the present state of MW surveys, and we discuss the Big Data in astronomy and related topics of Virtual Observatories and Computational Astrophysics. The review includes many numbers and data that can be compared to have a possibly overall understanding on the studied Universe, cosmic numbers and their relationship to modern computational possibilities.

Keywords: *Big Data, Astronomical Surveys, Astronomical Catalogues, Databases, Archives, Multi-wavelength Astronomy, Data Mining, Computational Astrophysics, Astrostatistics, Astroinformatics, Virtual Observatories, Laboratory Astrophysics.*

1. Introduction

Astronomy is the area of science where we deal with vast number of objects, phenomena and hence, big numbers. Astronomy and its results also enlarge most of other sciences, as any research on the Earth is limited in sense of the physical conditions, variety of objects and phenomena, and amount of data. During the last few decades astronomy became fully multiwavelength (MW); all-sky and large-area surveys and their catalogued data over the whole range of the electromagnetic spectrum from γ rays to radio wavelengths enriched and continue to enrich our knowledge about the Universe and supported the development of physics, geology, chemistry, biology and many other sciences. Astronomy has entered the Big Data era and these data are accumulated in astronomical catalogues, databases and archives. Astrophysical Virtual Observatories (VOs) have been created to build a research environment and to apply special standards and software systems to carry out more efficient research using all available databases and archives. VOs use available databases and current observing material as a collection of interoperating data archives and software tools to form a research environment in which complex research programs can be conducted. Most of the modern databases give at present VO access to the stored information. This makes possible not only the open access but also a fast analysis and managing of these data. VO is a prototype of Grid technologies that allows distributed data computation, analysis and imaging. Particularly important are data reduction and analysis systems: spectral analysis, spectral energy distribution (SED) building and

*aregmick@yahoo.com

DOI: 10.52526/25792776-2020.67.2-159

fitting, modelling, variability studies, cross-correlations, etc. This way, astronomers benefit from the usage of data coming from various ground-based and space telescopes, from various observing modes, from various time domains and from various wavelength ranges. Putting together all data (including old archival ones) allows discovering new objects, studying variability and finding high proper motion stars. Therefore, general knowledge of the important astronomical surveys, catalogues, databases and archives and main parameters of the available data is necessary for modern astrophysical research. Moreover, these accumulated data and the necessity of their quick reduction and analysis, as well as modelling and simulations in theoretical studies led to the creation of the Numerical or Computational Astrophysics (Astrostatistics, Astroinformatics), which is part of the Computer Science. It has become an indissoluble part of astronomy and most of modern research is being done by means of it. On the other side, Laboratory Astrophysics provides laboratory experiments related to space research to check the results by astronomical observations.

Big Data are characterized by 4 Vs:

- **Volume.** Quantity of generated and stored data. The size of the data determines the value and potential insight, whether it can be considered big data or not.
- **Variety.** The type and nature of the data. This helps people who analyze it to effectively use the resulting insight. Big data draws from text, images, audio, video; plus, it completes missing pieces through data fusion.
- **Velocity.** In this context, the speed at which the data is generated and processed to meet the demands and challenges that lie in the path of growth and development. Big data is often available in real-time.
- **Veracity.** The data quality of captured data can vary greatly, affecting the accurate analysis.

Present astronomical databases and archives contain billions of objects, both galactic and extragalactic, and the vast amount of data on them allows new studies and discoveries. Astronomers deal with big numbers and it is exactly the case that the expression "astronomical numbers" means "big numbers". Surveys are the main source for discovery of astronomical objects and accumulation of observational data for further analysis, interpretation, and achieving scientific results. Nowadays they are characterized by the numbers coming from the space; larger the sky and (in case of spectroscopic surveys) spectral coverage, better the spatial (in case of spectroscopic surveys, also spectral) resolution and sensitivity (deeper the survey), larger the covered time domain, more data are obtained and stored. Therefore, we give the highest importance to **all-sky and large area surveys**, as well as deep fields, where huge amount of information is available. These are:

- CGRO (Hartman et al., 1999), Fermi-GLAST (Acero et al., 2015) and INTEGRAL (Bird et al., 2010) in **γ-ray**,
- ROSAT (Voges et al., 1999, 2000), Swift (D'Elia et al., 2013), XMM-Newton (XMM-Newton, 2013) and Chandra (Evans et al., 2010) in **X-ray**,
- GALEX (Bianchi et al., 2011) in **UV**,
- SDSS (Ahumada et al., 2020) and POSS I / POSS II based several catalogues (APM (McMahon et al., 2000), MAPS (Cabanela et al., 2003), USNO (Monet et al., 1998, 2003) and GSC (Lasker et al., 2008)) in **optical range**,
- 2MASS (Cutri et al., 2003, Skrutskie et al., 2006) and DENIS (DENIS consortium, 2005) in **near infrared (NIR)**,
- WISE (Cutri et al., 2013), AKARI IRC (Ishihara et al., 2010) and Spitzer (Spitzer, 2015) in **mid-infrared (MIR)**,

- IRAS (Helou & Walker, 1985, IRAS, 1988, Moshir et al., 1989), AKARI FIS (Yamamura et al., 2010) and Herschel (Oliver et al., 2012) in **far infrared (FIR)**,
- ALMA (ALMA, 2015), Planck (Planck, 2011) and WMAP (Gold et al., 2011) in **sub-mm/mm**,
- GB6 (Gregory et al., 1996), NVSS (Condon et al., 1998), FIRST (Helfand et al., 2015), SUMSS (Mauch et al., 2012), WENSS (de Bruyn et al., 1998), 7C (Hales et al., 2007), VLA LFSS (Lane et al., 2014) and a few others in **radio**,
- as well as most important surveys giving **optical images** (DSS I / DSS II and SDSS),
- **proper motions** (Tycho (Høg et al., 2000), USNO, Gaia),
- **variability** (GCVS, NSVS, ASAS, Catalina, LINEAR, Pan-STARRS) and
- **spectroscopic data** (FBS (Markarian et al., 1989), SBS (Stepanian, 2005), Case, HQS (Hagen et al., 1999), HES (Wisotzki et al., 2000), SDSS, 2dF/6dF, CALIFA, GAMA, etc.).

Among the deep fields, HDF N/S, HUDF, CDF N/S, GOODS N/S, and COSMOS are most important. From the years of references, it is obvious that astronomical large-area surveys were carried out especially during the last years and significantly changed our knowledge in all wavelengths.

Very often dozens of thousands of sources hide a few very interesting ones that are needed to be discovered by comparison of various physical characteristics. Cross-correlations result in revealing new objects and new samples. The large amount of data requires new approaches to data reduction, management and analysis. Powerful computer technologies are required, including clusters and grids. Large volume astronomical servers have been established to host Big Data and giving high importance to their maintenance, the International Council of Scientific Unions (ICSU, at present: International Science Council, ISC) has created World Data System (WDS) to unify data coming from different science fields for further possibility of exchange and new science projects.

In this paper we give an overall understanding of the astronomical data by coverage along the whole wavelength range and comparisons between various surveys: galaxy redshift surveys, QSO/AGN, radio, Galactic structure and Dark Energy surveys. We describe surveys providing MW photometric data from γ-ray to radio, as well as proper motion, variability and spectroscopic surveys, including objective prism low-dispersion surveys and digital ones.

2. Astronomical Surveys: their importance and main characteristics

The Universe is very big; there are 100s billions of galaxies, each containing 100s billions of stars, nebulae, and other objects. Most of objects are very like each other, and standard approach may be applied to study their average physical properties, structure, and evolution. Classical explanations for stellar configurations, inner structure, stellar atmospheres, and radiation mechanisms have been developed. However, unique objects are needed to study and understand new physical mechanisms, origin and evolution of stars, galaxies, and the Universe as a whole. Some stars have extreme colours, peculiar chemical abundance, emission lines, extended envelopes, some stars are non-optical sources, variables (especially interesting are non-stable ones), binaries (especially interesting are physically connected close binaries), some stars are located in groups and clusters. Some galaxies are peculiar (blue, emission-line, etc.), there are starbursts (SB), active galactic nuclei (AGN), pairs and multiples (especially interesting are interacting ones), mergers, some galaxies have jets, some are non-optical sources, etc. All these peculiar objects comprise typically 5-10% of all observed objects.

It is impossible to study all astronomical objects and one of the main tasks of astronomers is to search and find those peculiar objects that may give more understanding on the physics of objects and phenomena. This task is being achieved by astronomical surveys; having observed large areas of the sky, one can select interesting objects by definite criteria. Selection and application of these criteria defines the value of a survey. Surveys are the backbone of astronomy, and the engine of discovery. They are of cultural importance, because they satisfy the desire to map our surroundings, and give us a feeling for where we live (Lawrence, 2007). Surveys are efficient, because once the sky has been imaged and catalogued, astronomers can do many different experiments using the same database. Surveys data are a resource that supports other astronomy research, e. g. when a γ- or X-ray source is found, one can check whether it is also an IR or radio source, without having to carry out new observations. Some surveys are aimed at mapping a large area of sky, either to build up a large sample to get relevant statistics, or because a large area is being studied like the Milky Way spreading all over the sky. The 20^{th} century technology allowed us to look at the Universe at different wavelengths and many new objects have been discovered at first in non-optical ranges and then identified in optical wavelengths; radio galaxies, quasars, pulsars, cosmic background, molecular clouds, the hot intra-cluster medium, ultraluminous starbursts and AGN (ULIRGs), brown dwarfs, hidden X-ray AGN, etc.

Most important characteristics of astronomical surveys are:

- **Observational method.** Surveys may be imaging (like POSS I and II), photometric, spectroscopic (in this case an objective prism, grism or multi-object spectrographs (MOS) are being used), polarimetric, etc. Some surveys use several modes to combine data and achieve better results. However, this requires more technical efforts and typically is not the case.

- **Sky area.** The selection of the sky area defines the task; e. g. for extragalactic surveys, high galactic latitudes are necessary to skip the heavy galactic absorption. For the galactic surveys, vice versa, definite regions of the Milky Way are being covered.

- **Sky coverage;** depending on this, larger area and more objects may be involved. However, for large sky areas deep surveys are not possible. From this point of view, surveys may be all-sky (totalling 41,253 sq. deg.) and large area ones (a few thousand or a few dozens of thousand sq. deg.) and deep fields (typically less than 1 sq. deg. and often only a few sq. arcmin).

- **Wavelength coverage;** even in optical surveys, wavelength range is important to reveal definite types of objects; e. g. most of the energy of high redshift QSOs is in red and IR part of the spectrum and having observations only in the blue part, one loses many QSOs due to their faintness in that range. Moreover, MW surveys are aimed at discovery of sources in all wavelength domains. In recent SDSS data releases (DR), wavelength range is 3000-10800Å, larger than in all previous optical surveys. Depending on covered wavelengths, the sky may be quite different, therefore this is a rather important parameter.

- **Time coverage.** Typically, most of the surveys make single observations in each field. However, large time domains are necessary for variability studies and repeated observations are being carried out for such purposes. Large time coverage is provided by archival observations that may be used due to digitization of old astronomical plates (variability data are provided by Samus' et al. (2011); Woźniak et al. (2004); Pojmanski (1998); Drake et al. (2014a,b)).

- **Spatial resolution.** The positional accuracy of a survey is derived from its spatial resolution. Recent optical surveys (DSS based catalogues, SDSS, Tycho, etc.) have reached 1 arcsec and better resolution, however in other wavelength ranges there still are technology-based limitations on the accuracy. This also creates inconvenience in cross-correlation of various sources.

- **Spectral resolution.** For spectroscopic surveys, this is one of the most important parameters, as most of the information comes from spectra and more accurate the spectroscopy, more information may be derived. However, high spectral resolutions take longer exposure times, therefore in large surveys, typically low and medium resolutions are being used.

- **Sensitivity.** In optical range, the limiting magnitude of a survey is important to reach fainter objects. Similarly, in other wavelength ranges, the sensitivity (typically given in magnitudes in optical range and UV, mJy-s in IR and radio, or eV-s in high energy astrophysics) defines how deep a survey can reach. In deepest surveys, such as HUDF, 30^m is achieved.

- **Photometric accuracy.** Along with the limiting magnitude or sensitivity, the accuracy of the photometric measurements is rather important. This is the case for estimation of the completeness, derivation of luminosities, colour and variability measurements, etc. Optical surveys reach 0.01^m and better photometric accuracy.

- **Homogeneity.** Any survey needs to be homogeneous, otherwise its value is not maintained. Homogeneous samples of objects or non-optical sources give an important material for statistics and further studies.
- **Completeness.** Based on the homogeneity limit, one may derive the completeness of any survey. As homogeneity, so as completeness gives understanding of the value for a survey. Typically, the completeness of the detection is being considered, however the completeness of classification is also crucial for spectroscopic surveys, which is based on more details, hence it is less than the detection limit.

There are many types of astronomical surveys that may be combined by following criteria:

- **Goals** (sky coverage, discovery of definite objects, etc.). E. g. redshift surveys are devoted to mapping the cosmos in three dimensions. Usually galaxies are the targets, but sometimes these are other objects, such as galaxy clusters or quasars.
- **Object types** (QSOs, AGN, galaxies, blue stars, late-type stars, SNe, variables, exoplanets, etc.).
- **Method** (colorimetric, spectroscopic, multi-band, variability, etc.).
- **Sky area** (all-sky, large area or deep surveys).
- **Wavelength range** (optical, γ-ray, X-ray, UV, IR, sub-mm/mm, radio, combined, MW).

The first systematic redshift survey was the CfA Redshift Survey of around 2,200 galaxies, started in 1977 with the initial data collection completed in 1982. This was later extended to the CfA2 redshift survey of 15,577 galaxies (Huchra et al., 1999). Later on, redshift surveys became most important for large scale structure of the Universe and cosmology.

3. Wide-field telescopes and their discoveries

Historically, astronomical surveys have been carried out with wide-field, mostly **Schmidt telescopes**. Here in **Table 1** we give the list of the largest Schmidt telescopes of the world, most of which at present have historical value. The consecutive columns give: telescope name, correcting lens size in cm, mirror size in cm, focal length in cm, focal ratio, field of view in degrees, plate size in cm, scale in arcsec/mm, location, country, altitude in m, and year of installation.

Table 1. Largest historical Schmidt telescopes.

Telescope name	Corr. cm	Mirror cm	Focus cm	Focal ratio	Field deg	Plate cm	Scale "/mm	Location	Country	Alt. m	Year
Alfred-Jensch	134	203	410	1:3.0	3.4×3.4	24×24	50.3	Tautenburg	Germany	331	1960
Samuel Oschin	122	183	307	1:2.5	6.6×6.6	36×36	67.2	Mt. Palomar	USA	1706	1948
UK Schmidt	122	183	307	1:2.5	6.6×6.6	36×36	67.2	Siding-Spring	Australia	1131	1973
Kiso Schmidt	105	150	330	1:3.1	6.0×6.0	36×36	62.5	Kiso	Japan	1130	1974
ESO Schmidt	102	162	306	1:3.0	5.5×5.5	29×29	67.4	Cerro La Silla	Chile	2400	1969
Jurgen Stock	102	152	301	1:3.0	5.5×5.5	29×29	68.5	Llano del Hato	Venezuela	3600	1976
Kvistaberg Schm.	102	135	300	1:3.0	4.6×4.6	24×24	68.8	Kvistaberg	Sweden	33	1964
BAO 1m Schmidt	102	132	213	1:2.1	4.1×4.1	16×16	96.8	Byurakan	Armenia	1397	1960
Uccle Schmidt	84	117	210	1:2.5			98.2	Uccle	Belgium	105	1958
Hamburg Schm.	81	122	240	1:3.0	5.5×5.5	25×25	86.2	Calar Alto	Spain	2160	1955
Baker-Schmidt	81	91	300	1:3.7			68.8	Bloemfontein	S. Africa	1387	1950
Baldone Schmidt	80	120	240	1:3.0	4.8×4.8	24×24	85.9	Baldone	Latvia	75	1967

Among these, especially **Palomar**, **Siding Spring** and **ESO** Schmidt telescopes are very well known for accomplishment of two Palomar Observatory Sky Surveys (POSS I and II; the two latter telescopes were used for the extension of POSS to the Southern sky). POSS I was carried out in 1948-1958 with Palomar Oschin 1.2m Schmidt telescope in blue and red colours, Kodak 103a-O and 103a-E, respectively. The limiting magnitudes are 21.0^m and 20.0^m. 937 different fields each 6.6°x6.6° were taken and the entire sky above δ $-33°$ was covered. Later on, the southern limit was extended to about $-45°$ (100 more plates); thus the survey as a whole includes 1037 fields. UKST SERC J Southern Survey was carried out in 1975-1987 with UKST 1.2m Schmidt telescope and complemented POSS I. POSS II was accomplished in 1987-2000 for the whole sky in blue IIIaJ, red IIIaF and IR IV-N bands, resulting in limiting magnitudes 22.5^m, 20.8^m and 18.5^m respectively. Both POSS I and II were digitized and Digitized Sky Surveys (DSS I and II) were created, respectively (Lasker et al., 1996, McGlynn et al., 1994). Large informative catalogues were created based on these data (USNO-A2.0, APM, MAPS, USNO-B1.0, GSC 2.3.2)

Byurakan and Hamburg Schmidt telescopes are well known for their spectroscopic surveys; famous Byurakan and Hamburg surveys, respectively (Hagen et al., 1999, Markarian et al., 1989), as well as Hamburg-ESO Survey (HES, Wisotzki et al. (2000)) was done with ESO Schmidt.

One of Byurakan 1m Schmidt telescope's advantages is the presence of its three objective prisms (1.5°, 3°, and 4°), which made possible wide-field spectroscopic observations with various dispersion: 1800 Å/mm, 900 Å/mm, 285 Å/mm near Hγ, respectively. The objective prisms can rotate in the position angle that allows obtaining spectra of any orientation. Markarian survey (or the First Byurakan Survey, FBS) carried out with BAO 1m Schmidt telescope, was one of the most efficient and most important survey in astronomy. It was the first systematic objective-prism survey, the largest objective-prism survey of the Northern sky (17,000 sq. deg) and it was a new method of search for AGNs. It resulted in discovery of 1515 UV-excess (UVX) galaxies, including more than 200 AGN and more than 100 SB galaxies. Markarian survey led to the classification of Seyferts into Sy1 and Sy2 (Weedman & Khachikyan, 1968), the definition of Starburst galaxies (Weedman, 1977), and several other projects, such as FBS Blue Stellar Objects (BSOs, Mickaelian (2008)), late-type stars (Gigoyan et al., 2019), optical identifications of IRAS sources (Byurakan-IRAS Galaxies (Mickaelian & Sargsyan, 2004) and Byurakan-IRAS Stars (Mickaelian & Gigoyan, 2006), BIG and BIS objects, respectively). The Second Byurakan Survey (SBS) was also carried out with BAO 1m Schmidt and was the continuation of FBS to fainter magnitudes (Stepanian, 2005). FBS is now digitized and the Digitized First Byurakan Survey (DFBS, Massaro et al. (2008), Mickaelian et al. (2007)) is available online. It provides 40,000,000 spectra for 20,000,000 objects at high Galactic latitudes. Detailed description of FBS, SBS and DFBS is given in Mickaelian (2014).

As mentioned, HQS and HES also are among most important astronomical surveys. HQS covers 14,000 deg^2 in the Northern sky and HES covers 9,000 deg^2 in the Southern sky. Digitized copies of both HQS and HES are available online. Hundreds of QSOs, other AGN, SB, emission-line galaxies, white dwarfs, cataclysmic variables and other hot stars were discovered using these surveys.

To compare the results obtained by Schmidt telescopes, particularly the spectroscopic surveys, we give in Mickaelian (2016a) a comprehensive table of main characteristics of major low-dispersion surveys and SDSS. Most of them are extragalactic surveys so that mainly high galactic latitudes are covered both in the North and South. This table gives an understanding on various parameters of low-dispersion objective prism surveys and SDSS and proves that many historical surveys are still useful.

In Table 1 we do not give the **Large Sky Area Multi-Object Fibre Spectroscopic Telescope** (**LAMOST**, Xinglong, China at 960 m altitude, installed in 2008), the 4m Schmidt telescope with reflective corrector, with collecting area of 18.86 m^2 and with 20m focal length, as its technology differs from all others and it is a meridian telescope. LAMOST is the first digital Schmidt telescope equipped with 2 4kx4k CCD cameras used in blue and red.

On the other hand, nowadays large (3-4 m) Ritchey-Chretien telescopes give relatively large field of view (up to 1 sq. deg.) and partially substitute Schmidt ones. Some of them are used as survey telescopes. Especially important are ESO's **VST (VLT Survey Telescope)** and **VISTA (Visible and Infrared Survey Telescope for Astronomy)** located in Paranal, Chile. VST is 2.6m optical survey telescope (its primary is 2.61m and secondary is 0.94m); its optical design is modified Ritchey-Chrétien reflector with correctors. VISTA is a 4m NIR survey telescope (its primary is 4.1m and secondary is 1.24m); its optical design is also a modified Ritchey-Chrétien reflector with corrector lenses in camera. Both VST and VISTA also use active optics to map the sky in more details and accuracy.

The future of the historical Schmidt-type and other wide-field telescopes is still disputable. Many of them at present are not used, however some are being modified for further studies. Though many historically important Schmidt telescopes are being closed, anyway such type of optics is extremely useful for new astronomical discoveries. The biggest Schmidt-type telescope, 4m LAMOST is the proof. Moreover, some of the space telescopes have used and now use Schmidt cameras, such as **HIPPARCOS** and **Kepler** telescopes. ESA's HIPPARCOS Space Astrometry Mission was launched in 1989 and operated till 1993 to measure accurate positions and magnitudes and resulted in Hipparcos Catalogue of 118,218 stars and Tycho Catalogue of 2,539,913 stars with the highest accuracy positions and proper motions (Høg et al., 2000). A small 29cm Schmidt camera did all this work. NASA's Kepler mission was launched in 2009 and is aimed at search for habitable planets. Kepler's telescope is a 95cm Schmidt camera with a very wide angle, 105 deg^2. Due to this, it is able to observe 100,000 stars.

Figure 1. World largest historical Schmidt telescopes. Upper row, from left to right: LAMOST, Tautenburg, Palomar and Siding-Spring Schmidt telescopes; bottom row from left to right: Kiso, ESO, Kvistaberg and BAO Schmidt telescopes.

Large Synoptic Survey Telescope (LSST, Vera Rubin Observatory) will be the largest Schmidt type telescope ever built. It is planned for 2021 (fully operational in 2022) and will be installed in Chile. The optical system is three-mirror anastigmat, Paul-Baker / Mersenne-Schmidt design. Its primary mirror will have 8.4 m, secondary, 3.4 m and the tertiary mirror, located in a large hole in the primary, is 5.0 m in diameter. The focal length is 10.31 m. The field of view will be 3.5 deg in diameter, or 9.6 sq. deg. Pixel size will be 0.2 arcsec and the resolution, 0.7 arcsec. Wavelength coverage is similar to SDSS one, 3200-10600 AA. LSST will measure orbits for 100,000 NEOs, it will discover 250,000 SNe per year, its observations will allow building light curves for 2 million QSOs, it will measure proper motions 4 magnitudes deeper than Gaia space mission, and it will construct the dark matter map. LSST will cover 10,000 sq. deg. every 3 nights (the whole sky area in 12 nights!)

and it will be the most powerful optical sky survey for the next two decades.

If comparing historical Schmidt cameras and modern (digital) ones, it is obvious that the beginning of digital era put limitations on fields because of restricted areas of CCDs. Only recently CCDs and their systems began to cover almost similar fields (several dozens of sq. deg.). E. g., POSS fields cover 6.6x6.6 degrees and after digitization and sampling, each pixel is 1.67 arcsec in DSS I and 1 arcsec in DSS II, which means that there are approximately 14kx14k pixels (193 Mpix) and 24kx24k pixels (538 Mpix) in each DSS I and DSS II field, respectively. DFBS sampling is 1.54 arcsec/pix and the field is 4.1x4.1 degrees, so that each DFBS field provides 9.6x9.6 kpix (88 Mpix). Only recently individual CCDs with 15 μm or smaller size pixels are reaching such numbers (the first 4kx4k CCD with 15 μm pixels was produced in 1989), otherwise systems of several CCDs were used to cover enough wide fields comparable to Schmidt telescopes. Anyway, given that CCD has linear response and high quantum efficiency, old observations will not have chance to compete by their quality with modern and future ones. LSST will have the world's largest camera with 3.2 Gpix. One can also compare CCDs of modern best digital photo cameras (40 Mpix) that give detailed images of anything on the Earth but far not enough for astronomical purposes. Here also astronomy proves its modern Big Data nature.

4. Historical Era and Wide-Field Plate Data Base (WFPDB)

Classical Schmidt telescopes gave the vast majority of new astronomical objects making all important discoveries possible. New Schmidt telescopes are now orbiting Earth and Sun and proved huge amounts of data for further astrophysical research. It is pretty obvious that almost all important objects for further astronomical studies have come from wide-field surveys, both colorimetric and spectroscopic. Among the colorimetric surveys, Palomar Observatory Sky Surveys are well known. However, very little information on the nature of these objects may be retrieved from these plates. Spectroscopic surveys give more information about the nature of objects and are much more important, though requiring rather harder work and are thus very rare. Unlike the colorimetric ones, there is no any all-sky spectroscopic survey and only several large area surveys exist.

Before 1609, eye observations and measurements were applied. Then, immediately after the first use of a telescope by Galileo and a number of discoveries, the rapid growth of telescope sizes (both lenses and mirrors) followed. We show in Figure 2 the historical growth of telescopes light collecting area. It is close to logarithmic law.

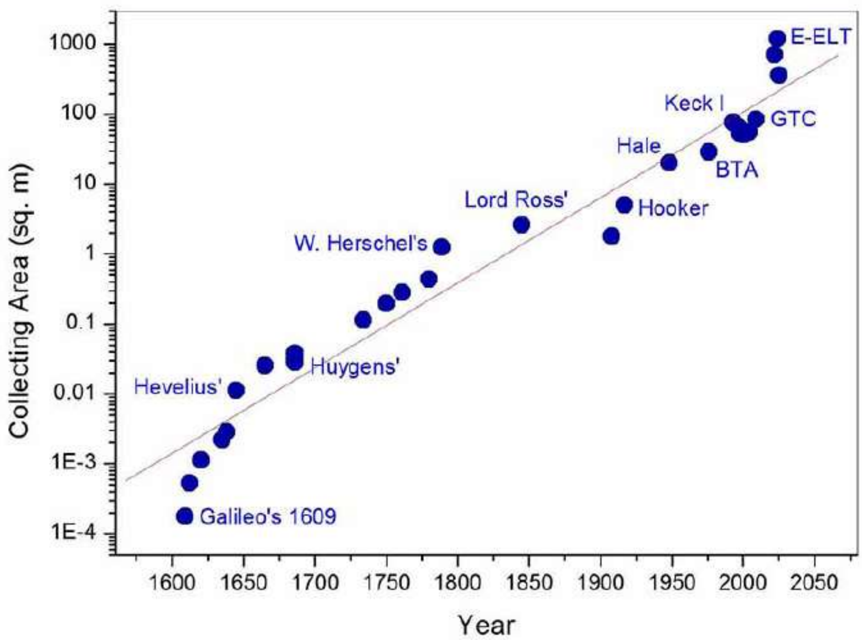

Figure 2. The growth of astronomical telescopes light collecting area since 1609. Largest telescopes of the time and some other important ones are given. The growth is close to logarithmic law.

However, the first telescopes didn't accumulate data, as eye observations were carried out. The telescope era without documentary recording lasted till 1840s, when photography was invented and applied in astronomy. Spectroscopy was an important method introduced in astronomy in early 1800s, even before the photographic era, when Joseph von Fraunhofer used his skills as a glass maker to create very pure prisms, which allowed him to observe 574 dark lines in a seemingly continuous spectrum. Later on, spectrographs were created to obtain and record spectra on photographic emulsion. In early 1900s J. S. Plaskett developed high-quality reflection gratings and more recently, grisms were invented for better quality spectroscopy. **Photographic Era** in astronomy lasted some 150 years and millions of images and spectra were obtained during these years until the beginning of 2000s, when Charge Coupled Devices (CCDs) completely substituted photographic emulsions. The **Digital Era** of astronomy began. However, many astronomers realize and appreciate old archival observations and accumulated data, which are especially useful for variability and proper motion studies (so-called **Time Domain Astronomy**, Mickaelian & Sinamyan (2010), Mickaelian et al. (2011)).

Table 2: Largest ground-based astronomical optical telescopes.

Diam. cm	Name	Year install.	Location	Altit. m	Country
1040	Gran Telescopio Canarias (GTC)	2007	La-Palma, Canarias	2267	Es / US / Mx
982	Keck I	1991	Mauna Kea, Hawaii	4123	USA
982	Keck II	1996	Mauna Kea, Hawaii	4123	USA
920	Hobby-Eberly Telescope (HET)	1997	Mt. Fowlkes, TX	2072	USA
910	South African Large Tel. (SALT)	2003	SAAO	1798	S.Africa / USA
840	Large Binocular Telescope (LBT) 1	2004	Mount Graham, AZ	3170	USA
840	Large Binocular Telescope (LBT) 2	2004	Mount Graham, AZ	3170	USA
830	Subaru	1999	Mauna Kea, Hawaii	4139	Japan
820	VLT Antu	1998	Cerro Paranal, Chile	2635	ESO
820	VLT Kueyen	1998	Cerro Paranal, Chile	2635	ESO
820	VLT Melipal	2002	Cerro Paranal, Chile	2635	ESO
820	VLT Yepun	2001	Cerro Paranal, Chile	2635	ESO
810	Gemini North (Gillett)	2000	Mauna Kea, Hawaii	4214	USA
810	Gemini South	2001	Cerro Pachon, Chile	2715	USA
650	Multiple Mirror Tel. (MMT)	1998	Mount Hopkins, AZ	2616	USA
650	Walter Baade Tel. (Magellan 1)	2002	Las Campanas, Chile	2282	USA
650	Landon Clay Tel. (Magellan 2)	2002	Las Campanas, Chile	2282	USA
605	BTA	1975	Mt. Pastukhovo, Caucasus	2070	Russia
600	Large Zenith Telescope (LZT)	2001	Maple Ridge, BC	395	Canada
508	Hale Telescope	1948	Mount Palomar, CA	1713	USA
425	South. Obs. Astroph. Res. (SOAR)	2002	Cerro Pachon, Chile	2701	Brazil / USA
420	William Herschel Tel. (WHT)	1987	La-Palma, Canarias	2369	UK / Netherl.
420	LAMOST	2008	Xinglong St., BAO	960	China
410	VISTA	2008	Cerro Paranal, Chile	2635	ESO
401	Victor Blanco	1976	Cerro Tololo, Chile	2200	USA

Wide-Field Plate DataBase (WFPDB) was created in Sofia, Bulgaria by Milcho Tsvetkov and colleagues (Tsvetkov et al. (1994); `http://www.skyarchive.org`) to accommodate all photographic wide-field ($> 1°$) observations. It contains 414 archives, 2,204,725 plates from 125 observatories obtained with more than 200 telescopes between 1879 and 2002. They include 2,128,330 direct and

64,095 objective prism plates (among them 1874 Markarian Survey and some 600 SBS ones). The biggest archives providing large amount of plates are Harvard – 600,000 plates and Sonneberg – 270,000 plates.

In Table 2 we give the list of the largest ground-based astronomical optical telescopes. One can see how fast the growth of sizes happens. Ex. BAO 2.6m telescope was the 7^{th} largest in the world when it was installed in 1975. However, at present it is not even in the list, being the 45^{th}. However, as most of the big telescopes are in the Western Hemisphere (Hawaii, Chile, etc.), BAO 2.6m is still very important (it is among the 10 biggest ones) for the European-Asian-African region.

5. Multiwavelength era in astronomy and multiwavelength surveys and catalogues

During many centuries optical wavelengths were the only source of information from the sky. However, modern astronomical research is impossible without various multiwavelength (MW) data present in numerous catalogues, archives, and databases. MW studies significantly changed our views on cosmic bodies and phenomena, giving an overall understanding and possibility to combine and/or compare data coming from various wavelength ranges. MW astronomy appeared during the last few decades and recent MW surveys (including those obtained with space telescopes) led to catalogues containing billions of objects along the whole electromagnetic spectrum. When combining MW data, one can learn much more due to variety of information related to the same object or area, as well as the Universe as a whole (Fig. 3).

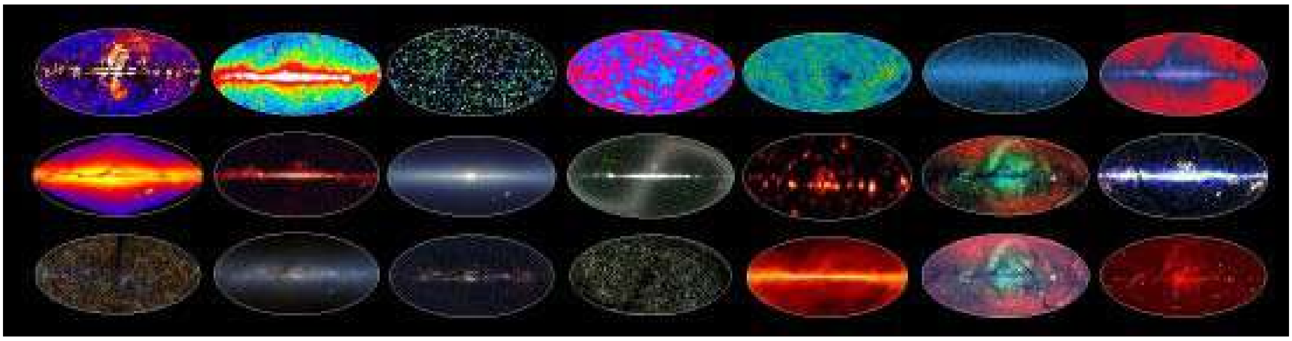

Figure 3. Different views of sky in various wavelength ranges showing the importance of MW studies to have an overall understanding about any given cosmic object and the Universe as a whole.

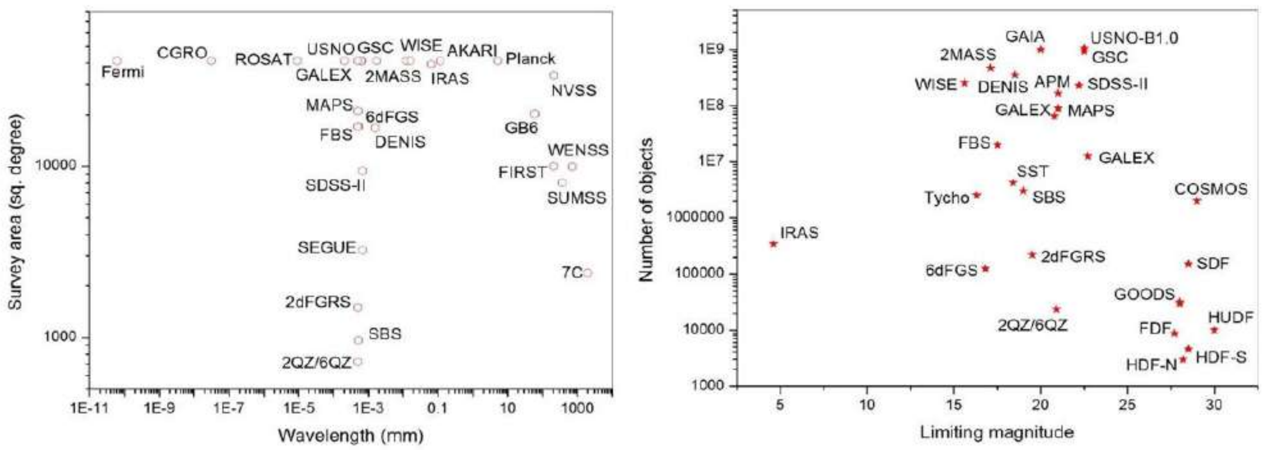

Figure 4. Comparative properties of large surveys. Left: survey area (in square degrees) vs. wavelength (in mm), right: number of survey objects vs. limiting magnitude.

In Mickaelian (2016a,b) we list most important recent surveys (those having homogeneous data for a large number of sources over large area) and resulted catalogues providing photometric data along the whole wavelength range, from γ-ray to radio. To summarize, we give in Table 3 a comparative list of multiwavelength all-sky and large-area surveys.

Table 3: Main data for all-sky and large-area astronomical surveys, as well as some other important projects providing multiwavelength photometric data. Catalogues are given in the order of increasing wavelengths.

Survey, Catalog	**Years**	**Spectral range**	**Sky area** *(deg^2)*	**Number of sources**	**Reference**
Fermi-GLAST	2008-2014	100MeV-300GeV	All-sky	3,033	Acero et al. (2015)
CGRO	1991-1999	20keV-30GeV	All-sky	1,300	Hartman et al. (1999)
INTEGRAL	2002-2014	15keV-10MeV	All-sky	1,126	Bird et al. (2010)
Swift	2004-2008	14-150 keV	All-sky	84,979	D'Elia et al. (2013)
XMM-Newton	1999-2014	0.25-12 keV	Pointed	372,728	XMM-Newton (2013)
Chandra	1999-2014	0.07-10 keV	Pointed	380,000	Evans et al. (2010)
ROSAT BSC	1990-1999	0.07-2.4 keV	All-sky	18,806	Voges et al. (1999)
ROSAT FSC	1990-1999	0.07-2.4 keV	All-sky	105,924	Voges et al. (2000)
GALEX AIS	2003-2012	1344-2831 Å	21,435	65, 266,291	Bianchi et al. (2011)
GALEX MIS	2003-2012	1344-2831 Å	1,579	12,597,912	Bianchi et al. (2011)
APM	2000	opt b, r	20,964	166,466,987	McMahon et al. (2000)
MAPS	2003	opt O, E	20,964	89,234,404	Cabanela et al. (2003)
USNO-A2.0	1998	opt B, R	All-sky	526,280,881	Monet et al. (1998)
USNO-B1.0	2003	opt B, R, I	All-sky	1,045,913,669	Monet et al. (2003)
GSC 2.3.2	2008	opt j, V, F, N	All-sky	945,592,683	Lasker et al. (2008)
FBS	1965-1980	3400-6900 Å	17,056	20,000,000	Markarian et al. (1989)
SBS	1978-1991	3400-6950 Å	965	3,000,000	Stepanian (2005)
HQS	1985-1997	3400-5300 Å	14,000		Hagen et al. (1999)
HES	1990-1996	3400-5300 Å	9,000		Wisotzki et al. (2000)
SDSS DR16	2000-2018	opt u, g, r, i, z	14,555	932,891,133	Ahumada et al. (2020)
SDSS DR16	2000-2018	3000-10800 Å	14,555	4,355,200	Ahumada et al. (2020)
Tycho-2	1989-1993	opt BT, VT	All-sky	2,539,913	Høg et al. (2000)
Gaia EDR3	2013-2020	opt GBP, GRP	All-sky	1,811,709,771	Brown et al. (2020)
DENIS	1996-2001	0.8-2.4 μm	16,700	355,220,325	DENIS consortium (2005)
2MASS PSC	1997-2001	1.1-2.4 μm	All-sky	470,992,970	Cutri et al. (2003)
2MASS ESC	1997-2001	1.1-2.4 μm	All-sky	1,647,599	Skrutskie et al. (2006)
WISE	2009-2013	3-22 μm	All-sky	747,634,026	Cutri et al. (2013)
AKARI IRC	2006-2008	7-26 μm	38,778	870,973	Ishihara et al. (2010)
Spitzer	2003-2009	3-180 μm	Pointed	4,261,028	Spitzer (2015)
IRAS PSC	1983	8-120 μm	39,603	245,889	IRAS (1988)
IRAS FSC	1983	8-120 μm	34,090	173,044	Moshir et al. (1989)
IRAS SSSC	1983	8-120 μm	39,603	16,740	Helou & Walker (1985)
AKARI FIS	2006-2008	50-180 μm	40,428	427,071	Yamamura et al. (2010)
Herschel	2009-2013	55-672 μm	Pointed	340,968	Oliver et al. (2012)
ALMA	2011-2014	0.3-9.6 mm	Pointed		ALMA (2015)

Planck	2009-2011	0.35-10 mm	All-sky	33,566	Planck (2011)
WMAP	2001-2011	3-14 mm	All-sky	471	Gold et al. (2011)
GB6	1986-1987	6 cm	20,320	75,162	Gregory et al. (1996)
NVSS	1998	21 cm	33,827	1,773,484	Condon et al. (1998)
FIRST	1999-2015	21 cm	10,000	946,432	Helfand et al. (2015)
SUMSS	2003-2012	36 cm	8,000	211,050	Mauch et al. (2012)
WENSS	1998	49/92 cm	9,950	229,420	de Bruyn et al. (1998)
7C	2007	198 cm	2,388	43,683	Hales et al. (2007)
VLA LFSS	2007	406 cm		92,965	Lane et al. (2014)

All-sky and/or large area surveys have been carried out in many wavelengths covering a very wide range, from 300 GeV energies (or 4x10^{-18} Å) to 74 MHz frequencies (or 4 m), which means a wavelength/frequency/energy ratio of 10^{-18}. Given that H.E.S.S. Gamma-ray telescope may observe up to 100 TeV energies (or 10^{-20} Å) and LOFAR is designed for up to 10 MHz frequencies (or 30 m), this ratio reaches 10^{-21}. MW approach is applied in astrophysical research. Table 4 gives photometric bands of all-sky and large area surveys, as well as some other important projects (e. g. XMM-Newton, Chandra, SST, Herschel, ALMA, Planck, etc.); this way one can get understanding what data at what wavelengths are available and may give new results.

Table 4: Available photometric bands in MW astronomy. All-sky and large-area surveys and some other important projects are given.

Survey, Catalogue	**Photom. band**	**Energy / wavelength**	**Sensitivity**	**Survey, Catalogue**	**Photom. band**	**Energy / wavelength**	**Sensitivity**
Fermi-GLAST	Fermi 5	10-100 GeV		AKARI IRC	L18W	18.0 μm	120 mJy
Fermi-GLAST	Fermi 4	3-10 GeV		WISE	W4	22 μm	6 mJy
Fermi-GLAST	Fermi 3	1-3 GeV		IRAS	25	24 μm	500 mJy
Fermi-GLAST	Fermi 2	0.3-1 GeV		SST	MIPS24	24 μm	0.1 mJy
Fermi-GLAST	Fermi 1	0.1-0.3 GeV		IRAS	60	61 μm	600 mJy
INTEGRAL	IBIS	15keV-10MeV		AKARI FIS	N60	65 μm	3.8 Jy
INTEGRAL	JEM-X	3-35 keV		Herschel	PACS	70 μm	6 mJy
XMM-Newton	Flux5	4.5-12 keV		SST	MIPS70	71 μm	6.0 mJy
Swift	Hard	2.0-10 keV		AKARI FIS	WIDE-S	90 μm	890 mJy
Chandra	h	2.0-7.0 keV		Herschel	PACS	100 μm	6 mJy
XMM-Newton	Flux4	2.0-4.5 keV		IRAS	100	102 μm	1 Jy
Chandra	m	1.2-2.0 keV		AKARI FIS	WIDE-L	140 μm	1.6 Jy
XMM-Newton	Flux3	1.0-2.0 keV		SST	MIPS160	156 μm	80 mJy
Swift	Medium	1.0-2.0 keV		AKARI FIS	N160	160 μm	7.6 Jy
ROSAT	D	0.9-2.0 keV		Herschel	PACS	160 μm	12 mJy
Chandra	s	0.5-1.2 keV		Herschel	SPIRE	250 μm	6 mJy
XMM-Newton	Flux2	0.5-1.0 keV		Herschel	SPIRE	350 μm	83 mJy
ROSAT	C	0.4-0.9 keV		Planck	HFI	350 μm	658 mJy
Swift	Soft	0.3-1.0 keV		SCUBA	450	450 μm	
Chandra	u	0.2-0.5 keV		ALMA	band10	470 μm	3.1 mJy
XMM-Newton	Flux1	0.2-0.5 keV		Herschel	SPIRE	500 μm	103 mJy
ROSAT	A	0.1-0.4 keV		Planck	HFI	550 μm	457 mJy
GALEX AIS	FUV	1539 Å	19.9^m	ALMA	band9	590 μm	1.3 mJy
GALEX AIS	NUV	2316 Å	20.8^m	SCUBA	850	850 μm	
SDSS	u	3551 Å	22.0^m	Planck	HFI	850 μm	289 mJy
POSS I	O	4050 Å	21.0^m	ALMA	band7/8	1.16 mm	140 μJy

Tycho-2	BT	4203 Å	16.6^m	Planck	HFI	1.38 mm	149 mJy
POSS II	j	4680 Å	22.5^m	ALMA	band6	1.70 mm	80 μJy
SDSS	g	4686 Å	22.2^m	Planck	HFI	2.10 mm	169 mJy
Tycho-2	VT	5319 Å	15.2^m	ALMA	band4	2.85 mm	80 μJy
SDSS	r	6165 Å	22.2^m	Planck	HFI	3.00 mm	266 mJy
POSS I	E	6452 Å	20.0^m	WMAP	W	3.20 mm	1 Jy
POSS II	F	6452 Å	20.8^m	ALMA	band3	4.00 mm	50 μJy
SDSS	i	7481 Å	21.3^m	Planck	LFI	4.26 mm	566 mJy
POSS II	N	8060 Å	18.5^m	WMAP	V	4.90 mm	750 mJy
SDSS	z	8931 Å	20.5^m	Planck	LFI	6.81 mm	825 mJy
2MASS	J	1.24 μm	17.1^m	WMAP	Q	7.30 mm	625 mJy
2MASS	H	1.66 μm	16.4^m	WMAP	Ka	9.10 mm	500 mJy
2MASS	K_s	2.16 μm	15.3^m	Planck	LFI	10.56 mm	461 mJy
WISE	W1	3.4 μm	70 μJy	WMAP	K	13.00 mm	500 mJy
SST	IRAC1	3.6 μm	0.6 μJy	GB6		6 cm	18 mJy
SST	IRAC2	4.5 μm	1.2 μJy	NVSS		21 cm	2.5 mJy
WISE	W2	4.6 μm	100 μJy	FIRST		21 cm	1 mJy
SST	IRAC3	5.8 μm	8.0 μJy	SUMSS		36 cm	1 mJy
SST	IRAC4	8.0 μm	9.8 μJy	WENSS		49 cm	18 mJy
AKARI IRC	S9W	9.0 μm	50 mJy	WENSS		92 cm	30 mJy
IRAS	12	11.6 μm	400 mJy	7C		198 cm	40 mJy
WISE	W3	11.6 μm	0.9 mJy	VLA LFSS		406 cm	700 mJy

Thus, MW astronomy provides 96 photometric points, out of which 64 come from all-sky or large area surveys, which means that these data are available for most of the studied sources, depending on the sensitivity.

Figure 5 gives the distribution of 58 photometric bands by their effective wavelengths and sensitivity from NIR to radio (most of the 64 bands coming from all-sly or large area surveys are in this ranges): 2MASS, WISE, SST, IRAS, AKARI, Herschel, ALMA, Planck, WMAP, GB6, NVSS, FIRST, SUMSS, WENSS, 7C, and VLA Low-Frequency Sky Survey (LFSS).

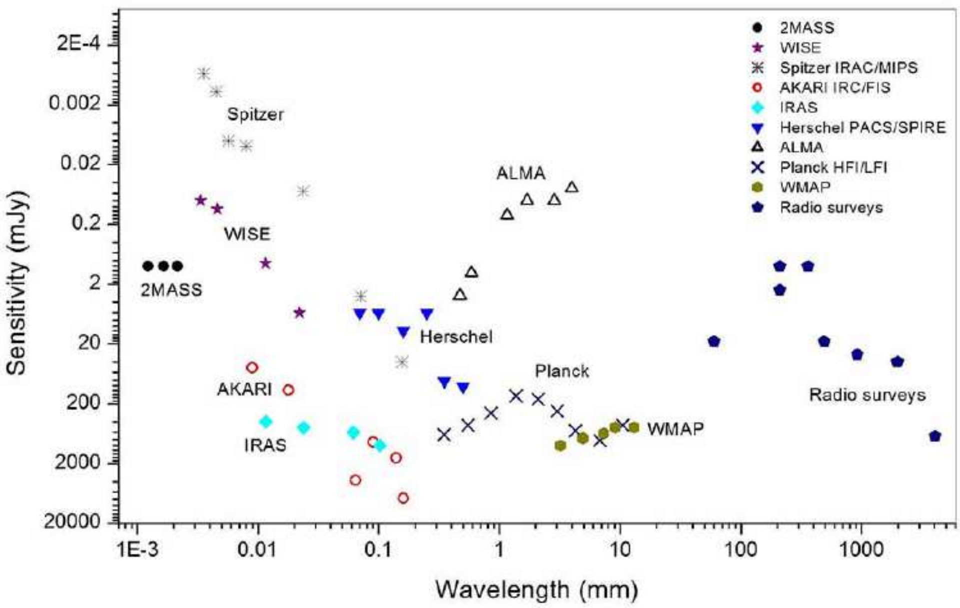

Figure 5. The distribution of 58 photometric bands by their effective wavelengths and sensitivity from NIR to radio. Spitzer and ALMA have especially high sensitivity.

Given that MW data exist in different lists, cross-matching of various astronomical catalogues becomes very important task. Moreover, establishing correspondence between sources revealed in different wavelengths is a tricky work (e. g. Abrahamyan et al. (2015)). Accurate cross-correlations between various MW catalogues are needed to establish genuine counterparts for each object/source. Quick cross-matching is being done for almost all catalogues, however; many objects/sources appear to have false associations, as in crowded regions large contamination with other neighboring objects is happening. Very often individual approach should be applied to such associations. Still, a number of cross-correlation software is in use and is being improved.

6. Big Data Era: numbers in astronomy

During the recent 2 decades, a number of giant projects were accomplished in astronomy completely changing the numbers of available information and requiring new approach in research. Among the biggest projects in astronomy one should mention the digitization of POSS I and II **(DSS I and II)** and creation of biggest catalogues (USNO-B1.0 is the biggest one with 1,045,913,669 objects and GSC 2.3.2 is more accurate with 945,592,683 objects), **SDSS** with its accurate optical images (932,891,133 objects) and spectroscopy providing 10 times more spectra (4,846,156) than available before in astronomy, **WISE** with very accurate positional and NIR/MIR photometric data for 563,921,584 sources that revolutionized astronomy in this wavelength domain. Out of upcoming projects we would like to mention Gaia, LSST and SKA. Table 5 gives the list of the biggest astronomical catalogs.

Table 5: World largest astronomical catalogs.

Survey	**Number of Objects**	**Sky Area**
SuperCOSMOS	1,900,000,000	All-sky
Gaia EDR3	1,811,709,771	All-sky
USNO B1.0	1,045,913,669	All-sky
GSC 2.3.2	945,592,683	All-sky
SDSS DR16	932,891,133	14,555 deg^2
AllWISE	747,634,026	All-sky
2MASS	470,992,970	All-sky

Due to SDSS, the number of QSOs increased up to some 2 million objects (though there is no unique catalog for 2020 (SDSS QSOs from DR16), our estimate is based on the combination of general catalogues of QSOs (Véron-Cetty & Véron, 2010) and QSOs discovered by SDSS DR16) compared to some 30,000 before the SDSS era in 2000, even counting 2QZ/6QZ surveys (Colless et al., 2001, Croom et al., 2004). Due to **Kepler** mission, the number of exoplanets increased to some 4900 (confirmed) and more than 5000 (to be confirmed by spectroscopic observations). More 500,000 QSOs will be provided by Gaia observations, as well as SDSS continues to discover more QSOs in its consecutive surveys (in the next decade, LSST will discover millions of new QSOs). Gaia will also discover some 10,000 or even more exoplanets.

Astronomical surveys give so much information that huge catalogues, dedicated archives and databases are being built to store, maintain and use these Big Data (Mickaelian, 2016a,b). At present astronomers deal with the following numbers in various wavelength ranges (Table 5), and these numbers increase exponentially. It is estimated that there are some 400 billion stars in the Milky Way galaxy and some 125-500 billion galaxies in the Universe, so that we are very far to catalogue all these objects. Even after Gaia space mission we will have much more accurate astrometric and photometric data for the stars but not much more completeness of detections. LSST and SKA will provide significantly more numbers, but again, full coverage of our estimated numbers in the Milky Way (stars) and especially in the Universe (galaxies and QSOs) will not happen in the nearest future.

As seen from Table 6, optical, UV and NIR/MIR wavelength ranges give most of the information from the sky, however MW astronomy was born in the recent decades and makes huge steps toward the overall understanding of the Universe with its various manifestations from γ-ray to radio and in the nearest future most of the objects (e.g. in our Galaxy or all galaxies in the Local Universe) will have their counterparts in all wavelengths.

Table 6: Number of catalogued sources at different wavelength ranges giving a comparative understanding about the wavelength coverage of the observed Universe.

Wavelength range	**Major missions, surveys/catalogues**	**Number of catalogued sources**
γ-ray	CGRO, Fermi-GLAST, INTEGRAL, Swift	10,000
X-ray	ROSAT, XMM-Newton, Chandra	1,500,000
UV	GALEX, HST	100,000,000
Optical	SDSS, DSS I, DSS II, HST, Gaia	2,400,000,000
NIR	2MASS, DENIS, HST	600,000,000
MIR	WISE, AKARI-IRC, Spitzer	600,000,000
FIR	IRAS, AKARI-FIS, Spitzer, Herschel	500,000
sub-mm/mm	Planck, WMAP, SCUBA, Herschel, ALMA	200,000
Radio	GB6, NVSS, FIRST, SUMSS, WENSS, 7C	2,000,000

Large astronomical surveys have become one of the most important directions of investigations in our science and they provide the main bulk of information that has been transformed into Big Data and approached astronomy and computer science posing new problems and inquiring new solutions.

As seen, astronomy deals with vast amount of data and big numbers. Table 7 gives some important numbers in astronomy compared to some other numbers known from our everyday life or other sciences. Numbers are given in increasing order from one of the smallest numbers in astronomy (Solar System planets) to the biggest known physical number (atoms in the Universe). Such a comparison allows having an understanding of numbers from different areas and helps remembering them for quick estimations.

Table 7: Numbers from the space +. Most important numbers in astronomy and some other ones for comparison.

Important astronomical and other numbers	**Numbers**
Solar System planets	**8**
Solar System planetary moons	219
Astronomical observatories	500
Trans-Neptunian Objects (TNO) (Dec 2020)	2 500
Discovered Exoplanets (Dec 2020, acc. to Exoplanet.eu)	**4 391**
Discovered Solar System comets	4 894

Astronomical catalogues (in Vizier, CDS, Strasbourg; Dec 2020)	20 398
Number of astronomers in the world (an estimate)	30 000
Number of square degrees in the sky	**41 253**
Human hair (average)	125 000
Astronomical units (AU) in a parsec	**206 265**
Spectral lines in NIST atomic spectra database	227 477
Solar System asteroids (Oct 2020)	998 030
Catalogued X-ray sources	1 500 000
Detected quasars (Milliquas Catalog 6.3, 2019)	1 986 800
Catalogued radio sources	2 000 000
Obtained photographic plates (according to WFPDB)	2 204 725
High and medium resolution spectra in astronomy	7 500 000
ADS abstracts of astronomy/physics papers (Dec 2020)	13 050 798
Seconds in a year	**31 556 926**
Low resolution spectra in astronomy (DFBS, HQS, etc.)	40 000 000
Catalogued astronomical objects	**3 000 000 000**
Age of the Earth in years	4 540 000 000
World population (Dec 2020 estimate)	7 833 166 000
Age of the Universe in years (acc. to Lambda-CDM model)	13 798 000 000
Stars in Our Galaxy	**400 000 000 000**
Galaxies in the Universe	**>500 000 000 000**
Seconds passed after Big Bang	4.35×10^{17}
Total number of animals on the Earth (according to Brian Tomasik)	2×10^{19}
Molecules in 1 cm^3 air (Loschmidt's number)	2.7×10^{19}
Stars in the Universe	$\mathbf{10^{22} - 10^{23}}$
Molecules in the Earth's atmosphere	1.09×10^{44}
Atoms in the Universe	$\mathbf{10^{78} - 10^{82}}$

The information size is given in bytes (B), KB, MB, GB, TB (Terabytes), PB (Petabytes), EB (Exabytes), etc. 1 PB = 1,125,899,906,842,624 or approx. 10^{15} B and 1 EB = 1,152,921,504,606,846,976 or approx. 10^{18} B. As various astronomical missions, surveys, catalogues, databases and archives give various types of information, the only way to compare their sizes is to give this information in bytes. Table 8 gives such a comparison. Thus astronomers, together with nuclear physicists, reach the largest possible numbers and put new requirements for computer science. As an example, LSST every night will provide 30 TB of data, which is much larger than many archives created and complemented during many years.

Table 8: Comparison of information stored in different present and future astronomical surveys or databases and archives.

Surveys, Projects	**Short**	**Range**	**Information Volume**
Digitized First Byurakan Survey	DFBS	opt	400 GB
Digitized Sky Survey (based on POSS)	DSS	opt	3 TB
Two Micron All-Sky Survey	2MASS	NIR	10 TB
Galaxy Evolution Explorer	GALEX	UV	30 TB
Sloan Digital Sky Survey	SDSS	opt	40 TB
SkyMapper Southern Sky Survey	SkyMapper	opt	500 TB
Panoramic Survey Telescope and Rapid Response System	PanSTARRS	opt	~40 PB
Large Synoptic Survey Telescope, *expected*	LSST	opt	~200 PB
Square Kilometer Array, *expected*	SKA	radio	~4.6 EB

The big surveys provided and will provide the following amount of data per year:

- 2008: 20 TB/year (UKIDSS)
- 2010: 100 TB/year (VISTA)
- 2019: 5 PB/year (LSST)
- 2022: 100 PB/year (SKA)

The increase is happening due to covered sky areas and data accuracy, i. e. both resolution and sensitivity, as well as due to many times coverage, i. e. creation of possibilities for time domain studies.

7. Virtual observatories

Astrophysical Virtual Observatories (VOs) have been created in a number of countries using their available databases and current observing material as a collection of interoperating data archives and software tools to form a research environment in which complex research programs can be conducted. The science goals are to define key requirements for large, complex MW astronomy projects. Interoperability includes the development and prototyping of new standards for data content, data description and data discovery. VO technology is the study and prototyping of Grid technologies that allow distributed computation, manipulation and visualization of data. A number of national projects have been developed in different countries since 2000, and an **International Virtual Observatory Alliance** (**IVOA**; www.ivoa.net) was created in 2002 to unify these national projects and coordinate the development of VO ideology and technologies. At present it involves 19 national and 2 European projects.

IVOA has Working Groups on Semantics, Data Access Layer, VO Event, Data Modeling, Resource Registry, Grid & Web Services, and VOTable and Interest Groups on Theory, Open Grid Forum Astronomy Research Group (OGF Astro-RG), Data Curation & Preservation, Knowledge Discovery in Databases. IVOA software and tools relate to Data discovery (Aladin, Astroscope, VOExplorer, Datascope), Spectral analysis (VOSpec, SPLAT, EURO-3D, Specview), Data visualization and handling (VOPlot, Topcat, VisIVO, STILTS), Spectral Energy Distribution (SED) building and fitting (VOSED, Yafit, easy-z, GOSSIP), etc. Spectral analysis tools allow combining spectral data coming from various telescopes at different wavelengths and joint analysis for line measurements, matching with theoretical models, etc., as for example in VOSpec. Building SEDs for AGN allow having an overall understanding on their energy distribution and better classifications. Examples of such software is given in Figure 6 and 7, VOSpec developed by Spanish VO and SED building tool developed by Italian Space Agency (ASI) Science Data Centre, respectively.

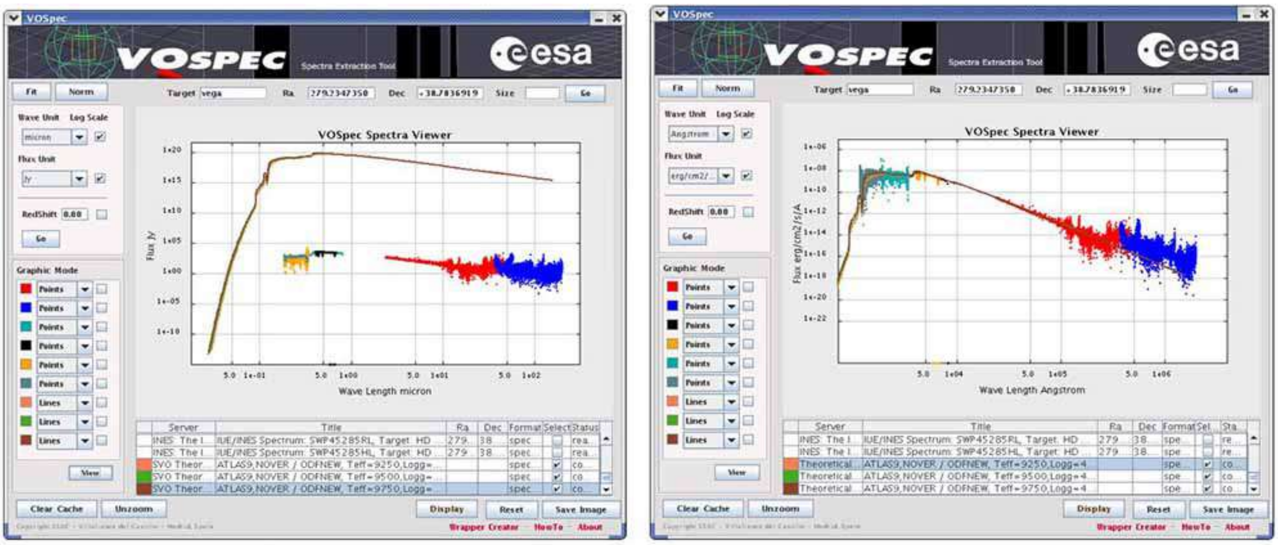

Figure 6. VO software VOSpec allowing superposition and analysis of spectral data coming from different telescopes and different wavelengths, as well as matching with theoretical model curves

Figure 7. SED building software developed at Italian Space Agency (ASI) Science Data Centre. SEDs are given for two Markarian galaxies: Mrk 180 and Mrk 231.

Armenian Virtual Observatory (**ArVO**, https://www.aras.am//Arvo/arvo.htm) was created based on the DFBS, Digitized Second Byurakan Survey (DSBS), and other digitization projects in Byurakan Astrophysical Observatory (BAO). ArVO project development includes the storage of the Armenian archives and telescope data, direct images and low-dispersion spectra cross-correlations, creation of a joint low-dispersion spectral database (DFBS / DSBS / HQS / HES / Case), a number of other science projects, etc. ArVO group at BAO was created in 2005 and it was authorized as an official project in IVOA also in 2005. An agreement on ArVO development between BAO and Institute for Informatics and Automation Problems (IIAP) was signed. The first science projects with DFBS/ArVO were the optical identifications of Spitzer Boötes sources in 2005. Joint projects were carried out between BAO and IIAP in 2007-2020. ArVO science projects are aimed at discoveries of new interesting objects searching definite types of low-dispersion spectra in the DFBS, by optical identifications of non-optical sources (X-ray, IR, radio) also using the DFBS and DSS/SDSS, by using cross-correlations of large catalogs and selection of objects by definite criteria, etc. We show in Fig. 8 the logos of DFBS and ArVO.

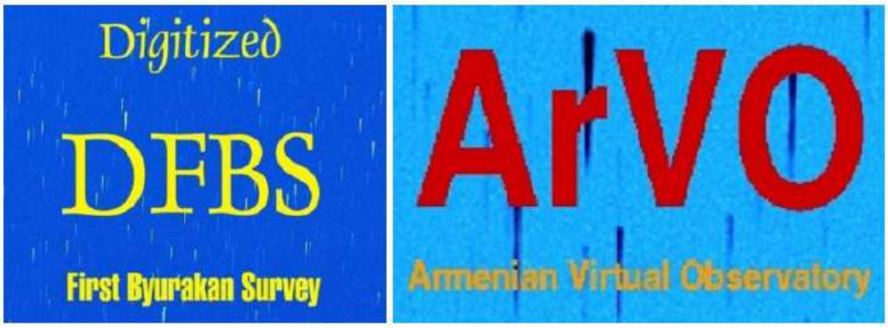

Figure 8. DFBS and ArVO logos.

8. Summary and Conclusions

In 1980s Viktor Ambartsumian was thinking about the growth of astronomical data by comparing the number of published papers. During his young years, 1920s-1930s, he could read ALL astronomical literature. In 1950s, with the growth of these numbers, he could manage to read ALL literature in GIVEN FIELDS, which was especially important for his research. In 1960s-1970s, he was selecting only the MOST IMPORTANT PAPERS from those given fields to read. And in 1980s he could not manage to read even this number of important papers (in 1985, the annual number of published astronomical refereed papers was about 11,000). Ambartsumian concluded that some new approach should be applied and new ways of study of astronomical (and any scientific) literature would be invented. Really, very soon search engines appeared and a new solution was suggested to manage to deal with this large number of information. In Astrophysical Data System (ADS), one can search the whole astronomical (and physical) literature by given keywords (found in the title or abstract), by authors, journals, years, etc. The same situation appeared with astronomical data when working in Internet and later on, by introducing VOs. Astrostatistics is a powerful tool for handling any size of information and providing results on very large datasets.

Modern astronomical research is impossible without various MW data present in numerous catalogues, archives, and databases. A user is able to search for any data in them, cross-correlate and make a comparative analysis. Surveys are much more valuable when various data can be compared and studied together. That is why it is so important to have easy access to all databases in a standard way. This is the task of the VOs. A number of efficient research projects have become possible, such as data discovery, spectral reduction and analysis, image processing, SED building and fitting, modeling, simulations, variability studies, cross-matching (cross-correlations), etc. Dedicated astronomical software is especially important to achieve the needed tasks. The main standard of astronomical data is FITS (Flexible Image Transfer System). It is being used in most of the software and systems. Most important software systems are MIDAS (Munich Image Data Analysis System, www.eso.org/sci/software/esomidas/) and IRAF (Image Reduction and Analysis Facility, http://iraf.noao.edu/).

In Astrophysics, main results of the 20^{th} century related to accomplishment of theoretical problems by using analytical methods. However, the complexity of many astrophysical phenomena shows that analytical methods are available only for limited cases. Therefore, to understand astrophysical phenomena, numerical methods have become irreplaceable and promise to have dominant role in the methodology of theoreticians. Very important is the presence of Big Data, which is the fourth axis of modern science (Hey et al., 2009). At present it is impossible to separate high performance computations and big data, as there is a need to analyze the vast amount of data coming from various telescopes, large instruments, space facilities and other sources. The Computational Astrophysics has become an important part of astronomical research, without which modern results are impossible.

References

ALMA 2015, http://www.almascience.org/

Abrahamyan H. V., Mickaelian A. M., Knyazyan A. V., 2015, A&C, 10, 99

Acero F., Ackermann M., Ajello M., et al 2015, ApJS, 218, 23

Ahumada R., Allende Prieto C., Almeida A., et al 2020, ApJS, 249, 3

Bianchi L., Herald J., Efremova B., Girardi L., Zabot A., Marigo P., Conti A., Shiao B., 2011, Ap&SS, 335, 161

Bird A. J., Bazzano A., Bassani L., et al 2010, ApJS, 186, 1

Brown A. G. A., Vallenari A., Prusti T., de Bruijne J. H. J., Babusiaux C., Biermann M., 2020, arXiv:2012.01533

Cabanela J. E., Humphreys R. M., Aldering G., et al 2003, PASP, 115, 837

Colless M., Dalton G., Maddox S., et al 2001, MNRAS, 328, 1039

Condon J. J., Cotton W. D., Greisen E. W., Yin Q. F., Perley R. A., Taylor G. B., Broderick J. J., 1998, AJ, 115, 1693

Croom S. M., Smith R. J., Boyle B. J., Shanks T., Miller L., Outram P. J., Loaring N. S., 2004, MNRAS, 349, 1397

Cutri R. M., Skrutskie M. F., van Dyk S., et al 2003, IPAC/California Institute of Technology

Cutri R. M., Wright E. L., Conrow T., et al 2013, WISE All-Sky Data Release, IPAC/Caltech, VizieR On-line Data Catalog II/328

DENIS consortium 2005, 3rd release, Vizier online data catalogue II/263

D'Elia V., Perri M., Puccetti S., et al 2013, A&A, 551, A142

Drake A. J., Graham M. J., Djorgovski S. G., et al 2014a, ApJS, 213, 9

Drake A. J., Gänsicke B. T., Djorgovski S. G., et al 2014b, MNRAS, 441, 1186

Evans I. N., Primini F. A., Glotfelty K. J., et al 2010, ApJS, 189, 37

Gigoyan K. S., Mickaelian A. M., Kostandyan G. R., 2019, MNRAS, 489, 2030

Gold B., Odegard N., Weiland J. L., et al 2011, ApJS, 192, 15

Gregory P. C., Scott W. K., Douglas K., Condon J. J., 1996, ApJS, 103, 427

Hagen H. J., Engels D., Reimers D., 1999, A&AS, 134, 483

Hales S. E. G., Riley J. M., Waldram E. M., Warner P. J., Baldwin J. E., 2007, MNRAS, 382, 1639

Hartman R. C., Bertsch D. L., Bloom S. D., et al 1999, ApJS, 123, 79

Helfand D. J., White R. L., Becker R. H., 2015, ApJ, 801, 26

Helou G., Walker D. W., 1985, IRAS small scale structure catalog, JPL, Pasadena, NASA

Hey T., Tansley S., Tolle K., (Eds.) 2009, The Fourth Paradigm: Data-Intensive Scientific Discovery

Høg E., Fabricius C., Makarov V. V., et al 2000, A&A, 355, L27

Huchra J. P., Vogeley M. S., Geller M. J., 1999, ApJS, 121, 287

IRAS 1988, Joint IRAS Science Working Group. IRAS PSC, Version 2.0, NASA RP-1190

Ishihara D., Onaka T., Kataza H., et al 2010, A&A, 514, A1

Lane W. M., Cotton W. D., van Velzen S., Clarke T. E., Kassim N. E., Helmboldt J. F., Lazio T. J. W., Cohen A. S., 2014, MNRAS, 440, 327

Lasker B. M., Doggett J., McLean B., Sturch C., Djorgovski S., de Carvalho R. R., Reid I. N., 1996, in Jacoby G. H., Barnes J., eds, Astronomical Society of the Pacific Conference Series Vol. 101, Astronomical Data Analysis Software and Systems V. p. 88

Lasker B. M., Lattanzi M. G., McLean B. J., et al 2008, AJ, 136, 735

Lawrence A., 2007, Astronomy and Geophysics, 48, 3.27

Markarian B. E., Lipovetsky V. A., Stepanian J. A., Erastova L. K., Shapovalova A. I., 1989, ComSAO, 62, 5

Massaro E., Mickaelian A. M., Nesci R., Weedman D., (Eds.) 2008, The Digitized First Byurakan Survey. ARACNE Editrice, Rome, 78 p.

Mauch T., Murphy T., Buttery H. J., et al 2012, MNRAS 342, 1117, 2003; Online version 2.1r, 16.02.2012

McGlynn T. A., White N. E., Scollick K., 1994, in 184th AAS Meeting, BAAS 26, 898

McMahon R. G., Irwin M. J., Maddox S. J., 2000, VizieR Online Data Catalog, p. I/267

Mickaelian A. M., 2008, Astron. J. 136, 946. VizieR On-line Data Catalog III/258

Mickaelian A. M., 2014, in Mickaelian A. M., Sanders D. B., eds, Vol. 304, Multiwavelength AGN Surveys and Studies. pp 1–10, doi:10.1017/S1743921314003147

Mickaelian A. M., 2016a, Baltic Astronomy, 25, 75

Mickaelian A. M., 2016b, Astronomy Reports, 60, 857

Mickaelian A. M., Gigoyan K. S., 2006, A&A 455, 765. VizieR On-line Data Catalog III/237A

Mickaelian A. M., Sargsyan L. A., 2004, Ap, 47, 213

Mickaelian A. M., Sinamyan P. K., 2010, MNRAS, 407, 681

Mickaelian A. M., Nesci R., Rossi C., et al 2007, A&A, 464, 1177

Mickaelian A. M., Mikayelyan G. A., Sinamyan P. K., 2011, MNRAS, 415, 1061

Monet D., Bird A., Canzian B., et al 1998, USNO Flagstaff Station and Universities Space Research Association (USRA)

Monet D. G., Levine S. E., Canzian B., et al 2003, AJ, 125, 984

Moshir M., Kopan G., Conrow T., et al 1989, IRAS FSC, Version 2.0, NASA

Oliver S. J., Bock J., Altieri B., et al 2012, MNRAS, 424, 1614

Planck 2011, A&A 536, A7, Vizier On-line Data Catalog VIII/88

Pojmanski G., 1998, Acta Astron., 48, 35

Samus' N. N., Durlevich O. V., Zharova A. V., et al 2011, GCVS database, Inst. Astron. and SAI, Moscow

Skrutskie M. F., Cutri R. M., Stiening R., et al 2006, AJ, 131, 1163

Spitzer 2015, http://www.spitzer.caltech.edu/

Stepanian J. A., 2005, RevMexAA, 41, 155

Tsvetkov M. K., Stavrev K. Y., Tsvetkova K. P., Ivanov P. V., Iliev M. S., 1994, in Astronomy from wide-field imaging: Proc. IAU Symp. 161, held in Potsdam, Germany, 1993. Ed. H. T. MacGillivray, E. B. Thomson, B. M. Lasker, I. N. Reid, D. F. Malin, R. M. West, H. Lorenz. Kluwer Acad. Publ., Dordrecht, p. 359

Véron-Cetty M. P., Véron P., 2010, A&A, 518, A10

Voges W., Aschenbach B., Boller T., et al 1999, A&A, 349, 389

Voges W., Aschenbach B., Boller T., et al 2000, MPE, Garching. The ROSAT Faint Source Catalogue

Weedman D. W., 1977, Vistas in Astronomy, 21, 55

Weedman D. W., Khachikyan E. E., 1968, Ap, 4, 243

Wisotzki L., Christlieb N., Bade N., Beckmann V., Köhler T., Vanelle C., Reimers D., 2000, A&A, 358, 77

Woźniak P. R., Vestrand W. T., Akerlof C. W., et al 2004, AJ, 127, 2436

XMM-Newton 2013, XMM-Newton Survey Science Centre Consortium, Leicester, UK, Online catalog 2013yCat.9044....0X

Yamamura I., Makiuti S., Ikeda N., et al 2010, AKARI/FIS All-Sky Survey Point Source Catalogues

de Bruyn G., Miley G., Rengelink R., et al 1998, WENSS Collab. NFRA/ASTRON and Leiden Obs., Vizier online catalogue VIII/62

Detecting shock waves in non-fundamental mode RR Lyrae using large sample of spectra in SDSS and LAMOST

Xiao-Wei Duan*[1,2,3], Xiao-Dian Chen[3,4,6], Li-Cai Deng[3,4,1,6], Fan Yang[3], Chao Liu[4,5], Anupam Bhardwaj[2], and Hua-Wei Zhang[1,2]

[1]Department of Astronomy, Peking University, Yi He Yuan Road 5, Hai Dian District, Beijing 100871,China
[2]Kavli Institute for Astronomy Astrophysics, Peking University, Yi He Yuan Road 5, Hai Dian District, Beijing 100871, China
[3]CAS Key Laboratory of Optical Astronomy, National Astronomical Observatories, Chinese Academy of Sciences, Beijing 100101, China
[4]School of Astronomy and Space Science, University of the Chinese Academy of Sciences, Huairou 101408, China
[5]CAS Key Laboratory of Space Astronomy and Technology, National Astronomical Observatories, Chinese Academy of Sciences, Beijing 100101, China
[6]Department of Astronomy, China West Normal University, Nanchong 637009, China

Abstract

Steps toward the nature inside RR Lyrae variables can not only improve our understanding of variable stars but also innovate the precision when we use them as tracers to map the structure of the universe. In this work, we develop a hand-crafted one-dimensional pattern recognition pipeline to fetch out the "first apparitions", the most prominent observational characteristic of shock.We report the first detection of hydrogen emission lines in the first-overtone and multi-mode RR Lyrae variables. We find that there is an anti-correlation between the intensity and the radial velocity of the emission signal, which is possibly caused by opacity changing in the helium ionization zone. Moreover, we find one RRd star with hydrogen emission that possibly shows Blazhko-type modulations. According to our discoveries, with an enormous volume of upcoming data releases of variable stars and spectra, it may become possible to build up the bridge between shock waves and big problems like the Blazhko effect in non-fundamental mode RR Lyrae stars.

Keywords: *Stars: variables: RR Lyrae, Emission lines, hypersonic shock wave, non-fundamental mode.*

1. Introduction

RR Lyrae stars represent the low-mass (0.5-0.7 $M_\odot$), old-age (¿10 Gyr) stellar population at the core helium (He)-burning stage of their evolution. Their pulsations are caused by k mechanism, when the opacity of ionized He changes with the temperature. They obey the absolute visual magnitude versus metallicity law $M_v - [F_e/H]$ (Muraveva et al., 2018) and the period-luminosity-metallicity law (PLZ, Catelan et al., 2004, Longmore et al., 1986)(PLZ, Longmore et al. 1986; Catelan et al. 2004) in the infrared bands, thus making them excellent standard candles for distance determinations to nearby galaxies. RR Lyrae stars are further classified based on the number of oscillation modes, as fundamental mode (RRab), the first overtone mode (RRc), and multi-mode (RRd) variables (Soszyński et al., 2011). Among them, RRc and RRd stars enjoy shorter periods and smaller amplitudes than RRab and occupy the blue side of RR Lyrae instability strip.

It is now a well-established fact that for RRab stars, three moderate-to-small emission lines appear sequentially in a pulsation cycle, which are the so-called "three apparitions" (Preston, 2011). They are considered to be generated by atoms de-exciting after being excited by the shock wave, which is compressing, heating, and accelerating the atmospheric gas when traveling into it (Gillet & Fokin,

*duanxw@pku.edu.cn, Corresponding author

DOI: 10.52526/25792776-2020.67.2-181

2014). The "first apparitions" are generated when the shock wave is close to the photosphere, which indicates the coming of maximum luminosity. The "second apparitions" are thought to be produced by the photospheric compression, when the inner deep expanding atmosphere collides with outer layers which are in ballistic infalling motion (Hill, 1972). Chadid & Preston (2013) interpreted the "third apparitions" as to be generated by the shock wave Sh_{PM}, a superposition of the compression resulted from the hydrogen recombination front, and an accumulation of several weak compression waves. Gillet et al. (2019)provided a general overview of the atmospheric dynamical structure of RRab over a typical pulsating cycle, using high-resolution spectra of Hα and sodium lines in RR Lyr (HD 182989), which describes the evolution picture of shock waves inside quite clearly.

Although the "apparitions" were generally detected in RRab, there is no detection of shock waves in RRc or RRd stars. Gillet (2013) suggested that the intensity of the shock waves is certainly lower in RRc than RRab. And it is possible that the coexistence of stable oscillations in fundamental mode and the first-overtone mode in the same pulsation cycle can reduce the development of the shock amplitude. Up to now, there hasn't been any atmospheric pulsation model for RRc or RRd with a comprehensive study of the dynamical evolution of shock waves. The research about the link between the Blazhko effect and the interaction of strong shock waves was strongly obstructed by this absence.

In this work, we develop a large sample searching algorithm to investigate shock waves in RR Lyrae stars, especially those in non-fundamental mode.We focus on the "first apparition", which is the most prominent signature of shock waves to be observed and allows for large searching. They show up as emissions on the blue wings of Balmer lines when $\phi\sim$ 0.9. We select this kind of features through our hand-crafted one-D pattern recognition pipeline, using low-resolution and single-epoch spectra. Here we report the first detection of hydrogen emission in the first-overtone and multi-mode RR Lyrae stars, which give us new insights into the nature of non-fundamental mode RR Lyrae variables.

2. Observations and methods

We need photometric and spectroscopic observations. Photometry was used to classify RR Lyrae stars, which can be provided by the Catalina Sky Surveys Drake et al. (2014, 2017), the Wide-field Infrared Survey Explorer (WISE, Chen et al., 2018), the All Sky Automated Survey for Supernovae (ASAS-SN, Jayasinghe et al., 2019), and the Asteroid Terrestrial-impact Last Alert System (ATLAS, Heinze et al., 2018). We combine these catalogs, remove duplicate data, and get 68,152 stars, which are identified as RR Lyrae. Light curves from the Zwicky Transient Facility (ZTF, Bellm et al., 2019, Chen et al., 2020) for our selected stars are collected if available.

We search for the pattern of the "first apparitions" among low-resolution and single-epoch spectra. The spectra are collected from the Sloan Digital Sky Survey (SDSS, Eisenstein et al., 2011) and the Large Sky Area Multi-Object Fiber Spectroscopic Telescope survey (LAMOST, Deng et al., 2012). Due to the fact that periods of RR Lyrae stars are quite short, and the "first apparition" only enjoys about 5 % of the whole period (Chadid, 2011), long-time exposures and co-addition of spectra smooths the relevant emission features.

The common practice to hunt the "first apparitions" is to visually check the profiles of hydrogen Balmer lines for any sign of emission for a small sample. As for large survey data, this becomes an enormous amount of work. So we built up a set of pipeline, using hand-crafted one dimensional pattern recognition method. We presuppose the pattern of the target feature as a Gaussian-like emission profile and a broad Gaussian-like absorption profile when both the two signals are more significant than 2σ compared to the mean level. We use the minimum value in the selected windows to locate Balmer absorption profile. The "hunting" results are adopted which at least show clear patterns of the "first apparition" in Hα and Hβ at the same time and contain at least two observational points on the profiles of emission. We apply this pipeline to the spectra of RR Lyrae stars from SDSS and LAMOST, with visual checks to ensure completeness.

The emission and absorption lines are fitted based on the scale width versus shape method for the Balmer lines (Clewley et al., 2002, Sersic, 1968). We adopted two Sérsic profiles (Xue et al., 2008, Yang et al., 2014) as:

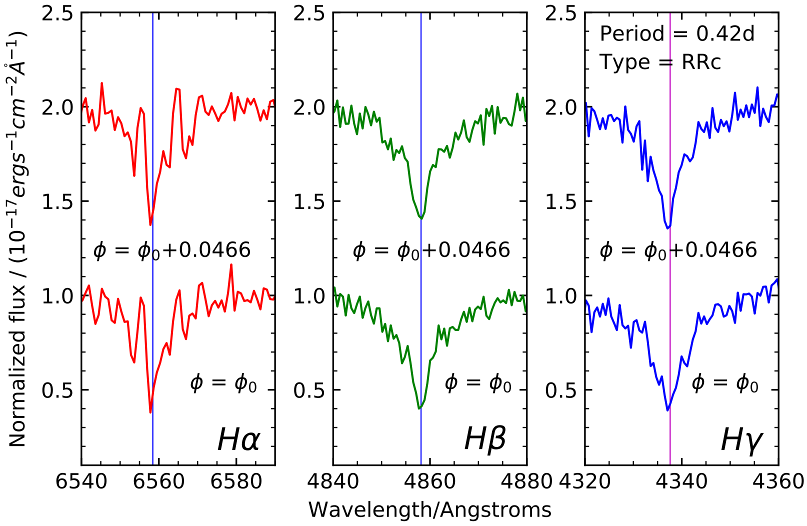

Figure 1. Emission in Hα, Hβ, and Hγ. The frame of reference for the wavelength axis is the stellar rest frame. The vertical blue lines indicate the Hα, Hβ, and Hγ line laboratory wavelength.

$$y = m - ae^{-\left(\frac{|\lambda-\lambda_\theta|}{b}\right)^c} \tag{1}$$

to fit the profile and make measurements of flux, intensity and full width at half maximum (FWHM) for the two components.We generate uncertainties by error propagation for covariance matrix and Monte Carlo method (Andrae, 2010), with limits based on observational resolutions.

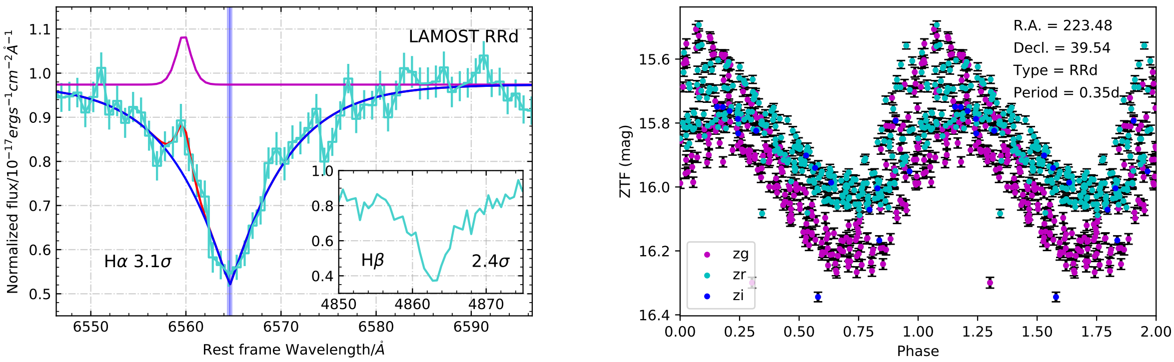

Figure 2. Left (a): Fitting result of the “first apparition” of the RRd star that may suffer from Blazhko effect. The unit of normalized flux is 10^{-17} ergs^{-1}cm $^{-2}$ $\mathring{A}^{-1}$. The reference frame for the wavelength axis is the stellar rest frame. The Hα emission lines are displayed as the pink profiles. The Vertical blue lines indicate the Hα line laboratory wavelength. The Hβ emission lines are displayed in the subplots. The significance of the emissions indicate the ratio between the flux of signal and noise. Right (b): The light curve from ZTF of the RRd star that may suffer from Blazhko effect.

.

3. Results of Searching

As one of the main results of the searching program, we find ten RRc stars in SDSS, ten RRc stars, and three RRd star in LAMOST, which all show intense shifted emission components on the blue wing of the Balmer absorption lines. The flux is normalized by the fitting result of the continuum. Figure

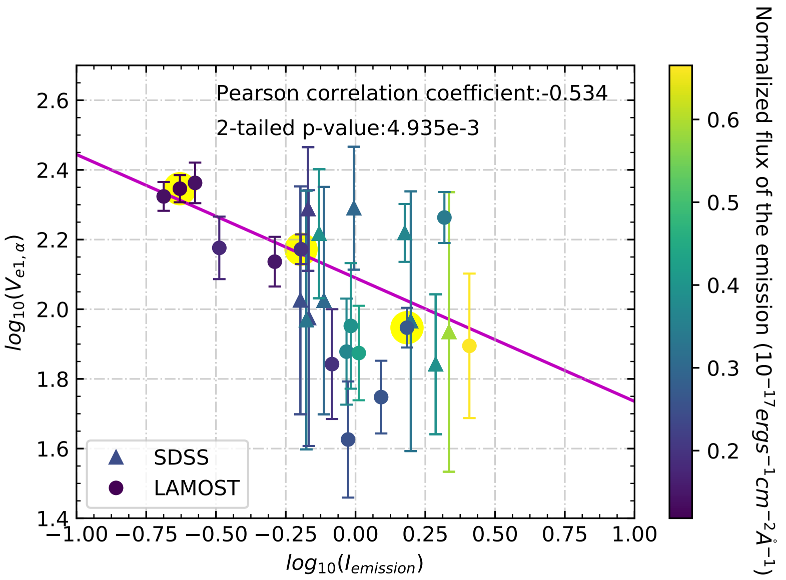

Figure 3. Relationship between the intensity and the radial velocity of the emission signal of the "first apparitions". The variation of the color shows different normalized flux of the emission part. Points highlighted with yellow edge are RRd stars, while others are RRc stars. Pink solid line indicates linear fitting results. Triangular points represent sample from SDSS, while circular points denote sample from LAMOST. The radial velocity of the emission is generated by the redshift measurements using Hα lines.

1 presents an example that the emission line appears at Hα, Hβ, and Hγ simultaneously. Figure 2 (left panel) shows a fitting example of one RRd star in LAMOST with hydrogen emission. Figure 2 (right panel) shows its light curve, provided by the Zwicky Transient Facility (ZTF). It may indicate that this RRd star suffer from long-term modulations (Blazhko effect).

4. Discussion

Emission features shown in the spectra of RR Lyrae stars can be considered as shocks propagating through their pulsating atmosphere. The "first apparition" can be generated by a shock forming below the photosphere near the time of the minimum radius. The shock is accelerating outward. The atoms de-excite after being excited by the shock in the radiative wake. Energy from the ramp pressure at the shock front is high enough to excite neutral hydrogen from the second quantum state upwards. Studies (Schwarzschild, 1952) show that hypersonic velocity shock is needed to make the emission observable. So we take our discoveries as evidence of the existence of hypersonic shock waves in non-fundamental mode RR Lyrae stars.

We measure the radial velocity of the emission line in the stellar rest frame. The equation is as:

$$V_{e1,\alpha} = c\frac{(\lambda_{e1,\alpha} - \lambda_{ab})}{\lambda_0} \tag{2}$$

where $\lambda_{e1,\alpha}$ is the wavelength corresponding to the central wavelength of the emission line. λ_{ab} indicates the central wavelength of the absorption component, while λ_0 is the laboratory wavelength.

An estimation of the temperature of the shock front for a strong shock can also be given by adiabatic Rankine-Hugoniot relationships (Chadid et al., 2008) as:

$$V_{shock} = \sqrt{\frac{16}{3}\frac{R}{\mu}T_{shock}} \tag{3}$$

where V_{shock} is in km/s, μ indicates the mean atomic weight, R stands for the universal gas constant. It shows that there is a linear correlation between $logT_{shock}$ and $logV_{shock}$.

We investigate the relationship between the radial velocity and the intensity of the emission part of the "first apparitions", visualized in Figure 3. It shows a clear anti-correlation, characterized by Pearson correlation coefficients of about -0.534. The variation of color shows that as the intensity of the emission becomes larger, the line width of the emission part gets broader, which indicates that the temperature of it gets higher. When the Mach number increases, the shock wave is getting more and more drastic. But from our results, if the radial velocity of the emission can represent the velocity of the shock, we learn that the intensity of the emission of the "first apparitions" is actually decreasing as the velocity and the temperature of the shock front are increasing. A probable explanation of this contradiction between theory and observation is the increase of the opacity. In a helium ionization zone, like the envelope of RR Lyrae, the environment becomes more opaque as temperature rises, so the light is harder to be delivered. Since RRc and RRd stars are hotter population in the whole sample of RR Lyrae and the anti-correlation between emission feature intensity and radial velocity (Figure 3), they are supposed to have less prominent shock signatures. It should be harder for them to deliver signatures of shock waves and it indicates that shock waves discovered in our sample are quite severe.

Theoretical analysis in Gillet & Fokin (2014), private communications told us that the different types of shock waves identified in RRab can also be found in RRc stars. Main shocks generated by the $k - \gamma$ *mechanism* in RRc have an amplitude three to four times lower than those in RRab.

The maximums of the flux of RRc is lower than RRab in our sample. The detailed comparisons between RRab and RRc sample with shock waves will be discussed in our upcoming paper. Gillet (2013) showed that statistically there is a striking amplitude jumping between stars with short-periods (RRc) and stars with long-periods (RRa) near the period $\sim$0.4 day. According to our result, the contribution of opacity should also be taken into account.

The Blazhko effect is considered a common effect among RRab and RRc stars. It has been suggested that this effect is generated by several strong shocks occurring during each pulsation cycle (Gillet, 2013). But it can't be confirmed that they share the same physical mechanism to suffer from this effect. It is mainly because of the lack of information on the observed shock wave signal in RRc. The large variety of resonant, nonresonant, and chaotic possible states should also be taken into considerations to interprete low-amplitude variations such as small modulations (Molnár et al., 2012a,b). Apparently, our research will strongly contribute to the investigation between shock waves and long-term modulations in non-fundamental mode stars.

5. Conclusions

We have detected the "first apparitions" in non-fundamental RR Lyrae stars for the first time, including ten RRc stars in SDSS sample, ten RRc stars, and three RRd star in LAMOST sample. We find an anti-correlation relationship between the radial velocity and the intensity of the emission signal, which is contrary to the theoretical behavior of shock waves but can be explained as the result of the changing opacity in a helium ionization zone. Moreover, one of the RRd stars we have selected may suffer from long-term modulation.

Nevertheless, due to the lack of observations of shock wave signals in non-fundamental mode RR Lyrae stars, the origin of the Blazhko effect in RRab and RRc stars has been suspected to be totally different. But since we have detected observational characteristics of hypersonic shock waves in non-fundamental mode stars, it may be possible for us to investigate the role of shock waves in long-term modulation of the first overtone and multi-mode RR Lyrae stars. As the cause of the formation of the Blazhko effect remains a mystery, steps toward the nature of shock waves may surprise us in the future.

Acknowledgements

We appreciate the help from Dr. Hao-Tong Zhang, Dr. Zhong-Rui Bai and Dr. Jian-Jun Chen for accessing the single-epoch spectra from LAMOST. We acknowledge research support from the Cultivation Project for LAMOST Scientific Payoff and Research Achievement of CAMSCAS. Li-Cai Deng acknowledges research support from the National Science Foundation of China through grants 11633005. Xiao-Dian Chen also acknowledges support from the National Natural Science Foundation of China through grant 11903045. Xiao-Wei Duan acknowledges support from the Peking University President Scholarship. Hua-Wei Zhang acknowledges research support from the National Natural Science Foundation of China (NSFC) under No. 11973001 and National Key RD Program of China No. 2019YFA0405504. The Guoshoujing Telescope (the Large Sky Area Multi-Object Fiber Spectroscopic Telescope LAMOST) is a National Major Scientific Project built by the Chinese Academy of Sciences. Funding for the project has been provided by the National Development and Reform Commission. LAMOST is operated and managed by the National Astronomical Observatories, Chinese Academy of Sciences.

References

Andrae R., 2010, arXiv e-prints,

Bellm E. C., et al., 2019, PASP, 131, 018002

Catelan M., Pritzl B. J., Smith H. A., 2004, ApJS, 154, 633

Chadid M., 2011, in McWilliam A., ed., Vol. 5, RR Lyrae Stars, Metal-Poor Stars, and the Galaxy. p. 29 (arXiv:1108.5682)

Chadid M., Preston G. W., 2013, MNRAS, 434, 552

Chadid M., Vernin J., Gillet D., 2008, A&A, 491, 537

Chen X., Wang S., Deng L., de Grijs R., Yang M., 2018, ApJS, 237, 28

Chen X., Wang S., Deng L., de Grijs R., Yang M., Tian H., 2020, ApJS, 249, 18

Clewley L., Warren S. J., Hewett P. C., Norris J. E., Peterson R. C., Evans N. W., 2002, MNRAS, 337, 87

Deng L.-C., et al., 2012, RAA, 12, 735

Drake A. J., et al., 2014, ApJS, 213, 9

Drake A. J., et al., 2017, MNRAS, 469, 3688

Eisenstein D. J., et al., 2011, AJ, 142, 72

Gillet D., 2013, A&A, 554, A46

Gillet D., Fokin A. B., 2014, A&A, 565, A73

Gillet D., Mauclaire B., Lemoult T., Mathias P., Devaux J. S., de France T., Garrel T., 2019, A&A, 623, A109

Heinze A. N., et al., 2018, AJ, 156, 241

Hill S. J., 1972, ApJ, 178, 793

Jayasinghe T., et al., 2019, MNRAS, 486, 1907

Longmore A. J., Fernley J. A., Jameson R. F., 1986, MNRAS, 220, 279

Molnár L., Kolláth Z., Szabó R., Plachy E., 2012a, AN, 333, 950

Molnár L., Kolláth Z., Szabó R., Bryson S., Kolenberg K., Mullally F., Thompson S. E., 2012b, ApJ, 757, L13

Muraveva T., Delgado H. E., Clementini G., Sarro L. M., Garofalo A., 2018, MNRAS, 481, 1195

Preston G. W., 2011, AJ, 141, 6

Schwarzschild M., 1952, AJ, 57, 57

Sersic J. L., 1968, Atlas de Galaxias Australes

Soszyński I., et al., 2011, AcA, 61, 1

Xue X. X., et al., 2008, ApJ, 684, 1143

Yang F., et al., 2014, NewA, 26, 72

Communications of BAO, Vol. 67, Issue 2, 2020, pp. 187-192

Properties of ISM in two star-forming regions

Nikoghosyan E.*, Azatyan N., Harutyunian H., Baghdasaryan D., and Andreasyan D.

Byurakan Astrophysical Observatory, 0213, Aragatsotn prov., Armenia

Abstract

The Hi-GAL provides an opportunity to make a complete and unbiased view of the continuum emission in the Galactic plane in five bands: 70, 160, 250, 350, and 500 μm. Our research focuses on two of star-forming regions. The first one is the molecular cloud, which includes G45.12+0.13 and G45.07+0.13 UC HII regions. Using the Modified blackbody fitting on *Herschel* images obtained in four bands: 160, 250, 350, and 500 μm, we determined the distribution of N(H_2) hydrogen column density and T_d dust temperature. The maps of N(H_2) and T_d show that UC HII regions clearly stand out against the general background of the molecular cloud with a relatively low density (from 1.0×10^{23} to 3.0×10^{23} cm^{-2}) and significantly higher temperature (up to 100 K), what is fully consistent with the basic concept of UC HII regions about the presence of a hot, high mass stellar source and stellar wind, which leads to the blowing out of matter. The second one is the elongated star-forming region, which includes five stellar subgroups around IRAS 05184+3635, 05177+3636, 05168+3634, 05162+3639 and 05156+3643 sources. Here, on the contrary, the N(H_2) is noticeably higher (from 1.0×10^{23} to 5.0×10^{23} cm^{-2}) than in the surrounding molecular cloud and the T_d does not exceed 25 K.

Keywords: *stars: pre-main sequence – infrared: stars – radiative transfer – ISM: hydrogen column density, dust temperature*

1. Introduction

The Hi-GAL provides an opportunity to make a complete and unbiased view of the continuum emission in the Galactic plane in five bands: 70, 160, 250, 350, and 500 μm. This range of wavelengths covers the peak of the spectral energy distribution (SED) of the cold dust emission and makes it possible to determine such important parameters of Interstellar medium (ISM) as the N(H_2) hydrogen column density and T_d dust temperature (Molinari et al., 2016).

For our study we choose two, relatively distant regions of star formation, which are different according to their properties and stellar content. The first is a pair of UC HII regions G45.07+0.13 and G45.12+0.13, associated with IRAS 19110+1045 and IRAS 19111+1048 sources, respectively (Wood & Churchwell, 1989). In Figure 1, we present the colour-composite image (left panel) with Hi-GAL three bands, where it is clearly seen that both regions are clearly distinguished by their brightness against the background of the surrounding molecular cloud. Moreover, it is clearly seen that they are connected by a relatively colder bridge. This can serve as further evidence that they belong to the same star-forming region and form a physically connected system. According to the results obtained in Han et al. (2015), the near and far kinematic distances of G45.07+0.13 and G45.12+0.13 regions are $\sim$4.0 and $\sim$8.0 kpc with tangent point distance of $\sim$6 kpc. The last, far distance estimation, is better consistent with a more recent estimate according to the trigonometric parallax (7.75 ± 0.45 kpc) in Wu et al. (2019). Following them, we adopt a distance of 7.8 kpc in our study.

The next star-forming region is a molecular cloud surrounding the five IRAS sources: 05168+3634, 05184+3635, 05177+3636, 05162+3639, and IRAS 05156+3643 (Azatyan, 2019). The right panel of Figure 1 presents the colour-composite image with Hi-GAL three bands, where we can see that there are relatively hot gas-dust matter concentrations in the vicinity of all IRAS sources. The distance

*elena@bao.sci.am, Corresponding author

DOI: 10.52526/25792776-2020.67.2-187

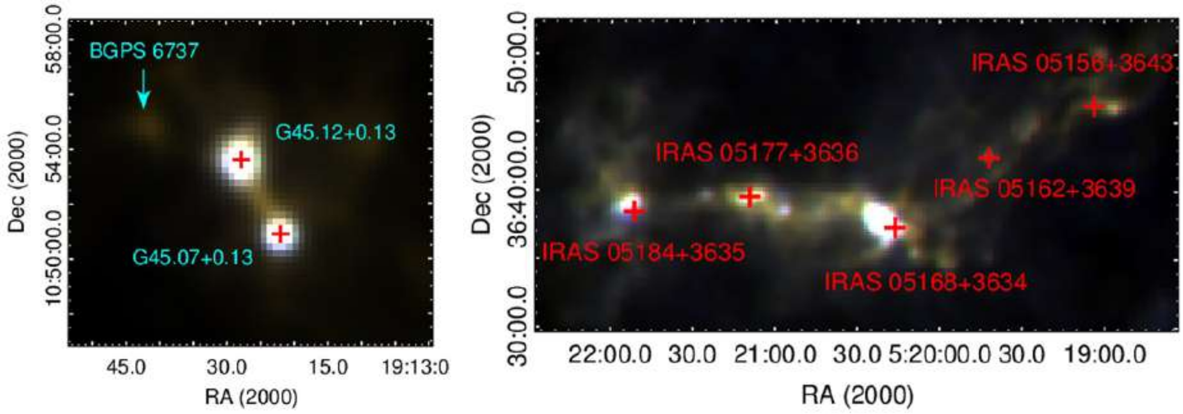

Figure 1. Colour-composite images with Hi-GAL three bands: PACS 160 μm (blue), SPIRE 350 μm (green), and 500 μm (red). *Left panel*: G45.07+0.13 and G45.12+0.13 UC HII regions; *right panel*: IRAS 05168+3634 (Mol 9) star-forming region. The positions of IRAS sources are marked by crosses.

estimations of this region are controversial. A kinematic distance estimated by Molinari et al. (1996) is 6.08 kpc. The distance of IRAS 05168+3634 estimated according to a trigonometric parallax with VERA is 1.9 ± 0.2 kpc (Sakai et al., 2012). Such a large difference in the calculated distances determines a significant difference in the assessment of the mass of gas-dust matter. Therefore, for our calculations, we used both distance estimates.

The both star-forming regions are associated with different manifestations of activity, including maser and continual molecular emission, outflows, etc (Varricatt et al., 2010, and ref. therein). Our previous studies shown that all IRAS sources in both star-forming regions are associated with dense young stellar clusters. The dense stellar clusters are associated with both G45.07+0.13 and G45.12+0.13 UC HII regions include a number of high-mass ZAMS stellar objects (Azatyan et al., 2020, Rivera-Ingraham et al., 2010, Vig et al., 2006). The molecular cloud in the second star-forming regions includes 240 candidates of YSOs within the radii of subclusters around all five IRAS sources. The age of the subclusters is estimated at 0.1-3 Myr (Azatyan, 2019).

2. Method

To obtain the physical parameters like N(H_2) and T_d, the Modified single-temperature blackbody fitting, as well as the thermal emission from cold dust lying in the *Herschel* FIR optically thin bands (160–500 μm) were used (Hildebrand, 1983). Following the discussion in the previous studies (e.g. Battersby et al., 2011), we excluded the 70 μm observational data as the optically thin assumption would not hold. Besides, the emission here would have a significant contribution from the warm dust component, thus modelling with a single-temperature blackbody would over-estimate the derived temperatures. For initial *Herschel* images processing, which includes the elimination of bad pixels effect, the transformation of surface brightness units to Jy pixel^{-1}, as well as the convolution of images resolution to the 500 μm image (the lowest among all images), we used the HIPE software.

The Modified single-temperature blackbody fitting, which was subsequently carried out on a pixel-by-pixel basis using the following formula:

$$S_\nu = B_\nu(\nu, T_d)\Omega(1 - e^{-\tau(\nu)}), \tag{1}$$

with

$$\tau(\nu) = \mu_{H_2} m_H k_\nu N(H_2), \tag{2}$$

where ν is the frequency, $S_\nu(\nu)$ is the observed flux density, $B_\nu(\nu, T_d)$ is the Planck function, Ω is the solid angle in steradians from where the flux is obtained (in this case for all bands the solid angle subtended by a 14 arcsec $\times$ 14 arcsec pixel), $\tau(\nu)$ is the optical depth, μ_{H_2} is the mean molecular weight (adopted as 2.8 here), m_H is the mass of hydrogen, and k_ν is the dust opacity.

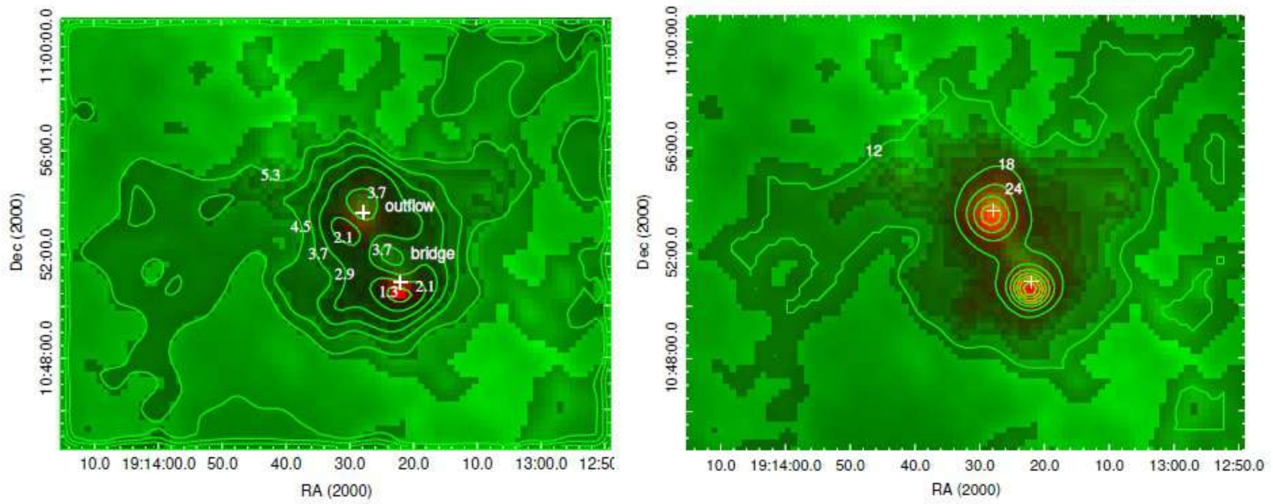

Figure 2. Colour-composite images of T_d (red) and $N(H_2)$ (green) distribution of the region surrounding G45.12+0.13 and G45.07+0.13 UC HII with overlaid contours of temperature in the left panel and $N(H_2)$ on the right panel. The temperature contours cover a range from 12 to 66 K with step in increments of 6 K. The $N(H_2)$ contours cover a range from 1.3×10^{23} to $5.3 \times 10^{23}\,\mathrm{cm}^{-2}$ with step in increments of $0.8 \times 10^{23}\,\mathrm{cm}^{-2}$. The positions of IRAS sources are marked by white crosses. On the right panel, the positions of G45.12+0.13 outflow and bridge between G45.12+0.13 and G45.07.0.13 UC HII are indicated (for more detail information see text).

For opacity, we adopted a functional form of $k_\nu = 0.1(\nu/1000\,GHz)^\beta\, cm^2 g^{-1}$, with $\beta = 2$ (see Hildebrand, 1983). For each pixel, equation (1) was fitted using the four data points (160, 250, 350, and 500 μm) keeping T_d and $N(H_2)$ as free parameters. Launhardt et al. (2013) used a conservative 15% uncertainty in the flux densities of the *Herschel* bands. We adopted the same value here for all bands. The uncertainties of the parameters were derived using Pearson's χ^2 statistics:

$$\chi^2 = \sum_{i=1}^{N} \frac{(D_i - F_i)^2}{F_i}, \tag{3}$$

where D_i is the observed flux and F_i is the flux predicted by the model, N is the number of bands.

From the derived column density values, we estimate the mass of the dusty clumps using the following expression:

$$M_{clump} = \mu_{H_2} m_H Area_{pix} \sum N(H_2), \tag{4}$$

where $Area_{pix}$ is the area of a pixel in cm^2.

3. Results

The results for both star-forming regions (see Sec. 1) are presented below.

3.1. G45.07+0.13 and G45.12+0.13 UC HII regions

The final obtained column density and dust temperature maps of the wider region surrounding G45.12+0.13 and G45.07+0.13 UC HII objects are shown in Figure 2. The map of temperature distribution clearly shows that the centers of both UC HII regions practically coincide with the temperature maxima, which reaches 49 K in G45.12+0.13 and 97 K in G45.07+0.13. On average, in the vicinity of IRAS 19110+1045, the value of $N(H_2)$ is $\sim 2 \times 10^{23}\ \mathrm{cm}^{-2}$, which is well coincides with the data in Churchwell et al. (2010) and almost an order of magnitude less than it was estimated from the 1.3 mm dust emission in Hernández-Hernández et al. (2014). On the other hand, the lower temperature estimation in the same work (82 K) is well consistent with ours.

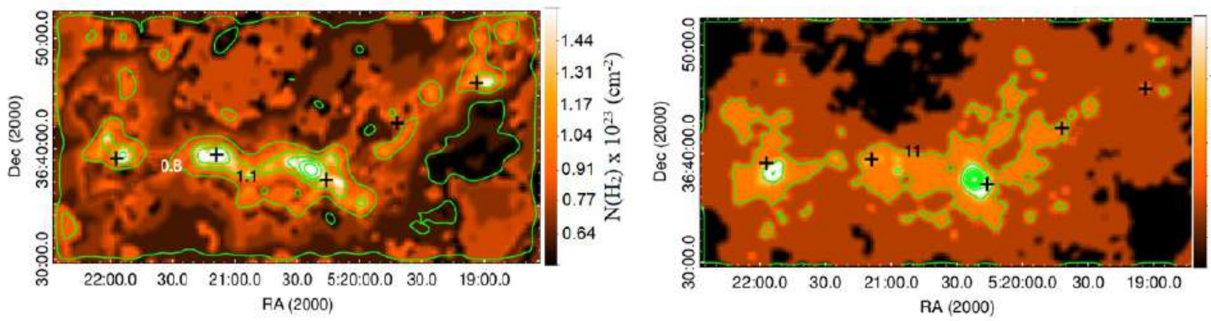

Figure 3. Maps of column density (*left panel*) and dust temperature (*right panel*) of IRAS 05168+3634 star-forming regions. On the N(H_2) map the isodenses corresponding to the values of 1.1×10^{23} and $0.8 \times 10^{23}\,\mathrm{cm}^{-2}$ shown. On T_d map isotherm corresponding to the value of 11 K is shown. The positions of IRAS sources are marked by crosses.

In the vicinity of IRAS 19111+1048, N(H_2) is equal to $\sim 4 \times 10^{23}\,\mathrm{cm}^{-2}$ that well consistents with the data of multi transition ^{13}CO and CS observations in the G45.12+0.13 core (Churchwell et al., 1992). IRAS 19111+1048 itself is located in a region with a relatively high column density, which coincides in coordinates with counters of blueshifted emission of the bipolar molecular outflow (Hunter et al., 1997). It can be assumed that the outflow is the cause of the formation of the region with increased N(H_2). It should be noted one more fact. One more region with a relatively high density and low temperature is located between the two UC HII regions. This region by coordinates coincides with the bridge between the UC HII regions, which is clearly distinguishable on *Herschel* colour-composite image (see Figures 1). This bridge is also clearly visible on the H30α map in Churchwell et al. (2010).

As can be seen in Figure 2, the temperature distribution in both UC HII regions has a pronounced spherical symmetry, and at a distance of 7 pix ($\sim$1.6 arcmin or $\sim$3.7 pc) in G45.12+0.13 and 5 pix ($\sim$1.2 arcmin or 2.6 pc) in G45.07+0.13 from IRAS sources, the temperature decline almost stops. These distances correspond to 18 K isotherm and $2.9 \times 10^{23}\,\mathrm{cm}^{-2}$ isodense, after which the column density begins to increase rapidly. We can assume that it is the region where the influence of the stellar wind, leading to blowing of matter, ends. The total masses of these regions were calculated by Formula 4 for G45.12+0.13 region is $\sim 2.2 \times 10^5\ M_\odot$ and for G45.07+0.13 is $10^5\ M_\odot$.

It should be noted that the parameters obtained by the Modified blackbody model are not without certain errors (Harutyunyan et al., 2020). Among other causes the errors are a strong function of the parameters' values. In general, the χ^2 in the UC HII regions does not exceed 0.1. However, the uncertainty of parameters significantly increases in the regions with the maximum temperature, reaching a value of 0.8.

Table 1. The parameter of gas-dust matter and stellar content in the vicinity of IRAS sources

Parameter	05156+3643	05162+3639	05168+3634	05177+3636	05184+3635
Radius (arcmin)	2.8	0.25	3.0	3.5	2.5
YSO's number	47	5	57	79	52
N(H_2) $\times 10^{23}\,cm^{-2}$	1.2	0.8	1.8	1.7	1.5
T_d (K)	12	12	24	13	14
M ($M_\odot$) for d = 1.9 kpc	1.2×10^4	1.9×10^2	1.9×10^3	2.2×10^4	1.0×10^4
M ($M_\odot$) for d = 6.1 kpc	1.4×10^5	2.2×10^3	2.1×10^4	2.5×10^5	1.2×10^5

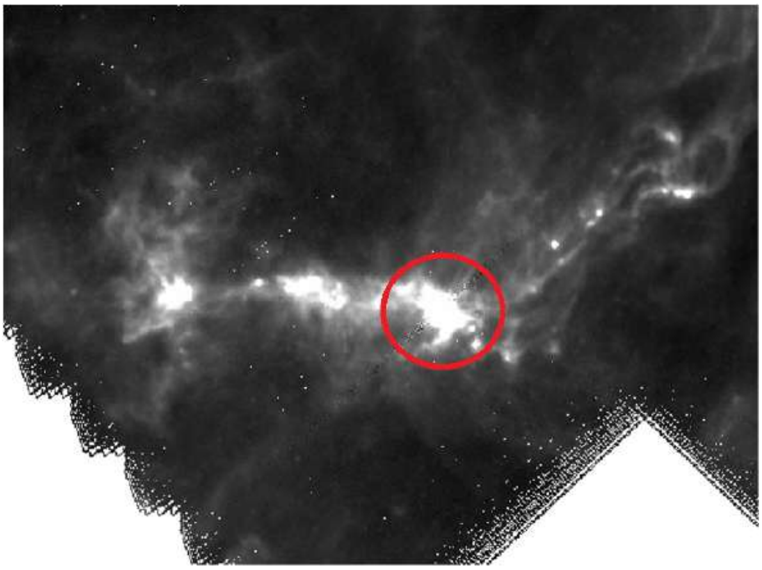

Figure 4. 2.5 level 250 μm *Herschel* image of IRAS 05168+3634 star-forming region. The red circle marks the vicinity of IRAS 05168+3634 source.

3.2. IRAS 05168+3634 star-forming region

The final obtained column density and dust temperature maps of the wider region surrounding five IRAS sources (05168+3634, 05184+3635, 05177+3636, 05162+3639, and IRAS 05156+3643) are shown in Figure 3. In contrast to the previous region, this star-forming region stand out against of the environment not only with a higher temperature, but also with a higher density. In general, N(H_2) in molecular clouds surrounding IRAS sources changes from $\sim 0.8 \times 10^{23}$ to $\sim 2.7 \times 10^{23}\,\mathrm{cm}^{-2}$, and T_d- from 11 to 26 K. We can see that the density in this star-forming region is only slightly less than in the previous one. However, the temperature of the gas-dust matter is much lower. Such a significant difference, of course, is primarily due to the stellar content. As mentioned above, stellar clusters in the UC HII regions include a significant number of high mass ZAMS stellar objects, accordingly with higher temperatures. In contrast, the subclusters in IRAS 05168+3634 star-forming region are mainly composed of younger, middle- and low-mass stellar objects with accordingly lower temperatures (Azatyan, 2019). The Table 1 lists some parameters that characterize both the stellar population and the gas-dust matter in the IRAS subclusters: the radii of the subclusters and the number of YSOs identified in them, as well as the hydrogen column density, dust temperature, and mass of the gas-dust component. Based on these data, a relationship is observed between the number of identified YSOs and the mass of the gas-dust component. Undoubtedly, the relationship between these parameters, including the evolutionary stage of the stellar objects, requires a more detailed study.

In general, in the molecular cloud, the uncertainty of parameters does not exceed 0.02. In general, the value of χ^2 is in this star-forming region noticeably lower than in the UC HII regions. This is most likely due to the fact that the temperature regime in this region is more suitable for the model we have applied. However, in the central part, in the vicinity IRAS 05168+3634, the uncertainty increases significantly, up to 0.9. In this case, this cannot be explained by the high temperature. The increase in the uncertainly of the parameters in this case is most likely explained by the quality of the images. Unfortunately, in all available *Herschel* images, this star-forming region is located at the very edge, where, of course, the image quality, especially in the 250 μm channel, is not good enough. The Figure 4 clearly shows that in the area around the IRAS 05168+3634 source, even in a 2.5 level image, there are many bad pixels that, most likely, is the reason for the increase in the χ^2 value.

4. Conclusion

Thus, the study of ISM in both star-forming regions of showed that with a small difference in density, they differ significantly in temperature. Undoubtedly, this difference is interconnected with the stellar composition. This once again confirms the well-known fact that any problem in astronomy, including the process of star formation, should be studied by a combination of many factors on the basis of extensive observational data, which can only be provided by survey observations made in different spectral ranges.

Acknowledgements

The authors are grateful to the organizers for holding the International Symposium "Astronomical Surveys and Big Data 2" and for publishing the paper.

References

Azatyan N. M., 2019, A&A, 622, A38

Azatyan N., Nikoghosyan E., Harutyunian H., Baghdasaryan D., Andreasyan D., 2020, ComBAO, 67, in press

Battersby C., et al., 2011, A&A, 535, A128

Churchwell E., Walmsley C. M., Wood D. O. S., 1992, A&A, 253, 541

Churchwell E., Sievers A., Thum C., 2010, A&A, 513, A9

Han X. H., Zhou J. J., Wang J. Z., Esimbek J., Zhang J. S., Wang N., 2015, A&A, 576, A131

Harutyunyan H. A., Nikoghosyan E. H., Azatyan N. M., 2020, Communications of the Byurakan Astrophysical Observatory, 67, 8

Hernández-Hernández V., Zapata L., Kurtz S., Garay G., 2014, ApJ, 786, 38

Hildebrand R. H., 1983, QJRAS, 24, 267

Hunter T. R., Phillips T. G., Menten K. M., 1997, ApJ, 478, 283

Launhardt R., et al., 2013, A&A, 551, A98

Molinari S., Brand J., Cesaroni R., Palla F., 1996, A&A, 308, 573

Molinari S., et al., 2016, A&A, 591, A149

Rivera-Ingraham A., et al., 2010, ApJ, 723, 915

Sakai N., Honma M., Nakanishi H., Sakanoue H., Kurayama T., Shibata K. M., Shizugami M., 2012, PASJ, 64, 108

Varricatt W. P., Davis C. J., Ramsay S., Todd S. P., 2010, MNRAS, 404, 661

Vig S., Ghosh S. K., Kulkarni V. K., Ojha D. K., Verma R. P., 2006, ApJ, 637, 400

Wood D. O. S., Churchwell E., 1989, ApJS, 69, 831

Wu Y. W., et al., 2019, ApJ, 874, 94

Uncertainties of the solar wind in-situ velocity measurements

Gogoberidze G.*and Gorgaslidze E.†

Ilia State University, 3/5 Cholokashvili ave., 0162 Tbilisi, Georgia

Abstract

We study spectral features of Alfvénic turbulence in fast solar wind. We propose a general, instrument independent method to estimate the uncertainty in velocity fluctuations obtained by in-situ satellite observations in the solar wind. We show that when the measurement uncertainties of the velocity fluctuations are taken into account the less energetic Elsasser spectrum obeys a unique power law scaling throughout the inertial range as prevailing theories of magnetohydrodynamic turbulence predict.

Keywords: *Solar Wind: Turbulence*

1. Introduction

In-situ satellite observations of the solar wind magnetic field and bulk flow span several decades in temporal scales and offer a 'natural laboratory' for the study of MHD turbulence (Bruno & Carbone, 2013). They have been extensively used to test theoretical predictions of MHD turbulence. The Elsasser fields, $\mathbf{Z}^{\pm} = \mathbf{v} \pm \mathbf{B}/\sqrt{4\pi\rho}$, where $\mathbf{v}$ and $\mathbf{B}$ are the velocity and magnetic fields, respectively, and ρ is the average density, represent eigen-functions of counter propagating (with respect to the mean magnetic field) Alfvén waves and therefore they are primary fields for the study of incompressible magnetohydrodynamic (MHD) turbulence. Fluctuations in the fast solar wind are strongly imbalanced - there is more power in Alfvén waves propagating outward from the sun than toward it so that the power in $\mathbf{Z}^{+}$ typically dominates over that in $\mathbf{Z}^{-}$.

Using high cadence WIND observations Wicks et al. (2010) studied spectral features of the Elsasser variables in the high frequency part of the inertial interval for the first time. They showed that at 1 AU (in accordance with earlier studies) in the low frequency part of the inertial interval (10^{-3}Hz $<$ $f < 10^{-2}$Hz) $\mathbf{Z}^{-}$ nearly follows Kolmogorov scaling which at higher frequencies ($f > 10^{-2}$Hz) is more shallow with $\gamma_{-} \approx -1.3$. The absence of single scaling of the subdominant Elsasser field in the entire inertial interval contradicts all recently developed models of strong, anisotropic imbalanced MHD turbulence which predict a single scaling for sub-dominant $\mathbf{Z}^{-}$ spectrum. They also are inconsistent with the results of recent high resolution direct numerical simulations of imbalanced MHD turbulence which showed single scaling of the subdominant Elsasser field in the inertial interval (Turner et al., 2012).

Control of observational uncertainty in the in-situ observations is non-trivial, although these errors often have known bounds. There are different challenges for magnetic field and velocity measurements; solar wind velocity observations are intrinsically more uncertain compared to the magnetic field data (Gogoberidze et al., 2012a,b, 2013, 2018, Hnat et al., 2011, Turner et al., 2012). Here we propose an instrument independent method to estimate the uncertainty on velocity field fluctuations directly from the data. We obtain the systematic shift that this uncertainty introduces into observed spectral exponents. We will see that the shallower $\mathbf{Z}^{-}$ spectrum at high frequencies can be entirely accounted for by this uncertainty in the velocity data and the observations of the $\mathbf{Z}^{\pm}$ spectra may in fact within

*grigol_gogoberidze@iliauni.edu.ge, Corresponding author

†egorgaslidze@gmail.com

DOI: 10.52526/25792776-2020.67.2-193

achievable accuracy of the observations, be in agreement with the predictions of theory and numerical simulations.

2. Data analysis

We use data obtained by the WIND spacecraft at 3 second resolution. Magnetic field data is provided by the MFI instrument and density and velocity data by the 3DP instrument. We use observations made during a quiet fast stream. The start time of the interval is 06:00 April 06, 2008 and stop time is 12:00 of April 08, 2008 (Gogoberidze et al., 2012b). During this interval the solar wind speed remained above 550 km/s. The energy of compressive fluctuations was an order of magnitude lower than that of incompressible fluctuations and, consequently, magnetic and velocity fluctuations, being mainly Alfvénic, were dominated by the components perpendicular to the local mean field. The mean field, $\bar{\mathbf{B}}(t,\tau)$, at some time t and on scale τ is defined as the magnetic field averaged over the interval $[t-\tau, t+2\tau]$. The fluctuations of the velocity and magnetic field are defined by standard expressions $\delta\mathbf{v}(t,\tau) = \mathbf{v}(t+\tau) - \mathbf{v}(t)$ and $\delta\mathbf{B}(t,\tau) = \mathbf{B}(t+\tau) - \mathbf{B}(t)$, respectively.

There are several sources of uncertainty in the solar wind velocity measurements (Gogoberidze et al., 2013, Podesta et al., 2002, Turner et al., 2012). The first source is the uncertainty in assessment of the proton distribution function. In addition, in common with all velocity in situ observations, the 3 s velocity observations on WIND are quantized before ground transmission and this quantization results in high frequency noise or quantization noise. These contributions to observational uncertainty decorrelate the velocity and magnetic field fluctuations at high frequencies. White, delta correlated noise provides a reasonable, instrument independent model for the uncertainty (Podesta et al., 2002). Any measurement of a velocity component fluctuation δv_o can then be represented as a sum of the 'real' turbulent signal δv_s and a noise δv_n which has zero mean and standard deviation ε, so $\delta v_o = \delta v_s + \delta v_n$. Note that the r.m.s. value of a single velocity measuremant v_n used to characterise velocity uncertainties in other studies (Podesta et al., 2002, Wicks et al., 2010) is, in our notations, $\varepsilon/\sqrt{2}$. In what follows we will neglect the uncertainties in the magnetic field measurements since generally these are small relative to those of the velocity measurements.

We will first quantify the velocity uncertainty from the data. We will exploit the fact that both the turbulent signal and the noise are random variables with distinct characteristic autocorrelation time scales. We make a key assumption- that the autocorrelation timescale of the underlying turbulent signal is that observed in the magnetic field component fluctuations δB_o (they have negligible noise) and that this is also the autocorrelation timescale of the 'true' turbulent velocity component fluctuations δv_s. Any difference in the autocorrelation functions of the observed δv_o and δB_o are thus attributable to the (delta correlated) noise δv_n on the velocity. The autocorrelation coefficient (AC) of

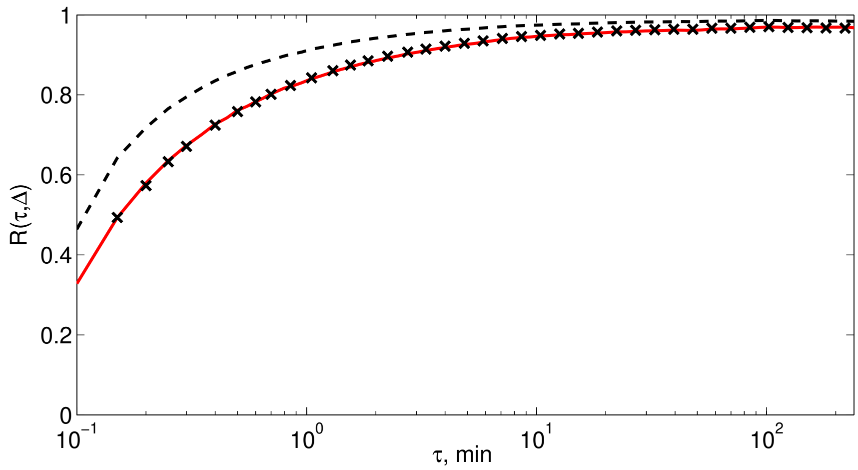

Figure 1. Autocorrelation functions $R_{\delta B_y}(\tau,\Delta)$ (black dashed line) of the GSE y component of the magnetic field fluctuation and $R_{\delta v_y}(\tau,\Delta)$ (red solid line) with the time lag $\Delta = 3$ s.

a component δv on time lag Δ is $R_{\delta v}(\tau,\Delta) \equiv \langle \delta v(t+\Delta,\tau)\delta v(t,\tau)\rangle / \langle \delta v(t,\tau)^2\rangle$, where angular brackets denote time averages with respect to entire studied interval (i.e., with respect to all possible values of t). The autocorrelation coefficients $R_{\delta B_o}(\tau,\Delta)$ and $R_{\delta v_o}(\tau,\Delta)$ for GSE y components of the magnetic field and velocity fluctuations are plotted in Figure 1 for lag $\Delta = 3$s as a function of scale τ with black solid and red dashed lines respectively. We see that the AC grows with scale τ for both signals and that the velocity AC is systematically lower that that of the magnetic field, consistent with the assumption of uncorrelated noise that principally affects the velocity signal. Given these assumptions one can construct a modelled noisy signal by adding uncorrelated noise to the magnetic field observations. The modelled noisy fluctuations $\delta B_{o+n} = \delta B_o + \delta B_n$, where δB_n are delta correlated Gaussian distributed random numbers with zero mean and standard deviation ε_B. The magnitude of the modelled noise ε_B can then be systematically varied. We first verify that this simple noise model is sufficient to reproduce the AC as a function of τ for the velocity fluctuations. The AC of the modelled δB_{o+n} is shown by the black crosses in Fig. 1 and this can be seen to closely coincide with the observed AC of velocity fluctuations δv_o. Assuming Alfvénic fluctuations the magnitude of ε_B used to generate this curve corresponds to an uncertainty in the velocity fluctuations of

$$\varepsilon_v \equiv \varepsilon_B \sqrt{\frac{\langle \delta v_o^2 \rangle}{\langle \delta B_{o+n}^2 \rangle}} = 4 \text{ km/s}. \tag{1}$$

Hereafter in this paper ε denotes r.m.s. value of observed velocity fluctuation δv, whereas ε_v denotes its estimate, derived using different methods described in the paper. Thus, $\varepsilon \sim 4$ km/s (which corresponds to the uncertainty of a single velocity component of $\varepsilon/\sqrt{2} \sim 2.83$ km/s) is a reasonable estimate of the amplitude of the noise on the turbulent velocity signal. We will develop this idea to obtain a general method to estimate the uncertainty direct from the data. In the next section we will compare our assessment of the velocity measurement uncertainties with the estimate derived in other studies. First, we will see how these uncertainties can affect measurements of scaling exponents and the conclusions that can be drawn from them. In Figure 2 we plot the observed second order

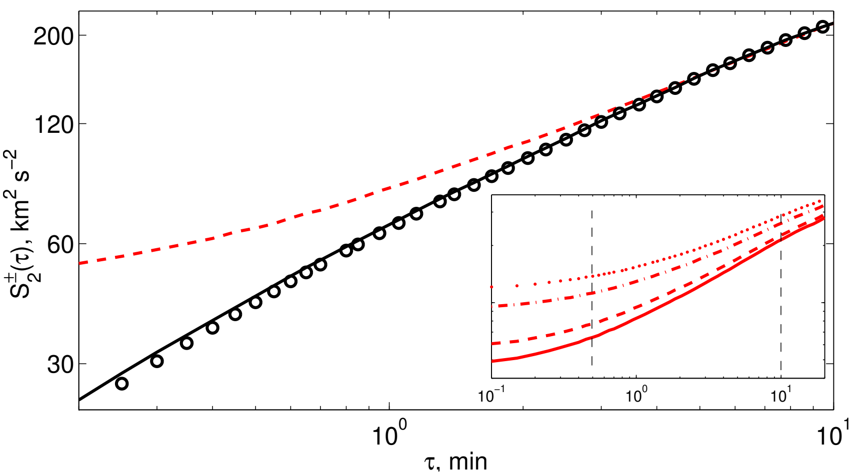

Figure 2. The normalized second order structure functions: of the GSE z component of the sub-dominant Elsasser variable Z_z^- (red dashed line), of the dominant Elsasser variable Z_z^+ (black solid line) and S_2^- (circles, see text for details). In the insert: the second order structure functions of the sub-dominant Elsasser variable for different values of added Gaussian noise. Raw observations are denoted by the solid line, and added noise is equivalent to $\varepsilon_v = 2$ km/s (dashed line), $\varepsilon_v = 4$ km/s (dash-dotted line) and $\varepsilon_v = 5$ km/s (dotted line).

structure functions S_2 of a component of the fluctuations in the Elsasser variables, where the Elsasser components are given by $\delta Z_i^{\pm}(\tau) = \delta v_i(t,\tau) \pm \delta B_i(t,\tau)/\sqrt{4\pi\bar{\rho}}$ and $\bar{\rho}(\tau)$ is the local mean value of the density averaged over the time scale of the fluctuations τ, i.e., over the interval $[t, t+\tau]$, and $S_2^{\pm} = \langle \delta Z_i^{\pm}(\tau)^2\rangle$. The solid lines are the structure functions of GSE z components of the dominant δZ_z^+ (black solid line) and subdominant δZ_z^- (red dashed line) fields. They are normalized to have the same values at $\tau = 10$ min scale on this plot; the power in δZ_z^+ is 20 times that in δZ_z^- at $\tau = 10$ min scale. For the ideal statistical scaling of fully developed MHD turbulence we anticipate the scaling $S_2 \sim \tau^{\zeta_\pm(2)}$ and turbulence theories predict constant values of $\zeta^\pm(2)$ over the entire inertial interval (they are directly related to the power spectral exponents $\gamma_\pm$ via $\gamma_\pm = -\zeta_\pm(2) - 1$). We can see that, consistent with earlier studies (e.g., Wicks et al. (2010)), the subdominant Elsasser variable does not follow a single power law in the inertial interval. A linear mean least square fit on log-log plot over scales 30 s $< \tau <$ 10 min gives $\gamma_+ = -1.54 \pm 0.02$ and $\gamma_- = -1.40 \pm 0.02$, consistent with previous observations (Bruno & Carbone, 2013, Wicks et al., 2010).

A quantitative demonstration of the effect of noise is provided by calculating $S_2^-(\delta B_{o+n}, \delta v_o) \equiv \langle \left[\delta v_{i,o} - (\delta B_{i,o} + \delta B_{i,n})/\sqrt{4\pi\bar{\rho}}\right]^2 \rangle$ which for uncorrelated noise is equivalent to $S_2^-(\delta B_o, \delta v_o) + \varepsilon_v^2$. Here a different 'Alfvénic' relation, $\varepsilon_v = \varepsilon_B/\sqrt{4\pi\bar{\rho}}$, is used to relate the velocity and magnetic field uncertainties. This is shown in the inset of Figure 2 for a range of amplitudes of δB_n, which are equivalent to velocity noise uncertainties of $\varepsilon_v = 2, 4$ and 5km/s. We can see that addition of 'white' (delta correlated) noise always systematically 'flattens' these curves, that is, it decreases the value of the scaling exponent; for $\varepsilon_v = 4$ km/s pseudo noise strongly affects S_2^- at all scales in the inertial interval. The 'flattening' of the pseudo-noisy $S_2^-(\delta B_{o+n}, \delta v_o)$ curve, that is, the change in the mean exponent over timescales 30 s $< \tau <$ 10 min is $\Delta\gamma_- \approx 0.13$, is close to the observed difference between exponents of the dominant and subdominant fields ($\gamma_- - \gamma_+ = 0.14$) hence this difference could be just due to noise in the velocity data.

We now obtain an estimate of the structure function in the absence of the noise in the velocity, $S_2^-(\delta B_o, \delta v_s) \equiv \langle (\delta Z_s^-)^2 \rangle$, where $\delta Z_s^- = \delta v_s - \delta B_o/\sqrt{4\pi\bar{\rho}}$. We have that the observed structure function $S_2^-(\delta B_o, \delta v_o) = \langle (\delta Z_s^- + \delta v_n)^2 \rangle = S_2^-(\delta B_o, \delta v_s) + 2\langle \delta Z_s^- \delta v_n \rangle + \varepsilon^2$. Assuming as before that the turbulent signal and the velocity error are uncorrelated ($\langle \delta Z_s^- \delta v_n \rangle = 0$) we obtain $S_2^-(\delta B_o, \delta v_s) = S_2^-(\delta B_o, \delta v_o) - \varepsilon^2$. The plot of our estimated $S_2^-(\delta B_o, \delta v_s)$ is given by black circles in Figure 2 for $\varepsilon = 4$ km/s. This error compensated subdominant $S_2^-(\delta B_o, \delta v_s)$ curve now has a single scaling throughout the inertial range, consistent with current theories and numerical predictions (Podesta et al., 2002). We can also see that the slope of $S_2^-(\delta B_o, \delta v_s)$ coincides quite closely with the observed slope of the dominant Elsasser variable S_2^+. The uncertainty in the velocity that we have estimated from the data is thus sufficient to account for the departure in scaling between the $\delta \mathbf{Z}^-$ and $\delta \mathbf{Z}^+$ Elsasser variables and these observations may in fact within the achievable accuracy be in agreement with theories (Podesta et al., 2002) that predict a *single scaling* for $\delta \mathbf{Z}^-$ and $\delta \mathbf{Z}^+$.

3. Conclusions

In summary, we have presented a general, instrument independent method to determine uncertainty in the velocity fluctuations in single point measurements. We have shown that this uncertainty is sufficient to account for both the absence of single scaling of the subdominant Elsasser field and for the difference of $\mathbf{Z}^\pm$ slopes in the inertial interval. Thus, our findings are able to report for the first time that the observations are, within the achievable accuracy, in agreement with the predictions of theory and numerical simulations.

Acknowledgements

This work has been supported by Shota Rustaveli National Science Foundation grant FR-18-19964.

References

Bruno R., Carbone V., 2013, Liv. Rev. Sol. Phys., 10, 2

Gogoberidze G., Chapman S. C., Hnat B., 2012a, Phys. Plasmas, 19, 102310

Gogoberidze G., Chapman S. C., Hnat B., Dunlop M. W., 2012b, MNRAS, 426, 951

Gogoberidze G., Perri S., Carbone V., 2013, ApJ, 769, 111

Gogoberidze G., Voitenko Y., Machabeli G., 2018, MNRAS, 480, 1864

Hnat B., Chapman S. C., Gogoberidze G., Wicks R. T., 2011, PRE, 84, 065401

Podesta J. J., Chandran B. D. J., Bhattacharjee A., Roberts D. A., Goldstein M. L., 2002, GRL, 29, 1839

Turner A. J., Gogoberidze G., Chapman S. C., 2012, PRL, 108, 085001

Wicks R. T., Horbury T. S., Chen C. H. S., ZastenkerSchekochihin A. A., 2010, MNRAS, 407, L31

M giants foundin the First Byurakan Spectral Sky data base. V. Gaia DR2 data.

Gigoyan K.S.*

V .A. Ambartsumian Byurakan Astrophysical Observatory, Armenia

Abstract

In this paper we study bright M–type giants found in the First Byurakan Survey (FBS) low-resolution (lr) spectroscopic data base. Phase dependence light-curves from large sky area variability data bases such as Catalina Sky Survey (CSS) and All-Sky Automated Survey for Supernovae (ASAS-SN), and the second Gaia data release data (Gaia DR2) high-quality photometric data are analyzed to estimate some important physical parameters for 1096 M-type giants found at high Galactic latitudes. Their Gaia DR2 broad-band G magnitudes are in the range 8.0 < G < 16.0 mag. Gaia DR2 radial velocities (RV) are available for 134 and luminosities for 158 stars out of 1096. The Gaia DR2 color–absolute magnitude diagram (CaMD), their Galactic distribution, also some other diagrams based on Gaia DR2 photometric data are presented. Absolute magnitudes cover the range +1.0 ≤ M(G)≤ -5.4 mag. They follow to the behaviors and occupy the same regions on the color-magnitude diagrams studied in many papers by different researches for long period variables (LPVs). Particularly, we consider the locations of the FBS giants on the new diagrams, using multi-band approaches in combination with Wesenheit functions, obtained recently by Lebzelter and colleagues (2018) for the oxygen-rich (O-rich) and carbon-rich (C-rich) LPVs in the Large Magellanic Cloud. Period-Luminosity (P-L) diagram was presented for 112 M Mira-variables. The upper limit of the initial stellar masses can be estimate near 5 $M_\odot$ for M giants according to the new diagnostic tools. The kinematic properties, space distribution also more interesting cases among the sample were considered.

Keywords: *Late-type stars: Astronomical data bases-Surveys.*

1. Introduction

The First Byurakan Survey (FBS), known also as the Markarian survey, was the first systematic objective-prism survey of the extragalactic sky. This survey was conducted by B. E. Markarian and collaborators from 1965 to 1980. The photographic plates were obtained at the Byurakan Astrophysical Observatory (BAO) using the 1-m Schmidt telescope, equipped with a 1.5^o prism, giving a reciprocal dispersion of 1800 Å/mm near H_γ throughout a useful field of $4° \times 4°$. FBS is large -area low-resolution (lr) spectral survey, covering a total of 17.000 deg^2. It is segmented into 28 parallel zones on all the Northern sky and part of the Southern sky at high Galactic latitudes with $\delta >$ -15° and |b| >15°. The limiting magnitude is 17.5-18.0 mag. in the photographic bandpass. Various Kodak emulsions were used during the observations (IIF, IIAF, IIaF, and 103aF), providing a spectral range of 3400-6900 $\AA$ (with a 70 $\AA$ - wide sensitivity gap at 5300 $\AA$), and spectral resolution of R = 96 near H_γ. The FBS was originally conducted to search for galaxies with an ultraviolet excess (UVX; Markarian, 1967). In total, 1515 UVX galaxies (Markarian galaxies) had been discovered, including many AGN, Starburst and Seyfert galaxies (Markarian et al., 1989). The discovery of UVX galaxies by Markarian and collaborators was the first and most important work based on the FBS spectroscopic plates. Several other interesting projects based on the FBS were started in 1987 (known as a second part of the FBS, Abrahamian & Mickaelian (1996)), which resulted in the discovery of new bright quasi-stellar objects (QSOs), Seyferts, white dwarfs (WDs), subdwarfs (sds), planetary nebula nuclei (PNNs), cataclysmic variables (CVs), and other interesting objects (Mickaelian, 2008).

DOI: 10.52526/25792776-2020.67.2-198

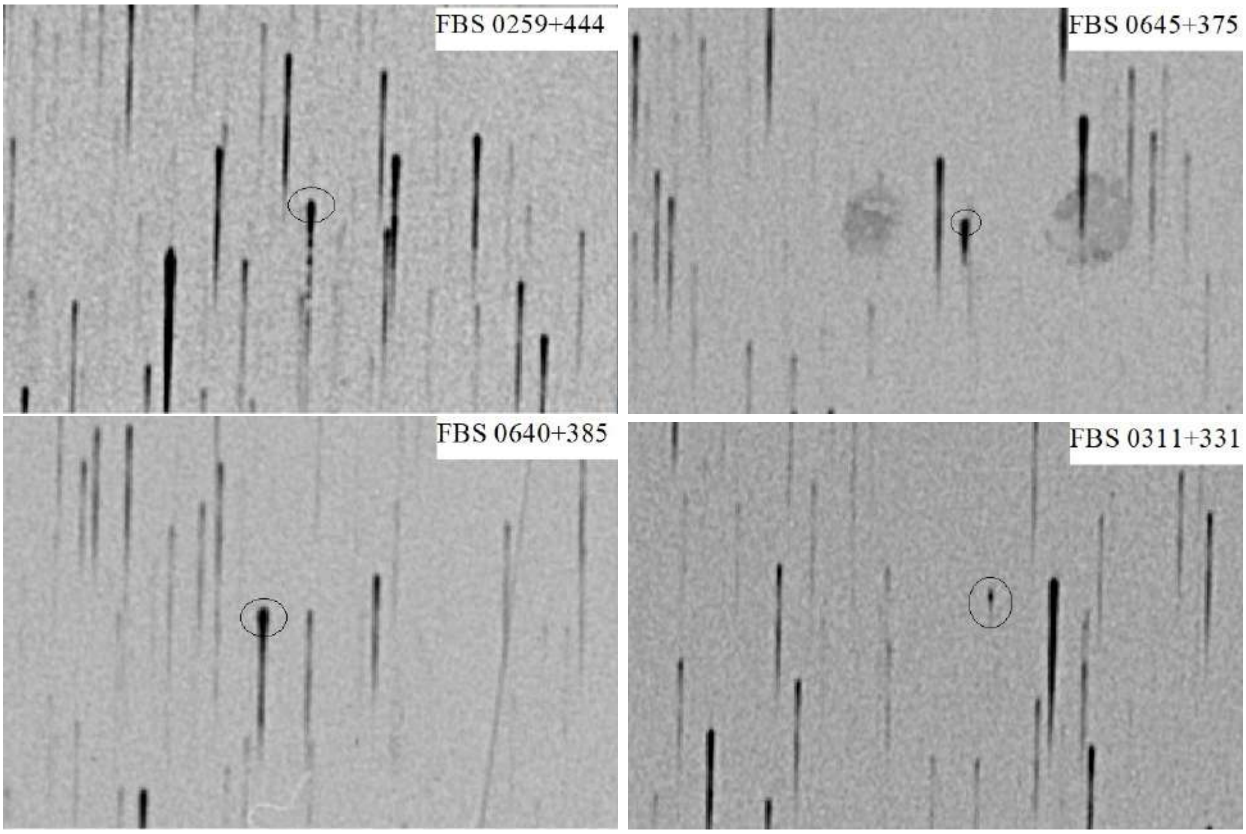

Figure 1. FBS lr spectral shapes for M and C stars

The second part of the FBS also included the selection, cataloguing and study of faint late-type stars (LTSs) at high Galactic latitudes. The large spectral range of the FBS is also suited to identify M-type and carbon (C)-stars. C stars can be identified through the presence of the Swan bands of the C_2 molecule (4383, 4737, 5165, and 5636 $\AA$), M-type spectra can easily be separated thanks to titanium oxide (TiO) molecular absorption bands (4584, 4762, 4954, 5167, 5448, 5862, 6159, and 6700 $\AA$). Since 2007 all FBS lr plates have been digitized, resulting in the creation of the Digitized First Byurakan Survey (DFBS) database (Mickaelian et al., 2007), for details see the web sites at http://www.ia2-byurakan.oats.inaf.it/ and http://www.aras.am/Dfbs/dfbs.html/). Figure 1 presents the FBS lr spectral shapes for early and late subclasses of the C and M stars. All DFBS plates were analyzed with the help of standard image analysis softwares. The sec- ond version of the "Revised And Updated Catalogue of the First Byurakan Survey of Late-Type Stars", containing data for 1471 LTSs (130 C-type stars, 235 M dwarfs, and 1096 M-type giants, was generated (Gigoyan et al. (2019), SIMBAD Vizier catalogue J/MNRAS/489/2030/catv2).

2. Optical Spectroscopy

For FBS LTSs, medium-resolution CCD spectra were obtained at different epochs with the BAO (Armenia) 2.6-m telescope (UAGS, ByuFOSC2 and SCORPIO spectrographs), moderate – and high-resolution CCD spectroscopy obtained with the Observatory de Haute-Provence (OHP, France) 1.93-m telescope (CARELEC spectrograph). For some FBS LTSs medium-resolution CCD spectra also were obtained with the Cima-Ekar 1.83-m telescope of the Padova Astronomical Observatory (Italy) equipped with the Asiago Faint Objects Spectrometer and Camera (AFOSC), and with the 1.52-m Cassini telescope of the Bologna Astronomical Observatory at Loiano (Italy) equipped with the Bologna Faint Objects Spectrometer and Camera (BFOSC; Gigoyan et al., 2019).

Figure 2 presents the 2.6-m BAO telescope moderate-resolution CCD spectra in the range 4000-7250 Å for some amount FBS LTSs.

*kgigoyan@bao.sci.am

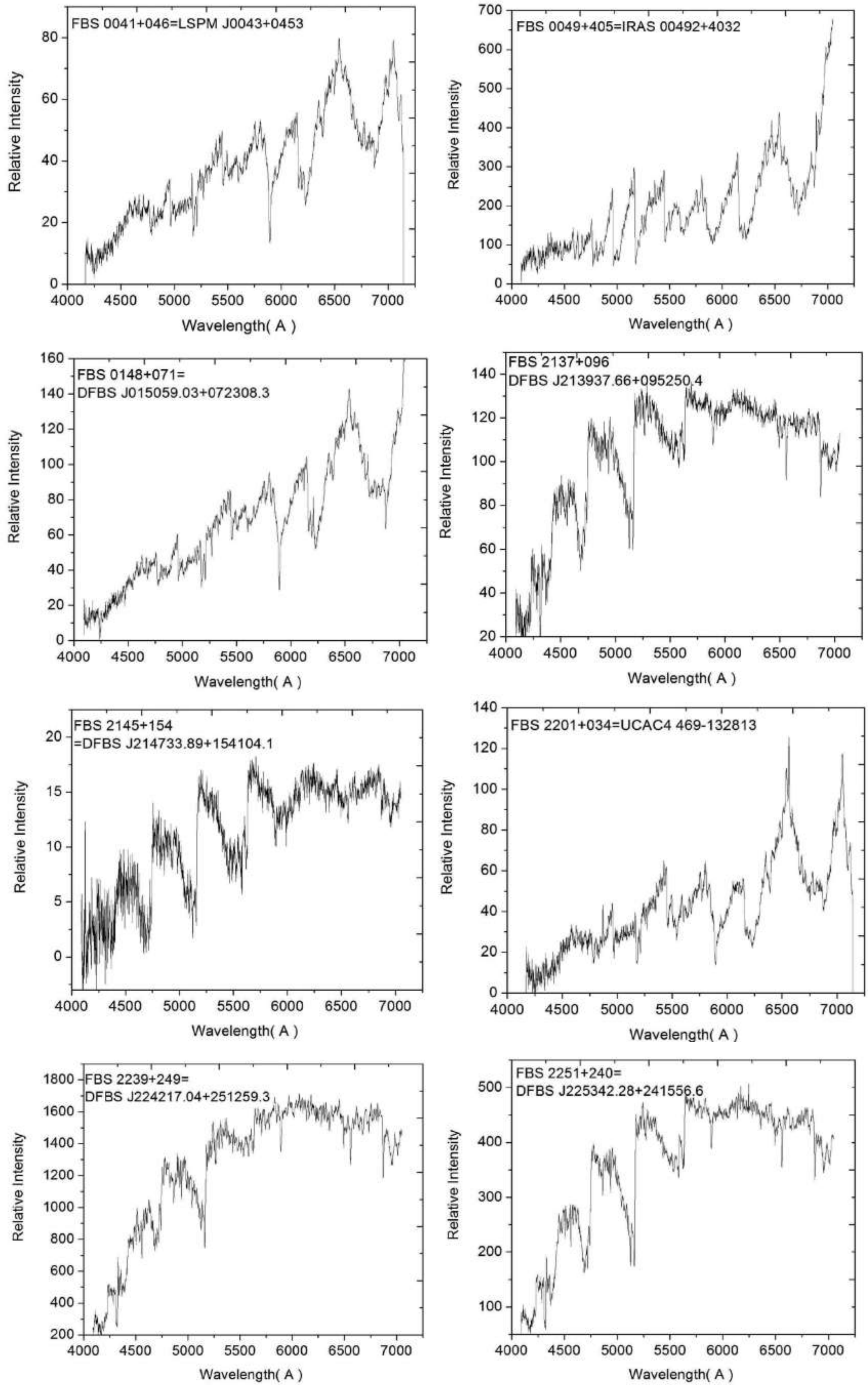

Figure 2. Figure 2. 2.6-m BAO telescope moderate-resolution CCD spectra for some FBS LTSs.

Moderate-resolution CCD spectra for more than 300 FBS LTS were sequred by LAMOST (Large Sky Area Multi-Object Fiber Spectroscopic Telescope) observations (LAMOST DR5; Luo et al., 2019),

Table 1. *Gaia* DR2 data for a sample of the FBS M giants.

FBS number	Var type	G mag (mag)	BP-RP color (mag)	T_{eff} (K)	Luminosity (solar units)	Other Association
0001+340	L	10.31	3.38	3304	340.28	
0212+858	SR	11.83	2.44	3615	999.79	
0519+021	SR	11.21	3.31	3306	139.47	
1014+819	SR	10.15	2.82	3529	1357.73	IRAS 10147+8159
1201+850	L	10.65	3.03	3297	1100.97	IRAS F12019+8503
1306+385	SR	10.06	3.30	3306	2024.77	NSVS 5041274
1454-069	SR	9.87	3.10	3302	388.26	IRAS 14544-0657
1737+428	SR	11.83	3.44	3670	319.70	ROTSE J173832.72+425112.8
1757+194	Mira	8.07	2.92	3304	927.80	IRAS 17575+1929
2147+023	SR	9.19	4.10	3326	761.05	IRAS 21465+0220

spectra available on-line at http://dr5.lamost.org/search/. The O-rich nature could be confirmed for the big part of the FBS M -giants.

3. Variability.

To determine the variability of the FBS M type giants, we exploit data from two primary sources, namely the Catalina Sky Survey (CSS, second public data release CSDR2, accessed via http://nesssi.cacr.caltech.edu/DataRelease/ (Drake et al., 2014, 2017) and the All-Sky Automated Survey for Supernovae ASAS-SN (accessed via https://asas-sn.usu.edu/variables). ASAS-SN is the first ground-based survey to monitor the entire visible sky to a depth of V $\leq$ 17.0 mag on a regular basis. As a consequence, ASAS-SN was used as the primary source for attributing variability types, periods, and amplitudes to the FBS M giants. Our final sample consist of 690 Semi-Regular (SR)-type, 294 L-type and 112 Mira-type variables.

Figure 3 presents phased ASAS-SN light curves for three FBS M-giants.

4. Gaia DR2 Data

With the advent of Gaia mission (Gaia Collaboration; Prusti et al., 2016) a new era in the astronomical research has started. The Gaia DR2 database containing astrometry, three-band photometry, radial velocities, effective temperatures, and information on astrophysical parameter and variability for approximately 1.7 billion sources brighter than G = 21.0 magnitude (Brown et al., 2018). This database opens a new area for investigations based on the Hertzsprung-Russell diagram (HRD).

All FBS M giants were cross-matched with the Gaia DR2 catalogue sources. The cross-match was carried out using a 5 arcsec aperture around the position of each of our sample stars. They are relatively bright, so that G − band brightnesses were in the range 8.0 mag < G < 16.0 mag, effective temperatures lay between 3200 K < T_{eff} < 4300 K.

4.1. Colors and Luminosities

The radii and luminosities (in Solar units) of 158 M giants of our sample (out of 1096) can be deduced from the Gaia DR2 data base. Luminosities of our target stars range between L=28.039$L_\odot$ (FBS 0255+193 = LAMOST J025756.28+193228.5, M1 star) and L = 2024.777$L_\odot$ (FBS 1306+385=LAMOST J130829.62+381801.4=IRAS 13061+3834, M6 subtype SR-variable). We computed the absolute V-band magnitudes for these objects, adopting that M_V = +4.81 mag for the Sun (see Table 3 in Andrae et al. 2018, for more details), resulting in an absolute V-magnitude range between M_V = +1.1 and M_V = -3.5. A representative sample table with Gaia DR2 data is given as Table 1.

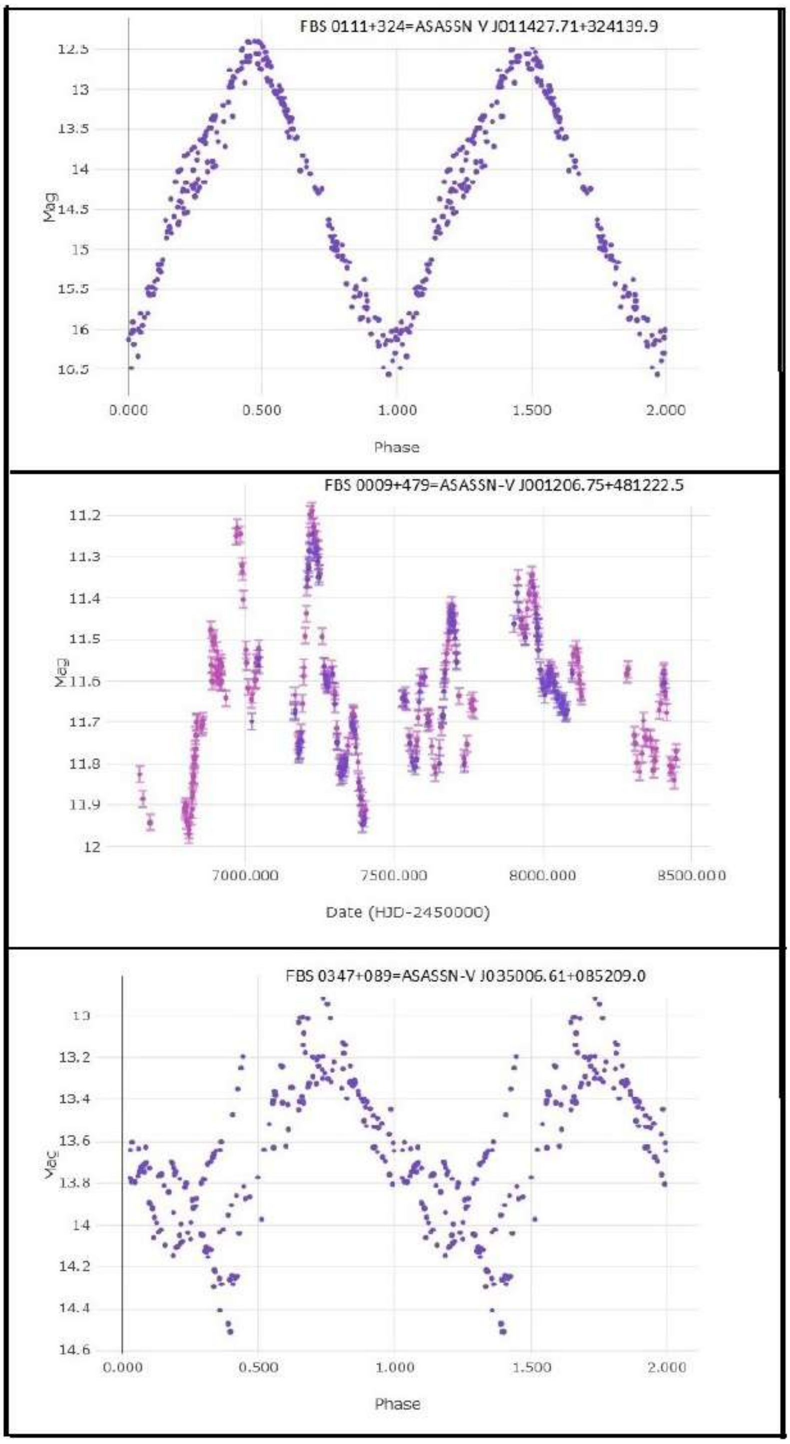

Figure 3. ASAS-SN Phased light curves for FBS 0111+324, FBS 0009+479, and FBS 0347+089, classified consequently as a Mira, SR, and L -type variables.

Figure 4 present the Gaia DR2 color-absolute magnitude (CaMD) diagram for 158 FBS M giants, with available luminosity value in Gaia DR2 data base.

Figure 4. Gaia color-absolute magnitude (MV vs. BP-RP) diagram of FBS M giants with available luminosity data in Gaia DR2 data base. Symbols are: blur circle - SR variables, green square - L variables, and red triangle – Mira - type variables.

We follow the paper by Lebzelter et al. (2018). We use also the distance information derived from Gaia DR2 by Bailer-Jones et al. (2018) (Gaia Collaboration, SIMBAD CDS VizieR catalogue I/347/gaia2dis) to plot the CaMD for FBS M giants.

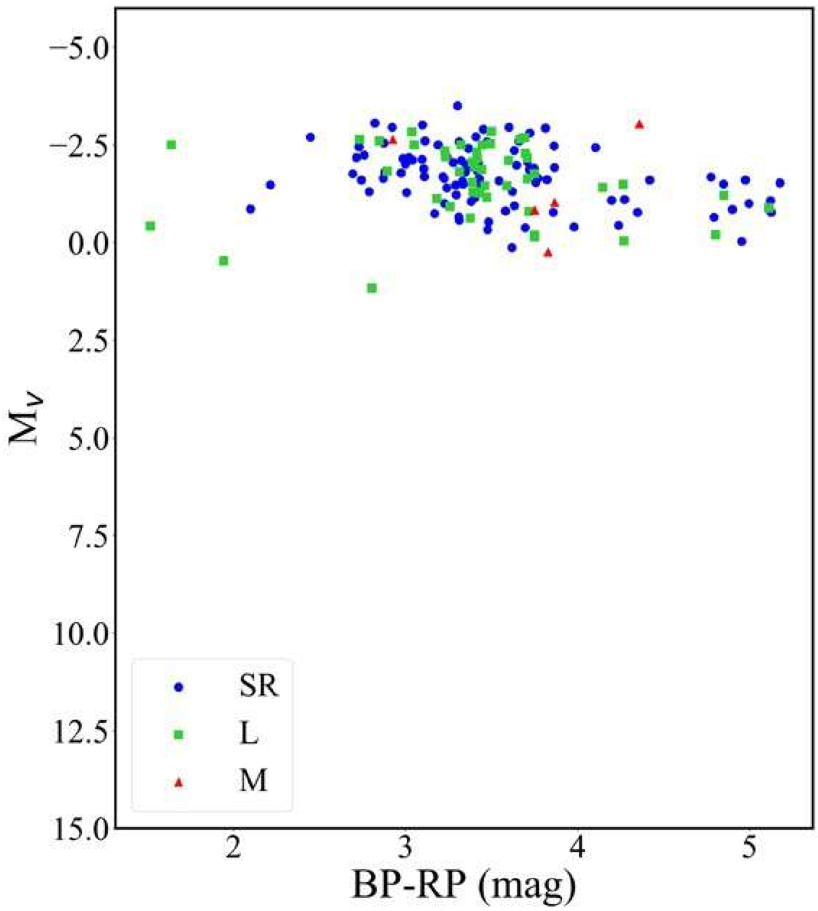

Figure 4. Gaia color-absolute magnitude (M_V vs. BP-RP) diagram of FBS M giants with available luminosity data in Gaia DR2 data base. Symbols are: blur circle - SR variables, green square - L variables, and red triangle – Mira - type variables.

5. 2MASS Colors

Figure 5 presents the 2MASS J- H versus H – Ks color – color diagram for FBS M stars. In the color – color diagram, objects having J – H > 0.8 and H – Ks > 0.2 are usually giants or asymptotic giant branch (AGB) stars (Bessell & Brett, 1988).

6. Discussion And Conclusion.

We explored the sample of 1096 relatively bright, spectroscopically confirmed M -giants. For this study, we cross-correlated our sample with the data bases from Gaia DR2, the Catalina Sky Survey (CSS), 2MASS, and All-Sky Automated Survey for Supernovae (ASAS-SN). Their Gaia DR2 broad-band G magnitudes are in the range 8.0 < G < 16.0 mag. Gaia DR2 radial velocities (RV) are available for 134 and luminosities for 158 stars out of 1096.

Acknowledgements

This research was made possible through the use of the ASAS-SN and Catalina Sky Survey variability data bases. We used the LAMOST telescope spectra. The LAMOST is a National Major Scientific project build by the Chinese Academy of Sciences. This work has made use of data from the European Space Agency (ESA) mission Gaia (https://cosmos.esa.int/gaia).

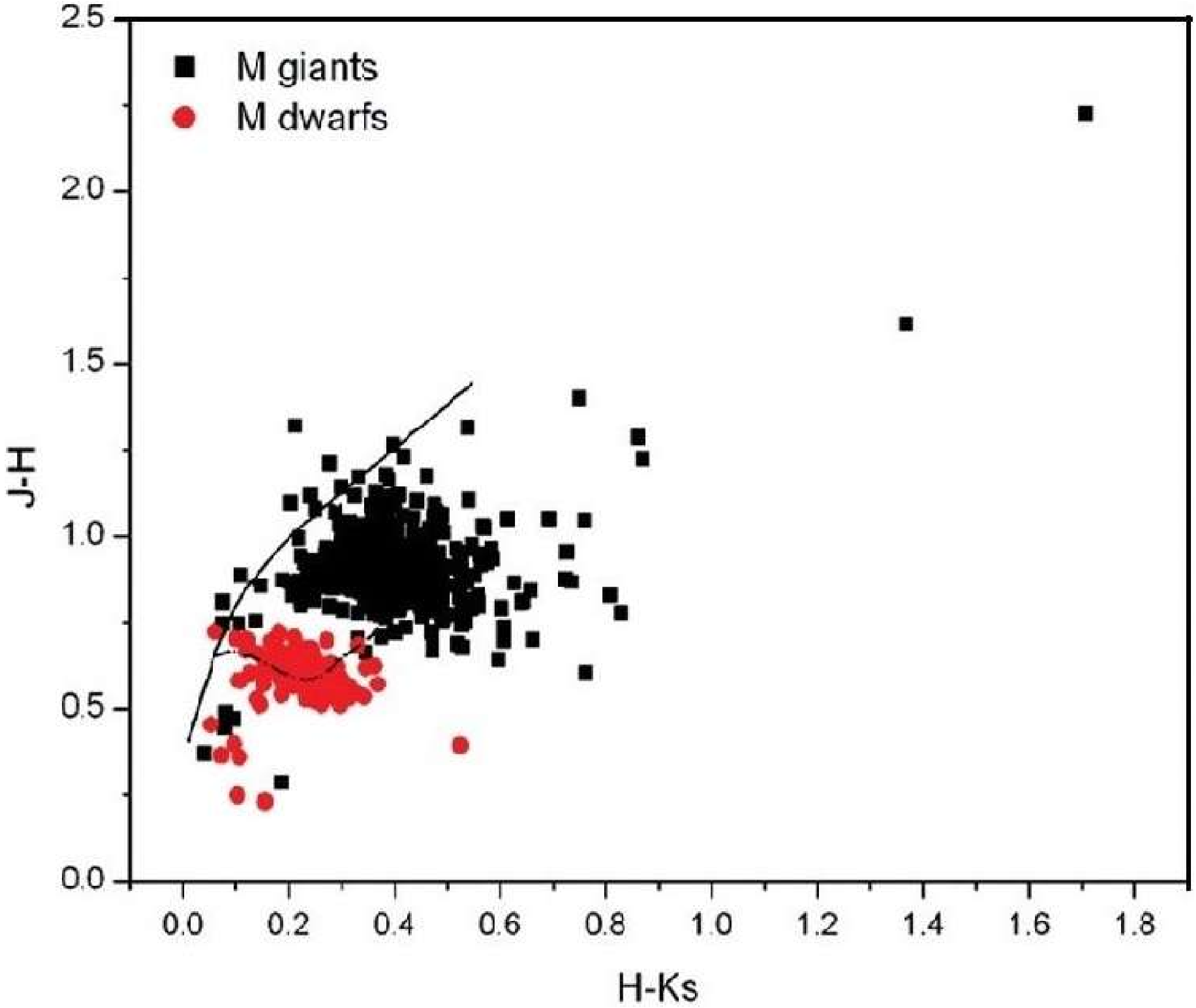

Figure 5. The 2MASS J-H versus H-Ks color-color diagram for FBS M giants. We present also on this diagram a some amount M dwarfs also for comparison. The solid line shows the M -giant equence and the dashed line with dots denotes the M-dwarf sequence (for more details, see Bessell & Brett (1988)

References

Abrahamian H. V., Mickaelian A. M., 1996, Astrophysics, 39, 315

Bailer-Jones C. A. L., Rybizki J., Andrae R., Fouesneau M., 2018, A&A, 616, A37

Bessell M. S., Brett J. M., 1988, PASP, 100, 1134

Brown A. G. A., et al., 2018, Astron. Astrophys. , 616, A1

Drake A. J., et al., 2014, Astrophys. J. Suppl. Ser. , 213, 9

Drake A. J., et al., 2017, Mon. Not. R. Astron. Soc. , 469, 3688

Gigoyan K. S., Mickaelian A. M., 2012, MNRAS, 419, 3346

Gigoyan K. S., Russeil D., Mickaelian A. M., Sarkissian A., Avtandilyan M. G., 2012, A&A, 544, A95

Gigoyan K. S., Mickaelian A. M., Kostandyan G. R., 2019, MNRAS, 489, 2030

Lebzelter T., Mowlavi N., Marigo P., Pastorelli G., Trabucchi M., Wood P. R., Lecoeur-Taïbi I., 2018, Astron. Astrophys. , 616, L13

Luo A. L., Zhao Y. H., Zhao G., et al. 2019, VizieR Online Data Catalog, p. V/164

Markarian B. E., 1967, Astrofizika, 3, 55

Markarian B. E., Lipovetsky V. A., Stepanian J. A., Erastova L. K., Shapovalova A. I., 1989, Soobshcheniya Spetsial'noj Astrofizicheskoj Observatorii, 62, 5

Mickaelian A. M., 2008, AJ, 136, 946

Mickaelian A. M., et al., 2007, Astron. Astrophys. , 464, 1177

Prusti T., et al., 2016, Astron. Astrophys. , 595, A1

Shappee B. J., Prieto J. L., Grupe D., Kochanek C. S., Stanek K. Z.and Walker Z., Yoon Y., 2014, Astrophys. J. , 788, 48

Investigation of faint galactic carbon stars from the First Byurakan Spectral Sky Survey. IV. GAIA DR2 data.

Kostandyan G. R.*

V .A. Ambartsumian Byurakan Astrophysical Observatory, Armenia

Abstract

The second Gaia data release (Gaia DR2) data are used to analyze and estimate a some important parameters for 127 carbon (C) type stars (56 are late N – type Asymptotic Giant Branch (AGB) C stars, 71 are early – type CH giants) detected on the First Byurakan Spectral Sky Survey (FBS) low – resolution (lr) spectral plates. Gaia DR2 G broad band magnitudes are in the range 9.4 mag < G < 18.2 mag. for FBS C stars. Radial velocities (RV) is available for 75 C stars out of 127. For 9 objects RV is greater than 200 km/s. Absolute magnitudes in V band are estimated for 18 FBS C stars, having luminosity data, from which 17 are CH giants. They are in the range between -3.5 ≤ M_V < +0.5 mag. For FBS 1918+869 absolute magnitude M_V = -3.4(±0.2) mag, which is typical for N type AGB C stars. Having distance estimations, the Hertzsprung – Russell diagram (HRD, or color – absolute magnitude diagram) was constructed for C stars. All FBS detected C stars are giants and AGB stars in the Galactic Halo. They are not far than 14 kpc from the Sun and 8 kpc from the Galactic plane.

Keywords: *carbon stars: surveys: late – type stars*

1. Introduction

The First Byurakan Survey (FBS, known also as a Markarian survey) is an objective – prism low – resolution (lr) survey. It is performed with the Byurakan Observatory 1 m Schmidt telescope, which covers about 17.000 sq. deg. of the Northern sky and part of the Southern sky at high Galactic latitudes defined by δ > -15^o and IbI > 15^o. The FBS was originally conducted for galaxies with ultraviolet excess (UVX, Markarian et al., 1989). Since 1990s, the lr plates of the FBS was used to select comparatively faint (fainter than 12 mag. in visual) late – type stars (LTS, M and carbon (C) stars) at high latitudes. The large spectral range of the FBS (λ 3400 – 6900 Å) is well suited to identify cool M – type or C – type stars. C stars can be identified through the presence of Swan bands of C_2 molecule at 4737, 5165, and 5636 $\AA$ (N – type C stars). Several objects showing the C_2 band-head at 4382 Å are early – type C stars (R or CH type stars). M – type stars can easily be distinguished because of the titanium oxide (TiO) molecule absorption bands at 4584, 4762, 4954, 5167, 5500 and 6200 $\AA$ (Gigoyan & Mickaelian, 2012). The eye – piece search (with magnification 15x) near 2000 FBS lr plates resulted to discovery 1045 new LTS. On the base of this selection the “Revised And Updated Catalogue of the First Byurakan Survey of LTS” was generated (Gigoyan & Mickaelian, 2012). Now the entire plate set of the FBS has been digitized (1874 plates for 1139 fields) leading to the Digitized First Byurakan Survey (DFBS) (Mickaelian et al., 2007) (online at http://byurakan.phys.uniroma.it or http://www.ia2-byurakan.oats.it /). Later, all DFBS lr spectral plates are analysed with help of standard image analysis Softwares (FITSView and SAOImage ds9). The advantages using these Softwares for selecting faint LTS on DFBS plates are described more detail in Gigoyan et al. (2012). “The Second Revised And Updated Version of the FBS LTS Catalogue”, containing comprehensive data for 1471 new objects, is available at CDS, SIMBAD VizieR data base (Gigoyan et al., 2019).

*kgayane@gmail.com

DOI: 10.52526/25792776-2020.67.2-206

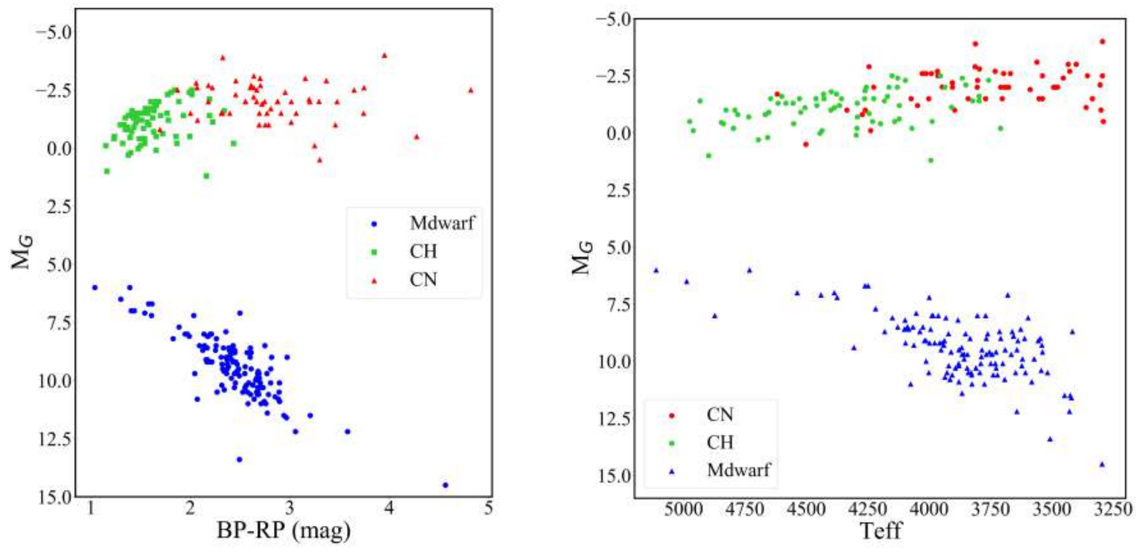

Figure 1. Hertzsprung – Russell diagramms for 127 FBS C stars

The goal of this paper is further exploitation of the Gaia Data Release 2 (DR2) (Gaia Collaboration et al., 2018) high accurate photometric and astrometric data, also the distance estimations, presented in catalogue of Bailer-Jones et al. (2018b), to estimate important parameters, such as absolute magnitudes and distribution in our Galaxy for carbon stars, selected on the lr FBS survey plates, and presented in the "Second and Updated Version of the FBS Late-Type Stars Catalogue (Gigoyan et al., 2019).

In Section 2 we describe Gaia DR2 data for FBS Carbon stars and some important physical parameter estimations. We discuss in Section 3 their Galactic distribution. Finally we conclude in Section 4.

2. FBS carbon stars. Gaia DR2 data and some important parameters

Gaia second data release (DR2), consists astrometry, photometry, radial velocities, effective temperatures, information on astrophysical parameters and variability, for sources brighter than G = 21.0 magnitude (approximately 1.7 billion sources, Gaia Collaboration et al., 2018). All FBS discovered C stars was cross - correlated with the Gaia DR2 catalogue sources (SIMBAD CDS VizieR Catalog I/345/gaia2). The search was made in catalogue with a search radius 5″ around their position. Their G broad – band photometric data values is in the range 9.4 mag. $<$ G $<$ 18.2 mag., and effective temperatures between 3291.00 K $<$ Teff $<$ 5000 K.

2.1. Colours, luminosities, and other characteristics

In Gaia DR2 data base the radiuses and luminosities (in Solar units)is presented for 18 FBS C stars only (out of 127). We estimate the absolute magnitudes (in V – band) for 18 objects adopting that $M_{V\odot} = +4.81$ mag for Sun. Figure 1 show positions on colour – absolute MG magnitude (Gaia DR2 G – band absolute magnitude) and T_{eff} versus absolute magnitude (Hertzsprung – Russell) diagram for 127 FBS C stars, also for near 150 M dwarfs from the "FBS Late – Type Stars Catalogue" (Gigoyan et al., 2019). All N - type AGB stars are distributed in the brightest region, where Long – Period Variables (Miras, Semi – Regular variables, slow irregular variables, and small – amplitude red giant) are located and Figure 2 and 3 by Gaia Collaboration et al. (2019). Absolute G – band magnitude was estimated via the usual equation (Gaia Collaboration et al., 2019):

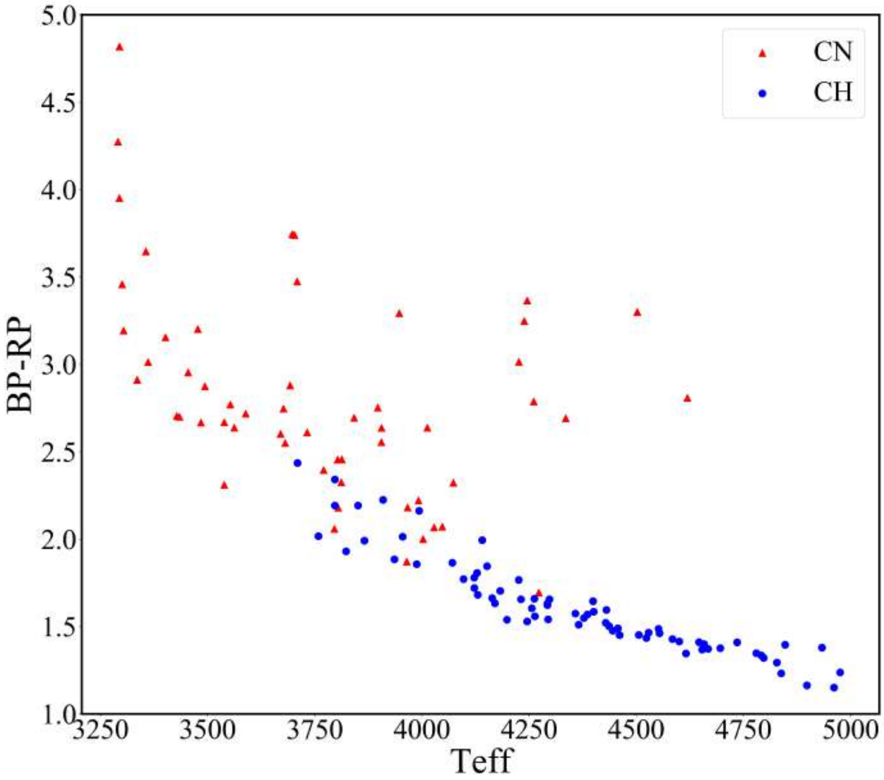

Figure 2. Gaia DR2 color – temperature relation for 127 FBS C stars.

$$M_G = G - 5Logr + 5 - A_G, \tag{1}$$

As we can see, FBS C stars occupy region on the HR diagram, where red giants and AGB stars are located. Figure 2 shows Gaia DR2 color – temperature relation for 127 FBS C stars. 11 N – type AGB stars are far from the line of distribution of stars. For all of them 2MASS (Two Micron All – Sky Survey, Skrutskie et al., 2006) J – K_S > 2.5 mag. Most probably there are thick gas-dust envelopes around these stars. Based on K- [12] and J – K colors indices mass-loss rates were estimated for 3 of them (Gigoyan et al., 2017). Three out of 11 N – type AGB stars show double – peaked SED Gigoyan et al. (2017), indicating the existence of the envelopes around them. We note also, that the effective temperatures, determined from the photometric data for CH – type FBS C stars (Gigoyan et al., 2015), are in the range of uncertainties, which gives Gaia DR2 catalogue (SIMBAD VizieR Catalog I/345/gaia2, Gaia Collaboration et al., 2018).

3. Distances

Distance estimations for all detected FBS C stars is presented in catalogue by Bailer-Jones et al. (2018a), which is based on Gaia DR2 parallaxes. In this catalogue distance estimation for more than 1.33 billion stars are reported. In the first paper of this series (Gigoyan et al., 2014) distances are estimated based on revised Period - Luminosity (PL) relations for N – type AGB C stars. According to Bailer-Jones catalogue data, the distances are in the range 735.64 pc < d < 14133.43 pc (FBS 0018+213, L = 82.779 $L_\odot$, RV = -13.87 (±1.54) km/s, and FBS 1811+462, RV = -164.8 (±0.65) km/s). Both stars are CH – giants. The hight (Z) above Galactic plane for FBS 0018+213 is ≈ 480 pc, and for FBS 1811+462 is ≈ 6.1 kpc consequently.

Figure 3 shows spatial distribution (Galactic longitude versus Galactic latitude) for all FBS C stars. Very little tendency is observable for CH giants distribution at high Galactic region.

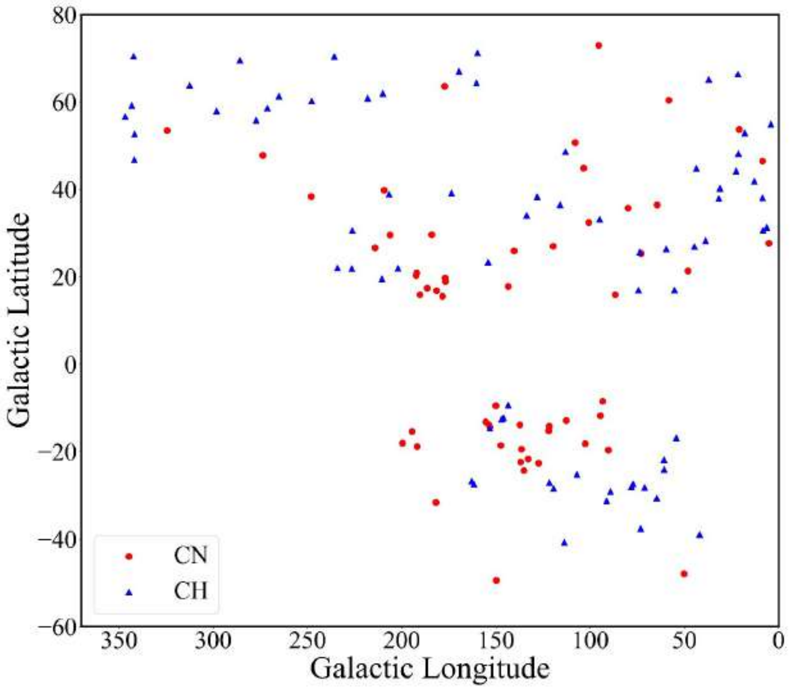

Figure 3. Spatial distribution for 127 FBS C stars.

4. Discussion and conclusion

Carbon stars, are excellent kinematics tracers of galaxies. They can also be served as visible standard candles for galaxies. Meanwhile, many problems remain not solved with this classes of objects, particularly estimation of absolute magnitudes for early – type of C stars, which are warm objects(R – type stars, CH- giants, and dwarf Carbon stars (dC)). Late N – type carbon stars are cool and luminous AGB stars and they follow Period–Luminosity (PL) relations. In this paper, the second Gaia Data Release 2 (DR2) high-precision astrometric and photometric data together with the CSS data base are used to analyse and estimate some very important physical characteristics for a limited number of carbon stars, discovered on the FBS plates, with a goal to clarify the nature of this objects at high latitudes. We study 127 FBS C stars from the light of Gaia, from which 56 are N – type AGB stars and 71 are CH – type giants. Having distance estimations, the Hertzsprung – Russell diagram (HRD, or color – absolute magnitude diagram) was constructed for C stars. All FBS detected C stars are giants and AGB stars in the Galactic Halo. They are not far than 14 kpc from the Sun and 8 kpc from the Galactic plane. Their Gaia DR2 G broad – band absolute magnitudes are estimated which is the range +1.0 $\leq$ G $\leq$ -4.0 mag. For 18 FBS C stars absolute V – band magnitudes are estimated, having luminosities in DR2 data base, from which 17 are CH giants. They are in the range between -3.45($\pm$0.2) $\leq$ M_V $<$ +0.5($\pm$0.1) mag. For FBS 1918+869 absolute magnitude M_V = -3.4($\pm$0.2)mag, which is typical for N – type AGB C stars. Radial velocities is available for 75 C stars out of 127. For 9 objects RV values is greater than 200 km/s. These stars are supplements to the objects with high radial velocity data discovered recently based on Gaia DR2 data base. We note that all these objects are Galactic Halo objects and they do not trace the Sagittarius (Sgr) dwarf spheroidal galaxy streams and their origin is unclear.

Meanwhile, it is worth to mention three FBS CH type giants among the 127 FBS C stars, for which

Bailer-Jones catalogue gives distances more than 13 kpc from the Sun. They are FBS 1629+156(r =13.04 kpc,), FBS 1811+462(r = 14.133 kpc, RV = -164.8 km/s), and FBS 1454+792 (r = 13.487 kpc, RV = -217.9 km/s). According to the Figure 15 in Huxor & Grebel (2015) the star FBS 1454+792 and FBS 1811+462 can be originated from the Sgr leading arm.

For FBS 1629+156 there are no RV information in Gaia DR2 data base. The object FBS 1811+462 show CSS phase-dependence light curve, which is typical for RS CVn type variable stars. In NSVS (Northern Sky Variability Survey, http://skydot.lanl.gov/) data base the object FBS 1629+156 can be also classified as RS CVn variable with amplitude $\triangle m \approx 0.4$ mag. In CSS data base this object do not show significant variability. Concerning to objects FBS 1454+792, this object is out of the CSS field and in NSVS data base do not show any variability.

We note also, that many – sided investigations which is based on Gaia DR2 for M – type giants and dwarfs from the 'Second Revised and Updated Catalogue Of the FBS LTS" is in progress and will be submitted for publication very soon.

References

Bailer-Jones C. A. L., Rybizki J., Fouesneau M., Mantelet G., Andrae R., 2018a, VizieR Online Data Catalog, p. I/347

Bailer-Jones C. A. L., Rybizki J., Andrae R., Fouesneau M., 2018b, A&A, 616, A37

Gaia Collaboration et al., 2018, A&A, 616, A1

Gaia Collaboration et al., 2019, A&A, 623, A110

Gigoyan K. S., Mickaelian A. M., 2012, MNRAS, 419, 3346

Gigoyan K. S., Russeil D., Mickaelian A. M., Sarkissian A., Avtandilyan M. G., 2012, A&A, 544, A95

Gigoyan K. S., Sarkissian A., Russeil D., Mauron N., Kostandyan G., Vartanian R., Abrahamyan H. V., Paronyan G. M., 2014, Astrophysics, 57, 510

Gigoyan K. S., Sarkissian A., Russeil D., Mauron N., Kostandyan G., Vartanian R., Abrahamyan H. V., Paronyan G. M., 2015, Astrophysics, 58, 369

Gigoyan K. S., Sarkissian A., Rossi C., Russeil D., Kostandyan G., Calabresi M., Zamkotsian F., Meftah M., 2017, Astrophysics, 60, 70

Gigoyan K. S., Mickaelian A. M., Kostandyan G. R., 2019, MNRAS, 489, 2030

Huxor A. P., Grebel E. K., 2015, MNRAS, 453, 2653

Markarian B. E., Lipovetsky V. A., Stepanian J. A., Erastova L. K., Shapovalova A. I., 1989, Soobshcheniya Spetsial'noj Astrofizicheskoj Observatorii, 62, 5

Mickaelian A. M., et al., 2007, A&A, 464, 1177

Skrutskie M. F., et al., 2006, AJ, 131, 1163

Communications of BAO, Vol. 67, Issue 2, 2020, pp. 211-218

Stellar population in two star-forming regions

N. Azatyan*, E. Nikoghosyan, H. Harutyunian, D. Baghdasaryan, and D. Andreasyan

Byurakan Astrophysical Observatory, 0213, Aragatsotn prov., Armenia

Abstract

Our research focuses on the stellar content of two star-forming regions. The first one is the molecular cloud which includes G45.12+0.13 and G45.07+0.13 UC HII regions around IRAS 19111+1048 and 19110+1045 sources, respectively. Based on infrared photometric data, we identified a rich stellar population, which includes 909 YSOs with different evolutionary stages. Among selected YSOs there are ZAMS objects. The second one is an elongated molecular cloud, which includes IRAS 05184+3635, 05177+3636, 05168+3634, 05162+3639, and 05156+3643 sources. We identified 1224 candidates of YSOs in the molecular cloud with different evolutionary stages. Selected YSOs are mostly younger then 0.1 Myr. The distribution of selected YSOs in both star-forming regions shows that there are dense clusters in the vicinity of all IRAS sources.

Keywords: *stars: pre-main sequence – stars: luminosity function – infrared: stars – radiative transfer*

1. Introduction

Presently, it is generally recognized that the stellar content of our Galaxy forms in clusters located within cold (T ~10-30 K) and dense ($n > 10^3$ cm^{-3}) giant molecular clouds (GMC) of the Galactic disk (e.g. Blitz, 1991, Lada & Lada, 2003). Therefore, the main properties of the stellar population in the embedded young clusters, such as the density distribution, the age and age spread, the star formation efficiency (SFE), and the shape of the initial mass function (IMF) might be very well closely related to the physical properties and mass distribution of the progenitor structures in the parental cloud (e.g. McKee & Ostriker, 2007). The development of sensitive, large-format imaging arrays at near- and mid-infrared (NIR and MIR), submillimeter, and radio wavelengths has made it possible to obtain statistically significant and complete sampling of young embedded clusters within molecular clouds.

In this paper, we present results of the NIR, MIR and far-infrared (FIR) study of two star-forming regions associated with IRAS 19110+1045 and IRAS 19111+1048 pair system and IRAS 05168+3634 multiple system. The latter system contains four more IRAS sources (IRAS 05184+3635, IRAS 05177+3636, IRAS 05162+3639, and IRAS 05156+3643) embedded in the same molecular cloud (Azatyan, 2019). Figure 1 presents the color-composite images of both regions on *Herschel* images.

IRAS 19110+1045 and IRAS 19111+1048 objects are also referred to as G45.07+0.13 and G45.12+0.13 UC HII regions, respectively (Wood & Churchwell, 1989). From the images obtained at 2 and 6 cm radio wavelengths, Wood & Churchwell (1989) determined that the morphology of the ionized gas in the G45.07+0.13 region has a spherical shape, and in G45.12+0.13 - cometary. On the 1.3 mm continual images, G45.12+0.13 has an elliptical shape, elongated from north-east to south-west (Hernández-Hernández et al., 2014). Given their proximity in the plane of the sky and similar LSR velocities, Hunter et al. (1997) suggested that G45.12+0.13 and G45.07+0.13 lie at the same distance equal to 8.3 kpc. A more recent distance estimate, according to the trigonometric parallax, is 7.75±0.45 kpc (Wu et al., 2019). We adopt a distance of ~7.8 kpc in our study. Many multi-wavelength studies suggest that both UC HII regions are sites of active massive star formation, at that IRAS 19111+1048 is a more advanced (Hunter et al., 1997, Vig et al., 2006). Both regions contain type I OH masers (Argon et al., 2000), but only IRAS 19110+1045 contains H_2O (Hofner &

*nayazatyan@bao.sci.am, Corresponding author

DOI: 10.52526/25792776-2020.67.2-211

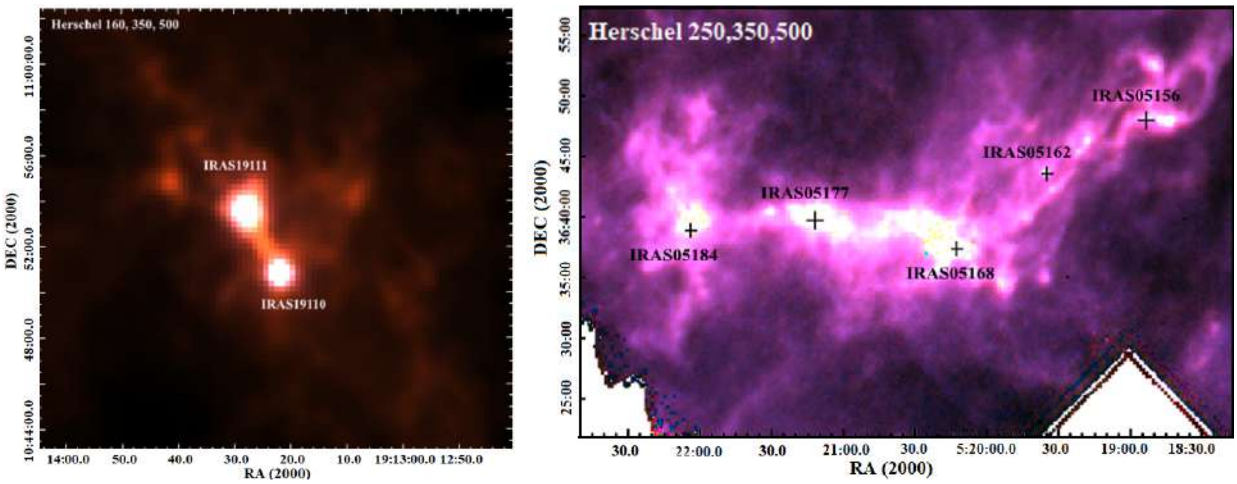

Figure 1. *(left panel)* Color-composite image of IRAS 19110+1045 and IRAS 19111+1048 pair system. *(right panel)* Color-composite image of IRAS 05168+3634 multiple system.

Churchwell, 1996) and methanol maser emissions (Breen et al., 2019, Hernández-Hernández et al., 2019). The NIR data, as well as high-resolution radio measurements, enabled Vig et al. (2006) and Rivera-Ingraham et al. (2010) to conclude that IRAS 19111+1048 region contains a larger number of ZAMS stars energizing compact and evolved HII region.

IRAS 05168+3634 is also known as Mol 9 in the catalog of Molinari et al. (1996). Zhang et al. (2005) have discovered a molecular outflow in this region. There have been various detections in the region: H_2O maser emission (Zhang et al., 2005), NH_3 maser emission (Molinari et al., 1996), CS emission (Bronfman et al., 1996), a new detection of 44 GHz CH_3OH methanol maser emission (Fontani et al., 2010), the SiO (J = 2–1) line (Harju et al., 1998), the main lines at 1665 MHz and 1667 MHz OH maser (Ruiz-Velasco et al., 2016), and four ^{13}CO cores (Guan et al., 2008). IRAS 05184+3635 and IRAS 05177+3636 are associated with dark clouds DOBASHI 4334 and 4326, respectively (Dobashi, 2011). IRAS 05162+3639 is associated with the H_2O maser (Sunada et al., 2007). A high proper-motion star has been detected in the LSPM-NORTH catalog 0.35 arcmin from the IRAS 05156+3643 (Lépine & Shara, 2005) probably compatible with IRAS 05156+3643 within the error bars. The distance estimations of this multiple system are different. A kinematic distance was estimated of 6.08 kpc (Molinari et al., 1996). The trigonometric parallax of IRAS 05168+3634 corresponds to a distance of $1.88^{+0.21}_{-0.17}$ kpc (Sakai et al., 2012). In Casoli et al. (1986), the distances of IRAS 05184+3635 and IRAS 05177+3636 were evaluated at the same 1.4 kpc distance. Both distances were used for further study. The embedded stellar cluster in this region was detected in the NIR and MIR by various authors (Azatyan et al., 2016, Faustini et al., 2009, Kumar et al., 2006). Azatyan et al. (2016) revealed a bimodal cluster with 1.5 arcmin radius from geometric center of the cluster that does not coincide with IRAS 05168+3634 source.

2. Used data

For our study, we used the data covering a wide range from NIR to FIR wavelengths. The first is the archival NIR photometric data in the J, H, and K bands of the Galactic Plane Survey DR6 (UKIDSS GPS, Lucas et al., 2008). Archival data of MIR observations were obtained from the Galactic Legacy Infrared Midplane Survey Extraordinaire (GLIMPSE, Churchwell et al., 2009), made with the *Spitzer* Infrared Array Camera (IRAC, Fazio et al., 2004). The four IRAC bands are centered at approximately 3.6, 4.5, 5.8, and 8.0 μm. We also used the Wide-field Infrared Survey Explorer (WISE, Wright et al., 2010) in 3.4, 4.6, 12, and 22 μm bandpasses. We used FIR wavelengths, in the range 70–500 μm, obtained by using the Photodetector Array Camera and Spectrometer (PACS, Poglitsch et al., 2010) and the Spectral and Photometric Imaging Receiver (SPIRE, Griffin et al., 2010) at the 3.5 m *Herschel* Space Observatory (Pilbratt et al., 2010).

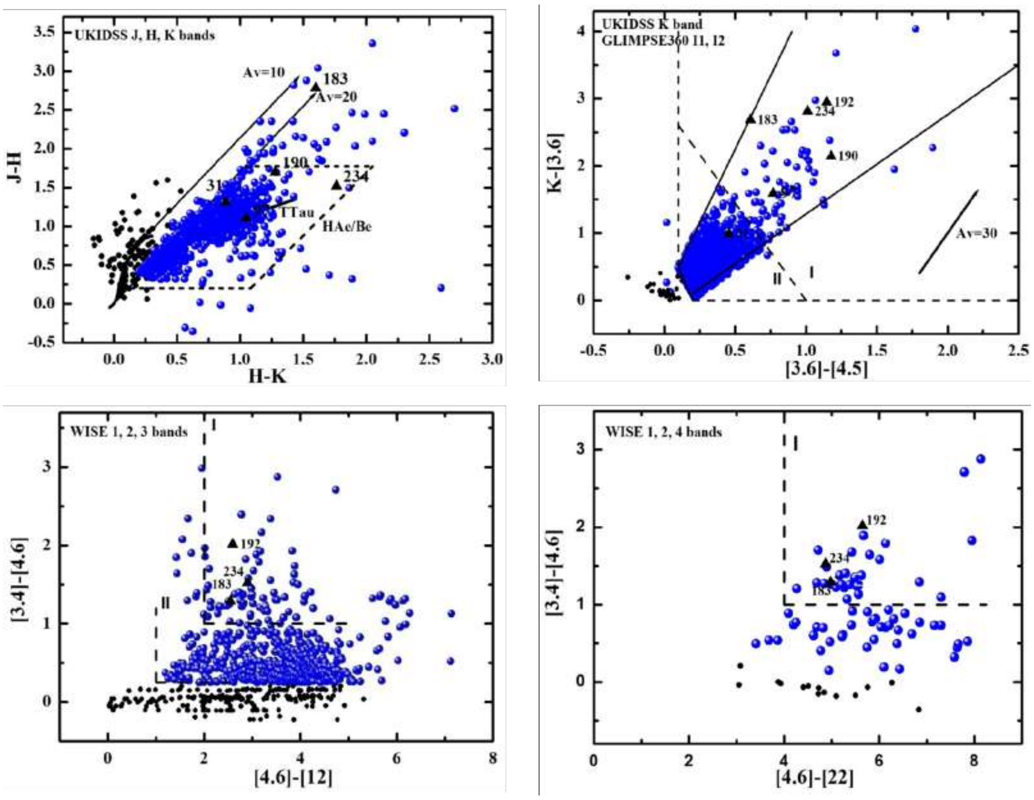

Figure 2. Color-color diagrams of the IRAS 05168+3634 multiple system. In the top left panel is shown the (J-H) vs. (H-K) diagram. In the top right panel the K-[3.6] vs. [3.6]-[4.5] diagram is presented. In bottom left and right panels are shown the [3.4]-[4.6] vs. [4.6]-[12] and [3.4]-[4.6] vs. [4.6]-[22] diagrams. The blue circles are selected YSOs and black circles are unclassified ones. IRAS and MSX sources are indicated by triangles and squares, respectively, and they are labeled as https://doi.org//10.26093/cds/vizier.36220038 catalog. For a detailed description of the references from which the locus of dwarf and giant stars, reddening vectors, and positions of different types of YSOs were obtained, see the text.

3. Results and Discussions

3.1. Color-color diagrams

For the selection of objects in both molecular clouds, we used the data of NIR, MIR, and FIR catalogs (see Section 2) within a radius of 6 arcmin concerning the geometric center of IRAS 19110+1045 and IRAS 19111+1048 pair system and a radius of 24 arcmin concerning the conditionally selected IRAS 05168+3634 source. We chose GPS UKIDSS-DR6 as the main catalog, and the other catalogs were cross-matched with it. The GPS UKIDSS-DR6 catalog for individual objects provides a probability (in percent) of being a star, galaxy, and noise; therefore, we selected objects with a probability of being noise $< 50\%$, and taking into account the completeness limit of UKIDSS survey in K band, the objects that have a measured magnitude of $K \geqslant 18.02$ were removed from the list. The MIR and FIR photometric catalogs were cross-matched with the GPS UKIDSS-DR6 catalog within $3\,\sigma$ of combined error matching radius.

One of the most powerful tools for identifying YSO candidates via reddening and excess is their location on color-color diagrams. The investigated regions are quite large and there is a high probability of selecting objects that do not belong to the considered molecular clouds; therefore, we chose as YSOs those stars that are classified as objects with IR excess in at least two color-color diagrams to minimize the likelihood of choosing incorrectly. Since IRAS 19110+1045 and IRAS 19111+1048 pair system has two saturated areas in the MIR around the IRAS objects, therefore within those areas the selection of YSOs was based on only NIR color-color diagram.

Figure 2 (top left panel) shows the (J-H) versus (H-K) color-color diagram of IRAS 05168+3634 where the solid and dashed curves represent the locus of the intrinsic colors of dwarf and giant stars, taken from Bessell & Brett (1988) after being converted to the CIT system using the relations given

Table 1. Properties of the cluster

IRAS	α(2000) (hh mm ss)	δ(2000) (dd mm ss)	α(2000) (hh mm ss)	δ(2000) (dd mm ss)	Radius (arcmin)	N
(1)	(2)	(3)	(4)	(5)	(6)	(7)
05184+3635	05 21 53.2	+36 38 20.4	05 21 52.6	+36 39 07.1	2.5	52
05177+3636	05 21 09.4	+36 39 37.1	05 21 02.8	+36 38 28.5	3.5	79
05168+3634	05 20 16.4	+36 37 18.7	05 20 22.3	+36 37 33.9	3	57
05162+3639	05 19 38.4	+36 42 25.0	05 19 38.4	+36 42 25.0	0.25	5
05156+3643	05 19 03.6	+36 46 15.7	05 19 04.0	+36 48 02.0	2.8	47
19111+1048	19 13 27.8	+10 53 36.7	19 13 27.3	+10 54 07.4	1.2	101
19110+1045	19 13 22.0	+10 50 54.0	19 13 23.1	+10 50 51.9	0.8	44

Notes. (1)-Name of clusters, (2),(3)-The coordinates of IRAS sources, (4),(5)-The coordinates of geometric centers of the clusters, (6)-The radius of each cluster according to YSOs surface density distribution, (7)-Number of objects within refined radii.

by Carpenter (2001). The parallel solid lines drawn from the base and tip of the dwarf and giant loci, are the interstellar reddening vectors (Rieke & Lebofsky, 1985). The locus of unreddened classical T Tauri stars (CTTSs) is taken from Meyer et al. (1997). The region bounded by the dashed lines where the pre-main sequence (PMS) stars with intermediate mass, i.e., Herbig Ae/Be stars are usually found (Hernández et al., 2005). For further study, we chose objects located to the right of reddening vectors that have a considerable, accurately expressed IR excess. Among the selected YSOs and objects within the reddening band of the MS and giant, we classified as Class I evolutionary stage objects those which have (J-K) > 3 mag color index (Lada & Adams, 1992) and located in the top right in the (J-H) versus (H-K) diagram. We used the same color-color diagram also for IRAS 19110+1045 and IRAS 19111+1048 pair system.

We used the K-[3.6] versus [3.6]-[4.5] color-color diagram for both star-forming regions. Figure 2 (top right panel) shows the K-[3.6] versus [3.6]-[4.5] color-color diagram of IRAS 05168+3634, where the diagonal lines outline the region of location of YSOs with both Class I and Class II evolutionary stages. The de-reddened colors are separated into Class I and II domains by the dashed line. Arrow shows the extinction vector (Flaherty et al., 2007). All the lines in the K-[3.6] versus [3.6]-[4.5] diagram are taken from Allen et al. (2007).

We also constructed two other color-color diagrams for both star-forming regions using the list of objects with good WISE detections, i.e., those possessing photometric uncertainty < 0.2 mag in WISE bands. Figure 2 (lower left panel) shows the [3.4]-[4.6] versus [4.6]-[12] color-color diagram of IRAS 05168+3634. As was mentioned for the previous color-color diagrams, the objects with different evolutionary stages are located in certain places in this diagram too (Koenig et al., 2012), i.e., Class I YSOs are the reddest objects, and are selected if their colors match [3.4]-[4.6] > 1.0 and [4.6]-[12] > 2.0. Class II YSOs are slightly less red objects and are selected with colors [3.4]-[4.6]-σ([3.4]-[4.6]) > 0.25 and [4.6]-[12]-σ([4.6]-[12]) > 1.0, where $\sigma(...)$ indicates a combined photometric error, added in quadrature.

We can check the accuracy of previous classification of stars that possess photometric errors < 0.2 mag in WISE band 4. Previously classified Class I sources were re-classified as Class II if [4.6]-[22] < 4.0 and Class II stars have been placed back in the unclassified pool if [3.4]-[12] < -1.7 × ([12]-[22]) + 4.3 (Koenig et al., 2012). However, there are no incorrect selections in the pre-classified objects with 1, 2, 3 bands and it confirms the results obtained in the [3.4]-[4.6] versus [4.6]-[12] color-color diagram (Figure 2, lower right panel).

In total, we selected 1224 YSOs within a 24 arcmin radius concerning the conditionally selected IRAS 05168+3634 source and 909 YSOs within a 6 arcmin radius of IRAS 19110+1045 and IRAS 19111+1048 system. Figure 3 shows the distribution of classified YSOs in both star-forming regions. Class I and Class II objects are indicated by filled red and blue circles, respectively. It can be seen that excluding the regions in the vicinity of the IRAS sources, all types of stellar objects are distributed relatively homogeneously in both molecular clouds. We also can see that in all cases, close to IRAS sources, the

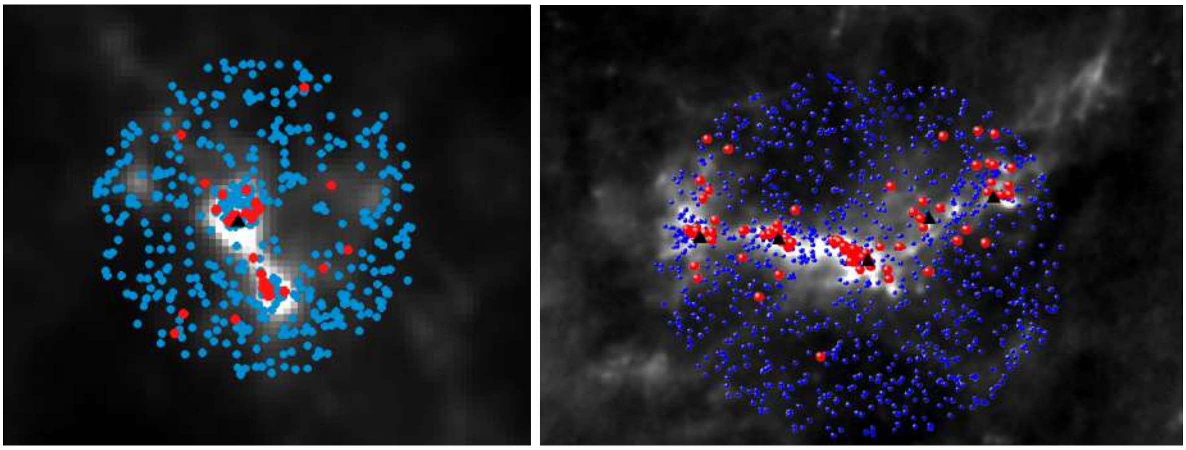

Figure 3. Distribution of YSOs in the regions on *Herschel* 500 μm images. *left panel* presents the distribution of YSOs in IRAS 19110+1045 and IRAS 19111+1048 pair system and *right panel* - in IRAS 05168+3634 multiple system. Class I and Class II objects are indicated by filled red and blue circles, respectively. IRAS sources are indicated by black triangles.

selected YSOs form relatively dense concentrations or clusters.

Since the regions are quite large, further investigations were performed on concentration areas. For that purpose, we refined the radius of each cluster relative to their geometric centers based on the density distribution of selected YSOs. Table 1 presents the coordinates of IRAS sources in Cols. 2 and 3, the coordinates of geometric centers are in Cols. 4 and 5, and the radii based on stellar density distribution are in the Cols. 6. The numbers of objects within selected radii are in the last column. There is no evidence of a real concentration only around IRAS 05162+3639. Therefore, the 0.25 arcmin value of radius given in Table 1 is conditional. So further studies were conducted for the 240 YSOs from IRAS 05168+3634 multiple system and 145 YSOs from IRAS 19110+1045 and IRAS 19111+1048 pair system; this total numbers of objects falls within the already-defined radii of the clusters.

3.2. Color-magnitude diagrams

The color-magnitude diagram is a useful tool for studying the nature of the stellar population within star-forming regions and for estimating its spectral types. The distribution of the identified YSOs in the K versus J-K color-magnitude diagrams are shown in Figure 4 with different symbols for each cluster. The zero age main sequence (ZAMS, thick solid curve) and PMS isochrones for ages 0.1, 0.5, and 5 Myr (thin solid curves) are taken from Siess et al. (2000). We used the conversion table of Kenyon et al. (1994). Figure 4 left panel shows K versus J-K color-magnitude diagram for members of IRAS 19110+1045 (blue circles) and IRAS 19111+1048 (red circles) clusters. To correct J and K magnitudes of the selected YSOs in IRAS 19110+1045 and IRAS 19111+1048 clusters, we used 7.8 kpc distance, and the average value of interstellar extinction $A_v = 13$ mag (see Section 3.3). According to the location of the stellar objects in the color-magnitude diagram, we can see that $\sim 80\%$ of the objects from IRAS 19110+1045 and IRAS 19111+1048 cluster are located to the left of 1 Myr isochrone. In general, the members of both clusters are brighter in the K band.

Figure 4 middle and right panels show K versus J-K color-magnitude diagrams for members of IRAS 05184+3635 (red circles), IRAS 05177+3636 (green circles), IRAS 05168+3634 (blue circles), IRAS 05162+3639 (yellow circles), and IRAS 05156+3643 (pink circles) clusters. The J and K photometry of the selected members are corrected for two different distances: 6.1 and 1.88 kpc, and estimated average A_v=4.5 mag toward five IRAS sources (Azatyan, 2019). In general, the selected YSOs are distributed to the right of 0.1 Myr isochrones, especially in the case of 6.1 kpc distance, and this distribution confirms that they are YSOs. Only a few identified YSOs are located to the left (black circles) of ZAMS.

The López-Chico & Salas (2007) correction can be used to obtain a lower limit of the stellar masses in both star-forming regions with excess vector, which has directions such as presented in Figure 4. Since all detected objects in IRAS 19110+1045 and IRAS 19111+1048 clusters are brighter in the K-

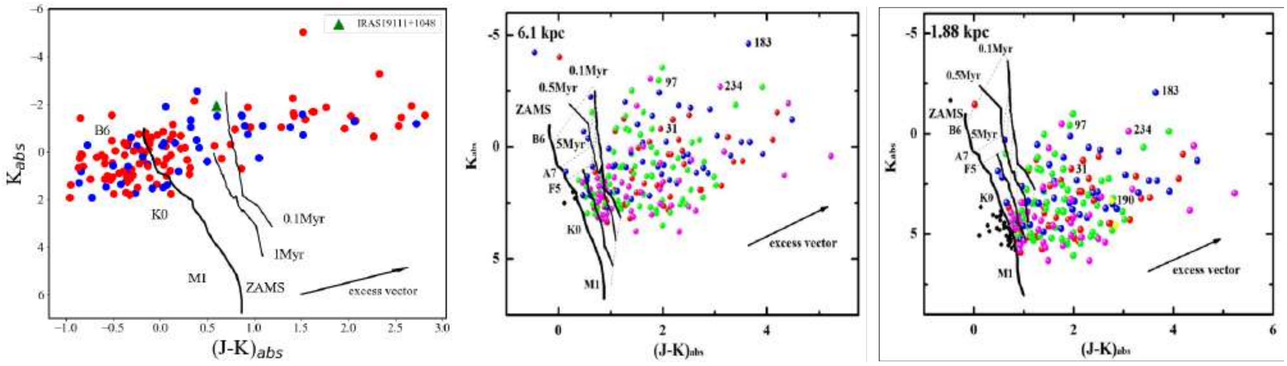

Figure 4. K vs. (J-K) color-magnitude diagrams for the identified YSOs in clusters. *(left panel)* The positions of the YSOs from IRAS 19110+1045 (blue circles) and IRAS 19111+1048 (red circles) pair system. IRAS 19111+1048 source is indicated by a green triangle and it is labelled. *(middle and right panels)* The positions of the YSOs from IRAS 05168+3634 multiple system for distances 6.1 and 1.88 kpc. The objects belonging to different clusters are shown as follows: IRAS 05184+3635 (red circles), IRAS 05177+3636 (green circles), IRAS 05168+3634 (blue circles), IRAS 05162+3639 (yellow circles), and IRAS 05156+3643 (pink circles). Black circles indicate objects considered members of clusters, but in the color-magnitude diagram they are located to the left of ZAMS. The IRAS and MSX sources are labeled as https://doi.org//10.26093/cds/vizier.36220038 catalog. The arrow indicates the average slope of NIR excesses caused by disks around YSOs, as determined by López-Chico & Salas (2007).

band than the estimation of lower mass obtained of 1.4 $M_\odot$ value. A large distance and interstellar extinction can play a crucial role in this result. At a distance of 1.88 kpc, approximately 80 % of the total content of the clusters in IRAS 05168+3634 multiple system has < 1 solar mass, and the remaining ∽20 % objects have 1–3 solar masses. At a distance of 6.1 kpc, approximately 20 % of the total content of the clusters has < 1 solar mass, about 70 % objects have 1–3 solar masses.

3.3. SED analysis

In order to learn about the evolutionary stages of the YSOs that have measured magnitudes in longer wavelengths, we constructed their spectral energy distributions (SEDs) and fitted them with the radiative transfer models of Robitaille et al. (2007). The SEDs are constructed for the members of clusters in both star-forming regions. This procedure was done using wavelengths ranging from 1.1 μm to 500 μm. The SED fitting tool was carried out using both distance estimations for IRAS 05168+3634 multiple system: 1.88 and 6.1 kpc. We used the ranges of A_v and the distances of 1–40 mag, and 5.5–6.5 kpc and 1.6–2 kpc, respectively. For IRAS 19110+1045 and IRAS 19111+1048 clusters, we used the ranges of A_v and the distances of 10–100 mag and 6.5–9.5 kpc, respectively.

Table 2 presents the parameters of IRAS sources estimated by SED fitting tool. For the clusters of IRAS 05168+3634 system at distances of 1.88 and 6.1 kpc, objects associated with IRAS sources can be classified as middle-mass YSOs. We applied SED fitting tool for 120 YSOs out of 240 selected ones in the clusters of IRAS 05168+3634 multiple system. We could obtained the parameters of only IRAS 19111+1048 source which is satisfy the conditions to create an UC HII region. For IRAS 19110+1045 source, we were unable to identify an object that could satisfy the conditions of central star(s) of this UC HII region. We carried out SED fitting tool only for 29 YSOs out of 145 selected ones in IRAS 19110+1045 and IRAS 19111+1048 clusters due to the saturation in MIR ranges and therefore the lack of photometric data. According to the SED fitting tool, the average value of interstellar extinction is equal to A_v=13 mag in this pair system, which was used for the correction of J and K photometry in K versus J-K color-magnitude diagram (see Section 3.2).

4. Conclusions

The search, identification, and classification of the young stellar population in the molecular clouds surrounding IRAS 19111+1048 and IRAS 19110+1045 pair system and IRAS 05168+3634 multiple

Table 2. Parameters of IRAS sources derived from Robitaille et al. (2007) models SED fitting.

IRAS	Distance (kpc)	A_v (mag)	Stellar age (Log)(yr)	Stellar mass ($M_\odot$)	Temperature (K)	L_{Total} (Log)($L_\odot$)	Class
(1)	(2)	(3)	(4)	(5)	(6)	(7)	(8)
05184+3635	1.88	12.1 ± 2.0	6.6 ± 5.9	3.1 ± 0.6	12589 ± 2000	1.9 ± 1.5	II/I
05184+3635	6.1	6.9 ± 0.3	5.9 ± 5.8	6.8 ± 0.7	12589 ± 8000	3.0 ± 2.8	II/I
05177+3636	1.88	4.4 ± 1.8	5.8 ± 5.9	2.6 ± 1.3	6309 ± 3981	2.4 ± 2.5	I
05177+3636	6.1	3.0 ± 1.0	4.1 ± 4.0	5.5 ± 0.9	3981 ± 630	2.6 ± 2.0	I
05168+3634	1.88	15.3 ± 1.0	6.0 ± 5.4	5.1 ± 0.3	15848 ± 1584	2.8 ± 2.0	I
05168+3634	6.1	6.9 ± 2.9	5.9 ± 5.5	7.1 ± 1.1	19952 ± 6309	3.4 ± 2.7	I
05162+3639.1	1.88	6.3 ± 3.1	4.8 ± 4.7	1.0 ± 0.4	3981 ± 501	1.2 ± 0.5	I
05162+3639.1	6.1	7.8 ± 2.5	4.2 ± 4.0	3.1 ± 0.6	3981 ± 630	2.1 ± 1.4	I
05162+3639.2	1.88	34.6 ± 3.0	5.9 ± 5.2	4.5 ± 0.3	7943 ± 1000	2.2 ± 1.8	I
05162+3639.2	6.1	19.5 ± 3.8	6.0 ± 5.2	5.4 ± 0.2	15848 ± 1000	2.8 ± 1.7	I
05156+3643	1.88	2.1 ± 0.8	6.2 ± 6.3	3.4 ± 3.6	12589 ± 7943	3.2 ± 3.4	I
05156+3643	6.1	1.4 ± 1.9	3.8 ± 2.7	2.9 ± 1.2	3981 ± 316	2.3 ± 0.4	I
19111+1048	7.8	12.0 ± 4.6	6.40 ± 6.07	9.4 ± 4.3	22928 ± 10771	3.8 ± 3.6	II

Notes. (1)-Name of IRAS source, (2)-Distance, (3)-(7)-the weighted means and the standard deviations of parameters obtained by SED fitting tool for all models with best $\chi^2 - \chi^2_{best} < 3N$, (8) - classification of YSOs.

system made it possible to obtain the following results: *(i)* Census of the young stellar population have been obtained in both regions, *(ii)* the distribution of selected YSOs shows clear concentrations in the vicinity of IRAS sources, *(iii)* in IRAS 05168+3634 multiple system unlike the Class II objects, the Class I objects are located mainly in vicinity of IRAS sources, *(iv)* selected YSOs in IRAS 05168+3634 multiple system are mostly younger then 0.1 Myr, *(v)* among selected YSOs in IRAS 19111+1048 and IRAS 19110+1045 pair system there are ZAMS objects.

Acknowledgements

The authors thanks to the organizers for the opportunity to take a part in International conference 'Astronomical Surveys and Big Data 2'

References

Allen L., et al., 2007, Protostars and Planets V, pp 361–376

Argon A. L., Reid M. J., Menten K. M., 2000, ApJS, 129, 159

Azatyan N. M., 2019, A&A, 622, A38

Azatyan N. M., Nikoghosyan E. H., Khachatryan K. G., 2016, Astrophysics, 59, 339

Bessell M. S., Brett J. M., 1988, PASP, 100, 1134

Blitz L., 1991, in Lada C. J., Kylafis N. D., eds, NATO Advanced Science Institutes (ASI) Series C Vol. 342, NATO Advanced Science Institutes (ASI) Series C. p. 3

Breen S. L., Contreras Y., Dawson J. R., Ellingsen S. P., Voronkov M. A., McCarthy T. P., 2019, MNRAS, 484, 5072

Bronfman L., Nyman L.-A., May J., 1996, A&AS, 115, 81

Carpenter J. M., 2001, AJ, 121, 2851

Casoli F., Dupraz C., Gerin M., Combes F., Boulanger F., 1986, A&A, 169, 281

Churchwell E., et al., 2009, PASP, 121, 213

Dobashi K., 2011, PASJ, 63, S1

Egan M. P., et al., 2003, VizieR Online Data Catalog, 5114

Faustini F., Molinari S., Testi L., Brand J., 2009, A&A, 503, 801

Fazio G. G., et al., 2004, ApJS, 154, 10

Fish V. L., Reid M. J., Wilner D. J., Churchwell E., 2003, ApJ, 587, 701

Flaherty K. M., Pipher J. L., Megeath S. T., Winston E. M., Gutermuth R. A., Muzerolle J., Allen L. E., Fazio G. G., 2007, ApJ, 663, 1069

Fontani F., Cesaroni R., Furuya R. S., 2010, A&A, 517, A56

Griffin M. J., et al., 2010, A&A, 518, L3

Guan X., Wu Y., Ju B., 2008, MNRAS, 391, 869

Han X. H., Zhou J. J., Wang J. Z., Esimbek J., Zhang J. S., Wang N., 2015, A&A, 576, A131

Harju J., Lehtinen K., Booth R. S., Zinchenko I., 1998, A&AS, 132, 211

Hernández-Hernández V., Zapata L., Kurtz S., Garay G., 2014, ApJ, 786, 38

Hernández-Hernández V., Kurtz S., Kalenskii S., Golysheva P., Garay G., Zapata L., Bergman P., 2019, AJ, 158, 18

Hernández J., Calvet N., Hartmann L., Briceño C., Sicilia-Aguilar A., Berlind P., 2005, AJ, 129, 856

Hofner P., Churchwell E., 1996, A&AS, 120, 283

Hunter T. R., Phillips T. G., Menten K. M., 1997, ApJ, 478, 283

Kenyon S. J., Gomez M., Marzke R. O., Hartmann L., 1994, AJ, 108, 251

Koenig X. P., Leisawitz D. T., Benford D. J., Rebull L. M., Padgett D. L., Assef R. J., 2012, ApJ, 744, 130

Kumar M. S. N., Keto E., Clerkin E., 2006, A&A, 449, 1033

Lada C. J., Adams F. C., 1992, ApJ, 393, 278

Lada C. J., Lada E. A., 2003, ARA&A, 41, 57

Lépine S., Shara M. M., 2005, AJ, 129, 1483

López-Chico T., Salas L., 2007, Rev. Mex. Astron. Astrofis., 43, 155

Lucas P. W., et al., 2008, MNRAS, 391, 136

McKee C. F., Ostriker E. C., 2007, ARA&A, 45, 565

Meyer M. R., Calvet N., Hillenbrand L. A., 1997, AJ, 114, 288

Molinari S., Brand J., Cesaroni R., Palla F., 1996, A&A, 308, 573

Molinari S., Brand J., Cesaroni R., Palla F., Palumbo G. G. C., 1998, A&A, 336, 339

Pilbratt G. L., et al., 2010, A&A, 518, L1

Poglitsch A., et al., 2010, A&A, 518, L2

Price S. D., Egan M. P., Carey S. J., Mizuno D. R., Kuchar T. A., 2001, AJ, 121, 2819

Rieke G. H., Lebofsky M. J., 1985, ApJ, 288, 618

Rivera-Ingraham A., et al., 2010, ApJ, 723, 915

Robitaille T. P., Whitney B. A., Indebetouw R., Wood K., 2007, ApJS, 169, 328

Ruiz-Velasco A. E., Felli D., Migenes V., Wiggins B. K., 2016, ApJ, 822, 101

Sakai N., Honma M., Nakanishi H., Sakanoue H., Kurayama T., Shibata K. M., Shizugami M., 2012, PASJ, 64, 108

Siess L., Dufour E., Forestini M., 2000, A&A, 358, 593

Sunada K., Nakazato T., Ikeda N., Hongo S., Kitamura Y., Yang J., 2007, PASJ, 59, 1185

Vig S., Ghosh S. K., Kulkarni V. K., Ojha D. K., Verma R. P., 2006, ApJ, 637, 400

Wood D. O. S., Churchwell E., 1989, ApJS, 69, 831

Wright E. L., et al., 2010, AJ, 140, 1868

Wu Y. W., et al., 2019, ApJ, 874, 94

Zhang Q., Hunter T. R., Brand J., Sridharan T. K., Cesaroni R., Molinari S., Wang J., Kramer M., 2005, ApJ, 625, 864

Communications of BAO, Vol. 67, Issue 2, 2020, pp. 219-226

Properties of Broad and Narrow Line Seyfert galaxies selected from SDSS

Vivek Kumar Jha*[1], Hum Chand[2], and Vineet Ojha[1]

[1]Aryabhatta research institute of observational sciences (ARIES), Nainital, Uttarakhand, India
[2]Central University of Himachal Pradesh (CUHP), Dharamshala, Himachal Pradesh, India

Abstract

A comparative study of a representative sample of Broad and Narrow line Seyfert galaxies is presented. These galaxies have been selected from the 16^{th} data release of the Sloan Digital Sky Survey (SDSS-DR16). Some of the properties derived from single epoch spectrum vary significantly between the two populations. We find that the emission regions of Narrow line Seyfert galaxies are rich in iron content and the accretion rate is higher compared to the Broad line Seyfert galaxies. In our analysis, the $H\beta$ emission line is found to be asymmetric in few of the galaxies with more number of Narrow-line Seyfert 1 (NlSy1) galaxies showing blue asymmetries i.e. traces of outflowing gas as compared to the Broad-line Seyfert 1 (BlSy1) galaxies. This behaviour may be explained by the higher iron content present in the emission line regions of NlSy1 galaxies.

Keywords: *galaxies: active – galaxies: nuclei – galaxies: Seyfert*

1. Introduction

Seyfert galaxies are characterized by a lower luminous active nucleus as compared to the general quasar population. Among the Seyfert galaxies, Type-1 galaxies show both narrow and broad emission lines (see Netzer, 2015, for a review). These lower luminous Type-1 galaxies are subdivided into narrow and broad line Seyfert classes based on the Full Width at Half Maximum (FWHM) of the $H\beta$ emission line. NlSy1 galaxies are understood to be a subclass of active galactic nuclei (AGN) which have narrower broad Balmer line widths with FWHM of broad $H\beta$ emission line ≤ 2000 km/sec^{-1}, a small intensity ratio of the [O III] λ5007 to $H\beta$ line ($[OIII]/H\beta \leq 3$), stronger optical Fe II emissions (see Rakshit et al., 2017, and references therein), and usually steeper soft X-ray spectra and more rapid X-ray and sometimes optical flux variability (see Ojha et al., 2020a) . It is assumed that these properties are due to the central black hole being less massive, but accreting at a very high rate. Low optical variability has also been reported in NlSy1 galaxies by Rakshit & Stalin (2017). It has been proposed by Mathur (2000) that the NlSy1 galaxies are a subcategory of BlSy1 galaxies only and can be assumed to be in evolutionary stages, while in Gaskell (2000) unusually high Fe-II strength, R_{fe} in NlSy1 galaxies is attributed to weak Balmer lines originating from a dense environment. The NlSy1 galaxies have been proposed as younger versions of the general broad line active galaxies.

The region responsible for the generation of broad emission lines is known as the Broad line Region (BLR). About 120 AGN been studied using the reverberation mapping technique (see Bahcall et al., 1972, Blandford & McKee, 1982), which is a powerful time domain method to probe the inner regions of type 1 galaxies. However, with the known number of AGN extending into hundreds of thousands, thanks to the all sky surveys such as the Sloan Digital Sky Survey (SDSS) (York et al., 2000) but precise knowledge of the structure and kinematics of BLR through reverberation mapping available for only a handful of AGN (see Bentz & Katz, 2015, for a comprehensive database of reverberation mapped AGN), studies have relied on statistical analysis on a selected sample of AGN constrained by

*vivek@aries.res.in, Corresponding author

DOI: 10.52526/25792776-2020.67.2-219

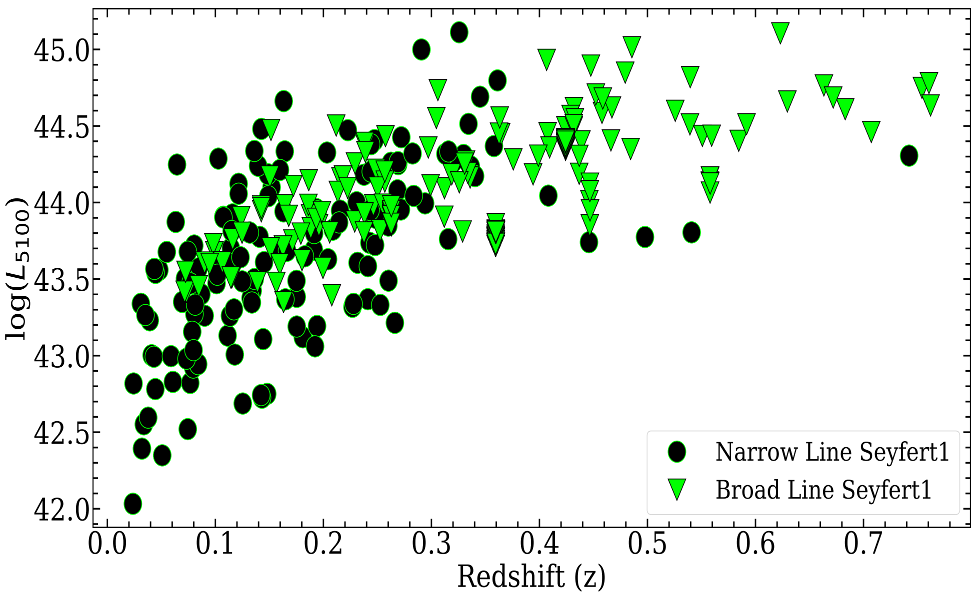

Figure 1. A representative sample of BlSy1 (green triangle) and the NlSy1 galaxies (black circle) galaxies matching in luminosity and redshift (L-z) plane being used for this work. The limit of redshift is put at 0.8 for clear $H\beta$ emission line detection in SDSS.

various limits, to infer the physical properties. A remarkable work was done by by Boroson & Green (1992), where they performed a Principal Component Analysis (PCA) on properties derived from X-ray, optical and radio wavelength data for a set of 87 quasars. They derived that the Eigenvector1 (E1), driven by the anti correlation of the ratio R_{Fe} of equivalent width (EW) of FeII emission lines in the optical band and the FWHM of $H\beta$ emission line is the primary cause of variability in the parameters. Since then, various aspects of E1 involving a variety of data sets as well multi-frequency parameters have been discussed in multiple works (see Marziani et al., 2018, and references therein). Sulentic et al. (2000) and later Zamfir et al. (2010) established the foundations of the four-dimensional EV1 (4DE1) formalism, including the (FWHM) of $H\beta$ and R_{fe} as two of the main components. These two quantities are respectively related to the black hole mass and the Eddington ratio and these studies have resulted in the so called quasar main sequence (see Marziani et al., 2018, Sulentic & Marziani, 2015)

In this work, we have compiled a representative sample of NlSy1 galaxies and BlSy1 galaxies and performed a statistical study based on the various physical parameters responsible for driving the variations in both types of galaxies. The primary objective of current study is to understand the diversity observed in the physical parameters for a representative sample of both broad line and narrow line Seyfert-1 galaxies and its correlation with the physical parameters obtained through optical and X-ray observations, and then establish a comparison between the two types of galaxies based on these parameters.

2. Data and fitting procedure

A sample comprising of both BlSy1 and NlSy1 galaxies with almost similar luminosity and matching in the redshift domain has been assembled in order to study the properties of these two seemingly different classes of galaxies. More information about this sample is available in Ojha et al. (2020b). The single epoch optical spectrum for all the sources was obtained from the SDSS archives (see Rakshit et al., 2017, Shen et al., 2011, York et al., 2000, etc.) using the SDSS-SAS DR16 server[1]. For all the sources we performed a search query for the optical spectrum on the SDSS-SAS server for a region around 0.05 arc minutes within the specified Right Ascension (RA) and Declination (DEC) positions of these sources. The spectra were brought to the rest frame using the redshift values available in the

[1]https://dr16.sdss.org/optical/spectrum/search

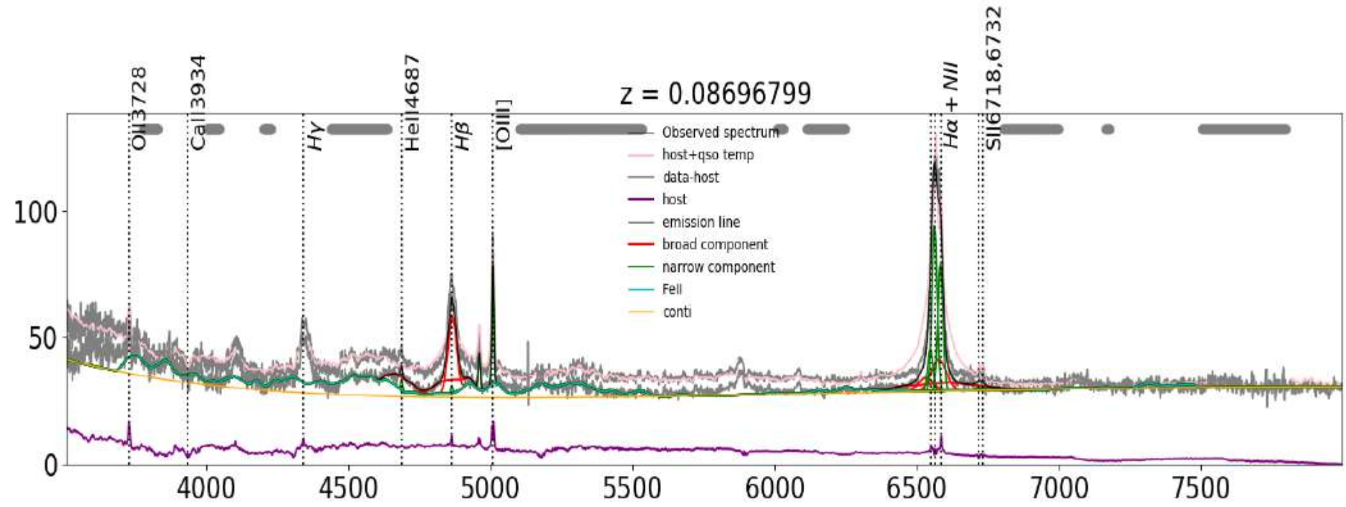

Figure 2. Demonstration of the fitting procedure. The continuum has been fit using a power law, the emission lines have been fit using a combination of gaussians, the host galaxy has been decomposed using already available tempelate in Yip et al. (2004) and the Fe blend has been removed using the tempelates available in Boroson & Green (1992).

header of the individual FITS files obtained from SDSS DR16. A limit of Signal to Noise Ratio (SNR) ≥ 5 was put for identifying the emission lines clearly. Out of the 225 NlSy1 galaxies in the sample, the SNR criteria reduced 10 sources while out of 164 BlSy1 galaxies from the sample, this criterion reduced 14 sources.

PyQSOFIT[2], a publicly available code to fit the quasar spectra has been used to analyse the individual spectra. It is written in Python language, and has been used for fitting the SDSS quasar spectra recently (see Gaur et al., 2019, Rakshit et al., 2020, etc.). Initially, the continuum model is prepared using the host galaxy components, contribution from the iron line and the accretion disk emission which reflects itself as a power law component (see Figure 2). We removed the host galaxy component using the PCA method, obtained from the host galaxy templates of (Yip et al., 2004) .For many of the sources in our sample the host galaxy decomposition could not be applied. The FeII blends were removed using the templates available in Boroson & Green (1992) which are available within the code itself. The accretion disk component was fitted as a polynomial and the final continuum model was subtracted from the original spectrum, which yielded the emission line components only. We were concerned with measuring the asymmetry in the $H\beta$ emission line, hence for the emission line fitting, we concentrated on the $H\beta$-OIII complex only. We assumed the emission line complex to be composed of a narrow and a broad central component representing the $H\beta$ emission arising from the Narrow line and Broad line regions respectively. The width of the narrow Gaussian components used for fitting the OIII doublet, was tied with the narrow component of the $H\beta$ emission line which physically indicates the emission coming from the same narrow line region. The limits for the width of the Gaussian profiles were set as 800 km/sec for narrow components, up to 2300 km/sec for broad components and beyond 10000 km/sec for very broad components for fitting the NlSy1 galaxies. The limit of 2300 km/sec was kept keeping in mind the previous works classifying the NlSy1 galaxies (for example, see Rakshit et al., 2017). For fitting the BlSy1 we removed the upper limit of 2300 km/sec on the broad component, while still allowing up to three Gaussian profiles including a very broad component. Out of 225 NlSy1 galaxies, we could fit and get proper measurements of physical quantities for 144 sources, while out of 164 BlSy1 galaxies, we could fit and get proper measurements for 110 sources.

[2]https://github.com/legolason/PyQSOFit

3. Analysis

We obtained the physical parameters from the spectral fitting and derived a few parameters based on empirical relations. The FWHM of the $H\beta$ emission line, area covered by the line, and its equivalent width (EW) were obtained from the direct decomposition of the spectra. The area covered by the $H\beta$ emission line was calculated by integrating the flux between 4700Åand 4920Å. We calculated the equivalent width (EW) of the emission line using the same wavelength window and the monochromatic luminosity at 5100 Å(L_{5100}) was obtained from the fit. The broad line region of NlSy1 galaxies is understood to be richer in FeII content as compared to the general population (Panda et al., 2019). The iron strength (R_{Fe}) was calculated as the ratio of area covered by the broad Fe line between 4433Åand 4684Å, and the area covered by the $H\beta$ emission line.

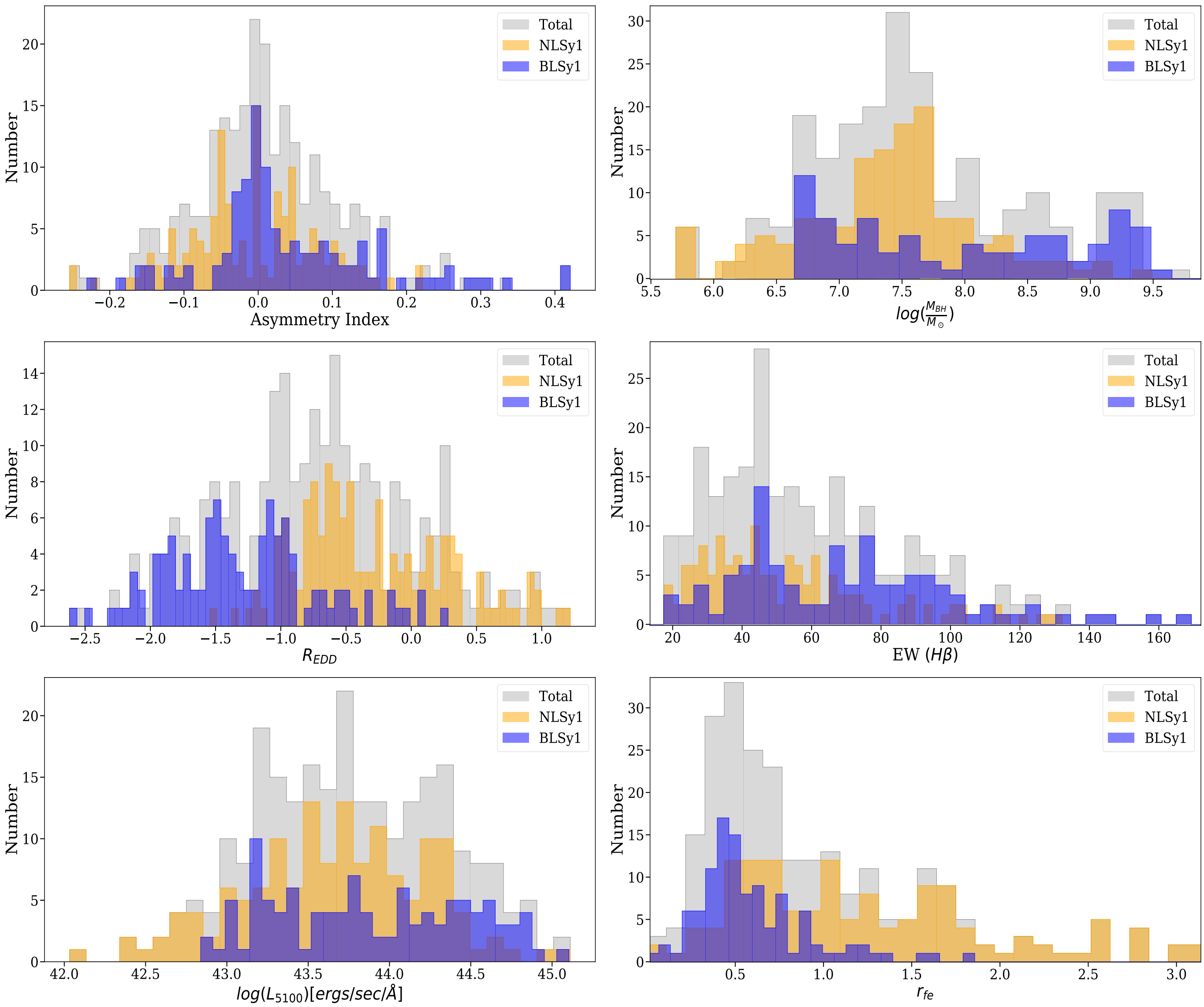

Figure 3. Distribution of various physical parameters for both the types of galaxies. Orange color denotes the NlSy1 galaxies, Blue color denotes the BlSy1 and the grey region is the combined number.

We found out the iron strength in NlSy1 galaxies to be higher than the BlSy1 galaxies for most of the AGN. The median R_{Fe} was 1.13 for the NlSy1 galaxies while it was less than half of that value, 0.49 for the BlSy1 galaxies. We estimated the flux ratio of the narrow OIII component to the broad $H\beta$ in order to understand the influence of the $H\beta$ on the emission from NLR gases. The NlSy1 galaxies have weak OIII emission and thus the OIII/$H\beta$ ratio was lower compared to the BlSy1 galaxies. Also, the ratio of broad components of $H\alpha$ and $H\beta$ was calculated using the area covered by the broad components of the two emission lines.

The central black hole mass has been estimated using various empirical relations in the recent past. Reverberation mapping based masses provide tighter constraints on the Supermassive Black Hole (SMBH) mass and thus far this technique has been the only reliable one for SMBH mass estimation to higher redshifts (Bentz et al., 2009). The single epoch SMBH mass estimation technique is based on the scaling relations obtained from local galaxy stellar velocity dispersion.

$$M_{BH} = f_{BLR} \frac{R_{BLR}(\Delta v)^2}{G} \tag{1}$$

In this equation, R_{BLR} is the BLR radius in light days and is estimated using the so called Radius Luminosity (R-L) relation available for a set of approximately 120 reverberation mapped AGN so far (Bentz et al., 2009, Du & Wang, 2019), Δv is obtained from the FWHM of the emission line being used for the SMBH mass estimation, assuming that the gas is in virialized motion around the SMBH. The NlSy1 galaxies have smaller SMBH mass, owing to the small FWHM of the $H\beta$ emission line.

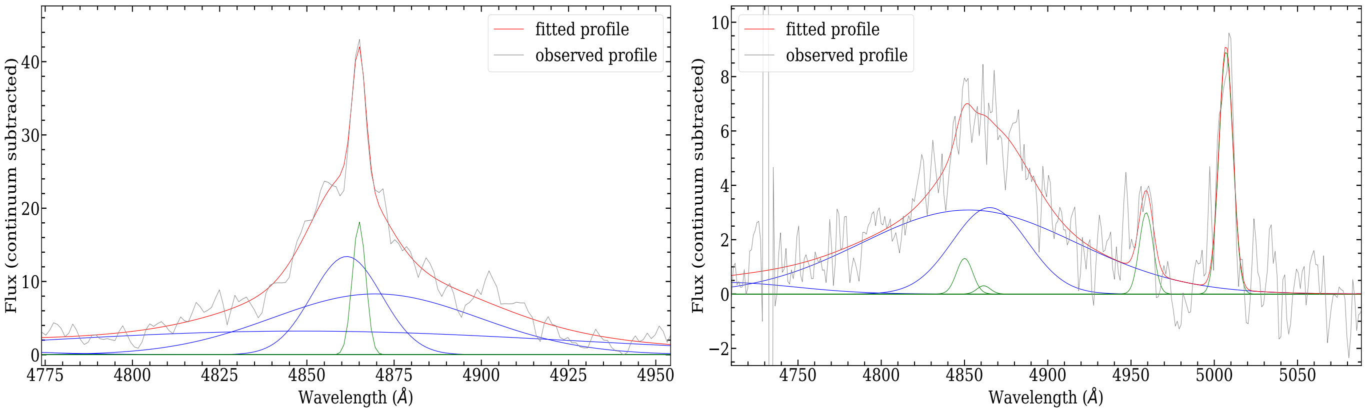

Figure 4. Example of blue (left) and red (right) asymmetric $H\beta$ profiles with AI values -0.14 and +0.12 respectively

The NlSy1 galaxies have been known to have higher accretion rates as compared to the BlSy1, which makes it one of the defining parameters in the classification. These AGN are understood to be younger in age but accreting very fast. In the eigenvector formalism of Boroson & Green (1992), the Eddington ratio, $R_{Edd} = \frac{L_{BOL}}{L_{Edd}}$ is understood to drive the variations in the parameters. The Eddington ratio is also interpreted as the age of the AGN in some recent works (Grupe, 2004). We estimated the Eddington ratio using optical spectra itself. In Ojha et al. (2020b), R_{Edd} was calculated using X-ray observations which was consistent with the estimation from that obtained from optical parameters hence we did not attempt to estimate R_{Edd} using other methods.

The asymmetry index has been used to trace the signatures of inflowing or outflowing gas in the broad line region of AGN. While the outflow asymmetry in the CIV line, known as the *blueshifting* is well known and documented (Gaskell & Goosmann, 2013) and possibly explained by the so called 2 component BLR model, the cause of similar asymmetry in a low ionisation line like $H\beta$ has not been known very well in the literature, although asymmetric $H\beta$ profiles have been known to exist. The characterisation of the AGN in terms of their emission line shapes and shifts and their correlation with physical parameters such as accretion rate etc. has been attempted in (Zamfir et al., 2010) where they conclude that the AGN with $H\beta$ FWHM $\geq$ 4000 km/sec show different characteristics than the ones with lower value of FWHM. We estimated the asymmetry indices for all the AGN in our sample. It has been calculated with different flux values in the recent past (Brotherton, 1996, Marziani et al., 1996). We chose a combination of 75% and 25% flux values to estimate the asymmetry index based on previous works. Basically the wavelength at which the broad emission line flux values reach the 75% and 25% of the flux values is recorded and the asymmetry index (AI) and Kurtosis Index (KI) are calculated. The correlation of AI with various physical parameters is shown in Figure 5. We also obtained the soft X-ray photon index as it is one of the fundamental components in the 4DE1 formalism. The X-ray photon indices were obtained from (Ojha et al., 2020b). The comparison between X-ray photon indices and the BLR asymmetry provides clues to the connection of the corona

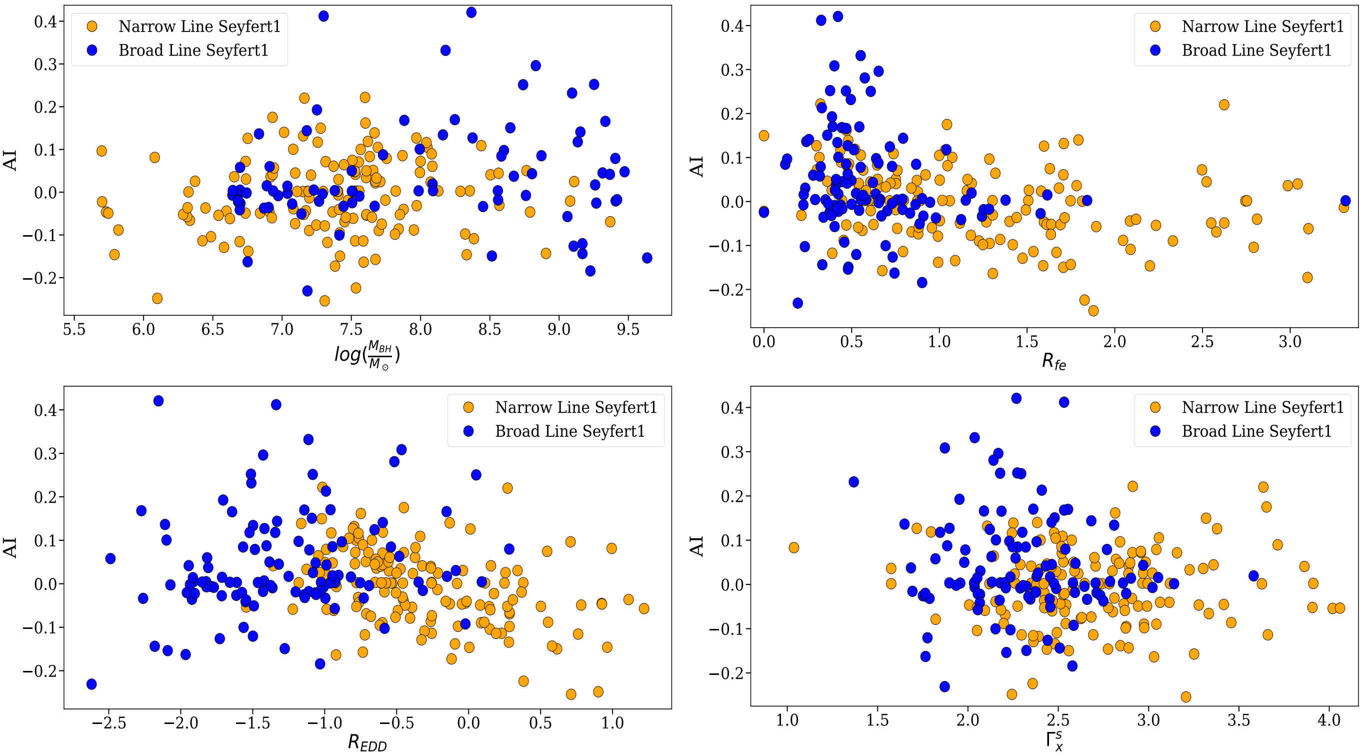

Figure 5. Correlation of asymmetry indices with various parameters for NlSy1 (orange) and BlSy1 (blue) galaxies.

in the accretion disk with the BLR. The distribution of the various parameters for the entire sample of BlSy1 and NLSy1 is presented in Figure 3. To understand the correlation among the various derived parameters, we calculated the spearman rank correlation coefficients. It is a statistical technique used to find out the strength and the direction of the association between two variables.

4. Results

The direct correlations point to higher anti correlation of the $H\beta$ FWHM with R_{fe} and R_{Edd} in the NlSy1. While there is a strong anti correlation of FWHM with R_{fe} in both the cases, it is slightly weaker in the case of BlSy1 galaxies. This may be because of the fact that R_{fe} is strongly dependent on the flux of the iron emission line and thus the emission region of NLSy1 being richer in iron content as compared to the BlSy1. The Eddington ratio is anti correlated with the $H\beta$ FWHM with the anti correlation coefficient of -0.43 for the whole sample. When the correlation is calculated separately, a positive correlation of +0.33 is present in the case of BlSy1 while it is highly anti correlated with the FWHM of $H\beta$ in the case of NlSy1 galaxies, it's correlation coefficient being -0.84. Most of the NlSy1 galaxies have higher Eddington ratios but lower FWHM than the BlSy1 hence, this skews the results for entire population in the favour of NlSy1 galaxies in this analysis.

More NlSy1 galaxies show blue asymmetries as compared to the BlSy1, which seems quite interesting. Blue asymmetries means there is outflowing gas arising from that region. In the literature (see Panda et al., 2019, Wolf et al., 2020) it has been recently known that the NlSy1 galaxies show more traces of outflow. The FWHM of Hβ correlates positively, although weakly with the asymmetry index. The correlation coefficent is 0.26 in the case of BlSy1 galaxies while it comes out to be 0.37 in the case of NlSy1 galaxies. Also it is anti correlated with R_{Fe} in both the cases of NlSy1 galaxies and BlSy1 galaxies. There has been a postulation to use the AI in the emission profile as a surrogate parameter in the 4DE1 formalism. The asymmetry index shows weak correlations and anti correlations with the other known parameters. Thus, we can't conclusively determine the asymmetry index to be a dominating factor in the AGN classification based on this analysis. Soft X-ray photon index has been one of the components of the 4DE1 formalism of Boroson & Green (1992) hence we tried to correlate it with other known parameters for this sample. Surprisingly, there is very weak correlation of the soft X-ray photon index with all the parameters in both the cases.

We tried to see if the differences in physical properties arise even when the NlSy1 galaxies are compared to the general Seyfert galaxies population. Naturally with the NlSy1 galaxies occupying extreme ends in some parameters space, it becomes imperative to understand the properties of these galaxies. In Grupe (2004), and more recently Ojha et al. (2020b) and Waddell & Gallo (2020) the properties of NlSy1 galaxies have been studied comparatively with BlSy1 galaxies. In Grupe (2004), a sample of 110 X-ray selected galaxies was available, which is around 250 in our case, owing to the availability of SDSS sepctrum. The results between the two studies are largely consistent. We conclude from this work that the NlSy1 galaxies are richer in iron content (indicated by their high R_{fe} values), accrete very fast and show more traces of outflow, signified by their blue asymmetries.

Acknowledgments

The authors acknowledge the financial support provided by DST-SERB (grant no: EMR 2016/001723) for this project.

References

Bahcall J. N. J., Kozlovsky B.-Z. B.-Z., Salpeter E. E., 1972, ApJ, 171, 467

Bentz M. C., Katz S., 2015, PASP, 127, 67

Bentz M. C., Peterson B. M., Netzer H., Pogge R. W., Vestergaard M., 2009, ApJ, 697, 160

Blandford R. D., McKee C. F., 1982, ApJ, 255, 419

Boroson T. A., Green R. F., 1992, ApJS, 80, 109

Brotherton M. S., 1996, Technical report, THE PROFILES OF Hß AND [O III] X5007 IN RADIO-LOUD QUASARS

Du P., Wang J.-M., 2019, ApJ, 886, 42

Gaskell C., 2000, New Astronomy Reviews, 44, 563

Gaskell C. M., Goosmann R. W., 2013, ApJ, 769, 30

Gaskell C. M., Goosmann R. W., 2016, Ap&SS, 361, 67

Gaur H., Gu M., Ramya S., Guo H., 2019, A&A, 631, A46

Grupe D., 2004, The Astronomical Journal, 127, 1799

Guo H., Shen Y., Wang S., 2018, PyQSOFit: Python code to fit the spectrum of quasars, Astrophysics Source Code Library (ascl:1809.008)

Kaspi S., Smith P. S., Netzer H., Maoz D., Jannuzi B. T., Giveon U., 2000, ApJ, 533, 631

Kaspi S., Smith P. S., Netzer H., Maoz D., Jannuzi B. T., Giveon U., 2002, ApJ, 533, 631

Marziani P., Sulentic J. W., Dultzin-Hacyan D., Calvani M., Moles M., 1996, ApJS, 104, 37

Marziani P., et al., 2018, Frontiers in Astronomy and Space Sciences, 5, 6

Mathur S., 2000, NewAR, 44, 469

Netzer H., 2015, ARA&A., 53, 365

Ojha V., Chand H., Krishna G., Mishra S., Chand K., 2020a, MNRAS, 493, 3642

Ojha V., Chand H., Dewangan G. C., Rakshit S., 2020b, ApJ, 896, 95

Panda S., Marziani P., Czerny B., 2019, ApJ, 882, 79

Rakshit S., Stalin C. S., 2017, ApJ, 842, 96

Rakshit S., Stalin C. S., Chand H., Zhang X.-G., 2017, ApJS, 229, 39

Rakshit S., Stalin C. S., Kotilainen J., 2020, ApJS, 249, 17

Shen Y., et al., 2011, ApJS, 194, 45

Sulentic J. W., 1989, ApJ, 343, 54

Sulentic J. W., Marziani P., 2015, Frontiers in Astronomy and Space Sciences, 2, 6

Sulentic J. W., Zwitter T., Marziani P., Dultzin-Hacyan D., 2000, ApJL, 536, L5

Sulentic J. W., et al., 2017, A&A, 608, A122

Waddell S. G. H., Gallo L. C., 2020, MNRAS, 498, 5207

Wang J.-M., Du P., Brotherton M. S., Hu C., Songsheng Y.-Y., Li Y.-R., Shi Y., Zhang Z.-X., 2017, Nature Astronomy, 1, 775

Wolf J., et al., 2020, MNRAS, 492, 3580

Yip C. W., et al., 2004, AJ, 128, 585

York D. G., et al., 2000, AJ, 120, 1579

Zamfir S., Sulentic J. W., Marziani P., Dultzin D., 2010, MNRAS, 403, 1759

Communications of BAO, Vol. 67, Issue 2, 2020, pp. 227-231

Temperature spectrum of the solar wind turbulence

Gogoberidze G.*[1], Machabeli G.†[1], and Voitenko Yu.‡[2]

[1]Ilia State University, 3/5 Cholokashvili ave., 0162 Tbilisi, Georgia
[2]Belgian Institute for Space Aeronomy, Ringlaan-3-Avenue Circulaire, B-1180 Brussels, Belgium

Abstract

We show that there exists apparent contradiction between the temperature spectra derived from the *Spektr-R* data and the temperature spectra predicted theoretically. We show that the temperature fluctuations can be correctly estimated from the *Spektr-R* data only if the mean temperature is isotropic. Since the mean temperature in the solar wind is usually anisotropic, the derived fluctuations appear to be pseudo-temperature rather than temperature. These pseudo-temperature fluctuations are driven by the high-amplitude magnetic fluctuations in Alfvén waves rather than the fluctuations of temperature or thermal velocity.

Keywords: *Solar Wind: Turbulence*

1. Introduction

Plasma ion moments (density, velocity and temperature) in the solar wind are usually derived using in-situ data collected by means of Faraday cups onboard a spacecraft. Although Faraday cups are quite simple devices, derivation of the plasma moments based on the currents measured by the Faraday cups is nontrivial and requires some kind of nonlinear fitting technique and some assumptions about particle distribution functions. Because of the complex fitting procedures, determination of the measurement errors in the obtained plasma moments is also nontrivial (Bruno & Carbone, 2013, Gogoberidze et al., 2012b, Hnat et al., 2011, Kasper et al., 2002).

Recently, Safrankova et al. (2013) analyzed spectra of velocity, density and thermal speed in the frequency range 0.001 – 2 Hz, therefore covering both magnetohydrodynamic (MHD) and kinetic ranges. These spectra were obtained using measurements of the Bright Monitor of the Solar Wind on board the *Spektr-R* spacecraft. The authors found that the spectral indices and spectral breaks between MHD and kinetic ranges were very similar for the bulk velocity and thermal speed, whereas the spectral behavior of the density fluctuations was entirely different. We found these results surprising because velocity perturbations are mostly due to the dominant Alfvénic component of the turbulence (Gogoberidze et al., 2012a), whereas the density and temperature fluctuations belong to the subdominant compressible fraction. This means it is natural to expect similar behavior of the temperature and density spectra rather than temperature and velocity.

In the present paper we attempt to understand this contradiction by analyzing dynamics of high frequency perturbations in the solar wind and methods of their measurements by *Spektr-R*. We show that some plasma parameters derived from the Faraday cup data can be strongly affected by the anisotropy of the proton distribution function. In particular, the derived thermal velocity is strongly dominated by perturbations of the magnetic field (and not parallel and/or perpendicular proton temperatures) and therefore the observed high frequency spectrum of the thermal speed is mainly produced by the incompressible part of the magnetic field perturbations, thus explaining its similarity with the proton velocity spectrum.

*grigol_gogoberidze@iliauni.edu.ge, Corresponding author
†g.machabeli@iliauni.edu.ge
‡voitenko@oma.be

DOI: 10.52526/25792776-2020.67.2-227

2. Thermal spectra from MHD to kinetic scales

For the proton velocity distribution $f(\vec{v})$ the current dI measured by the Faraday cup due to an elementary volume d^3v in the velocity space is (Kasper et al., 2002)

$$dI = eAf(\vec{v})\hat{n} \cdot \vec{v}d^3v. \tag{1}$$

Here A is the effective area of the Faraday cup and $\hat{n}$ is the direction along the main axes of the cylinder. The particle distribution function of protons in the solar wind is not isotropic and can be fitted by bi-Maxwelian distribution with different temperatures along and perpendicular to the mean magnetic field. The total Faraday cup current ΔI due to the bi-Maxwelian distribution can be calculated by integrating equation (1) over all proton velocities perpendicular to $\hat{n}$ and within some speed window along the line of sight. As showed by Kasper et al. (2002), the current ΔI measured by the Faraday cup depends not on the parallel ($T_\parallel$) and perpendicular ($T_\perp$) temperatures, but only on their linear combination

$$T_n = T_\parallel \left(\hat{n} \cdot \hat{b}\right)^2 + T_\perp \left[1 - \left(\hat{n} \cdot \hat{b}\right)^2\right]. \tag{2}$$

Here $\hat{b}$ is the unit vector in the direction of the magnetic field.

One can derive the the proton distribution function moments (density, velocity, parallel and perpendicular temperatures) using a fitting procedure for the current measurements ΔI either of different Faraday cups (as in the case of very high resolution data of *Spektr-R* or of the same Faraday cups in different speed intervals (Kasper et al., 2002). From the above consideration it is clear that if the proton distribution function is assumed isotropic, then the corresponding isotropic temperature in both fitting algorithms will be given by the weighted sum of parallel and perpendicular temperatures (2). This is exactly the case with the *Spectr-R* data. Indeed, the algorithm of derivation of the solar wind plasma parameters with extremely high resolution (32 ms) (Safrankova et al., 2013) implies using the simultaneous measurements of 6 Faraday cups to fit five plasma parameters: three components of the particle flux, flow speed and temperature. However, this method works fine only in the case of isotropic temperature $T_\parallel = T_\perp$. In the case of anisotropic temperature, $T_\parallel$ and $T_\perp$ separately cannot by found, only their linear combination T_n is accessible.

Let us introduce the angle θ between the total magnetic field $\mathbf{B}$ and $\hat{n}$, such that the measured temperature T_n (2) can be presented as (Gogoberidze et al., 2013, 2018)

$$T_n = \left(T_\parallel - T_\perp\right) \cos^2\theta + T_\perp. \tag{3}$$

Furthermore, we will distinguish the mean and fluctuating parts of anisotropic temperatures $T_{\parallel,\perp}$ and magnetic field $\mathbf{B}$:

$$T_\parallel = T_{0\parallel} + \delta T_\parallel; \quad T_\perp = T_{0\perp} + \delta T_\perp; \quad \mathbf{B} = \mathbf{B}_0 + \delta\mathbf{B} = \mathbf{B}_0 + \delta\mathbf{B}_\parallel + \delta\mathbf{B}_\perp \tag{4}$$

Then $\cos\theta$ can be expressed in terms of fluctuating magnetic fields exactly,

$$\cos\theta = \sqrt{1 - \left(\frac{\delta B_\perp}{B}\right)^2} \cos\theta_0 + \frac{\delta B_\perp}{B} \cos\phi \sin\theta_0, \tag{5}$$

where θ_0 is the angle between the mean magnetic field $\mathbf{B}_0$ and $\hat{n}$, ϕ is the angle between $\delta\mathbf{B}_\perp$ and $(\hat{n}, \mathbf{B}_0)$ plane, and $B = |\mathbf{B}|$,

$$B = \sqrt{B_0^2 + 2B_0\delta B_\parallel + \left(\delta B_\parallel\right)^2 + (\delta B_\perp)^2}. \tag{6}$$

Note that $\cos\theta$ does not depend on $\delta B_\parallel$ if $\delta B_\perp = 0$.

In general, as follows from (3-5), fluctuations of T_n are caused by the fluctuations of all involved parameters: $\delta T_\parallel$, $\delta T_\perp$, $\delta B_\parallel$, and $\delta B_\perp$. Therefore, the measured spectrum of T_n, or thermal velocity $\sim \sqrt{T_n}$ used by Safrankova et al. (2013), contains contributions of all these sources.

In what follows we show that, for the typical solar wind parameters, the dominant contribution to the spectra of T_n and $\sqrt{T_n}$ comes from the magnetic fluctuations rather than the fluctuations of parallel and perpendicular temperatures. First, we present

$$\cos^2\theta = \cos^2\theta_0 + \delta\left(\cos^2\theta\right), \tag{7}$$

where the $\delta\mathbf{B}$-dependent fluctuating part

$$\delta\left(\cos^2\theta\right) = \left((\cos\phi\sin\theta_0)^2 - \cos^2\theta_0\right)\left(\frac{\delta B_\perp}{B}\right)^2 + \sin\left(2\theta_0\right)\cos\phi\sqrt{1-\left(\frac{\delta B_\perp}{B}\right)^2}\frac{\delta B_\perp}{B} \tag{8}$$

All above expressions (3-8) are quite general, valid for any values of fluctuating parameters. To simplify further analysis we consider the limit of small perturbations, $\delta B_\perp/B$, $\delta T/T \ll 1$. Although this condition is not always satisfied for low frequency magnetic field perturbations it is always valid for the high frequency perturbations close to the spectral break between MHD and kinetic ranges. Then, using (8) in (3) and retaining only leading terms with respect to the small parameters $\delta B_\perp/B$, $\delta T/T \ll 1$, the fluctuating part of can be simplified to

$$\frac{\delta T_n}{T_{0\perp}} = \cos^2\theta_0\frac{\delta T_\parallel}{T_{0\perp}} + \sin^2\theta_0\frac{\delta T_\perp}{T_{0\perp}} + \left(\frac{T_{0\parallel}}{T_{0\perp}} - 1\right)\sin\left(2\theta_0\right)\cos\phi\frac{\delta B_\perp}{B_0}. \tag{9}$$

The dimensionless spectral power of T_n perturbations is thus

$$\frac{\left\langle \delta T_n^2\right\rangle}{T_{0\perp}^2} = \frac{\left\langle \delta T_n^2\right\rangle_T}{T_{0\perp}^2} + \frac{\left\langle \delta T_n^2\right\rangle_B}{T_{0\perp}^2}, \tag{10}$$

where we introduce the thermal contribution

$$\frac{\left\langle \delta T_n^2\right\rangle_T}{T_{0\perp}^2} = \left\langle\left(\cos^2\theta_0\frac{\delta T_\parallel}{T_{0\perp}} + \sin^2\theta_0\frac{\delta T_\perp}{T_{0\perp}}\right)^2\right\rangle \tag{11}$$

and the pseudo-thermal contribution due to magnetic fluctuations

$$\frac{\left\langle \delta T_n^2\right\rangle_B}{T_{0\perp}^2} = \frac{1}{2}\left(\frac{T_{0\parallel}}{T_{0\perp}} - 1\right)^2\sin^2\left(2\theta_0\right)\frac{\left\langle \delta B_\perp^2\right\rangle}{B_0^2}. \tag{12}$$

Here $\langle ...\rangle$ is the ensemble average and we assume that the turbulence is symmetric with respect to ϕ: $\langle\cos\phi\rangle = 0$; $\left\langle\cos^2\phi\right\rangle = 1/2$.

The spectral power density of the "thermal velocity" $V_{Tn} = \sqrt{V_{T\parallel}^2\cos^2\theta + V_{T\perp}^2\sin^2\theta}$ can be found similarly. Again, it consists of two parts, thermal

$$\frac{\left\langle|\delta V_{Tn}|^2\right\rangle_T}{V_{T0\perp}^2} = \frac{1}{4}\frac{\cos^2\theta_0\delta\left(V_{T\parallel}^2\right) + \sin^2\theta_0\delta\left(V_{T\perp}^2\right)}{V_{T0\perp}^2} \tag{13}$$

and pseudo-thermal (due to magnetic fluctuations)

$$\frac{\left\langle|\delta V_{Tn}|^2\right\rangle_B}{V_{T0\perp}^2} = \frac{1}{8}\frac{\left(T_{0\parallel}/T_{0\perp} - 1\right)^2\sin^2\left(2\theta_0\right)}{\left(T_{0\parallel}/T_{0\perp} - 1\right)\cos^2\theta_0 + 1}\frac{\left\langle\delta B_\perp^2\right\rangle}{B_0^2}. \tag{14}$$

It is long known that in the inertial interval of the solar wind turbulence the dimensionless magnetic fluctuations $\delta B_\perp/B_0$ associated with incompressible Alfvén waves are about one order of magnitude higher than the amplitudes of compressional fluctuations associated with perturbations of density and/or temperature, $\sim \delta T_{\parallel,\perp}/T_{0\perp}$ (Gogoberidze et al., 2018):

$$\frac{\delta B_\perp}{B_0} \gg \frac{\delta T_\parallel}{T_{0\perp}}, \frac{\delta T_\perp}{T_{0\perp}}.$$

Then from (12) it is seen that, excluding specific cases when $\sin 2\theta_0 \le 0.1$ or $\left|T_{0\|}/T_{0\perp} - 1\right| \le 0.1$, the measured power spectra of T_n (as well as the corresponding power spectra of V_{Tn}) are dominated by the Alfvénic magnetic fluctuations rather than the fluctuations of the temperature itself.

To estimate the maximum of the thermal contribution (the first term in the rhs of equation (10)) we assume that at any timescale τ the perturbations $\delta T_\perp(\tau)$ and $\delta T_\|(\tau)$ are equal $\delta T_\perp = \delta T_\| = \delta T$ and perfectly correlated. In this case after averaging the thermal contribution in the dimensionless rms power of perturbations is

$$\frac{\left\langle \delta T_n^2 \right\rangle_T}{T_{0\perp}^2} \approx \frac{\left\langle \delta T^2 \right\rangle}{T_{0\perp}^2}. \tag{15}$$

Now we estimate the magnetic contribution to the observed spectrum. As follows from equation (12), this contribution vanishes if $T_{0\|} = T_{0\perp}$ or $\sin 2\theta_0 = 0$. Although in the slow solar wind there are intervals with $T_{0\|} \approx T_{0\perp}$, usually difference between parallel and perpendicular temperatures is quite significant. Taking as the typical values $\sin^2 2\theta_0 \sim \left|\frac{T_{0\|}}{T_{0\perp}} - 1\right| \sim 0.5$ (Kasper et al., 2002), contribution of the Alfvén waves reduces to

$$\frac{\left\langle \delta T_n^2 \right\rangle_B}{T_{0\perp}^2} \approx \frac{1}{8} \frac{\left\langle \delta B_\perp^2 \right\rangle}{B_0^2}. \tag{16}$$

Estimations indicate that the ratio of dimensionless rms amplitudes $\lambda = (\delta T^2/T^2)/(\delta B_\perp^2/B_0^2)$ in the inertial range of stationary solar wind sub-intervals is usually of the order 10^{-2} and almost never exceeds 10% even in the slow streams of the solar wind, which are known to be much more compressible compared to perturbations in the fast solar wind.

3. Discussion and conclusions

We have shown that the nature of "temperature fluctuations" derived from the currents of Faraday cup(s) is strongly affected by the temperature anisotropy. If the temperature anisotropy is close to zero, then the derived "temperature fluctuations" are dominated by the perturbations of real temperature (thermal speed). However, when the temperature anisotropy is finite, as is typical for the solar wind, the "temperature fluctuations" change their source and nature being driven by the Alfvénic magnetic fluctuations rather than the fluctuating parallel and/or perpendicular temperatures. Such "temperature fluctuations", presented by (12) and (14), we call pseudo-thermal. The pseudo-thermal fluctuations and the bulk speed fluctuations have the common source, Alfvén waves, which explains a close similarity of their spectra.

The pseudo-thermal spectra should be even more similar (but with different amplitudes) to the magnetic spectra with which they share the same source - Alfvénic magnetic fluctuations. Therefore, as the magnetometer onboard *Spektr-R* is not operational (Safrankova et al., 2013) and *in situ* magnetic spectra are not available, a good proxy for them can be provided by the pseudo-thermal spectra. These spectra may be useful for testing some theoretical predictions even in the absence of magnetic data. Below we summarise several preliminary results in this direction.

1. Apparent fluctuations of the proton thermal velocity and the corresponding spectra deduced from the *Spektr-R* data are due to the Alfvénic magnetic fluctuations rather than the temperature fluctuations. Fluctuations of the bulk velocity and their spectra, observed simultaneously by *Spektr-R*, are produced by the Alfvénic velocity fluctuations. These two facts, together with the Alfvénic link between velocity and magnetic fluctuations, explain why the pseudo-thermal velocity spectra are so similar to the bulk velocity spectra.

2. We argued that the authentic thermal spectrum in the solar-wind turbulence (11) should closely resemble the density spectrum shown in Fig. 1c by Safrankova et al. (2013). However, this thermal spectrum is usually obscured by the magnetic pseudo-thermal spectrum and can rarely rise above it. As follows from equation (12) careful selection of the intervals with $T_{0\|} = T_{0\perp}$ or $\sin 2\theta_0 \approx 0$ could help in extracting authentic thermal spectra from the *Spektr-R* data and compare them with the density spectra.

3. In view of above, several previous conclusions about similarity between the thermal and bulk velocity spectra (Safrankova et al., 2013) appear to be incorrect. The reason behind these mistakes is

that the authors did not distinguish the proper thermal spectrum from the pseudo-thermal spectrum established by magnetic fluctuations. Between these two, only the latter spectrum can resemble the bulk velocity spectrum. On the contrary, the authentic thermal spectrum should resemble the density spectrum, which is still subject for future experimental verification.

Acknowledgements

This work has been supported by Shota Rustaveli National Science Foundation grant FR-18-19964.

References

Bruno R., Carbone V., 2013, Liv. Rev. Sol. Phys., 10, 2

Gogoberidze G., Chapman S. C., Hnat B., 2012a, Phys. Plasmas, 19, 102310

Gogoberidze G., Chapman S. C., Hnat B., Dunlop M. W., 2012b, MNRAS, 426, 951

Gogoberidze G., Perri S., Carbone V., 2013, ApJ, 769, 111

Gogoberidze G., Voitenko Y., Machabeli G., 2018, MNRAS, 480, 1864

Hnat B., Chapman S. C., Gogoberidze G., Wicks R. T., 2011, PRE, 84, 065401

Kasper J. C., Lazarus A. J., Gary S. P., 2002, GRL, 29, 1839

Safrankova J., Nemecek Z., Prech L., Zastenker G. L., 2013, PRL, 110, 025004

Turner A. J., Gogoberidze G., Chapman S. C., 2012, PRL, 108, 085001

Communications of BAO, Vol. 67, Issue 2, 2020, pp. 232-235

INT monitoring survey of Local Group dwarf galaxies: star formation history and chemical enrichment

T. Parto*[1,2], Sh. Dehghani[3], A. Javadi[1,4], E. Saremi[1], J. Th. van Loon[5], H. Khosroshahi[1], M. T. Mirtorabi[2], H. Abdollahi[2], M. Gholami[2], S.A. Hashemi[4], M. Navabi[1], M. Noori[6], S. T. Aghdam[1], M. Torki[6], and M. Vafaeizade[2]

[1]School of Astronomy, Institute for Research in Fundamental Sciences (IPM), PO Box 19395-5531, Tehran, Iran
[2]Physics Department, Alzahra University, Vanak, 1993891176, Tehran, Iran
[3]Physik. Institut, University of Cologne, Zulpicher Str. 77, D-50937 Cologne, Germany
[4]Department of Physics, Sharif University of Technology, Tehran, 11155-9161, Iran
[5]Astrophysics Group, Lennard-Jones Laboratories, Keele University, Staffordshire ST5 5BG
[6]Physics Department, Faculty of Science, University of Zanjan, Zanjan 45371-38791, Iran

Abstract

The Local Group (LG) hosts many dwarf galaxies with diverse physical characteristics in terms of morphology, mass, star formation, and metallicity. To this end, LG can offer a unique site to tackle questions about the formation and evolution of galaxies by providing detailed information. While large telescopes are often the first choices for such studies, small telescope surveys that perform dedicated observations are still important, particularly in studying bright objects in the nearby universe. In this regard, we conducted a nine epoch survey of 55 dwarf galaxies called the "Local Group dwarf galaxies survey" using the 2.5m Isaac Newton Telescope (INT) in the La Palma to identify Long-Period Variable (LPV) stars, namely Asymptotic Giant Branch (AGB) and Red Super Giant (RSG) stars. AGB stars formed at different times and studying their radial distribution and mass-loss rate can shed light on the structure formation in galaxies. To further investigate the evolutionary path of these galaxies, we construct their star formation history (SFH) using the LPV stars, which are at the final stages of their evolution and therefore experience brightness fluctuations on the timescales between hundred to thousand days. In this paper, we present some of the results of the Local Group dwarf galaxies survey.

Keywords: *stars: AGB and RSG - Stars: LPVs - Stars: dust - galaxies: evolution - galaxies: star-formation - galaxies: Local-Group - galaxies: dwarf*

1. Introduction

Dwarf galaxies are the most common type of galaxies in the universe. The importance of the internal and external processes (e.g., supernova explosion; interaction with the massive halos) on the evolution of these small galaxies are well known, though with many unanswered aspects (Weisz et al. 2014; Saremi et al. 2020). The star formation history (SFH) is a robust tracer of how different internal or external mechanisms affect the evolution of a galaxy (Saremi et al. 2019b).

The cool asymptotic giant branch (AGB) stars with luminosities of $\sim 10^4 L_\odot$ and wide age ranges, from 100 Myr to older than 10 Gry, are well-known probes of the stellar population of galaxies in the near-infrared (Habing et al. 2004; Javadi et al. 2011a, 2017)

especially in the nearby universe. Many evolved AGBs, to be specific, thermally pulsing AGBs (TP-AGB), are long-period variables (LPVs; Marigo et al. 2017), therefore they experience brightness fluctuations on the timescales between 100 to 1300 days due to the low surface gravity (Javadi & van Loon 2019). TP-AGBs are responsible for a significant fraction of the integrated light of a galaxy, they also contribute meaningfully to the chemical enrichment of the interstellar medium (ISM) through

*tahereparto@gmail.com, Corresponding author

DOI: 10.52526/25792776-2020.67.2-232

different mechanisms that drive the stellar wind. Red supergiant (RSG) stars with the look-back time 10^7 years are another major dust producers and are examples of LPVs and their brightness variates between 600 to 900 days (Javadi & van Loon 2019).

This survey aims to uniformly determine the SFH of 55 dwarf galaxies of the Local Group (LG) by adopting a novel method. This method was first proposed and applied to the M33 by (Javadi et al. 2011b) and relies on the identification of LPVs. There are some other successful applications of this method on dwarf galaxies in LG (e.g., IC 1613 Hashemi et al. 2018; LMC and SMC Rezaeikh et al. 2014; NGC 147 and NGC 185 Hamedani Golshan et al. 2017). Using this method, We can also monitor the amount of produced dust by LPVs, and investigate their role in the star formation and evolution of a galaxy. Surveying this large sample of LG dwarfs, enables us to determine the evolutionary dependense of dwarfs galaxies on the enviroment, such as proximity to the host galaxies and compare it with internal effects like the stellar mass or gas content (Saremi et al. 2019a).

2. Observations and Data

The sample of dwarf galaxies studied in this survey consists of all observable Andromeda system of satellites in the northern hemisphere, along with 20 satellites of Milky Way and some isolated and transitional dwarfs (Saremi et al. 2017). We exclude galaxies that have been studied with Javadi's method before.

The Observations were made in 9 epochs between 2015-2018 using the Wide Field Camera (WFC), an optical mosaic camera on the INT telescope. WFC consists of four 2048×4096 CCDs, with a pixel scale of 0.33 arcsec/pixel.

We used the i-band filter that is suited for identifying dusty AGBs. We also performed observations in the V-band to obtain the changes in the color (temperature) of stars. For each galaxy, the observation nights are separated by a month or more to identify LPV stars.

We reduce the WFC images using the THELI image processing pipeline (Erben et al. 2005). After the reduction process, We perform photometry for the crowded-field using DAOPHOT II (Stetson 1987) to construct a catalog for each galaxy. Furthermore, a completeness test carried out using the ADDSTAR task in the DAOPHOT II package to show the depth of our photometry. To remove the foreground contamination, we impose selection criteria on the proper motion and parallax of stars estimated in the *GAIA* Data Release 2 (Gaia Collaboration et al. 2018). The complete description of observations and details of the photometry procedure is available at (Saremi et al. 2020).

3. Method

3.1. LPV candidates detection

To identify LPV candidates, we employed a method described in (Stetson 1996) to determine the variability index L for each star. Then we estimated a threshold for variability, using the variability distribution for the stars in different magnitude bins (Javadi et al. 2011a; Saremi et al. 2020)

With insufficient observation night, we can not obtain a meaningful period for LPVs. However, there is a correlation between the amplitude and period of a variable star (Goldman et al. 2019), and large amplitude variables (LAV) are usually evolved AGBs at the late stage of their life.

Fig. 1 shows the color-magnitude diagram (CMD) of SagDIG, one of the dwarf irregular galaxies in our sample with the overplotted PARSEC–COLIBRI isochrones (Marigo et al. 2017). LPV candidates are shown as blue circles, with a size scaled to their amplitude in the i-band with values between $0.1 - 1.87$ *mag*.

3.2. SFH from LPV pulsation

The luminosity of AGB stars reaches a maximum at the final stage of life, hence can be used to estimate the birth mass of the star. For determining the mass, we construct the mass function of LPVs (for the suitable metalicity) by interpolating mass-luminosity relation using the PARSEC–COLIBRI isochrones. After estimating age of LPVs using the mass-age relation, we determine pulsation duration by fitting multiple Gaussian functions to the mass-pulsation values in the isochrones that show strong pulsations.

The star formation rate (SFR) function $\xi(t)$ introduced in (Javadi et al. 2011b) takes mass, age and pulsation duration of LPVs and estimates the stellar mass formed per year ($M_{\odot}y^{-1}$):

$$\xi(t) = \frac{\mathrm{dn(t)}}{\delta t} \frac{\int_{min}^{max} f_{IMF}(m)m\,dm}{\int_{m(t)}^{m(t+dt)} f_{IMF}(m)m\,dm}. \tag{1}$$

where f_{IMF} is the initial mass function (Kroupa 2001), dt represents different age bins, and dn is the number of observed LPVs in each age bins.

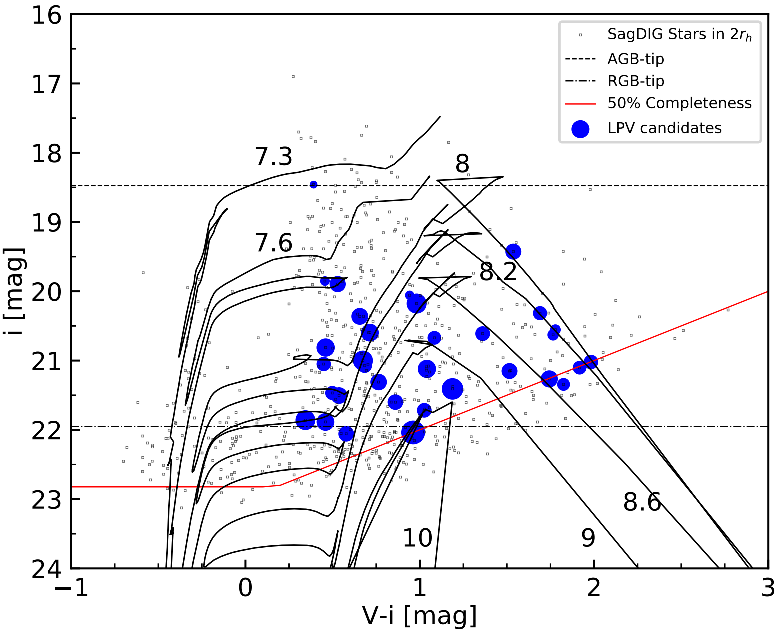

Figure 1. [i] vs. [V-i] CMD for SagDIG with the overplotted isochrones. Black dots denote the stars within the two half-light radius of this galaxy. Blue circles are the LPV candidates with a size scaled to their amplitude. The dotted line marks RGB-tip and AGB-tip. The 50% completeness is represented by the solid red line.

4. Results and On–going works

Here we present results of published papers for three galaxies: And I and And VII, two dwarf spheroidal and satellite of Andromeda, and IC 10, an irregular and isolated galaxy.

(Saremi et al. 2020) detected 59 LPV candidates within the two half-light radii of And I, including five extreme AGBs (X-AGB). They also modeled the spectral energy distribution (SED) of these stars, using *DUSTY* code (Ivezic & Elitzur 1997) and mid-IR bands measurement from Spitzer (3.6 and 4.5 μm), WISE (W1=3.4, W2=4.6, W3=11.6, and W4=22 μm) (Cutri & et al. 2014; Wright et al. 2010), INT near-infrared i-band catalog and SDSS (u, g, r ,z) filters. They evaluated the total mass-loss rate of $3.5 \times 10^{-5} M_{\odot}yr^{-1}$ from five X-AGBs and thirteen dusty AGBs, which suggest low growth of stellar mass ($\sim$ 10 %) in AND I in the next 10 Gyr.

(Navabi et al. Submitted, 2020) detected 43 LPV candidates within the half-light radii of And VII, and estimated the SFR peak of this area about 0.002 $M_{\odot}yr^{-1}$ at Z=0.0007. Probably, And VII was quenched by environmental impacts after infall into Andromeda's virial radius (Navabi et al. 2020a, 2020b).

(Gholami et al. 2019) detected around 10000 AGB stars in IC 10 in the area of CCD4 (~ 0.07 square-degree). They found that the AGB population concentrated more in the central region of IC 10, while the red giant branch (RGB) and RSG stars are more spread (Gholami & Mirtorabi 2019).

In the following, we complete this study for other dwarfs and construct the dust map of the galaxy. We later discuss our results in light of different structure formation scenarios and the importance of internal feedbacks in LG dwarf galaxies.

Acknowledgements

The observing time for this survey is provided by the Iranian National Observatory and the UK-PATT allocation of time to programs I/2016B/09 and I/2017B/04 (PI: J. van Loon). The authors thank the Iranian National Observatory and the School of Astronomy (IPM) for the financial support of this project.

References

Cutri R. M., et al. 2014, VizieR Online Data Catalog, p. II/328

Erben T., et al., 2005, AN, 326, 432

Gaia Collaboration et al., 2018, A&A, 616, A1

Gholami M., Mirtorabi M., 2019, IJAA, 6, 53

Gholami M., Javadi A., van Loon J. T., Khosroshahi H., Mirtorabi M. T., Saremi E., Eftekhari S., 2019, in McQuinn K. B. W., Stierwalt S., eds, Vol. 344, Dwarf Galaxies: From the Deep Universe to the Present. pp 70–72, doi:10.1017/S1743921318006531

Goldman S. R., et al., 2019, ApJ, 877, 49

Habing H., Olofsson H., Editors. 2004, Asymptotic Giant Branch Stars. Springer

Hamedani Golshan R., Javadi A., van Loon J. T., Khosroshahi H., Saremi E., 2017, MNRS, 466, 1764

Hashemi S. A., Javadi A., van Loon J. T., 2018, MNRAS, 483, 4751

Ivezic Z., Elitzur M., 1997, MNRAS, 287, 799

Javadi A., van Loon J. T., 2019, IAU Symposium, 343, 283

Javadi A., van Loon J. T., Mirtorabi M. T., 2011a, MNRS, 411, 263

Javadi A., van Loon J. T., Mirtorabi M. T., 2011b, MNRAS, 414, 3394

Javadi A., van Loon J. T., Khosroshahi H. G., Tabatabaei F., Hamedani Golshan R., Rashidi M., 2017, MNRAS, 464, 2103

Kroupa P., 2001, MNRAS, 322, 231

Marigo P., et al., 2017, ApJ, 835, 77

Navabi M., Noori M., Saremi E., Javadi A., van Loon J., Khosroshahi H., 2020a, in Neiner C., Weiss W. W., Baade D., Griffin R. E., Lovekin C. C., Moffat A. F. J., eds, Stars and their Variability Observed from Space. pp 383–385

Navabi M., Saremi E., Javadi A., Noori M., van Loon J., Khosroshahi H., 2020b, Proceedings of 27th Ipm Physics Spring Conference, 20

Rezaeikh S., Javadi A., Khosroshahi H., van Loon J. T., 2014, MNRAS, 445, 2214

Saremi E., et al., 2017, Journal of Physics: Conference Series, 869, 012068

Saremi E., Javadi A., van Loon J., Khosroshahi H., Torki M., 2019a, in Griffin R. E., ed., Vol. 339, Southern Horizons in Time-Domain Astronomy. pp 336–339, doi:10.1017/S1743921318002958

Saremi E., Javadi A., van Loon J. T., Khosroshahi H., Rezaei Kh S., Golshan R. H., Hashemi S. A., 2019b, in McQuinn K. B. W., Stierwalt S., eds, Vol. 344, Dwarf Galaxies: From the Deep Universe to the Present. pp 125–129 (arXiv:1812.09725), doi:10.1017/S1743921318005574

Saremi E., et al., 2020, Apj, 894, 135

Stetson P. B., 1987, PASP, 99, 191

Stetson P. B., 1996, PASP, 108, 851

Weisz D. R., Dolphin A. E., Skillman E. D., Holtzman J., Gilbert K. M., Dalcanton J. J., Williams B. F., 2014, ApJ, 789, 147

Wright E. L., et al., 2010, AJ, 140, 1868

Communications of BAO, Vol. 67 Issue 2, 2020, pp 236-240

Observational Data Related to the Largest Galaxies of the Universe: What they Tell?

Harutyunian H. A*

Byurakan Astrophysical Observatory, Armenia

Abstract

The physical mechanism of interaction between dark energy and ordinary baryonic matter is used to show that Ambartsumian's cosmogonic paradigm on the galaxy formation gets new support. This mechanism is considered to compare the cD galaxies observational properties with the model predictions in the framework of the suggested paradigm.

Keywords: *Dark energy; evolution, baryonic matter, mass growth, cD galaxies*

1. Introduction

For construction of galaxy formation scenarios one should study galaxies together with their local environments. Two mutually exclusive hypotheses concerning the genetic links between a galaxy and its local environment are possible ways for their birth and evolution. First scenario, widely discussed and repeatedly studied by researchers,is the possible physical influence of the environment on the galaxy's formation process. Second possibility,remaining on the hypothesis level, is the contrary situation when the galaxy forms its environment.

The most luminous galaxies of the Universe or Brightest Cluster Members (BCMs) are unique ones and their formation history is not physically transparent. cD galaxies form the special high luminosity end of the BCMs. These objects have been classified and named in mid 60s of the last century (Matthews et al., 1964) to distinguish them from large elliptical galaxies. The morphological and other appearance features definition of cD galaxies done almost at the same time when these galaxies have been identified as a separate type remains unchanged (Morgan & Lesh, 1965) and have been modified slightly in course of time. These galaxies have the following common features.They are located exclusively in regular rich clusters of galaxies where they are the BCMs or the Second Brightest Cluster Galaxies (SBCGs) and they are never found as field galaxies.They are located in the center or very close to the center of the hosting cluster.They are never very oblate (see also, Beers & Geller, 1983, Oemler, 1976, White, 1978). They have bright elliptical core or "main body" which is imbeddedinto an amorphous envelope (see, for example, Hoessel & Schneider, 1985, Schombert, 1988, Tonry, 1985).

Schombert (1988) mentions that cD envelopes are found in a range of cluster environments, from regular, compact clusters to irregular, highly subclustered systems.It changes slightly the first item in the enumerated initially features characterizing cD galaxies. There is one more modification stating that cD envelopes can be found around non-first-ranked ellipticals such as NGC 4839 in Coma (Oemler, 1976) or NGC 6034 in Hercules (Schombert, 1984). However, all cD envelopes were found at local cluster density maxima (see Beers & Geller, 1983), but never discovered in the field.

It is evident that one should consider the scenario of galaxies formation in a cluster parallel with the cluster formation. The very fact that the existence of a central galaxy and its morphological type clearly correlates with the cluster type, lies at the base of cluster classification in which the type I designate systems containing cD galaxy (Bautz & Morgan, 1970). Clusters belonging to this type of

*hhayk@bao.sci.am

DOI: 10.52526/25792776-2020.67.2-236

systems are the most regular ones, exhibiting obvious concentration of members towards the cluster center and possessing of mainly early types of galaxies. For the cD galaxies has been revealed a sharp correlation between the luminosities of the galaxy halo L_k and cluster L_{cl} (Oemler, 1976). The latter correlation got a firm corroboration when appeared that BCMs in poor clusters do not possess of an envelope (Albert et al., 1977, Morgan et al., 1975).

cD galaxies differ markedly from other elliptical galaxies by their internal kinematical features as well. Usually as the main kinematical characteristic of elliptical galaxies, one uses the velocity dispersion. As a rule, this feature has its greatest value at the center of the galaxy disk (higher for the high luminosity galaxies) named Faber-Jackson relation (Faber & Jackson, 1976) serves as a good tool for determination of absolute luminosities of elliptical galaxies. It was shown that this relation is shallower for the supergiant cD galaxies than for ordinary ones (Efstathiou et al., 1980, Lauer et al., 2006, Malumuth & Kirshner, 1981, Oegerle & Hoessel, 1991). It was shown also that they have larger radii than predicted by Kormendy relation (Hoessel & Schneider, 1985, Oegerle & Hoessel, 1991, Schombert, 1987, Thuan & Romanishin, 1981).

Differences of cD physical features from other elliptical galaxies prompted researchers to create special scenarios for their formation mechanism. Indeed, at the beginning, BCGs were suggested to form due to the merging mechanism when the cluster galaxies sink to the bottom of the cluster gravitational potential well and merge (so called, galactic cannibalism Ostriker & Tremaine, 1975, White, 1976). Meanwhile, theoretical analyses (Merritt, 1976) showed that this mechanism is not providing with the requested masses for building the BCGs. Moreover, the "merger scenario" should change the color of galaxies – they should be bluer for their luminosities. No such color differences have been revealed (Gallagher et al., 1980, Schombert, 1988).

2. Evolution Scenario via Energy Injection and Active Decay

Ambartsumian (Ambartsumian, 1958) was the first to suggest a scenario describing the galaxy formation from the Galactic Active Nuclei (AGN) through the initial bare nucleusgradual decay physical process. According this hypothesis all the cosmic objects form from denser (superdense) matter due to ejection of smaller portions of it, which forms stars and interstellar gas.

This idea was a natural sequel of his preceding series of researches devoted to the stellar associations (Ambartsumian, 1947) for the higher level of cosmic objects hierarchy. Stellar associations, the author showed, evolve from a smaller volume and are nests of young stars. The discovery and further studies of stellar associations showed that star formation is an ongoing process in our Galaxy and that in any galaxy there can exist different generations of stars. Today this assertion does not seem strange as was about seventy years ago, and the scientific community adopted the fact of newborn stars existence.

The next stage of our understanding of the cosmic objects formation and their evolution, we believe, should be the recognition of the fact that in our observable Universe adjoin different generations of galaxies, including ones born very recently. In any galaxy, star formation takes place in star formation regions and further evolution continues in stellar associations until they dissolve in the common field of galaxies. Evidently, this process goes on in the direction of decreasing the space density of stars. That was the main reason for the appearance of the hypothesis concerning the existence of matter in superdense state. On the other hand, this kind of expansion and decay process somehow reiterates the process of the Universe expansion for the smaller scales.

Although the fact that the formation of stars in our cosmogonic era is no longer in doubt, the idea that they are the result of the decay of very dense matter was rejected. The reason of rejection was very practical. The modern theoretical physics does not permit the existence of any stable superdense configuration of baryonic matter exceeding several solar masses.Actually, the same reason ceased future discussions on the galaxy formation by means of decay of superdense pre-stellar baryonic nucleus, existing as pre-galactic configuration and not populated yet by stars, gaseous and dust clouds.

However, the scientific community carried out all these discussions and made the suitable conclusions about half a century ago. After that no serious studies in this field appeared. Nonetheless, researchers managed to discover some new physical effects, which could change our approaches to problems discussed above. Above all, the mentioned concerns the discovery of the accelerated expansion of the Universe and introducing the idea of dark energy into the scientific toolkit. Having even very obscure ideas concerning the dark energy, one should try to understand the physical consequences of real interaction between the new substance and baryonic matter. One needs to apply the adopted physical laws in a self-consistent way, keeping in mind that almost all the mass of baryonic objects is concentrated in their nuclei, which have very specific structural properties, called mass defect and binding energy.

The most important conclusionmade on the base of this hypothesisis one asserting the Universe total mass growth in the course of evolution. This growing is due to interaction of the baryonic matter with the carrier of dark energy, taking place according to the second law of thermodynamics. It appears that if one applies the physical laws in a self-consistent way, one should inevitably arrive at the conclusion that owing to the interaction with the carrier of dark energy, in the atomic nuclei gradually decreases the lack of energy and therefore grows their mass (Harutyunian, 2017, Harutyunian & Grigoryan, 2018). It does mean that in the distant past all same atomic nuclei could have been lighter and possessing much greater binding energy.

Moreover, one arrives at a conclusion that in the past there could have been existed atomic nuclei consisting of much more nucleons than we know at present.Evolution of cosmic objects goes on simultaneously making the mass of atomic nuclei larger consequently growing the mass of objects consisted of these atoms.Therefore, a successive decay of atomic nuclei and baryonic objects consisted of atoms should happen if those exceed the maximal mass permitted by physical lows for the given epoch of the matter evolution.

The long-lasting evolutionary growth of the Universe mass explains also a paradox why the Universe continues expanding although it should close with a bang after its birth through big bang. Indeed, if the baryonic mass of the Universe really appeared at once from a cosmic vacuum in a small area it should have been located within the Schwarzchild radius for rather long time. The modern gravitational theories accepted by the scientific community the black whole conditions existed obviously, provided that, such a physical phenomenon is possible at all.

Returning to the Ambartsumian hypothesis and keeping in mind these new ideas on the atomic nuclei evolution during the cosmological time, one should speak not about the mass of the baryonic matter but about the number of baryons. It seems more plausible that baryonic matter physical properties are directly depending on the general physical conditions and loss their mass in expense of binding energy if these conditions are like ones the Universe had long ago. In any cosmic object, consisted of baryonic matter, should show evolutionary gradient toward its center. The closer any given area is to the center of an object, the more matter there lags behind in the evolutionary path.

Therefore, it is also plausible that in the interior of massive objects (e.g. stars, galactic nuclei) exist a vast quantity of matter. However, the large quantity here deals with the baryons number, which could possess of a comparatively smaller mass. The mass should grow gradually accumulating the injected into atomic nuclei dark energy. In some moment of evolution when the growing mass exceeds the limit of stability the object gets into the class of non-stability or activity. Like the radioactive atomic nuclei, such object should decay or eject some part of its internal baryonic mass, which has all chances to become a new object belonging to the same hierarchical class or lower.

3. 3. Formation of Cluster of Galaxies via Matter Ejection from the First Central Body

If the evolution of the cosmic objects takes place according the decay/ejection scenario, at any stage of the Universe evolution there should exist cosmic objects of various sizes consisted of baryonic matter. These objects evolve due to influence of dark mater, continuously fitting their physical state to the external space properties of the given epoch of expansion. We assume that the baryonic matter of the object's surface layers, bordering with the free space evolves faster than its interior. However, the evolution process is going on in the internal arias as well and the object gets more massive and energetically instable. Due to the energy interactions,some clots of baryonic matter can acquire the required amount of energy and escape from the object. This process resembles evaporation mechanism or cluster type decay of atomic nuclei.

Depending on the mass (or, rather, number of baryonic embryos) of the object and its spin value, the further evolution can have various scenarios. The simplest dynamics has the nonrotating object, which is subject of the dark energy influence only. Therefore, all the ejections, if any, have isotropic distribution in space. Obviously, possessing of an axial rotation adds new dynamical effect provided by the centrifugal acceleration, which is maximal on the equator. It does mean that ejection in the equator plane becomes more probable and one can see more clots of matter in the equatorial plane than in other directions. The bigger is the rotational velocity, the more is differences between the populations in the equatorial and any other planes.

We consider here the simplest model of a nonrotating baryonic clot interacting with dark energy. Then the dark energy is the only factor affecting such an object and baryonic matter clumps ejected by the parental object should have more or less isotropic distribution around it. This process, on the other hand, goes on comparatively calmly and clamps' formation takes place closer to the surface layers. These clamps can consist of very different number of baryonic embryos if the parental object consists of sufficiently large number of these particles. If the parental clamp consists of a vast number baryonic embryo enough for producing hundreds of galaxies, it will eject not only smaller ones but also larger proto-galaxies.

Considering this scenario, one should keep in mind that every new daughter-clump interacts with the dark energy and experiences changes similar to the parental one taking into account the scale differences. Baryonic matter will continue to accumulate a part of the dark energy and transform a part of it into the baryonic mass, simultaneously making the proto-object more and more instable, until it will eject its own daughter clumps. The common property in this picture is that every such clump can form various cosmic objects belonging to the parental hierarchical level or lower.

Now, let us consider the particular case of largest clump, consisted of so huge number of baryonic embryo, which is enough to form several thousand galaxies.It does mean that this scenario could describe the formation process of various mass galaxies, stellar clusters, individual stars. The process of mass ejection goes on involving formation of the next level objects in the daughter clumps, which, in its turn, entails mass ejection process as well. If the clump gained enough impulse during the ejection to get the escape velocity, it will continue its retreat movement gradually decreasing the initial speed.

On the other hand, if the daughter proto-object ejects next level clumps, the parental object might capture some part of those, depending on direction of its motion. The captured debris will form some kind of halo around the parental object. The halo evidently will have as higher luminosity, as more daughter clumps (to become galaxies) ejects the central (parental) galaxy. It is impossible to find such galaxy outside of a cluster of galaxies. The cluster formed in this way will have a regular spherical shape inasmuch as the paternal objects ejects daughter clumps in all directions equally. Nearly all galaxies, formed owing to the described here mechanism, should belong to the earlier classes, since the nonrotating, parental galaxy could not provide them with ample rotational moment to form a disk galaxy. Moreover, the richer is the cluster of galaxies the closer to the center is the cD galaxy. Evidently, when the number ejections form the cluster galaxies is small, the statistics is not enough yet for constructing the real distribution following from the isotropic ejection of proto-galaxies in the cluster.

4. Conclusion

The newly suggested hypothesis on the interaction between the baryonic matter and dark energy opens new perspectives for the further development of Ambartsumian's cosmogonic paradigm. The biggest obstacle for applying his paradigm was the assertion on the impossible existence of superdense matter of high mass. The refusing of his idea, based on the modern physics laws and axioms about half a century ago, made it hopeless without any possible way for further progress.

Nevertheless, the discovery of dark energy changed the situation drastically. It opens new rooms for the better understanding of the Nature of the Universe. One of the most important conclusions linked to the existence of this new type of energy is one, stating that in the course of evolution the mass of baryonic universe grows up at the expense of dark energy injection. It is interesting that known laws and axioms of modern physics solely allow one of making these conclusions. Actually, one arrives at this conclusion simply employing the second law of thermodynamics.

References

Albert C. E., White R. A., Morgan W. W., 1977, ApJ, 211, 309

Ambartsumian V. A., 1947, The evolution of stars and astrophysics

Ambartsumian V. A., 1958, in La structure et l'évolution de l'universe. pp 241–249

Bautz L. P., Morgan W. W., 1970, ApJL, 162, L149

Beers T. C., Geller M. J., 1983, ApJ, 274, 491

Efstathiou G., Ellis R. S., Carter D., 1980, MNRAS, 193, 931

Faber S. M., Jackson R. E., 1976, ApJ, 204, 668

Gallagher J. S., Faber S. M., Burstein D., 1980, ApJ, 235, 743

Harutyunian H. A., 2017, Astrophysics, 60, 572

Harutyunian H. A., Grigoryan A. M., 2018, Communications of the Byurakan Astrophysical Observatory, 65, 268

Hoessel J. G., Schneider D. P., 1985, AJ, 90, 1648

Hoessel J. G., Oegerle W. R., Schneider D. P., 1987, AJ, 94, 1111

Lauer T. R., Gebhardt K., Richstone D., Faber S. M., Tremaine S., 2006, The Most Massive Black Holes in the Local Universe, NOAO Proposal

Malumuth E. M., Kirshner R. P., 1981, ApJ, 251, 508

Matthews T. A., Morgan W. W., Schmidt M., 1964, ApJ, 140, 35

Merritt R., 1976, Instrum. Technol, 23, 27

Morgan W. W., Lesh J. R., 1965, ApJ, 142, 1364

Morgan W. W., Kayser S., White R. A., 1975, ApJ, 199, 545

Oegerle W. R., Hoessel J. G., 1991, ApJ, 375, 15

Oemler A. J., 1976, ApJ, 209, 693

Ostriker J. P., Tremaine S. D., 1975, ApJL, 202, L113

Schombert J. M., 1984, PhD thesis, Yale University., New Haven, CT.

Schombert J. M., 1987, ApJS, 64, 643

Schombert J. M., 1988, ApJ, 328, 475

Thuan T. X., Romanishin W., 1981, ApJ, 248, 439

Tonry J. L., 1985, AJ, 90, 2431

Von Der Linden A., Best P. N., Kauffmann G., White S. D. M., 2007, MNRAS, 379, 867

White S. D. M., 1976, MNRAS, 174, 19

White R. A., 1978, ApJ, 226, 591

The most evolved sources in the Hi-GAL survey

Elia D.*

INAF-IAPS, Roma, Italy

Abstract

Far-infrared and submillimetre surveys as the *Herschel* Galactic Plane Infrared Survey (Hi-GAL) represent an irreplaceable knowledge base about early phases of star formation, permitting statistical analysis based on thousands of Galaxy-wide distributed sources. Those with a regular spectral energy distribution in the *Herschel* wavelength range 70-500 μm span a variety of evolutionary stages, from quiescent to star forming clumps and, within the latter class, from mid-infrared dark clumps to sources appearing very bright also at shorter wavelengths (e.g. *Spitzer* 24 μm). A fraction of these clumps hosts the formation of high mass stars, which are expected to reach the zero age main sequence and to develop a HII region in their surroundings while they are still embedded in their parental large-scale dusty envelope. This paper aims at selecting and studying in detail a robust sample of Hi-GAL clumps supposed to be candidate to host a HII region in their interior. They are expected to be the most evolved sources in the Hi-GAL catalogue. The Galactic locations and the physical properties (temperature, mass, bolometric luminosity and temperature, and surface density) of these sources are discussed here. The large number (1199) of selected sources constitutes an important starting point for planning further interferometric programs, aimed at resolving possible cores hosting a young high-mass star.

Keywords: *Stars: formation – ISM: clouds – ISM: dust – Galaxy: local interstellar matter – Infrared: ISM*

1. Introduction

The influence of massive stars ($M > 8$ M$_\odot$) extends well beyond their immediate neighbourhoods, having effects on the interstellar medium and Galactic evolution. Through strong stellar winds and, finally, supernovae explosions, they enrich the interstellar medium by injecting mechanical energy and supplying it with processed material. Furthermore, their radiation output is the responsible of the ionization of the surrounding gas. Therefore they influence the subsequent star formation in their environments, being even a possible triggering mechanism of it. On a larger scale, stellar winds from massive stars and and supernovae lead to the formation of super-bubbles.

Despite their importance, massive stars represent a minority of the Galactic population, as it can be deduced from the slope of the well-known stellar initial mass function (Kroupa, 2001, Salpeter, 1955). Their evolutionary time scales, including that of the formation process, are considerably shorter than in their low-mass counterparts, so that the details of the phases of massive star formation are still elusive. Consequently, the need of observing sites of massive star formation to probe the early phases of this process and their connection with the surrounding environment clashes with the low availability of such regions in the Solar neighbourhoods: the large majority of known massive star forming regions are located beyond a few kiloparsecs from the Sun, and prospectively distributed on the Galactic plane.

In this respect, unbiased global-scale surveys of the Milky Way Galactic plane from infrared to radio wavelengths represent, compared with studies dedicated to single regions, a breakthrough in the direction of studying the impact of massive star formation on the whole Galactic ecosystem, and of offering the possibility of bridging the gap between local and extragalactic star formation studies.

*davide.elia@inaf.it

DOI: 10.52526/25792776-2020.67.2-241

The WISE, *Spitzer*, and *Herschel* mid- to far-infrared continuum surveys, together with surveys from ground-based facilities at millimetre and radio wavelengths, enabled us to reveal the Galactic distribution of dust, and to measure its physical properties on all scales of the ISM, from diffuse clouds to hundreds of thousands of dense clumps. Spectroscopic surveys in various atomic and molecular tracers provide, in turn, the chemical characteristics of dense clumps, as well as kinematic information which is essential to derive heliocentric distances and other distance-dependent parameters.

The *Herschel* Infrared Galactic Plane Survey (Hi-GAL, Molinari et al., 2010) plays a major role in this scenario, thanks to the unprecedented quality of *Herschel* observations, in terms of resolution, sensitivity and dynamical range, in a crucial spectral range (five photometric bands between 70 and 500 μm) for studying emission from cold dust in interstellar clouds. At these wavelengths, the early stages of star formation can be observed in almost point-like condensations, hereafter compact sources, that can correspond to cores or clumps, depending on their heliocentric distance (e.g., Elia et al., 2013, 2017, hereafter El17). A quiescent vs active character with regard to star formation can be attributed to such sources based on spectroscopic signposts (e.g., Giannetti et al., 2013), but also on a self-consistent photometric criterion that could be rougher but certainly applicable to all sources when spectroscopy is not available: a detection at 70 μm indicates a proto-stellar character, otherwise the source is classified as starless (Dunham et al., 2008, Elia et al., 2013, Giannini et al., 2012, Könyves et al., 2015).

A complete catalogue of Hi-GAL clump physical properties at inner longitudes ($-71^\circ \leq \ell \leq +68^\circ$) was released by El17, who identified a set of distance-independent parameters derived from spectral energy distributions (SED), namely the modified black body temperature T, the ratio of the bolometric luminosity to the mass L/M, the ratio of the bolometric luminosity to the portion in the sub-millimetre L/L_{smm}, and the bolometric temperature T_{bol}, able to provide a first evolutionary classification. In light of these parameters, a good degree of segregation was found between the starless and the proto-stellar classes. In particular, distributions of these quantities for proto-stellar sources appear generally broader than for starless sources, testifying a certain diversification of evolutionary stages within the phase globally labelled as proto-stellar.

This is consistent with other evidences offered by the comparison with other tracers: Molinari et al. (2016) calibrated the L/M ratio through CH3C2H(12–11) line observations. They find that this line is detected in sources with $L/M > 1$ $\mathrm{L}_\odot/\mathrm{M}_\odot$ (corresponding to a temperature $T < 30$ K in the inner part of the clump), and the temperature indicated by this tracer starts to increase at $L/M > 10$ $\mathrm{L}_\odot/\mathrm{M}_\odot$, so that this threshold is interpreted as the first appearance of one or more zero-age main sequence stars in the clump.

Cesaroni et al. (2015), analysing 200 Hi-GAL counterparts of CORNISH survey (carried out with VLA at 5 GHz and covering the area $10^\circ < \ell < 65^\circ$, $|b| < 1^\circ$, Hoare et al., 2012, Purcell et al., 2013) sources classified as “ultracompact” and “compact” HII regions, found a L/M ratio ranging from 1 to 250 $\mathrm{L}_\odot/\mathrm{M}_\odot$.

The work of Cesaroni et al. (2015) inspired El17 to establish a criterion to identify HII region candidates also in areas of the Galactic plane not covered by CORNISH and other radio surveys in general, and to discuss the statistics of their physical parameters in comparison with those of earlier evolutionary classes. However, locations of these sources were not shown, and internal correlations among physical parameters were not developed in detail. *The aim of this paper is therefore to better describe and characterize the sample of Hi-GAL HII region candidates*, presenting original analysis of their physical parameters estimated from infrared photometry.

The paper is organised as follows: in Sect. 2 the sample selection process is illustrated, and the Galactic locations and heliocentric distances of selected sources are shown; in Sect. 3 a discussion of different source physical parameters is provided; finally, in Sect. 4 main conclusions are summarised.

2. Sample selection

In El17, candidate HII regions have been identified starting from the work of Cesaroni et al. (2015), who built the histogram of the logarithm of the *Herschel*-based L/M ratio for these sources, where M is derived from the modified black body fit of the SED at $\lambda \geq 160$ μm, and the luminosity from the integral of the entire observed SED[1]. The ascending part of the distribution, corresponding to low values of L/M, can be interpreted as a genuine increase in cases at increasing L/M. On the contrary, the descending part to the right of the peak is due to a completeness effect: more evolved sources, at large L/M might not be included in the Hi-GAL catalogue of El17. Indeed, among the requirements for sources to be listed in this catalogue is the availability of a detection at 250 and 350 μm, which is necessary to ensure a reliable fit to the SED, but favours the colder sources and rejects flux combinations such as 70 μm-only, or 70-160 μm-only, or 70-160-250 μm-only, which correspond to warmer and more evolved sources.

El17 therefore pursue the idea of using the peak of this distribution as a conservative minimum threshold to identify candidate HII regions in their catalogue even at longitudes not covered by CORNISH. To identify this threshold more precisely, they plotted again the histogram of this distribution in bins of 0.1 and found a peak at 1.35, which corresponds to 22.4 $L_\odot/M_\odot$ (note that this value is also compatible with the aforementioned threshold of $L/M > 10\ L_\odot/M_\odot$ by Molinari et al., 2016). Applying this threshold to the sub-sample of proto-stellar clumps of their catalogue, El17 labelled 2377 sources as candidate HII regions (Fig. 1).

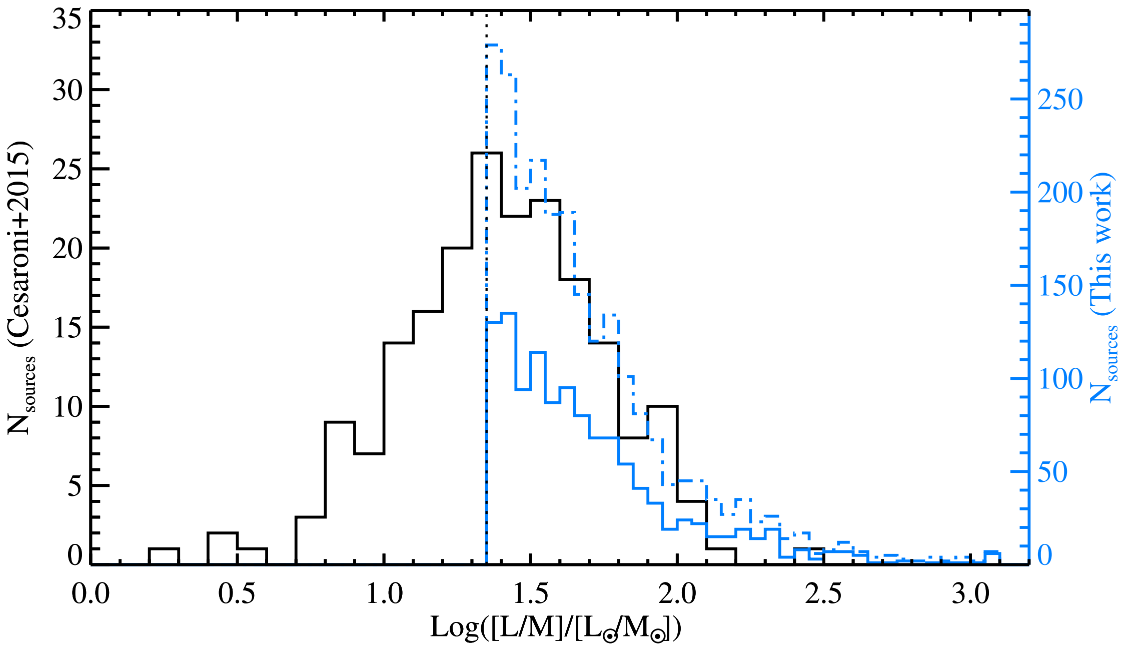

Figure 1. Black solid histogram: distribution, in logarithmic bins of 0.1, of the L/M quantity for Hi-GAL counterparts of CORNISH sources (data from Cesaroni et al., 2015). The peak position is marked with a vertical dashed line. Cyan dotted-dashed histogram: distribution, in logarithmic bins of 0.05, of the same parameter, but for all candidate HII regions from the catalogue of El17, i.e. sources with $L/M > 22.4\ L_\odot/M_\odot$. This histogram refers to the scale on the right y-axis. Cyan color is used here and throughout this paper for indicating HII region candidates for the sake of uniformity with notation of El17. Cyan solid histogram: same as dotted-dashed histogram, but only for sources selected for the present analysis, namely those fulfilling the condition $L > 1448\ L_\odot$.

In this work, a further selection is carried out, adding a further conservative constraint on the global luminosity, which must be compatible with the presence of a central high-mass star, namely $L > 8^{3.5} = 1448\ L_\odot$. The distribution of L/M for the selected sample of sources is also shown in Fig. 1. It can be noted that the second step of selection based on the luminosity filtered out about the 50% of sources, at least in the most populated and statistically relevant bins. A commented example

[1]Hi-GAL SEDs were complemented in the mid-infrared, where possible, with fluxes at 21, 22, and 24 μm from *MSX* (Egan et al., 2003), *WISE* (Wright et al., 2010), and *Spitzer*-MIPSGAL (Gutermuth & Heyer, 2015) surveys, respectively. Mid-infared fluxes are generally involved in the calculation of evolutionary parameters and produce an enhancement of them with respect to pure Hi-GAL SEDs; only modified black body temperature estimation is independent from mid-infrared fluxes.

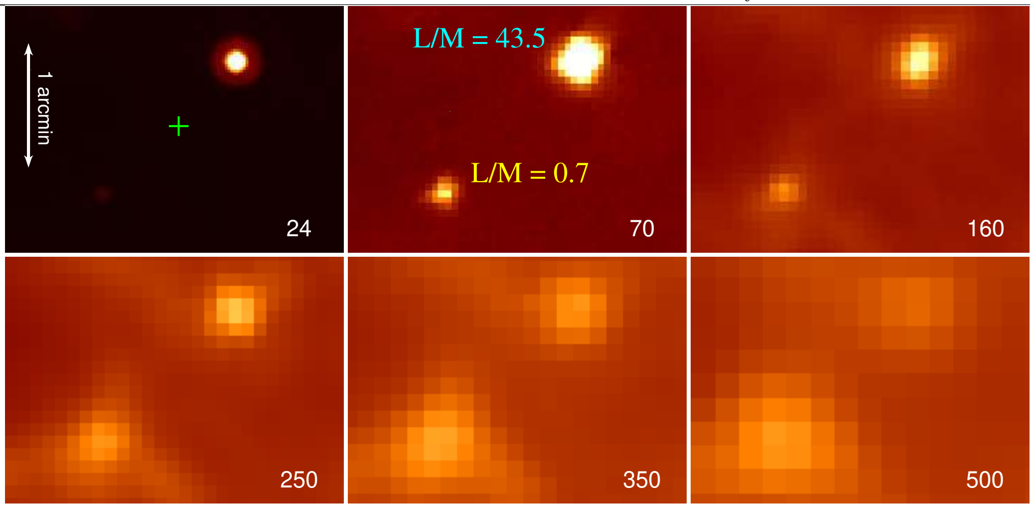

Figure 2. Multi-wavelength view of a Hi-GAL source selected as a HII region candidate. From top-left to bottom-right frame: MIPSGAL 24 μm image and Hi-GAL 70, 160, 250, 350, and 500 μm images, respectively. The wavelength is specified in the bottom-right corner of each frame. In the 24 μm frame the center of the image is indicated with a green cross and corresponds to coordinates $\ell = 17.20468°$ and $b = +0.11299°$. The angular scale of 1 arcmin is represented, in the same frame, with a white vertical segment. The selected source is located towards the top-right corner, and indicated with its peculiar $L/M = 43.5$ $L_\odot/M_\odot$ in the 70 μm frame. Another protostellar source, ruled out by the selection procedure, is located towards the bottom-left corner, and indicated with $L/M = 0.7$ $L_\odot/M_\odot$. It can be seen that the source with high L/M is bright at 24 μm, while the source at low L/M is dark, starting to be visible at 70 μm. Conversely, at the two longest wavelengths, 350 and 500 μm, the low-L/M source appears more extended and globally brighter than the high-L/M one.

of selected source is presented in Fig. 2, as it appears at wavelengths from 24 to 500 μm.

In El17 a comparison between *Herschel* colors of HII region candidates and of Hi-GAL counterparts of 16 bona-fide HII regions studied by Paladini et al. (2012) was carried out. The majority of candidates populate the region of the $\log(F_{\nu,70}/F_{\nu,160})$ vs $\log(F_{\nu,250}/F_{\nu,500})$ diagram occupied by the sources of Paladini et al. (2012), delimited by $\log(F_{\nu,70}/F_{\nu,160}) > -0.45$ and $\log(F_{\nu,250}/F_{\nu,500}) > 0.6$. In the sample considered in this paper, 1115 sources (i.e. 93% of the total) fulfil both these conditions.

The condition on the luminosity implicitly imposes that selected sources have a heliocentric distance estimate. In El17 only 57065 out of 100922 catalogue sources are provided with a distance, and, in particular kinematic distances in the longitude range $-10.°2 < \ell < 14.°0$ are not calculated, due to the difficulty in estimating them for sources in the direction of the Galactic Centre. The resulting distribution of sources in the Galactic plane is shown in Fig. 3. As already noted by El17 for the entire Hi-GAL source sample, the disposition of HII region candidates does not show a clear separation between populated spiral arm locations against void inter-arm regions. However, in limited portions of the displayed arms (from Hou et al., 2009) overdensities of HII region candidates are recognizable, both in the first and in the fourth quadrant. No specific trends are seen between source locations and their L/M.

Finally, in Fig. 4 the mass vs heliocentric distance plot for both the selected and ruled out sources is shown. The cut imposed on luminosity filtered out essentially sources at short distances and/or low masses, so that the 95% of selected sources lie at $M > 20$ $M_\odot$ and $d > 3$ kpc, respectively, compared to 8% for rejected sources.

3. Hi-GAL candidate HII regions physical parameters

The average dust temperature estimated through the modified black body fit has been proven by El17 to be an evolutionary indicator, although, compared with other parameters, it shows a lower power of separation between different stages. This is essentially due to the fact that the component

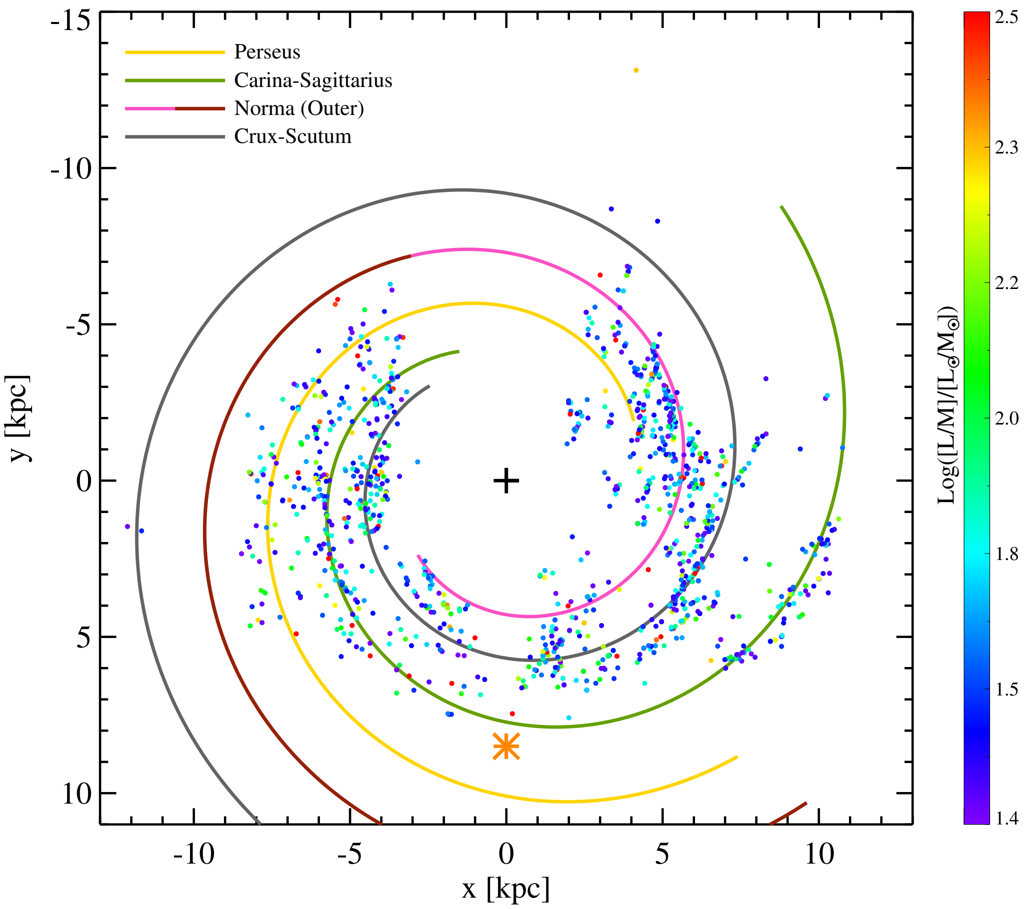

Figure 3. Plot of the positions in the Galactic plane of the Hi-GAL HII region candidates selected in this work. Symbol colors are encoded based on the logarithm of L/M, as reported in the color bar on the right. The inner zone ($-10.°2 < \ell < 14.°0$) is devoid of points, because distances were not reported in El17. The Galactic Centre is indicated with a large plus symbol at coordinates $[x, y] = [0, 0]$, and the Sun with an orange asterisk at coordinates $[0, 8.5]$. Spiral arms, from the four-arm Milky Way prescription of Hou et al. (2009), are plotted with different colours, according to the legend in the upper left corner. In particular, the Norma arm is represented using two colours: magenta for the inner part of the arm and brown for the portion of it generally designated as the Outer arm (see Momany et al., 2006). There is no link between the arm color choice and the color coding for source symbols.

observed at $\lambda \geq 160$ μm corresponds to the outer and coldest layer of a clump, which is only marginally influenced by the central source, if any.

Median kinetic temperatures of 23.3 K and 24 K for a set of 16 and 170 clumps known to host a HII region in their interior were estimated by Hofner et al. (2000) and Urquhart et al. (2013), respectively. These values are similar to the median temperature of 24.4 K found for the sources considered in this work, whose temperature distribution is shown in Fig. 5, left panel.

Another evolutionary parameter is the bolometric temperature, defined by Myers & Ladd (1993) as

$$T_{\mathrm{bol}} = 1.25 \times 10^{-11} \times \frac{\int_0^\infty \nu \, F_\nu}{\int_0^\infty F_\nu} \tag{1}$$

(where T_{bol} is expressed in K and ν in Hz), as a way to quantify spectral redness as the temperature of a blackbody whose spectrum has the same mean frequency (weighted with fluxes) of an observed SED. For a single star-forming core, and in the low-mass regime, Chen et al. (1995) identified a threshold of $T_{\mathrm{bol}} = 70$ K for separating Class 0 from Class I young stellar objects, according to the classification introduced by Lada & Wilking (1984), Lada (1987), and André et al. (1993).

For entire clumps, however, what is expected is that contained, unresolved cores can have different

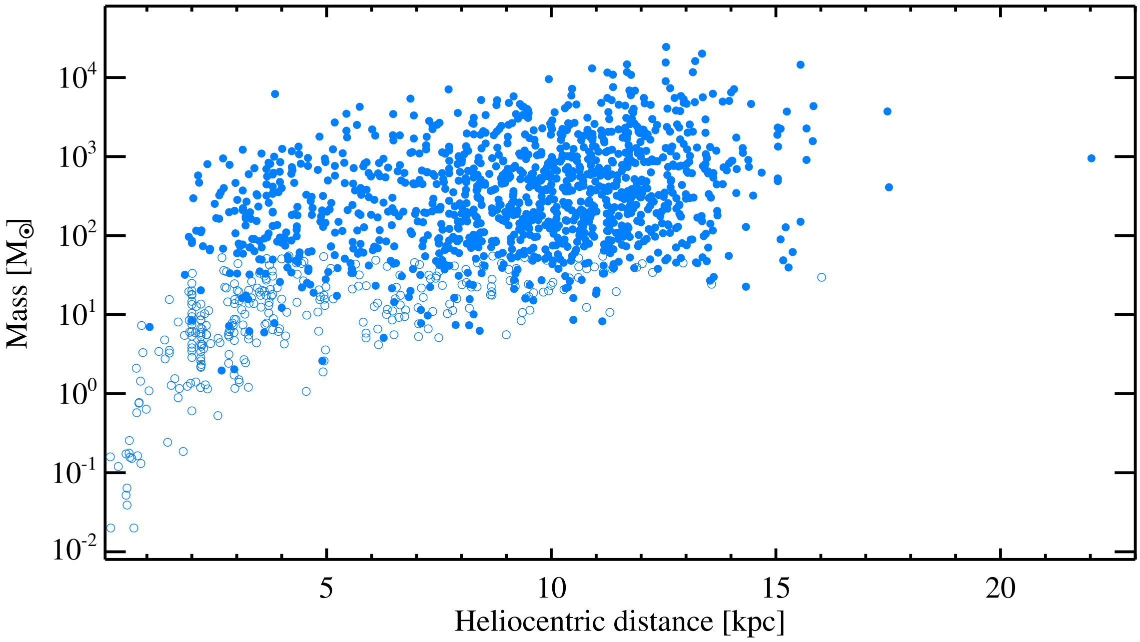

Figure 4. Mass vs heliocentric distance for Hi-GAL HII region candidate sources selected for the analysis presented in this work (filled circles) and filtered out (open circles).

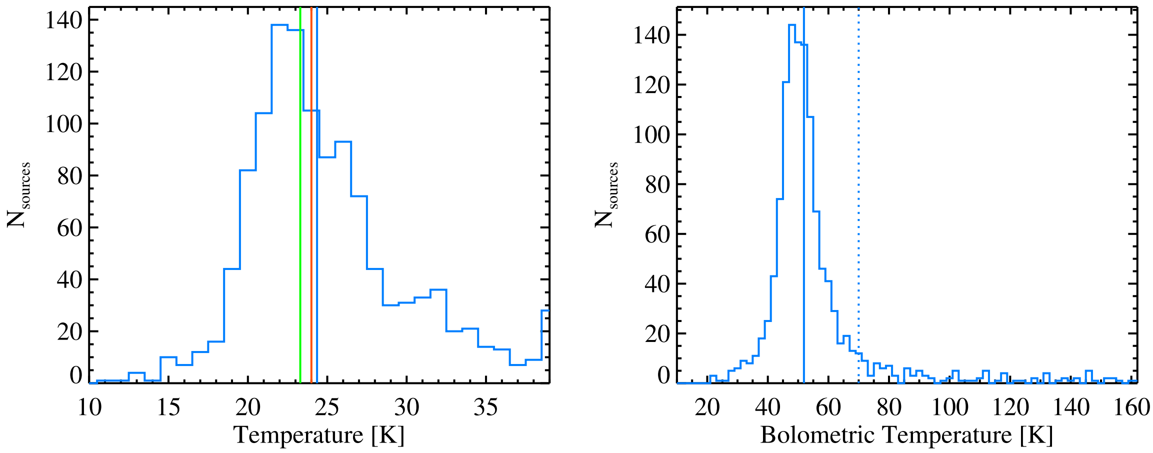

Figure 5. *Left*: histogram of modified black body fit temperature, in bins of 1 K, for Hi-GAL HII region candidates considered in this work. The cyan vertical line represents the median of this distribution, whereas the green and red vertical lines represent the median kinetic temperatures for the clump samples of Urquhart et al. (2013) and Hofner et al. (2000), respectively. *Right*: same as left panel, but for bolometric temperature, in bins of 2 K. The cyan solid and dotted vertical lines represent the median of this distribution and the $T_{\rm bol} = 70$ K threshold of Chen et al. (1995) for Class I sources, respectively.

evolutionary stages and this, together with the presence of quiescent inter-core material, leads to underestimate global evolutionary indicators, including $T_{\rm bol}$. For the selected sample of Hi-GAL HII region candidates, the median bolometric temperature id 52 K, and about 10% of sources have $T_{\rm bol} = 70$ K (Fig. 5, right panel), which corresponds to affirm that at least 10% of these clumps contain at least a young stellar object compatible with a classification of Class I (or equivalent in the high-mass regime).

Fig. 6 contains the plot of $T_{\rm bol}$ vs L/M for HII region candidates. This diagram was not explicitly shown by El17, who plotted this relation for the overall class of proto-stellar clumps. First, the different dynamical range for these two observables is evident, with L/M and $T_{\rm bol}$ spanning about two orders of magnitude and only half order of magnitude, respectively. This implies that any possible variation

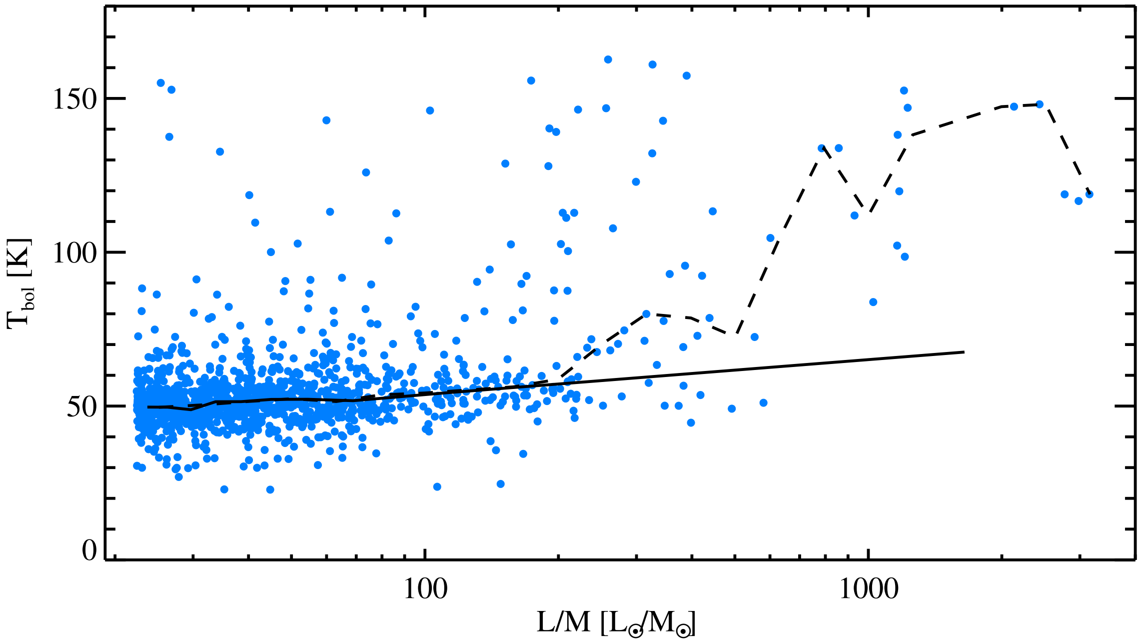

Figure 6. Bolometric temperature vs ratio of bolometric luminosity to mass for Hi-GAL HII region candidate sources selected for the analysis presented in this work. The two black lines connect the medians of $T_{\rm bol}$ in bins of $\log(L/M)$ with fixed width 0.1 (dashed), and in bins delimited by percentiles from 0% to 100% in steps of 10% (solid), respectively.

of $T_{\rm bol}$ as a function of L/M is expected to be very shallow. Even, Williams et al. (2004) did not recognize, in a similar plot for 19 objects, a clear trend between these two quantities. On the contrary, Fig. 6 shows a slightly increasing behaviour of $T_{\rm bol}$ for $L/M < 600\ {\rm L}_{\odot}/{\rm M}_{\odot}$, net of outliers found at high bolometric temperature (say $T_{\rm bol} > 70$ K). Moreover, for $L/M > 600\ {\rm L}_{\odot}/{\rm M}_{\odot}$, only values of $T_{\rm bol} > 80$ K are found. To better highlight a possible global trend, medians of $T_{\rm bol}$ in 0.1-wide logarithmic bins of L/M are connected with a dashed line in Fig. 6, so that the two aforementioned regimes can be easily noticed. However, to give the same statistical relevance to all points, the medians of $T_{\rm bol}$ were calculated also in bins corresponding to percentiles of $\log(L/M)$ (from 0% to 100% in steps of 10%), by definition all populated with the same number of sources (solid line). The two lines are practically indistinguishable for $L/M < 200\ {\rm L}_{\odot}/{\rm M}_{\odot}$, but the second one seems to follow a global linear behaviour over the entire range of L/M. A linear fit provides the empirical relation

$$T_{\rm bol}\,[K] = 0.1 \times \log[(L/M)/({\rm L}_{\odot}/{\rm M}_{\odot})] + 50.7 \tag{2}$$

(error bars for the two linear coefficients are 10% and 1%, respectively).

Finally, a look to source surface density Σ is given. El17 recognized an increase, on average, of this parameter from the pre-stellar to the protostellar phase. The most evolved sub-sample of this class, namely the HII region candidates, shows a decrease of average surface density, suggesting that envelope dissipation is already ongoing at this stage. However, on the one hand this average behaviour is accompanied by a wide spread of Σ, reaching also values larger than 1 g cm^{-2} ($A_V = 200$ mag), and on the other hand no clear correlation is found between Σ and evolutionary descriptors such as T, L/M, and $T_{\rm bol}$.

Left panel of Fig. 7 suggests that, despite in this paper a more stringent filtering of HII region candidates is made with respect to El17 in order to select a more realistic sample, the column density of sources in this sample still shows no clear evolutionary trend as a function of L/M. Surface density spans a wide range of about 3 orders of magnitude (central panel), and the only mild indication that can be drawn is that at very large values of the abscissa, $L/M \gtrsim 600{\rm L}_{\odot}/{\rm M}_{\odot}$, only surface density $\Sigma \lesssim 0.1$ g cm^{-2} are found. Surprisingly, this is the same value of L/M at which bolometric temperature is found to definitely increase over 80 K. However, at large L/M the catalogue is strongly incomplete (see Sect. 2), whereas a more robust statistics would be required to confirm a unequivocal

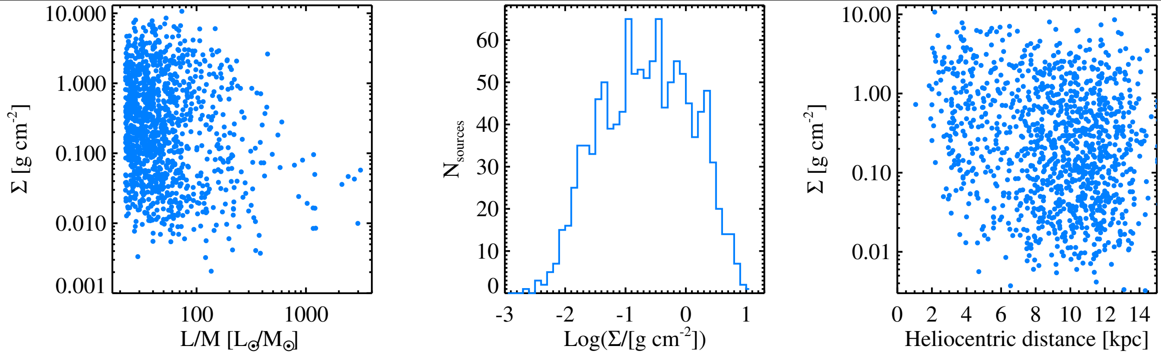

Figure 7. Diagnostics for surface density of Hi-GAL HII region candidates. *Left*: surface density vs ratio of bolometric luminosity to mass. *Center*: distribution of logarithm of column density. *Right*: surface density vs heliocentric distance.

trend indicating envelope dissipation at the most evolved stages probed in the Hi-GAL catalogue.

Finally, it is worth checking whether this spread of surface density may depend on a possible heliocentric distance bias. Indeed, although formally surface density is a distance-independent parameter, in practice its estimate can be affected by the distance. The Hi-GAL sources correspond to structures with different sizes and degree of internal complexity, depending on their distance. Their surface density is as an average parameter derived for the entire source, that in principle depends *i*) on the distribution of densities of single cores hosted by the clump and *ii*) on the amount of unresolved inter-core material included in such estimate. Baldeschi et al. (2017a,b) showed that global physical properties (including evolutionary indicators) of clumps detected at distances $d >> 1$ kpc mirror the average properties of the contained core population; this can hinder recognition of the presence of most evolved objects in these populations. All these considerations suggest the need of a check for a possible distance bias. The surface density vs distance plot in the right panel of Fig. 7, however, again suggests no particular correlation between these two observables.

4. Summary

The right tail of the L/M distribution of protostellar sources in the Hi-GAL catalogue, constituted by clumps candidate to host a HII region, has been examined in detail in this work. With respect to El17, who introduced this classification, an additional constraint for source selection has been imposed, and further relations among positional, photometric, and physical properties of selected sources have been explored. The main points of this analysis can be summarised as follows:

- A sample of 1199 HII region candidates has been selected by imposing not only $L/M > 22.4$ $L_\odot/M_\odot$, as in El17, but also $L > 1448$ $L_\odot$ as a necessary condition to have a central high-mass star.
- The distribution of Galactic positions of selected sources reveals overdensities in correspondence of spiral arm locations, but also a relevant fraction of inter-arm sources. No apparent link exists between position and evolutionary stage indicated by L/M, so that spiral arms do not seem to contain more evolved sources with respect to inter-arm regions.
- The dust temperature of the selected sources, estimated by fitting a modified black body to the SED at $\lambda \geq 160$ μm, and dominated by the outer envelope of the clumps, has a median 24.4 K, which is comparable with those found in the literature, estimated from line spectroscopy, for similar samples of sources.
- A median bolometric temperature of 52 K is calculated for the analysed sample, and a slightly increasing linear relation between $T_{\rm bol}$ and $\log(L/M)$ is found ($T_{\rm bol}$ $[K] = 0.1 \times \log[(L/M)/(L_\odot/M_\odot)] + 50.7$), once outliers of $T_{\rm bol}$ are filtered out.
- The surface density of selected sources spans about three orders of magnitude, showing no evolutionary trend. Additionally, this can not be even explained with a possible distance bias.

The source sample studied in this paper represents, at the same time, the right tail of the distribution of clump evolutionary stages than can be probed with Hi-GAL (i.e. sources still containing a relevant fraction of cold dust), and objects candidates to host high-mass stars with a surrounding HII region. To build a large statistics of bona-fide high-mass star forming objects it is necessary to carry out interferometric observations of these clumps, to resolve the level of clump-to-core fragmentation, and possibly reveal the presence of massive fragments (say $M > 30\ M_\odot$). The ALMAGAL large ALMA Cycle 7 programme (P.I.: S. Molinari), which is being currently observed, aims at resolving the internal structure and the degree of fragmentation of 1017 far-infrared clumps, selected to be candidate to host high-mass star formation (ongoing at present or in the future) and to explore a wide variety of conditions in terms of Galactic location and source evolutionary stage. It includes 79 of the sources analysed in this paper, for which the set-up with 0.1 mJy sensitivity will enable a complete study of the fragmentation process down to at least 1000 AU and 0.3 $M_\odot$. This implies that possible large-mass fragments will be easily resolved, and the high-mass star forming character of these sources will be definitely ascertained.

Acknowledgements

This research is supported by INAF through the Mainstream Grant 1.05.01.86.09 “The ultimate exploitation of the Hi-GAL archive and ancillary infrared/mm data”.

References

André P., Ward-Thompson D., Barsony M., 1993, ApJ, 406, 122

Baldeschi A., et al., 2017a, MNRAS, 466, 3682

Baldeschi A., Molinari S., Elia D., Pezzuto S., Schisano E., 2017b, MNRAS, 472, 1778

Cesaroni R., et al., 2015, A&A, 579, A71

Chen H., Myers P. C., Ladd E. F., Wood D. O. S., 1995, ApJ, 445, 377

Dunham M. M., Crapsi A., Evans II N. J., Bourke T. L., Huard T. L., Myers P. C., Kauffmann J., 2008, ApJS, 179, 249

Egan M. P., et al., 2003, VizieR Online Data Catalog, 5114, 0

Elia D., et al., 2013, ApJ, 772, 45

Elia D., et al., 2017, MNRAS, 471, 100

Giannetti A., et al., 2013, A&A, 556, A16

Giannini T., et al., 2012, A&A, 539, A156

Gutermuth R. A., Heyer M., 2015, AJ, 149, 64

Hoare M. G., et al., 2012, PASP, 124, 939

Hofner P., Wyrowski F., Walmsley C. M., Churchwell E., 2000, ApJ, 536, 393

Hou L. G., Han J. L., Shi W. B., 2009, A&A, 499, 473

Könyves V., et al., 2015, A&A, 584, A91

Kroupa P., 2001, MNRAS, 322, 231

Lada C. J., 1987, in Peimbert M., Jugaku J., eds, IAU Symposium Vol. 115, Star Forming Regions. pp 1–17

Lada C. J., Wilking B. A., 1984, ApJ, 287, 610

Molinari S., et al., 2010, PASP, 122, 314

Molinari S., Merello M., Elia D., Cesaroni R., Testi L., Robitaille T., 2016, ApJL, 826, L8

Momany Y., Zaggia S., Gilmore G., Piotto G., Carraro G., Bedin L. R., de Angeli F., 2006, A&A, 451, 515

Myers P. C., Ladd E. F., 1993, ApJL, 413, L47

Paladini R., et al., 2012, ApJ, 760, 149

Purcell C. R., et al., 2013, ApJS, 205, 1

Salpeter E. E., 1955, ApJ, 121, 161

Urquhart J. S., et al., 2013, MNRAS, 435, 400

Williams S. J., Fuller G. A., Sridharan T. K., 2004, A&A, 417, 115

Wright E. L., et al., 2010, AJ, 140, 1868

Astroinformatics: Statistically Optimal Approximations of Near-Extremal Parts with Application to Variable Stars

Andronov, Ivan L.*[1], Andrych, Kateryna D.†[1], Chinarova, Lidia L.‡[2,1], and Tvardovskyi, Dmytro E.§[1,3]

[1]Department of Mathematics, Physics and Astronomy, Odessa National Maritime University, Odessa, Ukraine
[2]Astronomical Observatory, Odessa I.I.Mechnikov National University, Odessa, Ukraine
[3]Department of Theoretical Physics and Astronomy, Odessa I.I.Mechnikov National University, Odessa, Ukraine

Abstract

The software MAVKA is described, which was elaborated for statistically optimal determination of the characteristics of the extrema of 1000+ variable stars of different types, mainly eclipsing and pulsating.

The approximations are phenomenological, but not physical. As often, the discovery of a new variable star is made on time series of a single-filter (single-channel) data, and there is no possibility to determine parameters needed for physical modelling (e.g. temperature, radial velocities, mass ratio of binaries).

Besides classical polynomial approximation "AP" (we limited the degree of the polynomial from 2 to 9), there are realized symmetrical approximations (symmetrical polynomials "SP", "wall-supported" horizontal line "WSL" and parabola "WSP", restricted polynomials of non-integer order based on approximations of the functions proposed by Andronov (2012) and Mikulasek (2015) and generally asymmetric functions (asymptotic parabola "AP", parabolic spline "PS", generalized hyperbolic secant function "SECH" and "log-normal-like" "BSK").

This software is a successor of the "Observation Obscurer" with some features for the variable star research, including a block for "running parabola" "RP" scalegram and approximation. Whereas the RP is oriented on approximation of the complete data set.

MAVKA is pointed to parts of the light curve close to extrema (including total eclipses and transits of stars and exoplanets). The functions for wider intervals, covering the eclipse totally, were discussed in Andronov (2017). Global and local approximations are reviewed in Andronov (2020).

The software is available at http://uavso.org.ua/mavka and https://katerynaandrych.wixsite.com/mavka.

We have analyzed the data from own observations, as well as from monitoring obtained at ground-based and space (currently, mainly, TESS) observatories. It may be used for signals of any nature.

Keywords: *Solar and Stellar Astrophysics: Instrumentation; Data Analysis; Time Series Analysis; Variable stars; Eclipsing binaries; Pulsating variables; RR Lyr*

1. Introduction

The variety of types of variability, as well as gaps in the astronomical observations, need a wide net of methods for analysis, which would allow statistically optimal determination of parameters using

*tt_ari@ukr.net, Corresponding author
†katyaandrich@gmail.com
‡llchinarova@gmail.com
§dtvardovskyi@ukr.net

DOI: 10.52526/25792776-2020.67.2-251

adequate approximations of the data. Many hundreds of monographs were published, the majority of them devoted to continuous signals or, at least, to signals, which are equidistantly spaced in time: $t_k = t_L + (k - L)\delta$. Here, $k, L = 1..n$, n is the number of observations, and $\delta-$ is the interval between each pair of the subsequent observations (sometimes called the "Time resolution").

In this paper, we describe the software MAVKA ("Multi-Analysis of Variability by Kateryna Andrych") elaborated mainly for determination of characteristics of extrema, primarily, Times of Maxima/Minima (current abbreviation "ToM", also known as "minima timings").

The software is a successor (add-on) of the computer program OO ("Observational Obscurer") and it's few realizations in different computer languages/operational systems (e.g. Andronov (2001)). The "running parabola" ("RP") scalegram and approximation of the complete data set (Andronov (1997)) are available.

The logo of MAVKA software is the letter "M" with 3 points showing a triple nature (third body at a distant orbit around an eclipsing binary) of the majority of objects we studied.

2. Why Phenomenological Modelling?

The aim of physical modelling is to determine physical parameters (e.g. masses, radii of stars) from the observations. However, till now, only 305 binary systems have been studies completely, with determination of masses, parameters etc. `caleb.eastern.edu`, while the number of catalogued eclipsing systems is 8955 (192 combinations of types) in the current GCVS (General Catalogue of Variable Stars, Samus et al. (2017), `www.sai.msu.su/gcvs/`). In the Variable Stars Index (VSX, `aavso.org/vsx`), there are currently 2105479 objects. So, only one system among 7000 is studied sufficiently. For the rest 99.986%, the only available methods of study are phenomenological modelling.

There are dozens of types of variability and hundreds of combinations, so there are some basic principles instead of a single method, There are numerous reviews on step-by-step improvements and extensions of the methods (Andronov (1994), Andronov (2003), Andronov (2005), Andronov (2020), Andronov et al. (2020a)).

The main idea was to make an (nearly) "all in one" software, which realizes main methods proposed in our group, as well as most important methods proposed by others.

3. Algorithms used in MAVKA

The algorithms with formulae were described by Andrych & Andronov (2019).

For an illustration, we have used the small part of observations (102 out of 629 in the filter V) of the pulsating variable RR Lyr made by Horace Smith (AAVSO code SHA). The approximations are shown in Fig. 2.

The methods may be grouped as follows:

- Generally asymmetric extrema, which are common in pulsating variables except RRc and DSct. The commonly used functions are polynomials of statistically optimal order (cf. Chinarova & Andronov (2000). Andrych et al. (2015) compared these approximations with the "Asymptotic Parabola" (AP) fits (Marsakova & Andronov (2015)). The "spline-like" extension of the AP function, is the parabolic spline (PS) (Andrych et al. (2020a)). For longer intervals of data, which are extended to opposite nearby extrema (e.g. to minima before and after the maximum), there are analytical functions, e.g. BSK (Bódi et al. (2016)) and SECH (asymmetrical hyperbolic secant, Andronov (2005)). SECH is more stable, makes asymptotic lines in a logarithmic scale (Fig.3). This allows determination of characteristic times of rise and fall of luminosity, if using the intensities instead of stellar magnitudes. BSK works exclusively with asymmetrical extrema. For positive parameters, the larger absolute slope at the preceding branch is needed. The function often has problems with convergence of the parameters to finite values. However, it was included to MAVKA for realizing existing methods, even if we do not recommend to use them.

- Generally symmetric extrema. Such approximations are common for the eclipses in the binary systems. For these, we implement symmetric polynomials with even powers of deviation $(t-t_e)^{2j}$

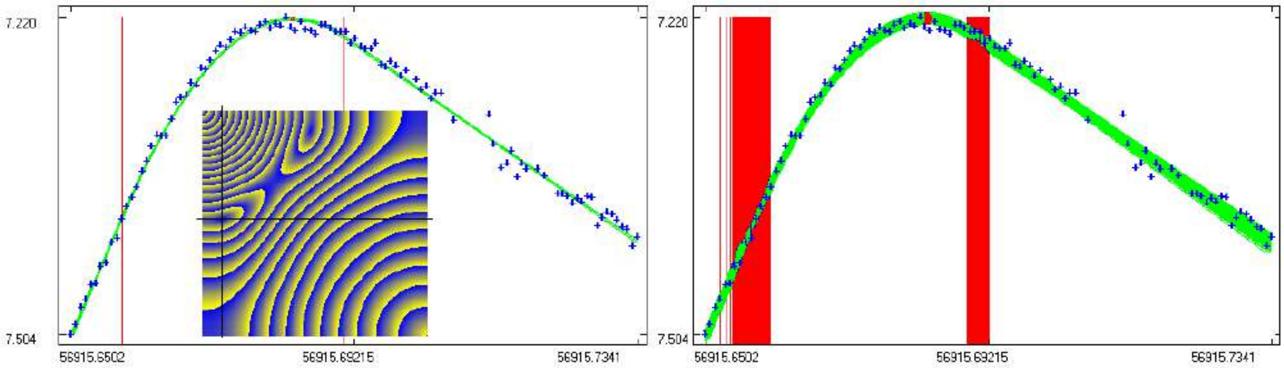

Figure 1. "Asymptotic parabola" approximation of the near-eclipse part of observations of RR Lyr using the program MAVKA. *Left:* the screenshot with the data (blue), approximation and $\pm 1\sigma$ "error corridor". Vertical red lines show the borders of intervals with lines connected with a parabola. The yellow-blue 2D dependence of the test function on positions of the borders of the inner interval, the black lines show position of the minimum of the test functions. *Right:* The approximations of the 2000 pseudo-data generated using the bootstrap algorithm. This sample data show much more stable bootstrap approximations than that discussed by Andrych et al. (2020a).

of argument from the time of extremum t_e. Also, we used the abbreviated Taylor series for the functions proposed by Mikulášek (2015) and Andronov (2012).

Andrych et al. (2017) introduced the "Wall-Supported Polynomial" (WSP) algoritms for statistically optimal modeling of flat eclipses and exoplanet transitions.

Obviously, these approximations are bad for asymmetric extrema, as one may see e.g. at the right part of Fig. 2.

- The moments of crossings of some fixed value m_0. In this case, it is recommended to use inverse approximation $t(m)$ and it's value $t(m_0$ (e.g. Andronov & Andrych (2014)).

Andrych et al. (2020b) and Tvardovskyi et al. (2020a) investigated the approximation stability for various methods implemented in MAVKA.

4. Applications to Concrete Stars

4.1. Eclipsing Binary Systems

During our studies of (O-C) diagrams, the initial data were taken either from own CCD photometrical observations, or the ground-based or space surveys. The original photometric observations were distributed into intervals near extremum and then analyzed with MAVKA.

Tvardovskyi et al. (2017) studied effects of the Mass Transfer and Presence of the Third Components in Close Binary Stellar Systems. Tvardovskyi et al. (2018) detected period variations and possible third components in the eclipsing binaries AH Tauri and ZZ Cassiopeiae. Tvardovskyi et al. (2020b) elaborated the code to model third components with elliptical orbits in the eclipsing binaries. Tvardovskyi (2020a) determined parameters of AB Cas, AF Gem, AR Boo, BF Vir and CL Aur. The catalogue of moments of Minima of 25 Eclipsing Binaries was computed by Tvardovskyi (2020b).

MAVKA is also used as a method complementary to the approximation of the complete light curves using the NAV ("New Algol Variable") algorithm (Andronov (2012), Tkachenko et al. (2016)). An example of such combined study is two eclipsing binaries V454 Dra and V455 Dra in the field of cataclysmic variable DO Draconis is shown by Kim et al. (2020).

A review on highlights of studies of interacting binary stars with instability of the light curves using these (and other) methods is presented by Andronov et al. (2017).

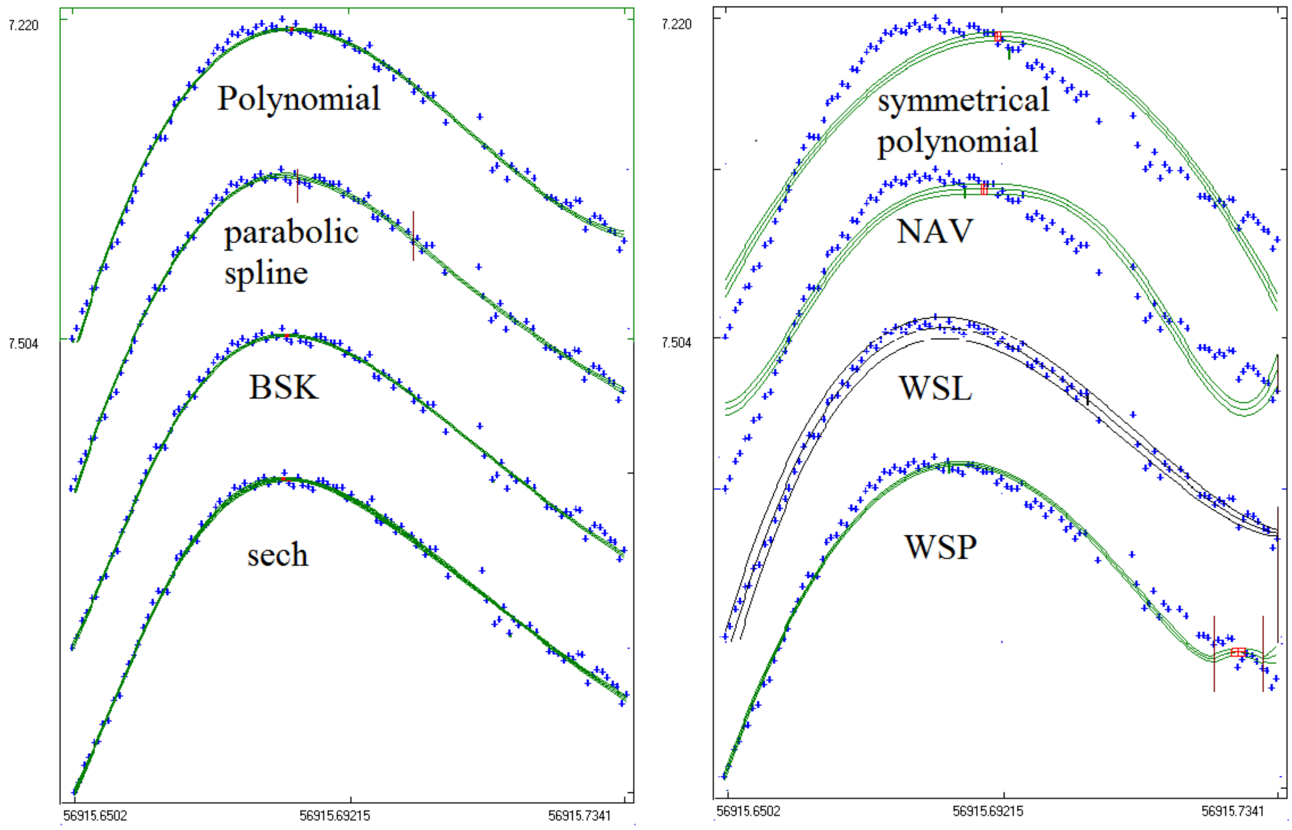

Figure 2. *Left:* approximations, which are generally oriented on asymmetric extrema, and show adequate quality of the fit. *Right:* The "bad" approximations of the asymmetric data using symmetric functions.

4.2. Intermediate Polars

Intermediate polars show a complicated behaviour because of at least two-period variations. One period is due to the orbital motion of a cataclysmic binary, and another period is due to "spin" (rotation of the magnetic white dwarf) and thus changing orientation of the accretion columns. In many cases, two accretion columns are seen alternately. So there are significant waves not only with the main (spin) period, but also the wave with a double frequency.

Such studies were made for nearly a dozen of intermediate polars. Two-Color CCD Photometry of the Intermediate Polar 1RXS J180340. 0 +401214 showed a remarkably stable period (Andronov et al. (2011)).

The variability of the spin period of the white dwarf in the intermediate polar V405 Aur is present, however, its type currently does not allow to decide, whether these variations are due to a light-time effect caused by a low-mass third body, or to the precession of the magnetic white dwarf surrounded by a (warped) accretion disk (Breus et al. (2013)).

A fast spin period decrease was detected in the intermediate polar V2306 Cygni (Breus et al. (2019)).

However, the phases of individual cycles of spin variability of MU Cam show a wave with an orbital phase (Kim et al. (2005)), which apparently may be interpreted as the orbital sideband of the spin period (Parimucha et al. (2020)).

4.3. Pulsating Stars

For the pulsating stars, we make a few-component analysis including period search and determination of the statistically optimal degree of the trigonometrical polynomial, phase plane analysis of the photometrical variations (Kudashkina & Andronov (2017b)).

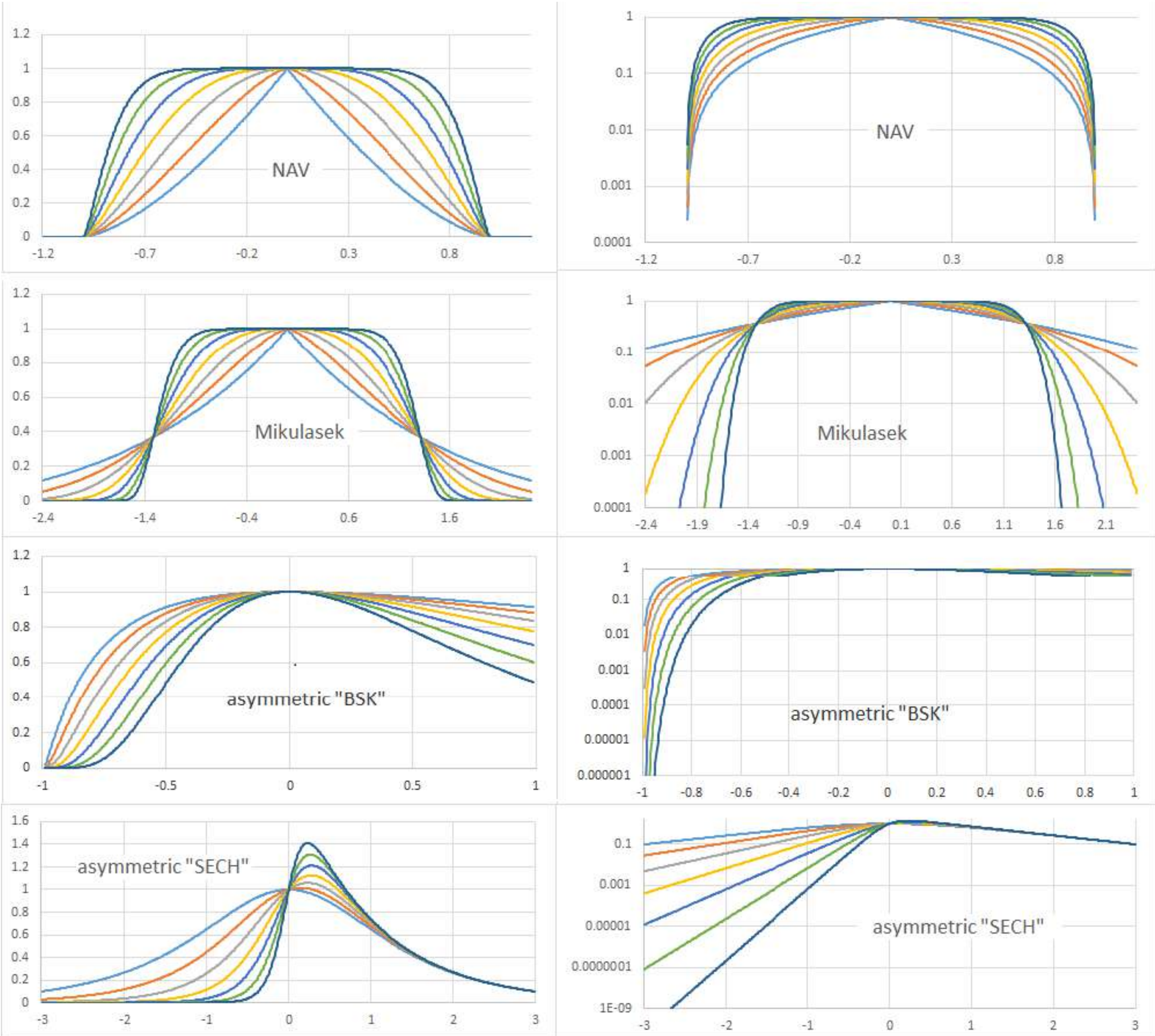

Figure 3. Some of functions implemented in MAVKA in linear *(left)* and logarithmic *right* scales.

Andronov et al. (2020b) made multi-algorithm analysis of the semi-regular variable DY Per, the prototype of the class of cool RCrB variables.

Impact of Pulsation Activity on the Light Curves of Symbiotic Variables was studied by Marsakova et al. (2015).

Wavelet Analysis of Semi-Regular Variables was made by Chinarova (2010) and Kudashkina & Andronov (2010).

A recent review on semi-regular variable stars is presented by Kudashkina (2019).

Acknowledgements

We thank Dr. Areg Mickaelian for fruitful discussions and the AFOEV (cdsarc.u-strasbg.fr/afoev/) and AAVSO (aavso.org) for numerous observations of variable stars. Special thanks to Horace Smith (AAVSO code SHA) for his photometrical observations of RR Lyr, some of which were used for the illustration of our methods.

References

Andronov I. L., 1994, Odessa Astronomical Publications, 7, 49

Andronov I., 1997, Astronomy & Astrophysics Supplement series, 125, 207

Andronov I. L., 2001, Odessa Astronomical Publications, 14, 255

Andronov I. L., 2003, ASP Conference Series, 292, 391

Andronov I. L., 2005, ASP Conference Series, 335, 37

Andronov I. L., 2012, Astrophysics, 55, 536

Andronov I. L., 2020, Knowledge Discovery in Big Data from Astronomy and Earth Observation, 1st Edition. Edited by Petr Skoda and Fathalrahman Adam. ISBN: 978-0-128-19154-5. Elsevier, pp 191–224

Andronov I. L., Andrych K. D., 2014, Odessa Astronomical Publications, 27, 38

Andronov I. L., Kim Y., Yoon J.-N., et al 2011, Journal of The Korean Astronomical Society, 44, 89

Andronov I. L., et al., 2017, ASP Conference Series, 511, 43

Andronov I. L., Breus V. V., Kudashkina L. S., 2020a, "Development Of Scientific Schools Of Odessa National Maritime University": Collective monograph. Riga, Baltija Publishing, 0, 3

Andronov I. L., Andrych K. D., Chinarova L. L., 2020b, Annales Astronomiae Novae, 1, 179

Andrych K. D., Andronov I. L., 2019, Open European Journal on Variable Stars, 197, 65

Andrych K., Andronov I. L. Chinarova L. L., Marsakova V. I., 2015, Odessa Astronomical Publications, 28, 158

Andrych K. D., Andronov I. L., Chinarova L. L., 2017, Odessa Astronomical Publications, 30, 57

Andrych K. D., Andronov I. L., Chinarova L. L., 2020a, Journal of Physical Studies, 24, 1902

Andrych K. D., Tvardovskyi D. E., Chinarova L. L., Andronov I. L., 2020b, Contributions of the Astronomical Observatory Skalnate Pleso, 50, 557

Breus V., et al., 2013, Journal of Physical Studies, 17, 3902

Breus V., Petrík K., Zola S., 2019, Monthly Notices of the Royal Astronomical Society, 488, 4526

Bódi A., Szatmáry K., Kiss L. L., 2016, Astronomy & Astrophysics, 596, id.A24, 8 pp.

Chinarova L. L., 2010, Odessa Astronomical Publications, 23, 25

Chinarova L. L., Andronov I. L., 2000, Odessa Astronomical Publications, 13, 116

Kim Y.-G., Andronov I., Park S.-S., Chinarova L., Baklanov A., Jeon Y.-B., 2005, Journal of Astronomy and Space Sciences, 22, 197

Kim Y., Andronov I. L., Andrych K. D., Yoon J.-N., Han K., Chinarova L. L., 2020, Journal of Korean Astronomical Society, 53, 43

Kudashkina L., 2019, Astrophysics, 62, 556

Kudashkina L. S., 2020, Annales Astronomiae Novae, 1, 199

Kudashkina L., Andronov I., 2010, Odessa Astronomical Publications, 23, 67

Kudashkina L., Andronov I., 2017a, Czestochowski Kalendarz Astronomiczny, 14, 283

Kudashkina L., Andronov I., 2017b, Odessa Astronomical Publications, 30, 93

Marsakova V. I., Andronov I. L., 2015, Odessa Astronomical Publications, 28, 158

Marsakova V. I., Andronov I. L., Chinarova L. L., Chyzhyk M. S., Andrych K. D., 2015, Czestochowski Kalendarz Astronomiczny, 12, 269

Mikulášek Z., 2015, Astronomy & Astrophysics, 584, id.A8, 13 pp.

Parimucha S., Dubovsky P., Kudzej I., Breus V., Petrik K., 2020, Contributions of the Astronomical Observatory Skalnaté Pleso, 50, 618

Samus N., Kazarovets E., Durlevich O., Kireeva N., E.N. P., 2017, Astronomy Reports, 61, 80

Tkachenko M., Andronov I. L., Chinarova L., 2016, Journal of Physical Studies, 20, 4902

Tvardovskyi D., 2020a, Advances in Astronomy and Space Physics, 10, 55

Tvardovskyi D. E., 2020b, Open European Journal on Variable stars, 204, 1

Tvardovskyi D. E., Marsakova V. I., Andronov I. L., 2017, Odessa Astronomical Publications, 30, 135

Tvardovskyi D. E., Marsakova V. I., Andronov I. L., Shakun L. S., 2018, Odessa Astronomical Publications, 31, 103

Tvardovskyi D. E., Andronov I. L., Andrych K. D., Chinarova L. L., 2020a, in Proceedings of the conference "Stars and their Variability Observed from Space". pp 381–382

Tvardovskyi D. E., Marsakova V. I., Andronov I. L., 2020b, Journal of Physical Studies, 24, 3904

Communications of BAO, Vol. 67, Issue 2, 2020, pp.257-263

Narrow-Band Survey of Star Forming Regions

Movsessian T.A.[*1], Magakian T.Yu.[†1], Dodonov S.N.[‡2], and Andreasyan H.R.[§1]

[1]Byurakan Astrophysical Observatory, Aragatsotn reg., Byurakan, 0213 Armenia
[2]Special Astrophysical Observatory, N.Arkhyz, Karachaevo-Cherkesia, 369167 Russia

Abstract

We present the results of a narrow-band Hα and [S II] imaging survey of the star-forming regions in Galaxy. Main tasks of this survey are the search and the studies of the new Herbig-Haro objects and collimated outflows, which are the main indicators of active processes of star formation. Besides, the eruptive stars of very rare types: FUors, EXors, UXors will be searched as well. As the main targets of this survey the R associations, young stellar objects associated with compact reflection nebulae as well as the deeply embedded infrared sources in molecular clouds are selected.

Observations are performed with 1-m Schmidt telescope at Byurakan Observatory, which is equipped with modern CCD detector. We plan to significantly expand the list of HH objects by using the high quantum efficiency of this system as well as the telescope's high focal ratio (F/2), which allows detecting low surface brightness objects, and its large field of view.

Keywords: *Star formation, Herbig-Haro objects, jets and outflows*

1. Introduction

For a long time Herbig-Haro objects (HH) are recognised as a sign of high activity of star formation in molecular clouds. In fact, they represent shocked excitation zones where supersonic flows from young stellar objects (YSO) collide with interstellar medium and form small cloudlets with pure emission spectrum including permitted and low excitation forbidden emission lines ([O I], [S II] etc). Thus, the discovering of new HH objects is important as for the further studies of the phenomenon of directed outflows from young stars, as well as for the searches for new star forming regions and groups.

On the other hand, it is well known that the stellar sources of directed outflows, which have low and intermediate mass, often are associated with compact reflection nebulae of characteristic conical shape. Moreover, deep images in the optical and infrared ranges reveal their bipolar nature. Such shape is a consequence of the presence of circumstellar disks and conical cavities, created by matter outflow, near the YSOs illuminating these nebulae. In the overwhelming majority of cases HH objects and HH flows are located along the axes of these cometary nebulae, which proves a direct relationship between all these phenomena.

We continue our searches for HH objects in the dark clouds, started in Byurakan observatory more than twenty years ago, with the new equipment and wider-field telescope. Among the first targets we included in our program the Mon R1 and southern area of Mon R2 association (Racine, 1968), as well as some deeply embedded infrared sources. Here we present the first successful results.

2. Observations

The images were obtained on the nights of Feb. 3–4 2019 with the 1-m Schmidt telescope at Byurakan observatory, which was upgraded during 2013–2015. The new detector is a reworked 4K×4K

*tigmov@bao.sci.am, corresponding author
†tigmag@sci.am
‡dodo@sao.ru
§handreasyan@bao.sci.am

DOI: 10.52526/25792776-2020.67.2-257

Apogee (USA) liquid-cooled CCD camera with a pixel size of 0.868 arcsec and a field of view of about 1 square degree (Dodonov et al., 2017).

Narrow-band filters centered on 6560 Å and 6760 Å, both with a full width at half-maximum (FWHM) of 100 Å, were used to obtain Hα and [S II] images, respectively. A mid-band filter, centered on 7500 Å with a FWHM of 250 Å, was used for the continuum imaging.

A dithered set of 5 min exposures was obtained in each filter. The effective exposure time in Hα equaled 6000 sec, in [S II] – 7200 sec and in the continuum – 2400 sec. Images were reduced in the standard manner using IDL package developed by one of authors (SND), which includes bias subtraction, cosmic ray removal, and flat fielding using "superflat field", constructed by several images.

3. Results

3.1. Mon R1

The area under study included three bright reflection nebulae (NGC 2245, NGC 2247 and IC 446), as well as several isolated dark lanes and emission-reflection filaments, which are stretched in SE-NW direction through the whole field. Mon R1 contains at least 30 YSOs, which were discovered in the optical range (Herbst et al., 1982). The distance of Mon R1 is usually assumed to be 800 pc, as is that of the nearby Mon OB1 (see Dahm (2003), for a detailed review). The YSOs in Mon R1 can be spatially divided into two groups: one group includes NGC 2245, 2247 and IC 446, and the other is projected on the large reflection nebula IC 2169. Recent infrared and radio observations indicate significant star-forming activity in the latter group (Bhadari et al., 2020). In comparison to the adjacent Mon OB1, Mon R1 has received much less attention. Nearly all observational studies were concentrated on IC 446, where a compact group of emission-line stars, including the HAeBe star VY Mon, was found by Cohen & Kuhi (1979). No searches for HH objects in the Mon R1 field have been performed to date.

Our observations immediately revealed a considerable amount of totally new HH knots and groups, standing out by their pure emission-line spectrum, in this area (Movsessian et al., 2021, in press). Besides, in the course of HH knots search, we noted several nebulous stars, which can be the probable members of Mon R1. Some of them can represent exciting sources of HH objects.

A Hα+[S II] image, which is covering one square degree field of the Mon R1 region, is shown on Fig.1. The zones with newly discovered HH objects and HH flows are marked by rectangles. Full results are presented in the forthcoming paper (Movsessian et al., 2021, in press). Here we show two most interesting outflow systems.

3.1.1. HH 1196 flow

This chain of HH objects contains at least six distinct knots with diffuse emission between them; its total length is about 4 arcmin (Fig. 2). All knots are aligned along an axis with position angle of 155. Knots A, B, E and F have bow-shape morphology with apexes pointing in S-SE direction. This fact confirms the impression of a single collimated outflow from a source, located in the northern direction.

As can be seen from the figure, the relative intensities of the individual knots in Hα and [S II] vary. Knots A, B, C and D are relatively brighter in Hα, while knot E has the ratio of Hα and [S II] near 1, and knot F is seen mainly in [S II].

Along the line connecting the HH 1196 knots, several objects, any of which can be suspected as a possible source of this outflow, can be found.

Total length of this HH outflow is about 1.6 pc; thus, it represents so-called giant HH outflow.

3.1.2. HH 1203

This HH flow includes four HH objects in a chain, embedded in the general diffuse emission (marked in Fig. 3 as knots A, B, C and D). Brightest knot (B) in this chain is somewhat displaced from the axis of whole complex. To the south-east from this HH group there is a compact cone-shaped reflection

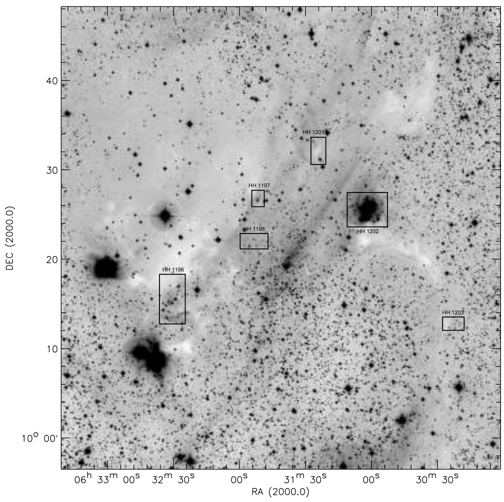

Figure 1. Whole observed field in Hα+[S II] emission, built from the images, obtained with 1 m telescope. The areas including newly discovered HH objects and outflows, are shown by rectangles. Also three major reflection nebulae are marked.

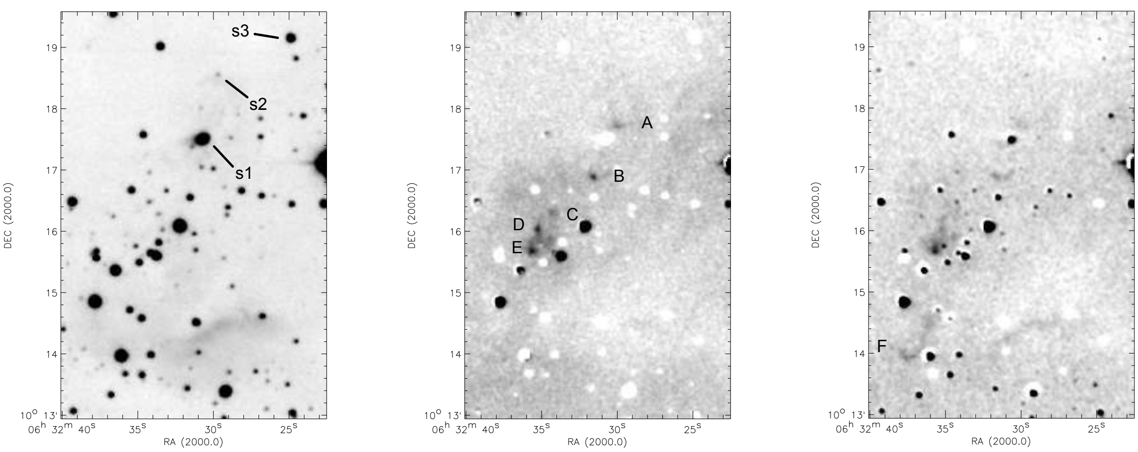

Figure 2. Images of HH 1196 outflow system: continuum image (left panel), continuum subtracted Hα (central panel) and continuum subtracted [S II] (right panel). By s1, s2 and s3 the 2MASS J06323159+1017352, IRAS 06297+1021 (E) and IRAS 06297+1021 (W) objects are marked respectively on the left panel.

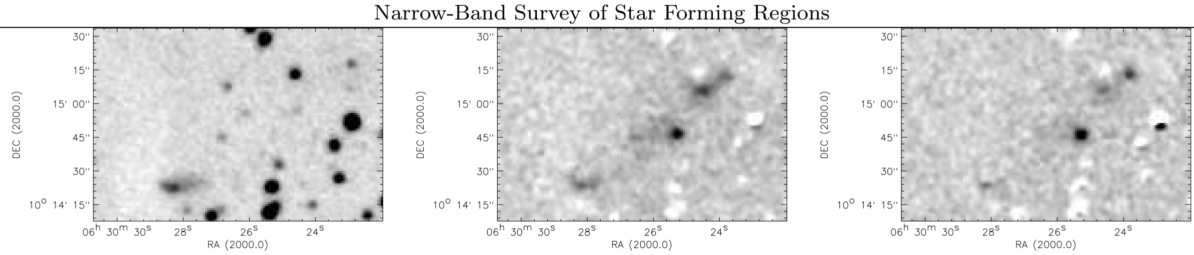

Figure 3. Images of HH 1203 outflow system: continuum image (left panel), continuum subtracted Hα (central panel) and continuum subtracted [S II] (right panel).

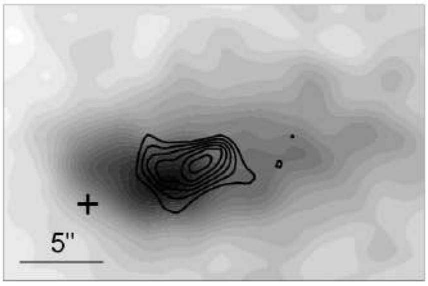

Figure 4. Image of the reflection nebula near HH 1203 in continuum (gray scale) and in [S II] emission (isolines). The position of IRAS 06277+1016 infrared source is marked by the cross. Short emission jet, pointing in the north-west direction along the axis of HH flow, is well seen.

nebula, which lies near the axis of this elongated group. On Fig. 4 the continuum image of this reflection nebula with [S II] image overlaid is presented. This combination reveals the short emission jet, elongated in the direction of the axis of HH 1203 flow. Its existence confirms the assumption that the star, obviously embedded into the nebula, and seen as an infrared source IRAS 06277+1016, also is the source of HH 1203.

3.2. Mon R2-south

Mon R2 is a well studied region of star formation which contains early-type stars (Racine, 1968), molecular outflows (Meyers-Rice & Lada, 1991), an embedded HII region (Downes et al., 1975) and clusters of infrared sources (Thronson et al., 1980). However, the amount of known before HH objects in this field is low; they were found mainly on the eastern side of Mon R2 (Carballo & Eiroa, 1993). The distance of Mon R2 is estimated as ≈900 pc (Lombardi et al., 2011). Our attention was drawn to the area to the south from the central part of Mon R2, where several nebulous objects and an eruptive star V899 Mon are located.

A Hα+[S II] image, which is covering one square degree field of the Mon R2 region, is shown on Fig.5. The zones with newly discovered HH objects and HH flows are marked by rectangles.

3.2.1. V899 Mon

A possible FUor-type eruption of V899 Mon(IRAS 06068−0641), the star, located near the Monoceros R2 region, was first discovered during the Catalina Real-time Transient Survey (CRTS) and reported by Wils et al. (2009). They announced the source as a FUor candidate, which suggestion was based on the constant brightening it has been undergoing since 2005. The spectrum published by Wils et al. (2009) showed strong Hα and CaII IR triplet lines, which identify the outbursting source as a YSO.

Further optical and near-infrared spectroscopy of V899 Mon confirmed it to be a member of the FUors/EXors family of outbursts. Photometrically and spectroscopically V899 Mon's properties lie between EXors and classical FUors (Ninan et al., 2015). But it is probably more similar to EXors than to the classical FUors.

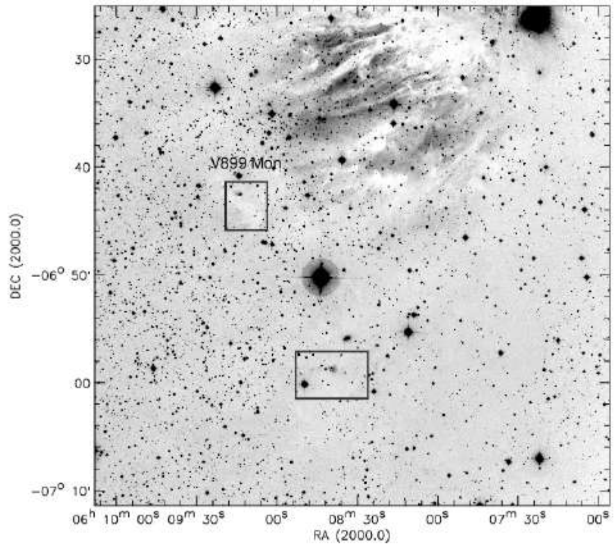

Figure 5. Whole observed field of Mon R2 south in Hα+[S II] emission, built from the images, obtained with 1 m telescope. The areas including newly discovered HH objects and outflows, are shown by rectangles.

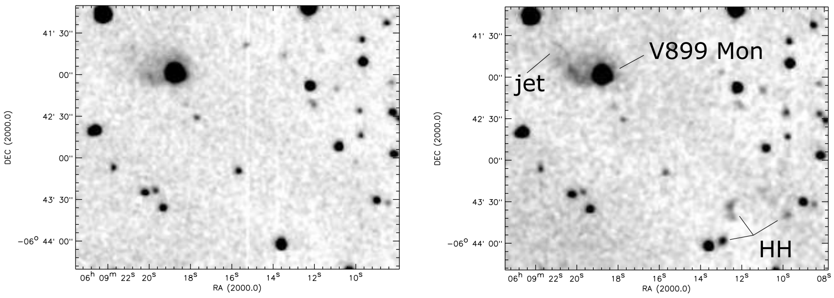

Figure 6. Images of V899 Mon and its outflow system: continuum image (left panel) and [S II] image (right panel).

On the distance of about 2.5 arcmin in south-west from V899 Mon we discovered four HH knots (Fig.6); besides, the narrow emission-line jet, oriented along the axis of the reflection nebula, associated with V899 Mon, was discovered (Fig.4). These data suggest that V899 Mon, like several other FU Ori type objects, is also a source of the collimated, possibly bipolar outflow, because the counter flow can be represented by newly found HH knots. However, one cannot exclude that these HH objects could be produced by other infrared sources in this area.

3.2.2. Curved HH flow

About 20 arcmin towards south-west from V899 Mon we revealed several HH knots near 2MASS 06084223-0657385 infrared source, which is associated with bipolar reflection nebula. HH objects lie on a parabolic curve at the apex of which this infrared source is located (Fig.7). It is remarkable that near the source this line coincides with the axis of the above mentioned bipolar nebula. Therefore, it can be argued that we are dealing with the bipolar collimated outflow of an unusual arc-shaped structure. Such a morphology is typical as for so-named irradiated jets as for outflows from the sources with high proper motion. We incline to choose the second scenario, because irradiated outflows usually are represented by very thin emission filaments without prominent internal knotty structures (Bally & Reipurth, 2001). Taking this scenario into account we estimated the value of the proper motion of the source, which turned to be about 50 km s^{-1}, which is quite reasonable. Estimated total length of this bipolar outflow for the distance of 900 pc will be about 1.5 pc. Thereby, this outflow system as well as HH 1196 represents giant or so called parsec-scale HH flow.

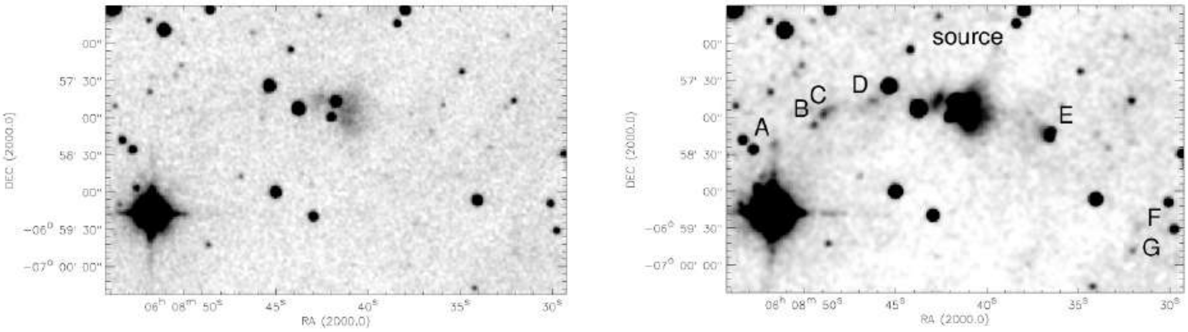

Figure 7. Images of curved HH outflow system: continuum image (left panel) and [S II] + Hα image (right panel).

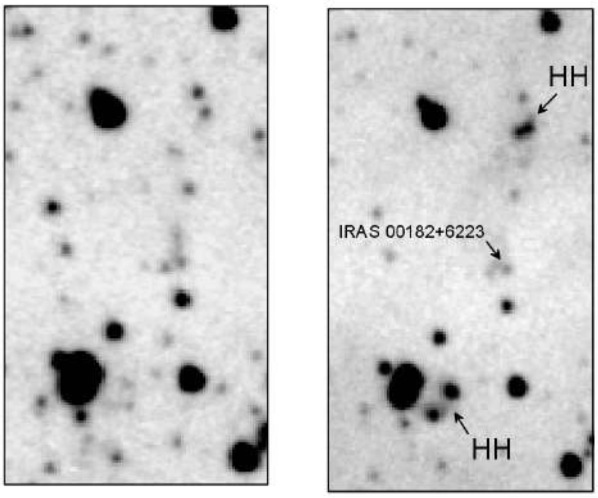

Figure 8. Images of IRAS 00182+6223 outflow system: continuum image (left panel), Hα image (right panel).

3.3. IRAS 00182+6223

This poorly investigated object, located at distance of 4.68 kpc firstly was mentioned as a source of CO outflow (Wouterloot & Brand, 1989). Observations in near-infrared range revealed small reflection nebula extending to the north from IRAS 00182+6223 (Connelley, Reipurth, & Tokunaga, 2007).

Our observations revealed two emission lobes in northern and southern sides of IRAS 00182+6223 with total length of about 1.7 arcmin (2.3 pc for the distance of 4.68 kpc) (Fig.8). It is worth to mention that this source is located in the dark cloud, which is covered by foreground stars of Milky Way. It would be one of the brightest known HH objects, if is was located at a distance of Orion star forming region.

4. Conclusion

Since the beginning of 2019, when the survey began, more than 30 new HH objects and outflow systems have been found. Among them several giant outflow systems, narrow jets as well as curved HH flow should be mentioned.

In addition to all the results presented above, this work demonstrates that the 1-m Schmidt telescope of Byurakan Observatory, which was used several decades ago for well-known surveys of active galaxies such as the First Byurakan Survey and Second Byurakan Survey, can still lead to important discoveries.

Acknowledgements

This work is based on observations conducted with the 1-m Schmidt telescope of the Byurakan Astrophysical Observatory of the National Academy of Sciences of Armenia. This work was supported by the Republic of Armenia State Committee of Science, in the framework of research project number 18T-1C-329.

References

Bally J., Reipurth B., 2001, ApJ, 546, 299.

Bhadari N. K., Dewangan L. K., Pirogov L. E., Ojha D. K., 2020, ApJ, 899, 167.

Carballo R., Eiroa C., 1993, in Stellar Jets and Bipolar Outflows, Proceedings of the 6th International Workshop, Ap&SpSc Lib. 186, p.213

Cohen M., Kuhi L.V., 1979, ApJS, 41, 743

Connelley M. S., Reipurth B., Tokunaga A. T., 2007, AJ, 133, 1528.

Dahm S.E, 2008, in Reipurth B., ed., Handbook of Star Forming Regions, Vol. I, Astron. Soc. Pac., p. 966

Dodonov S.N., Kotov S.S., Movsesyan T.A., Gevorkyan M. 2017, Astrophysical Bulletin, 72, 473

Downes D., Winnberg A., Goss W. M., Johansson L. E. B., 1975, A&A, 44, 243

Herbst W., Miller D.P., Warner J.W., Herzog A., 1982, AJ, 87, 98

Lombardi, M., Alves, J., Lada, C.J., 2011, A&A, 535, A16

Meyers-Rice B. A., Lada C. J., 1991, ApJ, 368, 445.

Movsessian T.A., Magakian T.Yu., Dodonov S.N., 2021, MNRAS, 500, 2440

Ninan, J.P., Ojha, D.K., Baug, T., Bhatt, B.C., Mohan, V., Ghosh, S.K., Men'shchikov, A., Anupama, G.C., Tamura, M., Henning, Th., 2015, ApJ, 815, 4

Racine R., 1968, AJ, 73, 233

Thronson H. A., Gatley I., Harvey P. M., Sellgren K., Werner M. W., 1980, ApJ, 237, 66.

Wils P., Greaves J., Drake A. J., Catelan M., 2009, Central Bureau Electronic Telegrams, 2033, 1

Wouterloot J. G. A., Brand J., 1989, A&AS, 80, 149

Big Data: Behind The Scenes

Kaustubh Vaghmare*

Persistent Systems Ltd., Pune, Maharashtra, India

Abstract

The phrase “big data” has become a highly common phrase in recent times. However the phrase ‘big data’, while it may have been coined to indeed vaguely refer to large volumes of data, has now evolved to mean something much more specific. The phrase ’big data’ actually refers to a family of technologies, platforms, software and techniques aimed at solving a variety of problems otherwise untenable through conventional or traditional solutions. The present article summarizes a traditional approach to a data management problem and presents limitations of this approach. The three ‘Vs’ used to characterize and define ‘big data’ are then elucidated upon. Finally, the article summarizes commonly used tools and technologies to solve the ‘big data’ problem.

Keywords: *big data, databases, hadoop, mapreduce, spark, nosql, rdbms*

1. Introduction

The phrase ‘big data’ is often used very informally. It maybe that there was a time when this word indeed was a vague term used to refer to very large volumes of data being generated by modern telescopes (or the Internet / Internet of Things / Social media etc.) but today the phrase has evolved to mean something more specific. The author’s personal favorite definition of the phrase ‘big data’ is *a phrase used to describe a characteristic(s) of data which makes the use of traditional solutions infeasible.*

However, a major problem with this definition of ’big data’ is that it is not self contained. To complete the definition, one needs to spell out what is meant by ’traditional solutions’ and also spell out under what circumstances or scenarios do those ’traditional solutions’ become infeasible. It is the endeavour in the rest of the article to spell out both these aspects.

The article is organized as follows - in Section 2, I summarize what is meant by a traditional solution and explore the circumstances under which this solution becomes infeasible; in Section 3, I describe the hardware and software requirements of handling big data; in Section 4, I briefly summarize the ecosystem of commonly used software technologies available for tackling big data processing challenges; in Section 5, I briefly explore the concepts related to database technologies needed to solve big data storage and organization; and Section 6 offers a brief summary of the article.

2. Traditional Solutions

A traditional solution can be decomposed into hardware and software components. The typical / traditional hardware can be characterized by

- A single monolithic unit of hardware.
- Presence of single or multiple CPUs with multiple cores per CPU
- Storage in the form of a single disk or a collection of disks arranged in a RAID (Redundant Array of Inexpensive Disks) configuration.

*kaustubh.vaghmare@gmail.com

DOI: 10.52526/25792776-2020.67.2-264

- Primary memory in the form of a collection of RAM chips

And the software ecosystem comprises of

- A conventional Operation System
- With processing implemented using standard software or programming languages.
- Unstructured data handled using simple file storage, and
- Structured data handled using relational database management systems (RDBMS) (such as MySQL, Postgres etc.)

There are however three main conditions under which these traditional solutions become infeasible - these are the 3Vs often invoked to characterize big data!

- high volume,
- high velocity, and
- variety

However, it is important to emphasize a subtle point here. It is not enough that the total volume, variety or velocity of data is high - what is important is that volume, variety or velocity of *single coherent unit of data* should be high. For example, if the total data volume is 100+ terabytes, but it is composed of images with each *independent* image being $\sim 1MB$, then each image can be processed using a traditional solution. As a contrary example, if the total volume of the data is $\sim 500GB$, but *all of it needs to be processed in one go*, then despite lower total data volume, a traditional solution is not feasible.

Traditional solutions are 'vertically scalable'. If a traditional solution becomes infeasible, it is quite hard to upgrade the existing hardware. And replacement of existing hardware with a new hardware of higher specifications, is non trivial.

3. Big Data Hardware and Software

To tackle the situations where traditional solutions no longer work, a different approach to hardware and software is needed. In terms of hardware, we need a cluster of machines interconnected to each other. However, it is important to emphasize that not all clusters are suitable for big data processing. A conventional HPC (High Performance Computing) setup is composed of many independent machines that work as a single whole but rely on a network mounted storage for bulk of their data storage. This results in a large amount of data flowing across the network and is not desirable for big data processing.

Big data clusters on the other hand, are composed of machines where each machine has its own substantial self storage. And the tools that are used to orchestrate big data processing work in a manner so as to allow each machine to work on data already stored on it. In other words, the emphasis is on *data locality.* Thus the total data transferred across a network is minimized. Another important aspect of big data clusters is that they are made of *commodity hardware.* This is important because it allows easy expansion of the capacity of a cluster.

On the software side, there are two main components required for big data processing.

- A distributed file system which presents a unified logical view of the total storage across all machines. Since commodity hardware is used, such a filesystem has to guard against fault tolerance.
- A scheduler which coordinates the data processing across all computers, typically designed to minimize network data transfer.

Big data clusters are *horizontally scaleable.* The augmentation of the capacity can be done by just adding more machines to the cluster. The software is designed to seamlessly adjust to the changing capacity.

4. The Big Data Software Ecosystem

Arguably, the most famous big data software is *Hadoop*. Hadoop can be thought of an Operating System for Big Data. It primarily comprises of two parts

- The Hadoop Distributed Filesystem (HDFS)
- The YARN (Yet Another Resource Negotiator), a distributed computing scheduler.

In a typical Hadoop data processing job, one uses the *MapReduce* framework. Under this framework, all data processing jobs must be decomposed as a series of map and reduce functions, with the map function responsible for a state independent local data process and the reduce function responsible for assembling the final results of individual map functions. While the MapReduce framework is excellent for immense data volume processing jobs, it is limited by a) the lack of flexibility of the framework itself and b) not being amenable to interactive analyses.

Spark solves this problem through graph based *in-memory* analytics. Spark is currently a very popular solution providing rich APIs which allow a user to solve several problems related to interactive data processing.

5. Big Data Databases

The most popular databases are the *relational databases* which organize data in the form of related or linked tables. These databases conform to the ACID properties (Atomicity, Consistency, Isolation and Durability). Because of this, it is often very hard to operate these databases successfully in a distributed environment. Also, it is very difficult to use these databases in the face of a large variety because of the emphasis on a rigid structure or schema. This has led to a whole family of databases popularly called *NoSQL* (Not only SQL) databases. Popular examples include HBase, MongoDB, Redis, Cassandra etc. One of the reasons for the existence of so many different NoSQL databases is the CAP theorem.

The CAP theorem says that it not possible for any database to achieve all three properties of Consistency, Availability and Partition-Tolerance simultaneously. Here, consistency refers to the condition that all clients see the same data at any given time, availability refers to the condition where system continues to respond even in the failure of one of the nodes in a cluster, and partition-tolerance refers to the condition that the system continues to operate even though data partitions can no longer communicate with each other. A given NoSQL database takes a different approach to balancing these three properties.

6. Conclusions and Summary

Big Data is not a term to be thrown about casually. It specifically refers to an ecosystem of hardware and software solutions designed to handle data processing workloads not feasible using a traditional solution. Big data hardware is a cluster of machines but there is a difference between an 'HPC' and a big data cluster. Relational databases are generally not capable of high volume distributed data storage and this has led to the rise of multiple databases known as NoSQL databses.

Acknowledgements

I would like to acknowledge the BAO for the opportunity to present the contents of this article as an invited speaker. *I also declare that views presented in this article are my own and should not be construed as the views of my present organization viz. Persistent Systems Ltd.*

Communications of BAO, Vol. 67, Issue 2, 2020, pp. 267-271

The Origin of LAMOST J1109+7459

Yazan Khrais and Nour Aldein Almusleh *

Department of physics al Al-Bayt university , al mafraq , 130040 Jordan

Abstract

We report a comprehensive Chemo-dynamical analysis of LAMOST J1109+0754, a relatively bright (V = 12.8), extremely metal-poor ([Fe/H] = −3.17), and prograde (J_ϕ and $V_\phi > 0$) star, with a strong r-process enhancement ([Eu/Fe] = +0.94 ± 0.12, [Ba/Fe] = −0.52 ± 0.15). 31 chemical abundances (from Lithium to Thorium) were derived. We suggest a possible progenitor with stellar mass of 13.4-29.5 $M_\odot$. We argue that J1109+0754 is representative of the main r-process component due to the well agreement with the scaled-solar r-process component. We analyze the orbital history of this star in a *time-varying Galactic potential*, based on a Milky-Way analogue model extracted from `Illustris-TNG` simulations. Using this model, we carry out a statistical estimation of the phase-space coordinates of J1109+0754 at a young cosmic age. Collectively, the calculated motions, the derived chemistry, and the results from the cosmological simulations suggest that LAMOST J1109+0754 most likely formed in a low-mass dwarf galaxy, and belongs to the Galactic outer-halo population.

Keywords: *Nucleosynthesis: r-process— Galaxy: halo– stars: abundances—stars: Chemically peculiar— stars: Population III — stars: dynamics —stars: Orbits — stars: individual (LAMOST J1109+0754)*

1. Introduction

Our universe is made up of a substantial number of elements (from hydrogen to oganesson) and their isotopes. This fact inspired astronomers and nuclear physicists, for more than six decades, to investigate the major physical processes and conditions that led to produce this wide variety of chemical species. Since the pioneer studies of Burbidge et al. (1957) and Cameron (1957), there has been a large number of studies in the literature focusing on the astrophysical site(s) of the rapid neutron capture (r)-process. However, the problem has not been solved, but some promising mechanisms were proposed: (i) the innermost ejecta of regular core-collapse supernovae (e.g., Farouqi et al., 2010), (ii) outer layers of supernova explosions (e.g., Qian, 2014), (iii) magneto-rotational jet-driven supernovae (e.g., Obergaulinger et al., 2018), and (iv) neutron stars (NSs) mergers (e.g., Thielemann et al., 2017).

The science of stellar archaeology is built on two fundamental assumptions: (i) Population II stars preserve in their atmosphere the chemical composition of the individual or a few Supernovae (SN) yields of the previous Population III (the so-called Population III chemical fingerprint, Mardini et al., 2019b) and (ii) Accurate chemical abundances (from lithium to uranium) can be acquired from high-resolution spectra. Therefore, metal-poor stars can contribute to reveal the first nucleosynthesis enrichment in the universe. In particular, the spectroscopic analysis of individual galactic halo stars with enhancement in r-process elements and lack/low s-process elements[1] (the so-called r-process-enhanced stars) bring us closer to solve the long-standing r-process puzzle (for a selected list see e.g., Placco et al., 2020, and references therein).

For the aforementioned reasons, increasing the numbers of the known r-process-enhanced metal-poor stars (i.e., expanding the chemical inventory of these stellar objects) has been one of the major interesting research subjects for individual researchers (e.g., Mardini et al., 2019a) and large projects

*nour.aldein002.2@gmail.com, Corresponding author

[1] The criterion [Ba/Fe] > 0 is included into the definitions of r-process-enhanced stars to avoid any possible contribution from the s-process.

DOI: 10.52526/25792776-2020.67.2-267

such as the Hamburg/ESO and the R-Process Alliance. In addition, Beers & Christlieb (2005) have proposed that r-process-enhanced stars can be classified, using the observed [Eu/Fe] ratio, into two main distinctive populations (i) r-I stars with $0.3 \leqslant$ [Eu/Fe] $\leqslant 1.0$ and (ii) r-II with [Eu/Fe] > 1.0. Based on the database for metal-poor stars (JINAbase, Abohalima & Frebel, 2018)[2] , the current statistics of r-I and r-II are $\sim$30 and 125, respectively.

Besides the chemical compositions of individual galactic stars, investigating the positions and kinematics of these stars will advance our understanding of the formation and evolution of our galaxy. During the past 30 years much more information has become available on the structure of the stellar halo of the Milky Way. These efforts suggested that the galactic halo is made-up of two distinguished populations of stars; the inner and outer stellar halo (e.g., Mardini et al., 2019c, Masda et al., 2019, Sommer-Larsen & Zhen, 1990, Taani et al., 2019a,b,c, 2020). Furthermore, in the era of the second data release of the Gaia mission (Gaia DR2; Gaia Collaboration et al., 2018), several studies are currently being expended investigating the kinematics and chemical abundance patterns of r-process-enhanced stars. These efforts attempt to combine the chemical abundance patterns, observed in r-process-enhanced stars, with kinematics derived from Gaia DR2 observations and results from cosmological simulations to assess the formation mechanisms and determine the role of r-process-enhanced stars as tracers of the accretion history of the galactic halo, i.e. the time at which these stars were ejected into our Galaxy.

2. Data, Results, and Discussions

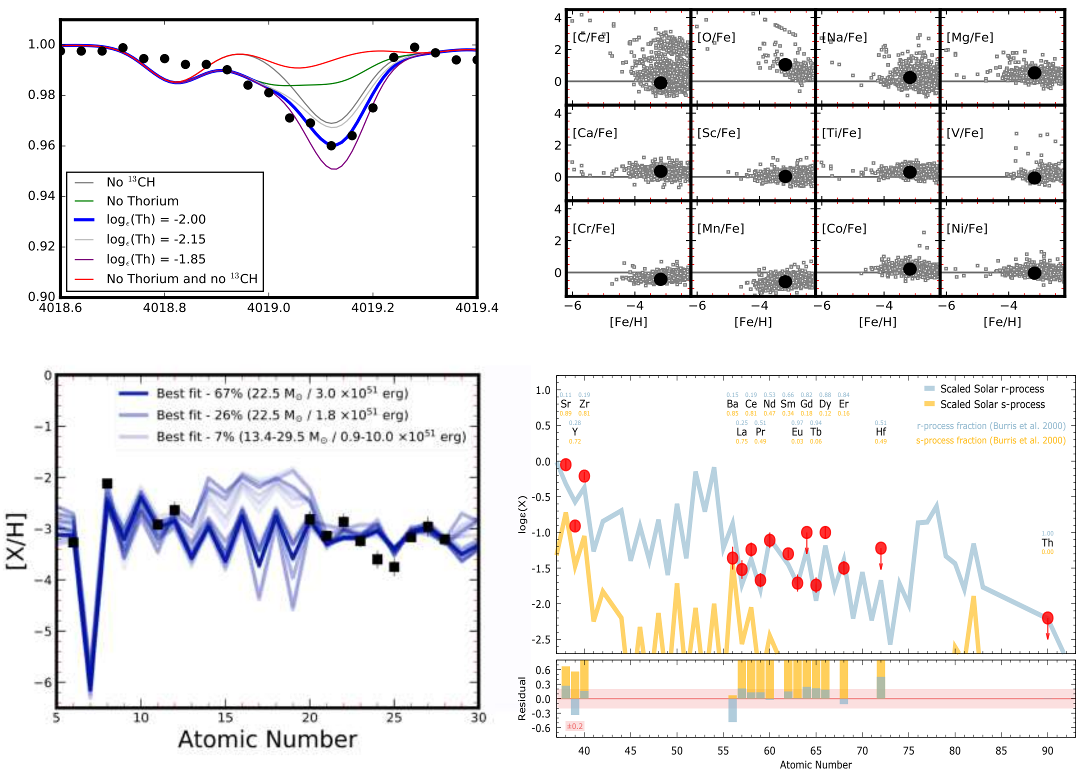

Figure 1. Upper left panel: portion J1109+0754 spectrum was used to derive the thorium (Z = 90) abundance and the associated uncertainty. Upper right panel: observed [X/Fe] ratios for elements up to the iron peak, as a function of [Fe/H]. Lower left panel: the observed [X/H] abundance ratios of J1109+0754 (filled black squares), as a function of atomic number, overlaid with the matched predicted nucleosynthetic SNe models. Lower right panel: heavy-element abundance pattern of J1109+0754 (filled circles), overlaid with the scaled Solar System abundances (SSSA).

[2] https://jinabase.pythonanywhere.com

In 2015, we observed J1109+0754 using Automated Planet Finder (APF) Telescope. We used IRAF to carry out a standard echelle data reduction. We measured the Radial Velocity using the same method presented in Mardini et al. (2019b), by cross-correlating the high-resolution reduced spectrum against synthesized template of the same spectral type, making use of the Mg I triplet at 5160–5190,Å. We used MOOG to determine stellar parameters and chemical abundances for 31 elements including Thorium.

The upper left panel of Figure 1 shows an illustrative example of spectral synthesis approach. The portion J1109+0754 spectrum was used to estimate the thorium abundance and its associated uncertainty. The upper right panel of Figure 1 shows the distribution of these abundances (large solid points), as you can see the light elements abundances of J1109+0754 do not scatter from the general trend observed in other literature metal-poor field stars (small opened gray squares). The lower left panel of Figure 1 speculate the stellar mass and the SN explosion energy of the progenitor of J1109+0754. The fitting result of this exercise supports the conclusion presented in Mardini et al. (2019b), which suggests that a stellar mass $\sim$ 20 $M_{\odot}$ may reflect the initial mass function of the first stars. Furthermore, it brings the possibility as to whether more massive SN might be more energetic and therefore destroy their host halo and not allow for EMP star formation afterward. The lower right panel of Figure 1 shows the heavy elements patterns overlaid with the scaled Solar components. The observed deviations of Sr, Y, and Zr from the scaled r-process peak indicate that the production of these elements (first r-process peak) is likely to be separated from the second and third r-process peaks. The universality of the r-process is shown in J1109+0754 due to the good agreement between the abundances of the elements with $Z > 56$ the scaled Solar r-process component. This suggest that there is no clear contribution from the s-process. Therefore, we argue that J1109+0754 can be used as a representative of the main component of the r -process (Abdusalam et al., 2020, Mardini et al., 2020).

The advent of the Gaia mission has fundamentally changed our view of the nature of the Milky Way. However, unraveling the full kinematic signature of J1109+0754 requires a less-idealized and more-realistic time-dependent galactic gravitational potential. We use the Illustris-TNG TNG100 simulation box, characterized by a length of ~110 Mpc to select potential Milky Way analogs. We then pared down an initial list of over 2000 candidates into using some sophisticated stellar parameters cuts. The best-fitting parameters are found for each snapshot using a smoothing spline fitting procedure. To obtain the gravitational force as a function of time, we interpolate between each snapshot's parameters. In order to show that our NFW + Miyamoto-Nagai model provides a reasonable description of the time evolving Galactic analogues, we calculated the gravitational acceleration of the star along its orbit using our model as well as the actual particle distribution from the Illustris-TNG simulation. This shows (see Figure 2) at the very least that our orbital integration of this particular star is approximately correct. To produce the figure, we used the orbital data from a randomly chosen integration in a randomly chosen MW analogue, and interpolated the spatial position at times where the full snapshots from the cosmological simulation were available. Then, the gravitational force was calculated at those spatial points using both our model routines, and direct summation. As one can see, the two calculations match quite closely, with relatively large error occurring only at particular points where the particle is closest to the centre of the halo (where naturally complex substructure is not fully captured by the simple model). This is especially the case in the second snapshot at around 4 Gyr; at this point in time the system has not yet settled into a simple disk+halo (note also that our integration is backward, so this datapoint has no practical importance in our orbit calculations). Barring this data point, the mean relative deviation between the model and the simulation is 0.04, and the standard deviation is 0.13. We generated 10,000 sets of the six-dimensional phase space coordinates from the corresponding measurement errors. This exercise shows that J1109+0754 has bounded (E= -87.05×10^3 km^2 s^{-2}), non-planar (Z_{max}=10.87 kpc), and eccentric orbit (e= 0.84). Moreover, J_ϕ and V_ϕ values (683.68 kpc km s^{-1} and 73.72 km s^{-1}, respectively) suggests that J1109+0754 is a prograde star. The right panel Figure 2 shows the last 10 periods orbit of J1109+0754, in x-y projection integrated in time for 4.2 Gyr.

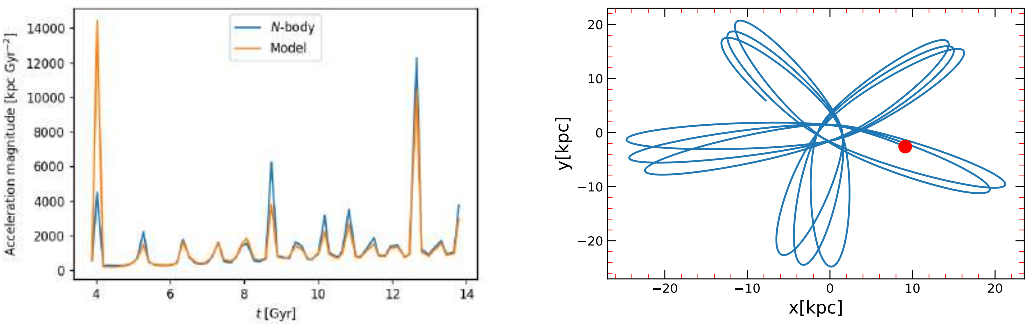

Figure 2. Left panel: the gravitational acceleration of J1109+0754 along its orbit using our model as well as the actual particle distribution from the Illustris-TNG simulation. Right panel: the last 10 periods orbit of J1109+0754, in x-y projection integrated in time for 4.2 Gyr

3. Conclusions

In this study, we carry out a statistical estimation of the stellar masses of the progenitors, the phase space coordinates, and orbital backward-time integrations of the relatively bright (V = 12.8), extremely metal-poor ([Fe/H] = −3.17), and prograde (J_ϕ and $V_\phi > 0$) star, with a strong r-process enhancement ([Eu/Fe] = +0.94 ± 0.12, [Ba/Fe] = −0.52 ± 0.15) LAMOST J1109+0754. The direct comparison of the observed atmospheric chemical abundances and the predicted SN yields suggest possible progenitors with stellar mass span the range of 13-22 $M_\odot$. In addition, the calculated motions suggest that our star is an outer-halo member. Furthermore, its peculiar atmospheric chemical composition suggest that our stars are might belong to a low-mass dwarf galaxy and have been accreted at a young cosmic age. The action-space map of our sample suggest that this r-process-enhanced star does not match the numerical criteria of *Gaia*-Sausage and *Gaia*-Sequoia remnant stars, but, it suggests that another accretion event might be responsible for the contribution of these r-process-enhanced stars to the Milky-Way.

To investigate the accretion scenario of r-process-enhanced stars, we strongly recommend future identification and observations to increase the numbers of these peculiar stars so that their full kinematics can be investigated in more detail, and thus be used to improve our understanding of their origin.

Acknowledgements

This work was supported by the National Natural Science Foundation of China under grant Nos. 11988101 and 11890694, and National Key R&D Program of China No.2019YFA0405502. This work has made use of data from the European Space Agency (ESA) mission *Gaia* (https://www.cosmos.esa.int/gaia), processed by the *Gaia* Data Processing and Analysis Consortium (DPAC, https://www.cosmos.esa.int/web/gaia/dpac/consortium). Funding for the DPAC has been provided by national institutions, in particular the institutions participating in the *Gaia* Multilateral Agreement.

References

Abdusalam K., Ablimit I., Hashim P., Lü G. L., Mardini M. K., Wang Z. J., 2020, Astrophys. J., 902, 125

Abohalima A., Frebel A., 2018, Astrophys. J. Suppl., 238, 36

Beers T. C., Christlieb N., 2005, Annu. Rev. Astronom. Astrophys., 43, 531

Burbidge E. M., Burbidge G. R., Fowler W. A., Hoyle F., 1957, Reviews of Modern Physics, 29, 547

Cameron A. G. W., 1957, Publ. Astronom. Soc. Pacific, 69, 201

Farouqi K., Kratz K. L., Pfeiffer B., Rauscher T., Thielemann F. K., Truran J. W., 2010, Astrophys. J., 712, 1359

Gaia Collaboration et al., 2018, Astronom. and Astrophys., 616, A1

Mardini M. K., et al., 2019a, The Astrophysical Journal, 875, 89

Mardini M. K., Placco V. M., Taani A., Li H., Zhao G., 2019b, The Astrophysical Journal, 882, 27

Mardini M. K., Ershiadat N., Al-Wardat M. A., Taani A. A., Özdemir S., Al-Naimiy H., Khasawneh A., 2019c, in Journal of Physics Conference Series. p. 012024 (arXiv:1904.09608), doi:10.1088/1742-6596/1258/1/012024

Mardini M. K., et al., 2020, arXiv e-prints, p. arXiv:2009.12142

Masda S. G., Docobo J. A., Hussein A. M., Mardini M. K., Al-Ameryeen H. A., Campo P. P., Khan A. R., Pathan J. M., 2019, Astrophysical Bulletin, 74, 464

Obergaulinger M., Just O., Aloy M. A., 2018, Journal of Physics G Nuclear Physics, 45, 084001

Placco V. M., Santucci R. M., Yuan Z., Mardini M. K., Holmbeck E. M., Wang 2020, Astrophys. J., 897, 78

Qian Y.-Z., 2014, Journal of Physics G Nuclear Physics, 41, 044002

Sommer-Larsen J., Zhen C., 1990, Monthly Notices Roy. Astronom. Soc., 242, 10

Taani A., Karino S., Song L., Al-Wardat M., Khasawneh A., Mardini M. K., 2019a, Research in Astronomy and Astrophysics, 19, 012

Taani A., Abushattal A., Mardini M. K., 2019b, Astronomische Nachrichten, 340, 847

Taani A., Karino S., Song L., Mardini M., Al-Wardat M., Abushattal A., Khasawneh A., Al-Naimiy H., 2019c, in Journal of Physics Conference Series. p. 012029, doi:10.1088/1742-6596/1258/1/012029

Taani A., Khasawneh A., Mardini M., Abushattal A., Al-Wardat M., 2020, arXiv e-prints, p. arXiv:2002.03011

Thielemann F. K., Eichler M., Panov I. V., Wehmeyer B., 2017, Annual Review of Nuclear and Particle Science, 67, 253

Stellar and interstellar parameters from large photometric surveys

Malkov O*[1], Karpov S†[2,3,4], Kovaleva D‡[1], Murthy J§[5], Sichevsky S¶[1], Sytov A‖[1], Zhao G**[6], Zhukov A††[1,7,8], and Zakharov A‡‡[9]

[1]Institute of Astronomy, Moscow 119017, Russia
[2]Institute of Physics, Czech Academy of Sciences, 182 21 Prague 8, Czech Republic
[3]Special Astrophysical Observatory, Nizhnij Arkhyz 36916, Russia
[4]Kazan Federal University, Kazan 420008, Russia
[5]Indian Institute of Astrophysics, Bengaluru 560034, India
[6]National Astronomical Observatories, Beijing 100012, China
[7]"MPEI Special Design Bureau" Corporation, Moscow, Russia
[8]Federal State Budgetary Scientific Institution "Expert and Analytical Center", Moscow, Russia
[9]Sternberg Astronomical Institute, Moscow, Russia

Abstract

The parameterization of stars is a well known problem and used for various purposes in astronomy. We have shown that multicolor photometric data from large modern surveys can be used for parameterization of stars. With sufficiently good quality photometry, one may compute a 3D extinction map by comparing catalogued multicolor photometry with photometry derived from the secondary estimators such as the distance modulus and the interstellar extinction law with suitable calibration tables for absolute magnitudes with reasonable spectral types, extinctions and distances.

Keywords: *Sky surveys · Photometry · Cross-matching · Interstellar extinction*

1. Introduction

Three-dimensional (3D) extinction models have been constructed using spectral and photometric stellar data, open cluster data, star counts, Galactic dust distribution models. The standard approach to construct a 3D extinction model has been to parcel out the sky in angular cells, each defined by boundaries in Galactic coordinates (l,b). The visual extinction (A_V) in each cell may then be obtained as a function of distance (d): A_V (l,b,d) from the stars in the cells. The angular size of the cells has varied from study to study, although each cell was generally chosen to be large enough to contain a statistically significant number of calibration stars at different distances.

Published 3D models, using spectral and photometric data, were based on 10^4-10^5 stars, or were constructed for a very limited area in the sky (see, e.g., Sale et al. (2014), Green & et al (2015), Lallement et al. (2018), the earlier studies were reviewed in Malkov & Kilpio (2002)). Modern large surveys contain photometric (3 to 5 bands) data for $10^7 - 10^9$ stars. However, to make those data (obtained at different wavelengths and with different observational techniques) useful for a 3D extinction model construction, one needs to run a correct cross-identification of objects between surveys. Such cross-identification was laborious and time consuming, but using Virtual Observatory (VO) data access and

*malkov@inasan.ru, Corresponding author
†karpov.sv@gmail.com
‡dana@inasan.ru
§murthy@iiap.res.in
¶s.sichevskij@gmail.com
‖sytov@inasan.ru
**gzhao@nao.cas.cn
††aozhukov@mail.ru
‡‡zakhster@gmail.com

DOI: 10.52526/25792776-2020.67.2-272

cross-correlation technologies, a search for counterparts in a subset of different catalogues can now be carried out in a few minutes. It is now feasible to obtain information on interstellar extinction from modern large photometric surveys.

In Section 2 we give a review of sky surveys, and present principles of their cross-matching. Section 3 contains description of our procedure for parameterization of stars, and in Section 4 we present principles and pilot results of determination of interstellar extinction. We draw our conclusions in Section 5.

2. Sky Surveys and Cross-matching

2.1. Sky Surveys Selection

The number of surveys available at any wavelength is large enough to construct detailed spectral energy distributions (SED) for any kind of astrophysical object. Sky surveys, we select for parameterization of stars, should satisfy the following criteria:

- the number of objects exceeds $\sim 10^7$,
- the survey covers a large area in the sky,
- the photometric accuracy is better than about 0.05 mag,
- the depth of the survey exceeds V$\sim$20 mag.

Table 1. Large photometric surveys

Survey	N[a]	Sky coverage	Photometric bands	Limiting magnitude
DENIS	355	Southern hemisphere	Gunn-i, J, K_S	18.5, 16.5, 14.0
2MASS	471	All sky	J, H, K_S	15.8, 15.1, 14.3
SDSS 12	325	25%	u, g, r, i, z	g,r=22.2
GALEX DR5 (AIS+MIS)	78	90%	FUV, NUV	$\sim$25
UKIDSS DR9 LAS	83	15%	Z, Y, J, H, K	K=18.3
AllWISE	748	All sky	W1, W2, W3, W4	16.6, 16.0, 10.8, 6.7
IPHAS DR2	219	Northern Galactic plane	r, i, H_α	r=21-22
Pan-STARRS PS1 - DR1	1919	All sky but southern cap	g, r, i, z, y	i$\sim$20
GAIA DR2	1693	All sky	G, BP, RP	G=20

[a]N is number of objects, 10^6.

The following sky surveys are selected for our study.

- The DENIS database DENIS Consortium (2005)
- 2MASS All-Sky Catalog of Point Sources Cutri & et al (2003)
- The SDSS Photometric Catalogue, Release 12 Alam et al. (2015)

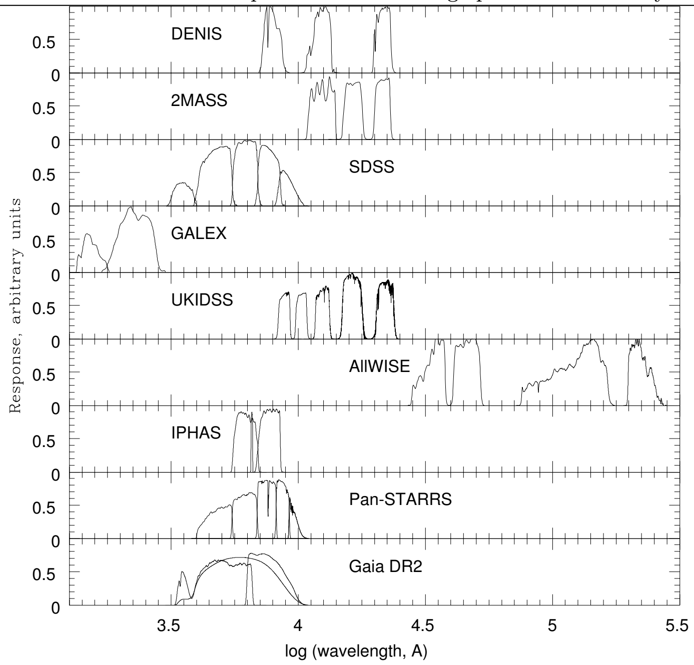

Figure 1. Response curves of the photometric surveys.

- GALEX-DR5 (GR5) sources from AIS and MIS Bianchi et al. (2011), Bianchi et al. (2017)
- UKIDSS-DR9 LAS, GCS and DXS Surveys Lawrence & et al (2007)
- AllWISE Data Release Cutri & et al (2014)
- IPHAS DR2 Source Catalogue Barentsen & et al (2014)
- The Pan-STARRS release 1 (PS1) Survey - DR1 Chambers & et al (2016)
- Gaia DR2 Gaia Collaboration et al. (2018), Bailer-Jones et al. (2018)

Some information on the surveys is given in Table 1, their photometric systems response curves are shown in Fig. 1.

The presented surveys basically satisfy the criteria listed above. The number of objects vary from $\sim 10^8$ to $\sim 10^9$. The most local survey, IPHAS, covers a relatively small but important area in the sky. The photometric accuracy of all surveys (except, probably, ultraviolet GALEX) is better than 0.05 mag. The limiting magnitudes, converted to V-band, are not less than $\sim$20 mag.

2.2. Cross-matching of Surveys

Different surveys/instruments have different positional accuracy and resolution. In addition, the depth of each survey is different and, depending on sources brightness and their SED, a given source might or might not be detected at a certain wavelength. All this makes the pairing of sources among surveys not trivial, especially in crowded fields.

We have implemented an algorithm of fast positional matching of some of the sky surveys in small (up to one degree) areas with filtering of false identification Malkov & Karpov (2011). In particular, for each area and each pair we estimated the matching radius. As a result, we drew in a number 0.1-degree radius areas samples of point-like objects counterparts from the DENIS, 2MASS, SDSS, GALEX, and UKIDSS surveys, and performed a cross-identification within these surveys Karpov et al. (2012), Malkov et al. (2012). We have compiled the corresponding subcatalogues in the VOTable format. The tool developed as a result of this work can be used to cross-identify objects in arbitrary sky areas for the further classification and determination of stellar parameters, including the measurement of the amount of interstellar extinction.

In some surveys (e.g., GALEX, SDSS, UKIDSS) more than one observation per object was made and, consequently, more than one entry per object is present in the survey. In such cases we use weighted average values for the photometry.

In the cross-identification process (and later for the parameterization) we use all positional information and all photometry available in surveys. To select objects for further study we also pay attention to various flags, presented in the surveys. The flags can indicate quality of observations and provide information on a nature of object (duplicity, variability, extended shape). As it was mentioned above, on this stage we do not use trigonometric parallax as an input parameter.

It can be seen from Fig.1 that response curves of photometric bands in different surveys are sometimes the same or similar (e.g., K_S-band in DENIS and K_S-band in 2MASS). The comparison of brightness of objects in such pairs of bands provides us an additional filter to discard objects irrelevant for the parameterization: a large magnitude difference may indicate variability, a rare evolutionary stage, or non-stellar nature of the object.

We have to remove all non-stellar objects, unresolved photometric binaries, variable stars and other contaminating objects, based on flags included in the original surveys. Too bright and too faint objects for this particular survey (i.e., overexposed and underexposed, respectively) can also be spotted and omitted at this stage.

3. Multicolor Photometry and Parameterization of Stars

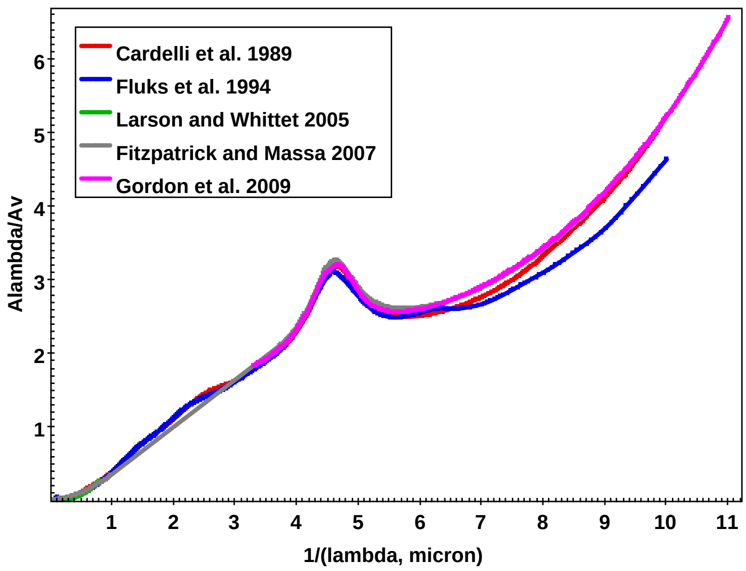

Figure 2. Interstellar extinction law. Red curve: Cardelli et al. (1989) for R_V=3.1. Blue curve: Fluks et al. (1994) for R_V=3.1. Green curve: Larson & Whittet (2005). Grey curve: Fitzpatrick & Massa (2007) for R_V=3.1. Purple curve: Gordon et al. (2009) for R_V=3.1.

We studied a problem of classification and parameterization of stars from multicolor photometry in detail (see, e.g., Sichevskiy et al. (2013), Sichevsky & Malkov (2016)). In particular, a problem of binary stars parameterization was studied in Malkov et al. (2010) and Malkov et al. (2011).

We have developed a method, which allows us to determine stellar parameters from multicolor photometry. For the studied objects MK (Morgan-Keenan) spectral types (SpT), distances (d) and interstellar extinction values (A_V) can be estimated, minimizing the function

$$\chi^2 = \sum_{i=1}^{N} \left(\frac{m_{obs,i} - m_{calc,i}}{\sigma m_{obs,i}} \right)^2, \qquad (1)$$

where $m_{obs,i}$ and $\sigma m_{obs,i}$ are the apparent magnitude and its observational error, respectively, in the i-th photometric band from a given survey. The summation is over up to N$\sim$30 photometric bands

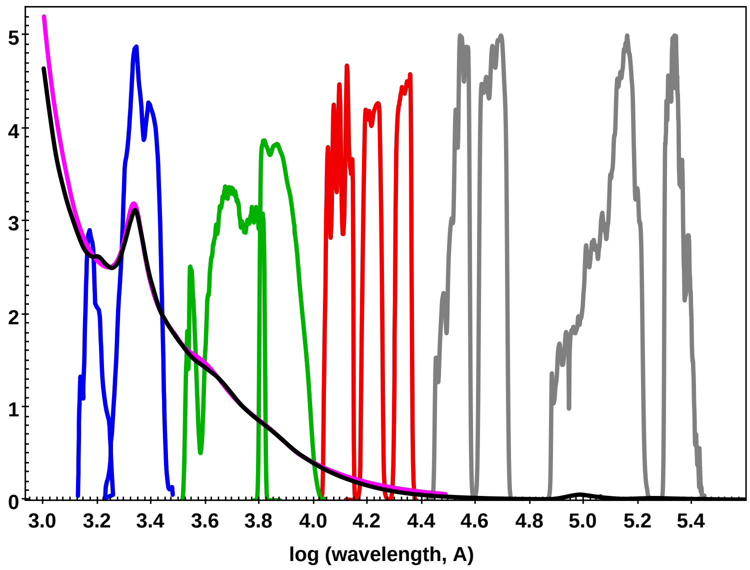

Figure 3. Response curves of all-sky photometric surveys and IEL. Response curves, from left to right: GALEX (FUV, NUV), Gaia (BP, RP), 2MASS (J, H, K_S), AllWISE (W1, W2, W3, W4); the Y-axis represents the capacity in arbitrary units. IELs for $R_V = 3.1$: Cardelli et al. (1989) (purple curve), Fluks et al. (1994) (black curve); the Y-axis represents A_λ/A_V.

(see Table 1), and

$$m_{calc,i} = M_i(\mathrm{SpT}) + 5\log \mathrm{d} - 5 + \mathrm{A_i}(\mathrm{A_V}), \tag{2}$$

Here $A_i = f(A_V)$ is the extinction in the i-th photometric band, and can be determined from the interstellar extinction law (Fluks et al. (1994), Cardelli et al. (1989), Fitzpatrick & Massa (2007)).

A calibration relation $M_i(\mathrm{SpT})$ should be available for each of the i photometric bands included in the original surveys. It is true for 2MASS, SDSS and GALEX photometric systems (Kraus & Hillenbrand (2007), Findeisen et al. (2011)) but corresponding calibration tables for UKIDSS and other surveys can not be found in literature. In the absence of such information, it is necessary to construct corresponding relations from theoretical spectral energy distributions (SED) and photometric system response curves. The best source for theoretical SED are libraries of synthetic spectra Lejeune et al. (1997), Castelli & Kurucz (2003), Gustafsson et al. (2008), and the SEDs are computed there for a given set of atmospheric parameters ($\log T_{\mathrm{eff}}$, $\log g$, $[M/H]$) rather than spectral classes. Thus, for the decision of this problem it is necessary to design and use relations between spectral class and atmospheric parameters, for different luminosity classes. To construct analytic (spectral class – atmospheric parameters) formula, we have used data from the empirical stellar spectral atlases ELODIE (Prugniel et al., 2007), Indo-US (Valdes et al., 2004), MILES (Falcón-Barroso et al., 2011), and STELIB (Le Borgne et al., 2003), and made a polynomial approximation. The results are presented in Table 3 (see Malkov et al. (2020) for details).

Another source of SED for different types of stars (which can be used to model observational photometry), are empirical spectrophotometric atlases (e.g., Pickles (1998), Wu et al. (2011)). We have made a comparative analysis of the most known semi-empirical and empirical spectral atlases. The results show that the standard error of synthesized stellar magnitudes calculated with SED from best spectral atlases reaches 0.02 mag. It has been also found that some modern spectral atlases are burdened with significant systematic errors Kilpio et al. (2012).

To parameterize the stars it is necessary to have an understanding of the relation of interstellar extinction in V-band and in photometric bands of the used surveys, $A_i(A_V)$ (see Eq. 2). However, $A_i(A_V)$ values are calculated and available in the literature only for a small number of modern photometric systems, namely: Rieke & Lebofsky (1985) (UBVRIJHKLMN, 8.0,8.5,...13.0 μm), Cardelli et al. (1989) (UBVRIJHKL), Draine (2003) (Johnson, Cousins, SDSS), Indebetouw et al. (2005) (2MASS, Spitzer), Schlafly & Finkbeiner (2011) (Landolt, UKIRTJHKL, Gunn, Stromgren, SDSS), Yuan et al. (2013) (2MASS, SDSS, GALEX, AllWISE), Hanson & Bailer-Jones (2014) (u,g,i,z,Y,J,H,K), Bono

Table 2. Spectral class — effective temperature — surface gravity relations

			std. dev.	valid for	Eq.
LC=V					
$\log T_{\rm eff}$	=	$4.80223 - 0.0465961S + 0.00157054S^2$	0.004	O3–O9	(T1)
$\log T_{\rm eff}$	=	$5.30408 - 0.111312S + 0.00284209S^2 - 2.51285e^{-5}S^3$	0.011	B0–G7	
$\log T_{\rm eff}$	=	$3.25745 + 0.0285452S - 0.000388153S^2$	0.008	G8–M9	
S	=	$-77.4025 - 208.506T - 72.7616T^2$	0.36	$3.38 \leq \log T_{\rm eff} < 3.75$	(T2)
S	=	$13.0566 + 68.6827T + 404.486T^2 + 751.011T^3 + 497.913T^4$	0.75	$3.75 \leq \log T_{\rm eff} < 4.10$	
S	=	$5.53554 - 34.2627T - 4.78570T^2 + 191.168T^3 + 317.065T^4$	0.34	$4.10 \leq \log T_{\rm eff} \leq 4.72$	
$\log g$	=	$4.23248 + 0.0194541S_1 + 0.000552749S_1^2 - 4.30515e^{-5}S_1^3-$			
		$-1.09920e^{-6}S_1^4 + 7.61843e^{-8}S_1^5 + 8.20985e^{-10}S_1^6 - 3.27874e^{-11}S_1^7$	0.055	O3–M9.5	(T3)
S	=	$-0.117642 + 1.07059G + 192.069G^2 - 183.386G^3 + 49.7143G^4$	4.02	$3.8 \leq \log g \leq 5.3$	(T4)
LC=I					
$\log T_{\rm eff}$	=	$5.37107 - 0.132197S + 0.00447197S^2 - 7.12416e^{-5}S^3 + 4.17523e^{-7}S^4$	0.049	O7–M3	(T5)
S	=	$5.87386 - 49.0805T - 135.952T^2 - 119.090T^3 + 124.459T^4 + 108.708T^5$	3.14	$3.45 \leq \log T_{\rm eff} < 4.60$	(T6)
$\log g$	=	$5.26666 - 0.289286S + 0.00728099S^2 - 6.33673e^{-5}S^3$	0.485	O7–M3	(T7)
S	=	$5.26199 - 10.2492G + 2.79561G^2 + 0.526251G^3$	9.74	$-0.2 \leq \log g \leq 3.8$	(T8)
LC=III					
$\log T_{\rm eff}$	=	$5.07073 - 0.0757056S + 0.00147089S^2 - 1.03905e^{-5}S^3$	0.034	O5–M10	(T9)
S	=	$8.49594 - 49.4053T - 191.524T^2 - 335.488T^3 - 144.781T^4$	2.59	$3.45 \leq \log T_{\rm eff} < 4.65$	(T10)
$\log g$	=	$3.79253 - 0.0136260S + 0.000562512S^2 - 1.68363e^{-5}S^3$	0.513	O5–M10	(T11)
S	=	$33.3474 - 18.3022G - 5.33024G^2 - 0.667234G^3$	7.03	$-0.5 \leq \log g \leq 4.7$	(T12)

S is spectral class code: 3 for O3, ..., 10 for B0, ..., 60 for M0.
$S_1 = S - 35$
T = $\log T_{\rm eff} - 4.6$
G = $\log g - 3.7$

et al. (2019) (Gaia). To calculate the missing $A_i(A_V)$ values it is necessary to know the interstellar extinction law, IEL (see a summary of published IELs in Table 3 and Figs. 2 and 3). The value $x \equiv (\lambda, \mu m)^{-1}$ is commonly used as argument in the IEL.

Table 3. Interstellar extinction law

Reference	x, $(\mu m)^{-1}$	λ, A	IEL
Cardelli et al. (1989)	0.3 - 1.1 (IR)	9100 - 33,000	A_λ/A_V
	1.1 - 3.3 (Opt/NIR)	3000 - 9100	
	3.3 - 8 (UV)	1250 - 3000	
	8 - 10 (Far-UV)	1000 - 1250	
O'Donnell (1994)	1.1 - 3.3 (Opt/NIR)	3000 - 9100	A_λ/A_V
Fluks et al. (1994)	0 - 10 (IR/Opt/UV)	1000 - 2,500,000	A_λ/E_{B-V}
Larson & Whittet (2005)	0 - 0.8 (IR)	>12,500	A_λ/A_V
Fitzpatrick & Massa (2007)	0 - 1 (IR)	>10,000	$E_{\lambda-V}/E_{B-V}$
	3.7 - 8.7 (UV)	1150 - 2700	
Gordon et al. (2009)	3.3 - 11 (UV/Far-UV)	900 - 3000	A_λ/A_V

To properly obtain astrophysical parameters from catalogued photometry one also needs to study the possibility and sphere of application of the parameterization method. We indicate areas in the parameter space [effective temperature $\log T_{\rm eff}$, gravity $\log g$, metallicity $[Fe/H]$, visual extinction A_V, total-to-selective extinction ratio R_V], where observational photometry precision, achieved in modern large multi-color surveys, allows us to obtain astrophysical parameters with acceptable accuracy Sichevskij et al. (2014).

4. Determination of Interstellar Extinction

Using the method pf parameterization, described in Section 3, one can construct A_V(l,b,d) relation. This method allows one to plot parameterized objects in the distance-extinction (d-A_V) plane, approximate them (by the cosecant law or more complicated function) and estimate interstellar extinction parameters in a given direction on the sky.

Note that for high galactic latitude areas ($|b| > 15^o$ or so) the interstellar extinction is thought to be (roughly) uniformly distributed and to satisfy the so-called cosecant (barometric) law, suggested by Parenago (1940). That function should be modified (complicated) for lower latitudes, as dust clouds concentrated in the Galactic plane, will have to be taken into account.

A preliminary analysis of applicability of SDSS and 2MASS photometry for determining the properties of stars and interstellar extinction was made by in Sichevskij (2018).

Then to test the procedure, described in Section 3, we have selected sky areas which are interesting from astrophysical point of view and where our results can be compared with independent studies. In particular, it is instructive and useful to apply the model to estimate interstellar extinction for several areas of the sky where individual estimates were made by Schlegel et al. (1998), and used to calculate extinction for SNs in the Universe accelerating expansion study Perlmutter & et al (1999).

In our study Malkov et al. (2018b) we have cross-matched objects in 2MASS, SDSS, GALEX and UKIDSS surveys in selected areas at high galactic latitudes, using Virtual Observatory facilities. As a result of the cross-matching, we obtained multi-wavelength (i = 9 to 13 bands) photometric data for each object. We have applied the method, described in Section 3, to parameterize the stars and to construct A_V(l,b,d) relations for selected areas in the sky.

We have compared our results with LAMOST Luo & et al (2015) data and extinction values to distant SNs (based on IRAS and DIRBE microwave data), available in the literature. The comparison exhibits a good agreement (see Malkov et al. (2018b) for details). A comparison of our results with recently released Gaia DR2 data also demonstrates a good agreement for stars as faint as $19^m.6$ g_{SDSS}, and shows that our method allows us to determine spectral type, distance and interstellar extinction of objects out to 4.5 kpc Malkov et al. (2018a). It indicates that the proposed algorithm (after some modifications, required for low galactic latitudes) can be used for construction of a 3D map of interstellar extinction in the Milky Way Galaxy.

5. Conclusions

The study of the stellar physical properties as well as the spatial distribution of interstellar extinction, is important for many investigations of galactic and extragalactic objects. We have developed a method for determination of stellar parameters and interstellar extinctions from multicolor photometry. This method was applied to objects drawn from modern large photometric surveys and, in this work, we give a review of the surveys and discuss problems of cross-identification.

Our procedure may be modified to use the astrometric and spectral information on the studied objects as input parameters. In particular, our procedure can be modified to determine stellar parameters and interstellar extinction values from not only multicolor photometry but also using additional information such as precise parallaxes and spectral classification, where available, thus reducing the number of unknowns in Eq. (2). One notable improvement has come with the recent release of the Gaia DR2 set of parallaxes, which allows us to use distance as an input (rather than as a free) parameter. It should significantly increase the accuracy of our results, especially when we can substitute the more precise parallaxes from Gaia DR3 for the DR2 data we currently use. Our procedure can also be modified for stars with spectral classification available from LAMOST Luo & et al (2015), the largest source of spectral classification of objects in the northern sky. LAMOST Data Release 4 contains data on 7.6×10^6 objects and is available through VizieR database (V/153).

Also, our experience is thought to be a practical guide to issues that will be particular important as soon as the new surveys become available (LSST Ivezić et al. (2019), SAGE Zheng et al. (2018), UVIT Tandon & et al (2017)).

Acknowledgements

The work was partly supported by the Russian Foundation for Basic Researches (project 19-07-01198), by NSFC/RFBR grant 20-52-53009, and by DST grant INT/RUS/RFBR/P-265 to JM. OM thanks the CAS President's International Fellowship Initiative (PIFI). SK was supported by European Structural and Investment Fund and the Czech Ministry of Education, Youth and Sports (Project CoGraDS – CZ.02.1.01/0.0/0.0/15 003/0000437). The work is partially performed according to the Russian Government Program of Competitive Growth of Kazan Federal University. This research has made use of NASA's Astrophysics Data System, and use of the VizieR catalogue access tool, CDS, Strasbourg, France. This research made use of TOPCAT, an interactive graphical viewer and editor for tabular data (Taylor, 2005). The acknowledgements were compiled using the Astronomy Acknowledgement Generator.

References

Alam S., et al., 2015, Astrophys. J. Suppl. Ser. , 219, 12

Bailer-Jones C. A. L., Rybizki J., Fouesneau M., Mantelet G., Andrae R., 2018, Astron. J. , 156, 58

Barentsen G., et al 2014, VizieR Online Data Catalog, 2321

Bianchi L., Herald J., Efremova B., Girardi L., Zabot A., Marigo P., Conti A., Shiao B., 2011, Astrophys. Space. Sci. , 335, 161

Bianchi L., Shiao B., Thilker D., 2017, Astrophys. J. Suppl. Ser. , 230, 24

Bono G., et al., 2019, Astrophys. J. , 870, 115

Cardelli J. A., Clayton G. C., Mathis J. S., 1989, Astrophys. J. , 345, 245

Castelli F., Kurucz R. L., 2003, in Piskunov N., Weiss W. W., Gray D. F., eds, IAU Symposium Vol. 210, Modelling of Stellar Atmospheres. p. A20 (arXiv:astro-ph/0405087)

Chambers K. C., et al 2016, arXiv e-prints,

Cirasuolo M., MOONS Consortium 2016, in Skillen I., Balcells M., Trager S., eds, Astronomical Society of the Pacific Conference Series Vol. 507, Multi-Object Spectroscopy in the Next Decade: Big Questions, Large Surveys, and Wide Fields. p. 109

Cutri R. M., et al 2003, VizieR Online Data Catalog, 2246

Cutri R. M., et al 2014, VizieR Online Data Catalog, 2328

DENIS Consortium 2005, VizieR Online Data Catalog, 1

Draine B. T., 2003, Ann. Rev. Astron. Astrophys. , 41, 241

Drew J. E., et al., 2014, Mon. Not. R. Astron. Soc. , 440, 2036

Eker Z., et al., 2018, Mon. Not. R. Astron. Soc. , 479, 5491

Falcón-Barroso J., Sánchez-Blázquez P., Vazdekis A., Ricciardelli E., Cardiel N., Cenarro A. J., Gorgas J., Peletier R. F., 2011, Astron. Astrophys. , 532, A95

Findeisen K., Hillenbrand L., Soderblom D., 2011, Astron. J. , 142, 23

Fitzpatrick E. L., Massa D., 2007, Astrophys. J. , 663, 320

Fluks M. A., Plez B., The P. S., de Winter D., Westerlund B. E., Steenman H. C., 1994, Astron. and Astrophys. Suppl. Ser. , 105, 311

Gaia Collaboration et al., 2018, Astron. Astrophys. , 616, A1

Gordon K. D., Cartledge S., Clayton G. C., 2009, Astrophys. J. , 705, 1320

Green G. M., et al 2015, Astrophys. J. , 810, 25

Gustafsson B., Edvardsson B., Eriksson K., Jørgensen U. G., Nordlund Å., Plez B., 2008, Astron. Astrophys. , 486, 951

Hanson R. J., Bailer-Jones C. A. L., 2014, Mon. Not. R. Astron. Soc. , 438, 2938

Indebetouw R., et al., 2005, Astrophys. J. , 619, 931

Ivezić Ž., et al., 2019, Astrophys. J. , 873, 111

Karpov S. V., Malkov O. Y., Mironov A. V., 2012, Astrophysical Bulletin, 67, 82

Kilpio E. Y., Malkov O. Y., Mironov A. V., 2012, in Prugniel P., Singh H. P., eds, Astronomical Society of India Conference Series Vol. 6, Astronomical Society of India Conference Series. p. 31 (arXiv:1208.1960)

Kraus A. L., Hillenbrand L. A., 2007, Astron. J. , 134, 2340

Kunder A., et al 2017, Astron. J. , 153, 75

Lallement R., et al., 2018, Astron. Astrophys. , 616, A132

Larson K. A., Whittet D. C. B., 2005, Astrophys. J. , 623, 897

Lawrence A., et al 2007, Mon. Not. R. Astron. Soc. , 379, 1599

Le Borgne J.-F., et al., 2003, Astron. Astrophys. , 402, 433

Lejeune T., Cuisinier F., Buser R., 1997, Astron. and Astrophys. Suppl. Ser. , 125, 229

Luo A.-L., et al 2015, Research in Astronomy and Astrophysics, 15, 1095

Luo A. L., Zhao Y. H., Zhao G., et al. 2019, VizieR Online Data Catalog, p. V/164

Malkov O., Karpov S., 2011, in Evans I. N., Accomazzi A., Mink D. J., Rots A. H., eds, Astronomical Society of the Pacific Conference Series Vol. 442, Astronomical Data Analysis Software and Systems XX. p. 583

Malkov O., Kilpio E., 2002, Astrophys. Space. Sci. , 280, 115

Malkov O. Y., Sichevskij S. G., Kovaleva D. A., 2010, Mon. Not. R. Astron. Soc. , 401, 695

Malkov O., Mironov A., Sichevskij S., 2011, Astrophys. Space. Sci. , 335, 105

Malkov O., Dluzhnevskaya O., Karpov S., Kilpio E., Kniazev A., Mironov A., Sichevskij S., 2012, Baltic Astronomy, 21, 319

Malkov O., et al., 2018a, Galaxies, 7, 7

Malkov O., et al., 2018b, Open Astronomy, 27, 62

Malkov O. Y., et al., 2019, CEUR Workshop Proceedings, 2523, 217

Malkov O., Kovaleva D., Sichevsky S., Zhao G., 2020, Research in Astronomy and Astrophysics, 20, 139

O'Donnell J. E., 1994, Astrophys. J. , 437, 262

Ochsenbein F., et al., 2004, in Quinn P. J., Górski K. M., eds, Toward an International Virtual Observatory. p. 118, doi:10.1007/10857598˙18

Parenago P. P., 1940, Astron. Zh., 13, 3

Pecaut M. J., Mamajek E. E., 2013, Astrophys. J. Suppl. Ser. , 208, 9

Perlmutter S., et al 1999, Astrophys. J. , 517, 565

Pickles A. J., 1998, Publ. Astron. Soc. Pac. , 110, 863

Prugniel P., Soubiran C., Koleva M., Le Borgne D., 2007, arXiv Astrophysics e-prints,

Reis I., Poznanski D., Baron D., Zasowski G., Shahaf S., 2018, Mon. Not. R. Astron. Soc. , 476, 2117

Rieke G. H., Lebofsky M. J., 1985, Astrophys. J. , 288, 618

Sale S. E., et al., 2014, Mon. Not. R. Astron. Soc. , 443, 2907

Samus' N. N., Kazarovets E. V., Durlevich O. V., Kireeva N. N., Pastukhova E. N., 2017, Astronomy Reports, 61, 80

Schlafly E. F., Finkbeiner D. P., 2011, Astrophys. J. , 737, 103

Schlegel D. J., Finkbeiner D. P., Davis M., 1998, Astrophys. J. , 500, 525

Sichevskij S. G., 2018, Astrophysical Bulletin, 73, 98

Sichevskij S. G., Mironov A. V., Malkov O. Y., 2014, Astrophysical Bulletin, 69, 160

Sichevskiy S. G., Mironov A. V., Malkov O. Y., 2013, Astronomische Nachrichten, 334, 832

Sichevsky S., Malkov O., 2016, Baltic Astronomy, 25, 67

Skvortsov N. A., et al., 2016, Astrophysical Bulletin, 71, 114

Smith D. J. B., et al 2016, in Reylé C., Richard J., Cambrésy L., Deleuil M., Pécontal E., Tresse L., Vauglin I., eds, SF2A-2016: Proceedings of the Annual meeting of the French Society of Astronomy and Astrophysics. pp 271–280 (arXiv:1611.02706)

Straižys V., 1992, Multicolor stellar photometry. Tucson : Pachart Pub. House, c1992.

Tandon S. N., et al 2017, Astron. J. , 154, 128

Taylor M. B., 2005, in Shopbell P., Britton M., Ebert R., eds, Astronomical Society of the Pacific Conference Series Vol. 347, Astronomical Data Analysis Software and Systems XIV. p. 29

Valdes F., Gupta R., Rose J. A., Singh H. P., Bell D. J., 2004, Astrophys. J. Suppl. Ser. , 152, 251

Wu Y., Singh H. P., Prugniel P., Gupta R., Koleva M., 2011, Astron. Astrophys. , 525, A71

Yanny B., et al 2009, Astron. J. , 137, 4377

Yuan H. B., Liu X. W., Xiang M. S., 2013, Mon. Not. R. Astron. Soc. , 430, 2188

Zheng J., Zhao G., Wang W., Fan Z., Tan K.-F., Li C., Zuo F., 2018, Research in Astronomy and Astrophysics, 18, 147

de Jong R. S., et al., 2019, The Messenger, 175, 3

Biermann battery mechanism and its role in evolution of astrophysical magnetic fields

Mikhailov E A*[1] and Andreasyan R R[2]

[1]M.V.Lomonosov Moscow State University, Moscow, Russia
[2]V.A.Ambartsumian Byurakan Astrophysical Observatory, Byurakan, Armenia

Abstract

Nowadays it is well-known that a wide range of astrophysical objects have large-scale magnetic fields. Their observations are usually carried using Faraday rotation measurements. One of the possible mechanisms of their generation (at least the seed ones) can be connected with the Biermann battery mechanism. It is connected with difference between masses of protons and electrons, which are interacting with the cosmic medium. They produce the circular currents which can be generate the magnetic field which is perpendicular to the rotation plane. Here we present the mechanism of the magnetic field generation by the Biermann mechanism in the disc objects which can be useful for galaxies, accretion discs and another objects. One of the important features is connected with the influence of the existing magnetic fields (which can be induced by another charged particles) while studying the movement of the particles.

Keywords: *magnetic fields, Biermann battery, galaxies*

1. Introduction

Now it is well-known that a lot of different astrophysical objects have regular magnetic field structures (Zeldovich et al, 1983). There is a wide range of research of magnetic fields of the Sun, another stars, planets, galaxies, accretion discs and another objects. They are well studied using both observational and theoretical methods.

From the observational point of view, first studies of the magnetic fields in space were connected with description of dark spots. As for the galactic magnetic fields, first assumptions have been made by studying the cosmic rays. After that, the estimates of the magnetic field were done using the study of the synchrotron emission spectra (Fermi, 1949). Nowadays most of the studies are done using measurements of the Faraday rotation of the polarization plane of the radio waves (Beck et al, 1996; Arshakian et al, 2009). For the Milky Way, such research is usually done basing on the data about pulsars (Andreasyan et al, 2020). As for another galaxies, the extragalactic sources are used. Sometimes they are taken for our Galaxy, too (Oppermann et al, 2012) Also the Faraday rotation is useful to study the magnetic fields of another cosmic objects.

As for the theory, the magnetic fields are usually described by the dynamo mechanism (Beck et al, 1996). It is based (Moffatt, 1978) on joint activity of the differential rotation (which is connected with the non-solid rotation of the galaxies) and alpha-effect (it describes the vorticity of the turbulent motions of the interstellar medium). If they are more intensive than the turbulent diffusivity, the magnetic field will grow according to the exponential law. However, it is necessary to have the initial field. It is very difficult to describe it using only dynamo, so we should take another processes.

One of the possible mechanisms is connected with so-called Biermann battery (Biermann, 1950). Principally it is based on outflows from the central objects to the outer parts (Andreasyan, 1996). They contain protons and electrons which interact with the rotating medium. The different masses of these particles make them interact in different way. So, the velocity of them is different and there

*ea.mikhajlov@physics.msu.ru, Corresponding author

DOI: 10.52526/25792776-2020.67.2-281

are circular currents. Such currents produce magnetic fields which can play a great role in galactic magnetism.

It is important to take into account, that every particle moves in the existing magnetic field. For example, this field can be connected with the magnetic fields of another particles. So, the growth of the magnetic field can be limited by the interaction between the particles and the existing magnetic field.

Here we present the model for the motion of the particles and estimate the typical values of the velocity and circular currents. Also we calculate the magnetic field induced by it.

2. Basic equations and their solution

We can consider the motion of the charged particle which outflows from the central body in the galaxy or another object of disc shape (fig. 1). The acceleration $\mathbf{w}$ of the particle will be the following:

$$\mathbf{w} = -\frac{1}{\tau}(\mathbf{v} - \mathbf{V}) + \mathbf{F}_L + \mathbf{F}_g,$$

where $\mathbf{v}$ is the velocity of the particle, $\mathbf{V}$ is the velocity of the medium, τ is the typical timescale of the interaction between the rotating medium and the particle, $\mathbf{F}_g$ is the gravitational force and $\mathbf{F}_L$ is the Lorentz force.

It is quite reasonable to assume, that the radial velocity of the particle has the uniform value V. Also, the magnetic field is directed vertically, and the Lorentz force will be:

$$F_L = \frac{q}{mc}\dot{r}B.$$

So, the main component of the equation is associated with $\varphi-$component:

$$w_\varphi = -\frac{1}{\tau}r(\dot{\varphi} - \Omega) - \frac{q}{mc}\dot{r}B.$$

As for the component of the acceleration we shall have:

$$w_\varphi = r\ddot{\varphi} + 2\dot{r}\dot{\varphi}.$$

The equation for the angle evolution will be the following:

$$r\ddot{\varphi} + 2\dot{r}\dot{\varphi} = -\frac{r}{\tau}(\dot{\varphi} - \Omega) - \frac{q}{mc}\dot{r}B.$$

We can take into account that $\dot{r} = V$ and assume that the distance from the center changes quite slowly. So we can rewrite the equation as:

$$\ddot{\varphi} = -\frac{2V}{R}\dot{\varphi} - \frac{1}{\tau}(\dot{\varphi} - \Omega) - \frac{q}{Rmc}VB.$$

This equation can be rewritten as:

$$\ddot{\varphi} + \left(\frac{2V}{R} + \frac{1}{\tau}\right)\dot{\varphi} = \frac{\Omega}{\tau} - \frac{qVB}{Rmc};$$

$$\frac{d}{dt}\left(\dot{\varphi}\exp\left(\left(\frac{2V}{R} + \frac{1}{\tau}\right)t\right)\right) = \left(\frac{\Omega}{\tau} - \frac{qVB}{Rmc}\right)\exp\left(\left(\frac{2V}{R} + \frac{1}{\tau}\right)t\right).$$

3. Solutions of the equations

Both parts of the equation can be integrated as:

$$\dot{\varphi}\exp\left(\left(\frac{2V}{R}+\frac{1}{\tau}\right)t\right)+C=\frac{\left(\frac{\Omega}{\tau}-\frac{qVB}{Rmc}\right)\exp\left(\left(\frac{2V}{R}+\frac{1}{\tau}\right)t\right)}{\frac{2V}{R}+\frac{1}{\tau}};$$

where C is some constant connected with the initial conditions.

If in the beginning $\varphi=0$, we can take that:

$$C=\frac{\left(\frac{\Omega}{\tau}-\frac{qVB}{Rmc}\right)}{\frac{2V}{R}+\frac{1}{\tau}};$$

so the equation for the velocity will be:

$$\dot{\varphi}\exp\left(\left(\frac{2V}{R}+\frac{1}{\tau}\right)t\right)+\frac{\left(\frac{\Omega}{\tau}-\frac{qVB}{Rmc}\right)}{\frac{2V}{R}+\frac{1}{\tau}}=\frac{\left(\frac{\Omega}{\tau}-\frac{qVB}{Rmc}\right)\exp\left(\left(\frac{2V}{R}+\frac{1}{\tau}\right)t\right)}{\frac{2V}{R}+\frac{1}{\tau}};$$

For the derivative of the angle we shall have:

$$\dot{\varphi}=\frac{\left(\frac{\Omega}{\tau}-\frac{qVB}{Rmc}\right)}{\frac{2V}{R}+\frac{1}{\tau}}\left\{1-\exp\left(-\left(\frac{2V}{R}+\frac{1}{\tau}\right)t\right)\right\}.$$

If we are speaking about the radial velocity, it will come to the value:

$$\dot{\varphi}=R\frac{\Omega-\frac{q\tau VB}{Rmc}}{1+\frac{2V\tau}{R}}\left\{1-\exp\left(-\frac{t}{\tau}\left(1+\frac{2V\tau}{R}\right)\right)\right\}.$$

So the velocity will reach the limit value:

$$v_{\varphi}=V_0\left\{1-\exp\left(-\frac{t}{T}\right)\right\};$$

where

$$V_0=R\frac{\Omega-\frac{q\tau VB}{Rmc}}{1+\frac{2V\tau}{R}};$$

$$T=\frac{\tau}{1+\frac{2V\tau}{R}}.$$

The time period T is usually much smaller than another typical times of the problem, so the azimuthal velocity soon becomes close to V_0. Taking into account that $\frac{2V\tau}{R}\ll 1$, for the velocity we shall have:

$$v_{\varphi}\approx R\frac{\Omega-\frac{q\tau VB}{Rmc}}{1-\frac{2V\tau}{R}}\approx R\Omega-2V\Omega\tau-\frac{q\tau VB}{mc}.$$

The typical period of the particle is the following:

$$T=\frac{2\pi R}{v}=\frac{2\pi}{\Omega-\frac{2V\Omega\tau}{R}-\frac{q\tau VB}{Rmc}}$$

It is connected with the current:

$$I=\frac{q}{T}=\frac{q}{2\pi}\left(\Omega-\frac{2V\Omega\tau}{R}-\frac{e\tau VB}{Rmc}\right)$$

We describe two different types of particles. For the protons we will have:

$$I_p=\frac{e}{2\pi}\left(\Omega-\frac{2V\Omega\tau_p}{R}-\frac{e\tau_p VB}{Rm_p c}\right);$$

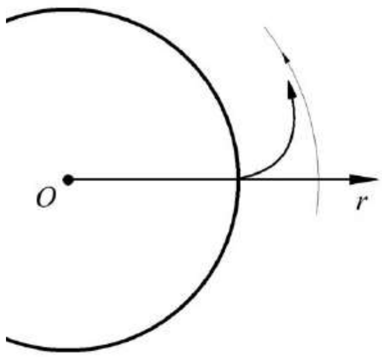

Figure 1. Motion of the particle.

where τ_p is the typical collision time for protons, m_p is the proton mass. For electrons:

$$I_e = -\frac{e}{2\pi}\left(\Omega - \frac{2V\Omega\tau_e}{R} + \frac{e\tau_e VB}{Rm_e c}\right);$$

where τ_e is the typical electron collision time, m_e is the mass of the electron. Each pair corresponds to the full current:

$$I = I_p + I_e = -\frac{eV\Omega(\tau_p - \tau_e)}{\pi R} - \frac{e^2 VB}{\pi Rc}\left(\frac{\tau_p}{m_p} + \frac{\tau_e}{m_e}\right).$$

If we take into account that τ is proportional to squared mass, the part which is connected with the electrons can be neglected, and the current will be the following:

$$I = -\frac{eV\Omega\tau_p}{\pi R} - \frac{e^2 VB\tau_p}{\pi Rcm_p}.$$

This current corresponds to the magnetic momentum:

$$m = \frac{IS}{c};$$

where $S = \pi R^2$, so

$$m = -\frac{eV\Omega R}{c} - \frac{e^2 VB\tau_p R}{c^2 m_p}.$$

The first part corresponds to the effect, which is connected with the linear mechanism (Andreasyan, 1996). The second is connected with the influence of the magnetic field. This field can be connected both with the external part and the self magnetic field induced by such particles.

4. Conclusion

We have studied the role of the Biermann battery mechanism in the evolution of the magnetic fields of objects of disc geometry. We have taken into account the influence of the existing magnetic field. Such mechanism can describe the saturation of the magnetic field growth for this case. The full magnetic field generated by the Biermann battery can be described by the self-consistent model, which takes into account the integral effect of the growth of the magnetic momentum.

References

Andreasyan R. R., 1996, Astrophysics, 39, 58

Andreasyan R. R., Mikhailov E. A., Andreasyan H. R., 2020, Astronomy Reports, 64, 189

Arshakian T., Beck R., Krause M., Sokoloff D., 2009, Astronomy and Astrophysics, 494, 21

Beck R., Brandenburg A., Moss D., et al. 1996, Annual Review of Astronomy and Astrophysics, 1, 155

Biermann L., 1950, Zeitschrift Naturforschung Teil A, 5, 65

Fermi E., 1949, Physical Review, 75, 1169

Moffatt H., 1978, Magnetic field generation in electrically conducting fluids. University Press, Cambridge

Oppermann E., Junklewitz H., Robbers G. e. a., 2012, Astronomy and Astrophysics, 542, A93

Zeldovich Y., Ruzmaikin A. A., Sokoloff D. D., 1983, Magnetic Fields in Astrophysics. Gordon and Breach, New York

Communications of BAO, Vol. 67, Issue 2, 2020, pp. 286-292

Catalogs of celestial bodies from digitized photographic plates of the Ukrainian Virtual Observatory Archive

Protsyuk Y.*[1], Vavilova I.†[2], Andruk V[2], Pakuliak L.‡[2], Shatokhina S.§[2], and Yizhakevych O.[2]

[1]Research Institute 'Mykolaiv Astronomical Observatory', Mykolaiv, Ukraine
[2]Main Astronomical Observatory of the NAS of Ukraine, Kyiv, Ukraine

Abstract

The Ukrainian Virtual Observatory (UkrVO, http://ukr-vo.org) database is compiled from observations conducted in 1898-2018 at observational sites of 8 Ukrainian observatories with about 50 instruments. Now the UkrVO archive covers data of about 40,000 astroplates, from which 15,000 are digitized at three observatories: Main Astronomical Observatory of the NAS of Ukraine (MAO NASU), Research Institute 'Mykolaiv Astronomical Observatory' (RI MAO), and Astronomical Observatory of the Taras Shevchenko National University of Kyiv (AO TSNU).

Astroplates were digitized using *Epson*^{TM} and *Microtek*^{TM} commercial scanners with 16-bit gray levels and resolution of 1200-1600 dpi. Images of all objects registered on plates were processed using the advanced software complex for CCD images' treatment MIDAS/ROMAFOT in the LINUX environment. Additional software modules developed and implemented at the MAO NASU and RI MAO provide both the digitized images' processing and the final products as the catalogs of positions and stellar magnitudes of all the registered objects.

The processing of the digitized Northern Sky Survey observations (the FON project) resulted in a few catalogs of coordinates and B-magnitudes for more than 19 million stars and galaxies from the FON-Kyiv part and more than 13 million objects from the FON-Kitab part. Besides, based on these data, two catalogs for more than 5,000 positions and B-magnitudes of asteroids were compiled. Now, in cooperation with Hissar Astronomical Observatory (Dushanbe, Tajikistan), we are preparing similar catalogs based on digitized observations of the third part (1985-1992) of the FON project. The digitized data of open star clusters in UBVR color bands obtained at the Baldone observatory (Latvia) were used to enhance the photometric content of the resulted catalogs.

The developed methods of digitization, image processing, and reduction with the latest reference catalogs allowed us to achieve good positional and photometric accuracy of objects.

Other digitized data of photographic observations stored in UkrVO archives formed the basis of several Solar System Bodies positional catalogs. The compiled catalogs of 90 positions and B-values of Pluto, 1500 positions of satellites of outer planets are available on the UkrVO website and in the Strasbourg Data Center.

Keywords: *Virtual Observatory, catalogs, database, stars, asteroids*

1. Introduction

The Ukrainian Virtual Observatory (UkrVO, http://ukr-vo.org) database is compiled from observations conducted in 1898-2018 at observational sites of 8 Ukrainian observatories with about 50 instruments (Sergeeva et al. (2004), Protsyuk et al. (2005)). UkrVO database includes data from over 40 thousand direct astroplates, about 15 thousand of them have been digitized at three observatories and included in UkrVO Joint Digital Archive (UkrVO JDA): MAO NASU, RI MAO, and AO TSNU

*yuri@mao.nikolaev.ua, Corresponding author
†irivav@mao.kiev.ua
‡pakuliak@mao.kiev.ua
§svetash@mao.kiev.ua

DOI: 10.52526/25792776-2020.67.2-286

(http://gua.db.ukr-vo.org/, http://nao.db.ukr-vo.org) (Vavilova et al. (2011), Vavilova et al. (2012), Vavilova (2016)).

Additionally, as an independent part of JDA, RI MAO hosts a digital archive of 140,000 CCD frames, having been obtained since 2001 with KT-50 (D = 500 mm, F = 3000 mm, 43'x 38', scale = 0.8"/pix), FRT (D = 300 mm, F = 1500 mm, 83'x 83'), and AMC (D = 180 mm, F = 2480/12360 mm, scale 1"/mkm) telescopes.

Besides direct plates' collections, UkrVO glass archive accumulates about 50,000 spectra astronegatives obtained in 1960-1995 (Pakuliak et al. (2014)), mostly with variable stars. At the moment, the project of their classification and digitization is in progress (Zolotukhina et al. (2020)).

The digitization of astroplates was carried out in all three observatories using $Epson^{TM}$ and $Microtek^{TM}$ commercial scanners with 16-bit gray levels, resolution of 1200-1600 dpi (Protsyuk et al. (2014b), Protsyuk et al. (2014c)) and stored in FITS format.

Digitization of astroplates and the newest digitized data processing services allowed us to develop a new approach for the creation of catalogs of astrometric and photometric characteristics of the various celestial objects. The accuracy of newly determined positions is higher than in traditional determinations from photographic observations, but it cannot be comparable to the accuracy of modern CCD observations. Modern observations far exceed the previous ones in the accuracy of coordinates and number of positions, but we hope to find from digitized photographic archives new original data about the Universe that could be useful in modern kinematic and dynamic solutions.

2. Software for digitized images' processing

Images of all objects registered on plates were retrieved using the advanced software complex for CCD images' processing MIDAS/ROMAFOT in the LINUX environment. Additional software modules developed and implemented at the MAO NASU and RI MAO provide both the object image extraction and the final products as the catalogs of positions and stellar magnitudes of all the registered objects. The detailed description of all steps of astronomical image processing is given in Protsyuk et al. (2014a), Protsyuk et al. (2014b), Andruk et al. (2014), Andruk et al. (2015), Pakuliak & Andruk (2020). These steps are as follows: preliminary filtering, choosing PSF (point spread function) of objects, and the scheme of astrometric reduction to calculate positions and magnitudes in systems of the selected reference catalogs.

For all catalogs mentioned here, we used Tycho2 and UCAC4 catalogs as reference. Combined with developed methods of digitization, image processing, and plate reduction, these catalogs allowed us to achieve the best positional and photometric accuracy available for used photographic material and digitizing appliances. For example, mean internal errors of the FON-Kyiv resulted catalog (Tycho-2 as reference) are of 0.23" in coordinates and 0.14^m in magnitudes for all stars down to $16^m.5$.

Using the Gaia DR2 as a reference showed that when compared with the results of the reduction in Tycho2 and UCAC4 reference frames, there was no significant improvement in the random and systematic components of residual differences $(O-C)$ for the EPSON scans from the UkrVO archive. On the other hand, the repeatability tests for the scans of the same plates obtained with the scanning machine of the Shanghai Astronomical Observatory (PRC) (Yu et al. (2017)) allow us to suppose that re-processing of old photographic observations in the Gaia DR2 reference system could improve the positional accuracy of old photographic observations, raising it to the level of modern ground-based CCD observations (Protsyuk & Maigurova (2020)). It also can be assumed that these tests can be the indirect evidence of the advantages of the purpose-built machines against the flatbed scanners for scanning photographic plates.

Other UkrVO software and web-services are described in Vavilova et al. (2017). All software and web-services of the UkrVO are compatible with IVOA standards (Allen et al. (2019)).

3. Catalogs of celestial bodies from digitized photographic plates

The results of digitization, processing, and reduction are stellar catalogs with positional and photometric data for all objects fixed on the plates (Vavilova (2016), Vavilova et al. (2020)). Some catalogs can comprise proper motions of stars, which makes it possible to use them to obtain kinematic characteristics of objects and their groups. Since the start of the digitization of photographic archives of the UkrVO, we have created a set of catalogs of celestial bodies based on digitized images of photographic plates from the UkrVO JDA. Some of them are as follows:

- catalogs of coordinates and B-magnitudes for more than 19 million stars and galaxies from the Kyiv part and more than 13 million stars and galaxies from the Kitab part of the FON project (Andruk et al. (2016); Andruk et al. (2017); Yuldoshev et al. (2017); Yuldoshev et al. (2018); Yuldoshev et al. (2019));
- catalog of coordinates of 274485 stars (8-16 mag, Epoch J1981.6) from the observations of 1970-1990 using Zonal Astrograph of RI MAO (Protsyuk et al. (2014d));
- catalog of coordinates of 195 thousand stars down to 15^m in circumpolar areas (Protsyuk et al. (2015a));
- catalog of proper motions of 30 thousand stars down to 15^m in circumpolar areas (Protsyuk et al. (2015a));
- catalog of positions and proper motions of 2.3 million stars in the vicinity of open clusters NAO2015; (Protsyuk et al. (2014d); Protsyuk et al. (2017a));
- catalogs of more than 5,000 positions and B-magnitudes of asteroids (Shatokhina et al. (2018a); Shatokhina et al. (2018b); Shatokhina et al. (2019));
- catalog of 90 positions and B-magnitudes of Pluto; (Eglitis et al. (2019b));
- catalog of 1500 positions of satellites of Saturn, Jupiter, Uranus, and Neptune based on historical observations at MAO NAS of Ukraine. (Yizhakevych et al. (2017b); Yizhakevych et al. (2017a); Yizhakevych et al. (2018); Yizhakevych et al. (2019)).

Currently, in cooperation with Hissar Observatory (Dushanbe, Tajikistan), we are preparing similar catalogs based on the digitized observations of the third part (1985-1992) of the FON project. The digitized data of open star clusters in UBVR color bands obtained at the Baldone observatory (Latvia) were used to enhance the photometric content of the resulted catalogs.

The digital data from UkrVO JDA were used for the identification of optical counterparts of gamma-ray burst sources GRB110213A and GRB101224A. Catalogs of coordinates and magnitudes for all fixed faint objects in the areas around GRB110213A and GRB101224A were also created (Golovnia et al. (2015)). For these and other gamma-ray burst sources, the results were published in GCN Circulars Archive.

Re-processing of the digitized archive of Uranus and Neptune observations from RI MAO collection is carried out (Protsyuk et al. (2017b)).

The catalogs mentioned above cover both the whole northern hemisphere (the FON project) and its separate areas (near-polar, equatorial, local (open clusters, areas around GRB sources)). Observations carried out in different spectral bands are used.

3.1. Catalogs of the FON project

- Main idea for the FON project:
  - FOUR-FOLD OVERLAP of the sky with instruments of the same type (Fig.1);
  - SIX OBSERVATORIES: Kyiv(Ukraine), Kitab (Uzbekistan), Zelenchuk (Russia), Abastumani (Georgia), Zvenigorod (Russia), Dushanbe(Tajikistan);
  - INSTRUMENTS: Double wide-angle astrographs, D/F=40/200, D/F=40/300;
  - YEARS of observations: 1981-1998.
- Observational data for the compiled catalogs:
  - FON-KYIV: 2260 plates, 24 752 709 stars and galaxies, epoch 1988.16, B color band, sky area from $-04°$ to $+90°$ on declination;

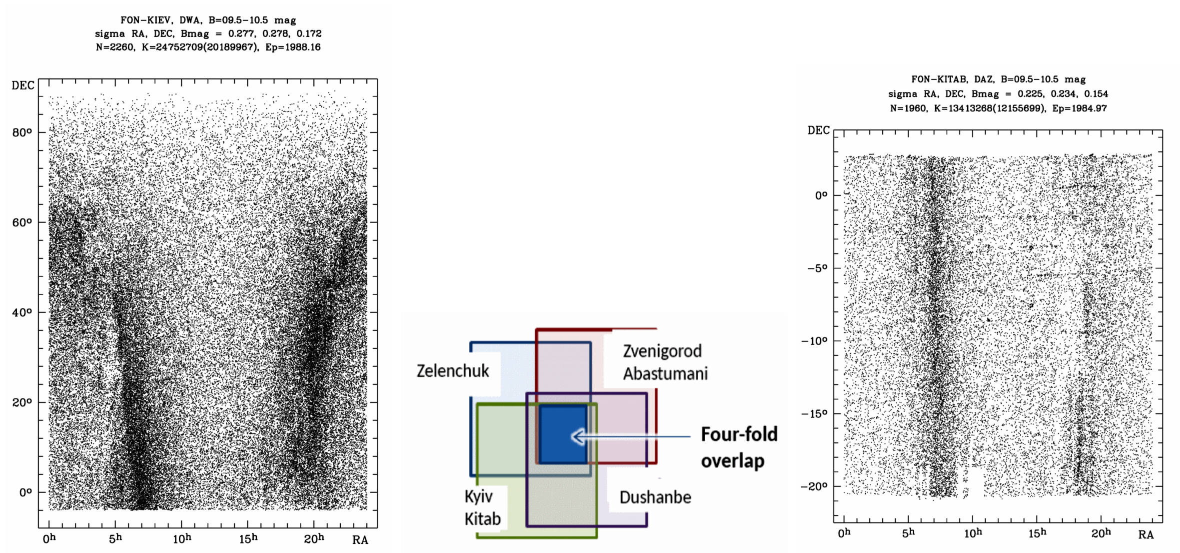

Figure 1. The scheme of the FON four-fold overlap (center). Bright part of the FON-KYIV catalog (left) and the FON-KITAB catalog (right).

- FON-KITAB: 1963 plates, 13 413 268 stars and galaxies, epoch 1984.97, B color band, sky area from $-20.5°$ to $+2.5°$ on declination;
- FON-DUSHANBE: 1560 plates, B color band, sky area from $-04°$ to $+90°$ on declination
- ADDITIONAL DATA:
  - 1.2m Schmidt telescope, Baldone: 779 plates, U color band;
  - 1.2m Schmidt telescope, Baldone : 4656 plates, V color band

- Results of the digitized images processing (Fig.1):
  - FON-KYIV: declination zone: $-4.0°$ to $+90.0°$, 24.7 million objects, B $<= 16.5^m$, $\sigma_{RA,DE} = \pm 0.28''$, $\sigma_B = \pm 0.17^m$
  - FON-KITAB: declination zone: $-20.5°$ to $+2.5°$, 13.4 million objects, B $<= 17.5^m$, $\sigma_{RA,DE} = \pm 0.23''$, $\sigma_B = \pm 0.15^m$.
  - FON-DUSHANBE: in progress, preliminary estimated $\sigma_{RA,DE} = \pm 0.33''$, $\sigma_B = \pm 0.12^m$.

FON-KYIV and FON-KITAB parts of the observational program are digitized, processed, and resulted in individual catalogs of positions and photometric data. The combination of digitizing technique with developed algorithms of scanner errors elimination and reduction models provided the accuracy of resulted data comparable to that of classical methods of photographic astrometry. The digitization of FON-DUSHANBE observational data makes it possible to create a final combined catalog of positions and proper motions of the Northern Sky, taking into account the main idea of the FON project - the multiple overlapping of the sky by several instruments of the same type (Akhmetov (2016); Akhmetov et al. (2018); Protsyuk & Relke (2016)).

3.2. Catalog of coordinates and proper motions from common reduction of CCD observation and plate archive images

The combined processing of coordinates from digitized photographic (1953-1993) and modern CCD (1997-2020) observations has led to a new definition of the stars' proper motions. The VO world archives contain numerous original observational data in free access without any restrictions on their use. The possibility of downloading and processing files from these archives solves the problem of missing data. Based on CCD image files from various astronomical databases and joint processing of virtual and own CCD and photographic observations, the set of catalogs of positions and proper motions of stars was obtained in the areas of open star clusters (Fig.2).

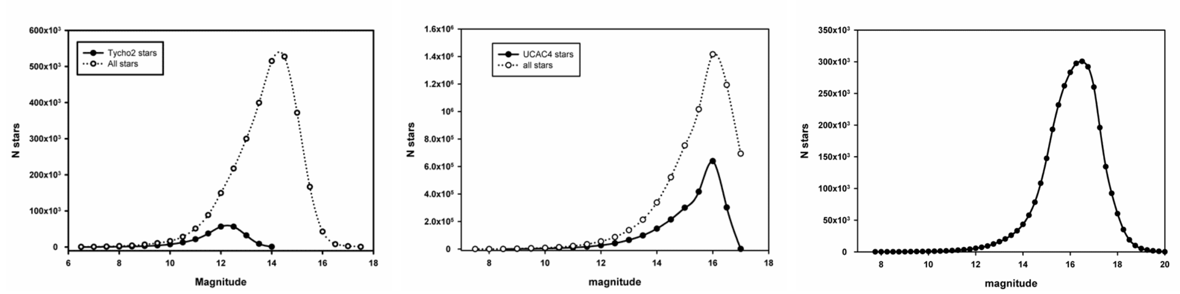

Figure 2. Distributions by magnitude of photographic catalog (left), CCD catalog (in the middle) and compiled catalog of positions and proper motions (right).

Catalogs which were obtained in 2012-2015:

- Photographic catalog for epoch 1983.2: 2.7 mln stars $(7-16)^m$, $\sigma_{RA} = \pm 0.09'', \sigma_{DE} = \pm 0.10''$
- CCD catalog for epoch 2013.6: 4.2 mln stars $(8-17)^m$, $\sigma_{RA} = \pm 0.06'', \sigma_{DE} = \pm 0.07''$
- 6 catalogs for different epochs from IVOA images: 51 mln stars $(7-19)^m$, $\sigma_{RA,DE} = \pm(0.03-0.07)''$

∗ Catalog of coordinates and proper motions NAO2015: 2.3 mln stars $(8-18)^m$, $\sigma_{RA} = \pm 0.035'', \sigma_{DE} = \pm 0.040''$, $\sigma_\mu = \pm 0.004''/year$

The accuracy of the obtained coordinates and proper motions corresponds to the level of accuracy for modern ground-based CCD observations. The catalog also includes the stars of the open clusters of the Galaxy, which allows one to determine their stellar population and their average proper motions.

3.3. Catalogs of asteroid positions and B-magnitudes from the FON-KYIV and FON-KITAB parts of the FON observational collections

In addition to the star images, the massive photographic surveys of the sky comprise the records of moving objects of the Solar system. Extracting these data, we create some positional catalogs of asteroids, comets, outer planets and their satellites. Unlike the classical methods of image visualization, we used an analytical method to identify asteroids, based on a comparison of the obtained processing results and the calculated ephemeris of asteroids from on-line services.

We identified several thousand asteroids and derived 5020 their positions from the digitized observations of FON-KYIV and FON-KITAB collections. The preliminary catalog of about 1800 asteroid positions and UBVR-magnitudes was compiled in combination with the digitized observations from Baldone. Asteroids down to 16^m stellar magnitude were identified from the FON-KYIV part, down to $(17-17.5)^m$ from the FON-KITAB, and down to 18^m from the Baldone archive (Fig. 3). Comparison of all asteroid positions with ephemeris demonstrates a good agreement between the results obtained from the FON-KYIV and FON-KITAB digitized images.

Besides, mainly in the Baldone collection observed in 1967-1995, a large number of the faint asteroid precovery observations were found, and their positions and magnitudes were determined. The discovery of these objects took place only 20-30 years later, and they had no observations at all in the 20th century (Eglitis et al. (2019a)).

4. Conclusion

The external accuracy of star positions in our new photographic catalogs is in good agreement with their internal accuracy. The random positional error lies within 50 to 250 mas for most of them, which is due to the quality of the scanned material. Some of the catalogs, which comprise proper motions of stars, make it possible to use them to obtain kinematic characteristics of objects and their groups. We suppose that the usage of a high-precision reference catalog in the whole range of magnitudes

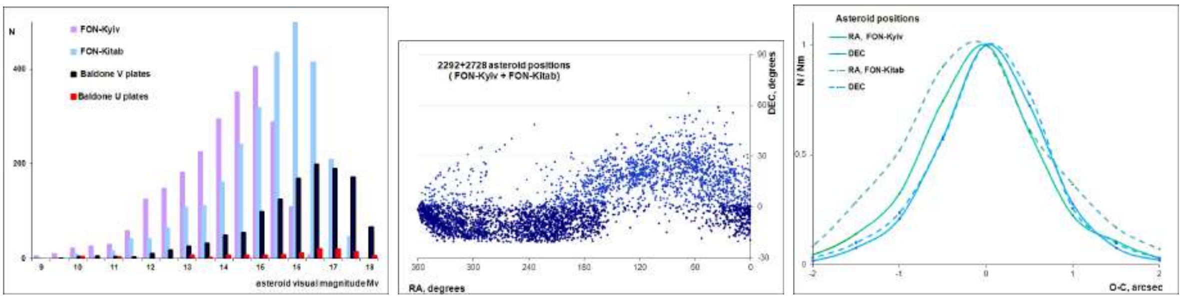

Figure 3. Distributions of asteroids positions by magnitude intervals (left), by equatorial coordinates (in the middle) and differences O-C (right), obtained from a comparison with ephemeris.

(for example, Gaia DR2) for the reduction will improve the star positions both systematically and randomly.

The use of new digital technologies for processing observations made it possible to increase the total number of positions of small bodies of the Solar System by searching for images from various digitized archives of observations, as well as to increase their accuracy. The combination of the Gaia DR2 (or DR3) stellar catalog with digital archives of the UkrVO gives a good possibility for data mining. As an example, the re-processing of some selected minor planets' observations using their digitized images and state-of-the-art star catalogs as a reference has led to increasing in positional accuracy compared to previous results (Protsyuk et al. (2016), Protsyuk & Maigurova (2020)).

The covering of certain time intervals with missing data of asteroid positions and their analysis can be useful not only for modern ephemeris calculations but also for studying the evolution of asteroid orbits along time. The digital observational archives of UkrVO and other databases give a possibility to spot these missing data, retrieve them, and subject them to analysis (Savanevych et al. (2015), Savanevych et al. (2018)).

References

Akhmetov V. S., 2016, Odessa Astron. Publ., 29, 116

Akhmetov V. S., Khlamov S. V., Andruk V. M., et al. 2018, Odessa Astron. Publ., 31, 199

Allen M. A., Dowler P., Evans J. D., et al. 2019, arXiv e-prints, p. arXiv:1912.01481

Andruk V. N., Golovnya V. V., Ivanov G. A., et al. 2014, Odessa Astron. Publ., 27, 53

Andruk V. M., Pakuliak L. K., Golovnia V. V., et al. 2015, Odessa Astron. Publ., 28, 192

Andruk V. M., Pakuliak L. K., Golovnia V. V., et al. 2016, Kinem. Phys. Cel. Bod., 32, 260

Andruk V. M., Pakuliak L. K., Golovnia V. V., et al. 2017, VizieR Online Data Cat., I/342

Eglitis I., Yizhakevych O., Shatokhina S., et al. 2019a, Odessa Astron. Publ., 32, 189

Eglitis I., Eglite M., Kazantseva L. V., et al. 2019b, VizieR Online Data Cat., VI/155

Golovnia V., Protsyuk Y. I., Andruk V., et al. 2015, Odessa Astron. Publ., 28, 196

Pakuliak L., Andruk V., 2020, Applications of Big Data in Astronomy and Geosciences: Algorithms for Photographic Images Processing and Error Elimination. Škoda, P. and Adam, F., doi:10.1016/B978-0-12-819154-5.00029-1

Pakuliak L., Shlyapnikov A., Rosenbush A., et al. 2014, in Astronomical Society of India Conference Series. H. P. Singh, P. Prugniel and I. Vauglin, pp 103–106

Protsyuk Y. I., Maigurova N. V., 2020, Odessa Astron. Publ., 33

Protsyuk Y., Relke E., 2016, Odessa Astron. Publ., 29, 144

Protsyuk Y., Pinigin G., Shulga A., 2005, Kinematika i Fizika Nebesnykh Tel Supplement, 5, 580

Protsyuk Y. I., Andruk V. N., Kazantseva L. V., 2014a, Odessa Astron. Publ., 27, 59

Protsyuk Y. I., Andruk V. N., Muminov M. M., et al. 2014b, Odessa Astron. Publ., 27, 61

Protsyuk Y. I., Kovylianska O. E., Protsyuk S. V., et al. 2014c, Odessa Astron. Publ., 27, 63

Protsyuk Y. I., Martynov M. V., Mazhaev A. E., et al. 2014d, Kinem. Phys. Cel. Bod., 30, 296

Protsyuk Y., Andruk V., Mazhaev A., et al. 2015a, Odessa Astron. Publ., 28, 202

Protsyuk Y., Yizhakevych O., Kovylianska O., et al. 2015b, Odessa Astron. Publ., 28, 204

Protsyuk Y., Maigurova N., Protsyuk S., et al. 2016, Odessa Astron. Publ., 29, 147

Protsyuk Y. I., Kovalchuk O. M., Mazhaev O. E., 2017a, Sci. innov., 13, 54

Protsyuk Y. I., Kovylianska O. E., Protsyuk S. V., et al. 2017b, Sci. innov., 13, 89

Savanevych V. E., et al., 2015, Monthly Notices of the Royal Astronomical Society, 451, 3287

Savanevych V. E., et al., 2018, Astronomy&Astrophysics, 609, A54

Sergeeva T. P., Sergeev A. V., Pakulyak L. K., Golovnya V. V., 2004, Baltic Astronomy, 13, 677

Shatokhina S., Relke H., Yuldoshev Q., et al. 2018a, Odessa Astron. Publ., 31, 235

Shatokhina S., Kazantseva L., Yizhakevych O., et al. 2018b, Kinem. Phys. Cel. Bod., 34, 270

Shatokhina S., Kazantseva L., Yizhakevych O., et al. 2019, VizieR Online Data Cat., J/other/KFNT/34

Vavilova I., 2016, Odessa Astron. Publ., 29, 109

Vavilova I. B., Pakuliak L. K., Protsyuk Y. I., et al. 2011, Kosm. nauka tehnol., 17, 74

Vavilova I. B., Pakulyak L. K., Shlyapnikov A. A., et al. 2012, Kinem. Phys. Cel. Bod., 28, 85

Vavilova I., Yatskiv Y., Pakuliak L., et al. 2017, in Astroinformatics. Brescia, M. and Djorgovski, S.G. and Feigelson, E.D. and Longo, G. and Cavuoti, S., pp 361–366, doi:10.1017/S1743921317001661

Vavilova I., Pakuliak L., Babyk I., et al. 2020, Surveys, Catalogues, Databases, and Archives of Astronomical Data. Škoda, P. and Adam, F., doi:10.1016/B978-0-12-819154-5.00015-1

Yizhakevych O., Andruk V., Pakuliak L., 2017a, Odessa Astron. Publ., 30, 201

Yizhakevych O. M., Andruk V. M., Pakuliak L. K., 2017b, Kinem. Phys. Cel. Bod., 33, 142

Yizhakevych O., Andruk V., Pakuliak L., 2018, VizieR Online Data Cat., J/other/KFNT/33

Yizhakevych E., Andruk V., Pakuliak L., 2019, VizieR Online Data Cat., J/other/OAP/29

Yu Y., Zhao J.-H., Tang Z.-H., et al. 2017, Research in Astronomy and Astrophysics, 17, 28

Yuldoshev Q. X., Ehgamberdiev S. A., Muminov M. M., et al. 2017, Kinem. Phys. Cel. Bod., 33, 250

Yuldoshev Q. X., Ehgamberdiev S. A., Muminov M. M., et al. 2018, VizieR Online Data Cat., I/346

Yuldoshev Q., Protsyuk Y., Relke H., et al. 2019, Astron. Nachr., 340, 494

Zolotukhina A. V., Pakuliak L. K., Vavilova I. B., Kaminsky B. M., 2020, Odessa Astron. Publ., 33

BAO plate archive project: digitization, electronic database and scientific usage

A. M. Mickaelian*, K. S. Gigoyan, G. A. Mikayelyan, G. M. Paronyan, M. V. Gyulzadyan, and G. R. Kostandyan

NAS RA V. Ambartsumian Byurakan Astrophysical Observatory (BAO), Byurakan 0213, Aragatzotn province, Armenia

Abstract

Observational archives are the main source for most of the astronomical studies, as given observations cannot entirely solve any problem and need to be complemented by related observing data both for construction of the time domain, multiwavelength, multi-technique and multi-method picture. This relates to both modern observations and historical ones preserved at many observatories. Therefore, digitization and accessibility of all possible data are rather important. The Byurakan Astrophysical Observatory (BAO) Plate Archive consists of some 37,500 photographic plates and films, obtained with 2.6m telescope, 1m and 0.5m Schmidt telescopes and other smaller ones during 1947-1991 and then by digital methods since 1996. Its most important part, the famous Markarian Survey (or the First Byurakan Survey, FBS) 1874 plates were digitized in 2002-2007 and the Digitized FBS (DFBS, www.aras.am/Dfbs/dfbs.html) was created. New science projects have been conducted based on this low-dispersion spectroscopic material. Several other smaller digitization projects have been carried out as well, such as part of the Second Byurakan Survey (SBS) plates, photographic chain plates in Coma, where the blazar ON 231 is located and 2.6m film spectra of FBS Blue Stellar Objects. However, most of the plates and films were not digitized. In 2015, we have started a project on the whole BAO Plate Archive digitization and its scientific usage. It was aimed at digitization, extraction and analysis of archival data and building an electronic database and interactive sky map. Armenian Virtual Observatory (ArVO, www.aras.am/Arvo/arvo.htm) database will accommodate all new data. The project runs in collaboration with the Armenian Institute of Informatics and Automation Problems (IIAP) and continued during 4 years in 2015-2018. Later on, the project was renovated for 2020-2021. The final result will be an Electronic Database and online Interactive Sky map to be used for further research projects. ArVO will provide all standards and tools for efficient usage of the scientific output and its integration in international databases.

Keywords: *photographic plates – photographic films – digitization – astrometry – photometry – spectroscopy – astronomical archives – databases – virtual observatories*

1. Introduction

The astronomical archives created on the basis of numerous observations at many observatories are the most important part of both astronomical observational heritage (plate and film archives) and modern observations (modern archives). The necessity of digitization of astronomical plates was emphasized and current progress in various national and international projects was given at Astroplate workshops (e. g. Osborn (2014); Hudec (2014); Kazantseva (2014); Nesci et al. (2014a); Stupka & Benesova (2014)).

The **Byurakan Astrophysical Observatory (BAO) Plate Archive** is one of the largest astronomical archives in the world and is considered to be BAO main observational treasure. It is the results of decades' hard work of Armenian astronomers and the work of BAO telescopes and other expensive equipment, as well as the results of their activities. Today BAO archive holds some 37,500

*aregmick@yahoo.com, Corresponding author

DOI: 10.52526/25792776-2020.67.2-293

astronomical plates, films or other carriers of observational data. However, previous observational and informational registration methods currently do not make it available to wide range of scientists, and especially its usage for solution of new research problems. Digitization of BAO plates is a significant contribution to the Wide-Field Plate DataBase (WFPDB) developed in Sofia, Bulgaria (Tsvetkov & Tsvetkova, 2012).

A project on Digitization of BAO Plate Archive and creation of BAO Interactive Astronomical Database (shortly BAO Plate Archive project, BAO PAP) started in February 2015. It was aimed at preservation of BAO valuable observational material accumulated during 1947-1991, creation of full Database of all BAO observations, creation of BAO Interactive Sky Map with visualization of all observations and quick access to the data, development and accomplishment of new research projects based on the existing observational material, and integration of BAO observations into the international databases. A number of BAO young astronomers were involved in this project and it lasted 4 years. Later on, the project was renovated for 2020-2021 to complete the full tasks.

The project objectives are the preservation of BAO observational archive, preservation of scientific information contained in photographic plates and other careers, creation of opportunity of dissemination and wide usage of observational data, putting in correspondence of observational material to modern standards and usage methods, proposing new science projects and creation of possibility of their further accomplishment, and making BAO activities visible.

A short description of BAO Plate Archive was given by Mickaelian (2014a) and more detailed paper is given in Mickaelian et al. (2016b).

2. BAO telescopes and observing programmes

BAO observers worked with a number of BAO telescopes during 1947-1991 and obtained several dozens of thousands of plates, films and other products. The table gives general understanding on observations of 10 BAO telescopes that worked on photographic photometry, electrophotometry, slit and objective prism spectroscopy, and polarimetry of many thousands astronomical objects.

Table 1. Overview of BAO telescopes and produced observational material.

Telescope	**Sizes** (cm)	**Years**	**Observing methods**	**Plates**
5” double–astrograph	13	1947–1950	photometry	3000
6”	15	1947–1950	photometry	3000
8” Schmidt	20/20/31	1949–1968	photometry	4500
20” Cassegrain	51/800	1952–1991	electrophotometry	
10” telescope–spectrograph	25	1953–19??	spectra	
Nebular spectrograph		1954–19??	spectra	
16” Cassegrain	41/400	1955–1991	electrophotometry	
21” Schmidt	53/53/183	1955–1991	photometry	12000
40” Schmidt (AZT–10)	102/132/213	1960–1991	photometry, spectra	7500
ZTA–2.6m	264/1016	1975–1991	photometry, spectra	7000
All telescopes		**1947–1991**		**37000**

We give in Table 1 an overview of BAO telescopes and produced observational material. Telescope “Sizes” are given for the mirror and focal length for classical telescopes and for the correcting lens, mirror and focal length for Schmidt type telescopes. Here we list the main observational projects accomplished on the three most important BAO telescopes (2.6m classical reflector, 1m Schmidt and 0.5m Schmidt; Figure 1).

21” (0.5m) Schmidt telescope:

- Polarization of cometary nebula NGC 2261
- Nuclei of nearby Sa and Sb galaxies

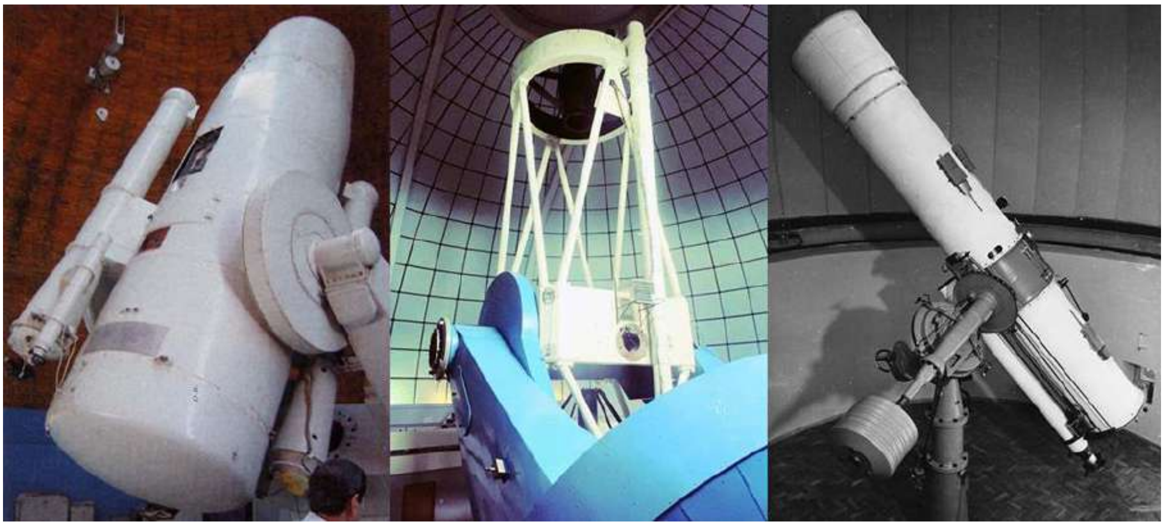

Figure 1. BAO most important telescopes (from left to right): 1m Schmidt, 2.6m classical reflector and 0.5m Schmidt.

- Nuclei of nearby Sc galaxies
- Search for flare stars in Pleiades
- Search for flare stars in Orion
- Search for flare stars in NGC 7000 (Cygnus)
- Search for flare stars in Praesepe
- Search for flare stars in Taurus Dark Clouds (TDC)
- Variability of Markarian galaxies
- Monitoring of extragalactic supernovae in certain areas

40" (1m) Schmidt telescope:

- Detailed colorimetry of bright galaxies
- First Byurakan Survey (FBS, Markarian survey; Markarian et al. (1989))
- Search for flare stars in Pleiades
- Search for flare stars in Orion
- Search for flare stars in NGC 7000 (Cygnus)
- Search for flare stars in Praesepe
- Search for flare stars in Taurus Dark Clouds (TDC)
- Second Byurakan Survey (SBS; Stepanian (2005))
- Extension of the FBS in the Galactic Plane

ZTA-2.6m telescope:

- Morphological study of Markarian galaxies
- Investigation of star clusters
- Investigation of groups and clusters of galaxies
- Spectroscopy FBS blue stellar objects
- Spectroscopy FBS late–type stars
- Spectroscopy SBS galaxies and stellar objects (BAO/SAO)
- Direct images of the central regions of Markarian galaxies
- Spectroscopy of T Tauri and flare stars
- Spectroscopy of Byurakan-IRAS Galaxies (BIG objects)
- Spectroscopy of ROSAT AGN candidates (BAO/HS/OHP/INAOE)

Summarizing, the main observational projects run on these telescopes were:

21" (0.5m) Schmidt: Polarization of cometary nebula NGC 2261, Nuclei of nearby Sa and Sb galaxies, Nuclei of nearby Sc galaxies, Search for flare stars in Pleiades, Orion, NGC 7000 (Cygnus), Praesepe and Taurus Dark Clouds (TDC), Variability of Markarian galaxies, Monitoring of extra-galactic supernovae in certain areas, etc.;

40" (1m) Schmidt: the First Byurakan Survey (FBS, Markarian survey; Markarian et al. (1989)), the Second Byurakan Survey (SBS; Stepanian (2005)), Extension of the FBS in the Galactic Plane, Detailed colorimetry of bright galaxies, Search for flare stars in Pleiades, Orion, NGC 7000 (Cygnus), Praesepe and Taurus Dark Clouds (TDC), etc.;

ZTA-2.6m telescope: Morphological study of Markarian galaxies, Investigation of star clusters, Investigation of groups and clusters of galaxies, Spectroscopy of FBS blue stellar objects, FBS late–type stars, SBS galaxies and stellar objects (BAO/SAO), T Tauri and flare stars, Byurakan-IRAS Galaxies (BIG objects) and ROSAT AGN candidates (BAO/HS/OHP/INAOE), and Direct images of the central regions of Markarian galaxies.

Especially efficient were Byurakan spectroscopic surveys accomplished by Markarian and colleagues with 1m Schmidt telescope: FBS and SBS.

3. BAO Plate Archive Project

The digitization of astronomical plates and films pursues not only the maintenance task, but also it will serve as a source for new scientific research and discoveries, if only the digitized material runs according to modern standards and, due to its accessibility, it will become an active archive. The project is aimed at compilation, accounting, digitization of BAO observational archive photographic plates and films, as well as their incorporation in databases with modern standards and methods, providing access for all observational material and development of new scientific programs based on this material.

Scientific Programs Board (SPB) was created to evaluate the existing observational material, to select sets of priorities to be scanned first and to propose new research projects. It consists of BAO most experienced observers, as well as researchers from NAS RA Institute of Informatics and Automation Problems (IIAP) are involved for their experience in computer science related to databases and computational methods. **Project Executing Team (PET)** consists of more than 10 members led by the Head of BAO Astroinformatics Department Gor Mikayelyan, and the members are involved in scanning and reduction of data.

The project consists of the following tasks:

- Development of technical principles of the Project, necessary Equipment, Timeline and the Budget
- Collection of all photographic plates (until recently only plates obtained before 1974 had been collected in BAO Plate Archive)
- Revision and accounting of the plates and observing journals in BAO Plate Archive,
- Scanning of a few dozens of plates for test and educational reasons to set up the necessary parameters for the scanning in frame of the main Project
- Input of data from observing journals; Creation of the Project Database and development of the principles of organization of data in it
- Creation of the Project Webpage and User Interface
- Scanning of photographic plates and films
- Astrometric solution; Extraction of images and spectra; Wavelength calibration; Density and flux calibration; Multiband (UBVR) photometry
- Making up template low-dispersion spectra; Numerical classification of low-dispersion spectra
- Visualization of BAO observations on sky map; Creation of electronic interactive sky map and search system
- Scientific analysis of existing observational material and providing new research possibilities; Proposing and discussing new research projects

BAO PAP webpage (http://www.aras.am/PlateArchive/; Figure 2) is open and contains a lot of information on BAO observations, previous digitization projects, present Project details, teams, follow-up research projects, deliverables and related links (many items will be filled in during the next months). The main products will be **"Data Access"** and **"Interactive Sky Map"**. The first one will contain BAO Observational Database, Search by any parameter (Dates / Julian dates, Telescope, Observing modes/methods, Instrument, Receiver, Emulsion, Filters, Seeing, Project name, Project PI, Observers, Targets / coordinates, Sky area, Surface, Scale, Spatial resolution, Spectral range, Spectral resolution, Limiting magnitude, Number of nights, Number of exposures, Links), Data Visualization and Download of the digitized plates, films, part of them or individual objects images or spectra. "Interactive Sky Map" will visualize the observed by BAO telescopes sky and will give possibility to check observed areas for a given observational project, given telescope, observer, observing method, limiting magnitude, etc. There will be possibility to check individual fields for presence and number of plates to propose further research projects. Main expected projects are supposed to be those on variability and proper motions, as well as studies of the Solar System objects.

4. DFBS and other digitization projects at BAO

So far, a number of digitization projects have been accomplished at BAO, including the most important one, **Digitized First Byurakan Survey (DFBS**; http://www.aras.am/Dfbs/dfbs.html; Mickaelian et al. (2007a); Massaro et al. (2008); Mickaelian et al. (2019a)) based on the digitization of the famous Markarian Survey (Markarian et al., 1989).

The Second Byurakan Survey (SBS; Stepanian (2005)) plates are also subject for digitization, as they are hypersensitized and their emulsion is more sensitive for deterioration. 180 plates have been digitized so far. Due to SBS smaller photographic grains, 2400 dpi (10μm pixel size) is being used and 512 MB files are being obtained for each plate.

Photographic spectra of the FBS blue stellar objects (BSOs) have been obtained using 2.6m telescope and UAGS spectrograph on photographic films. ~700 such spectra have been scanned with 1600 dpi, 16 bit and 650×21 pix sizes images were obtained (FBS BSOs; Mickaelian (2008) and late-type

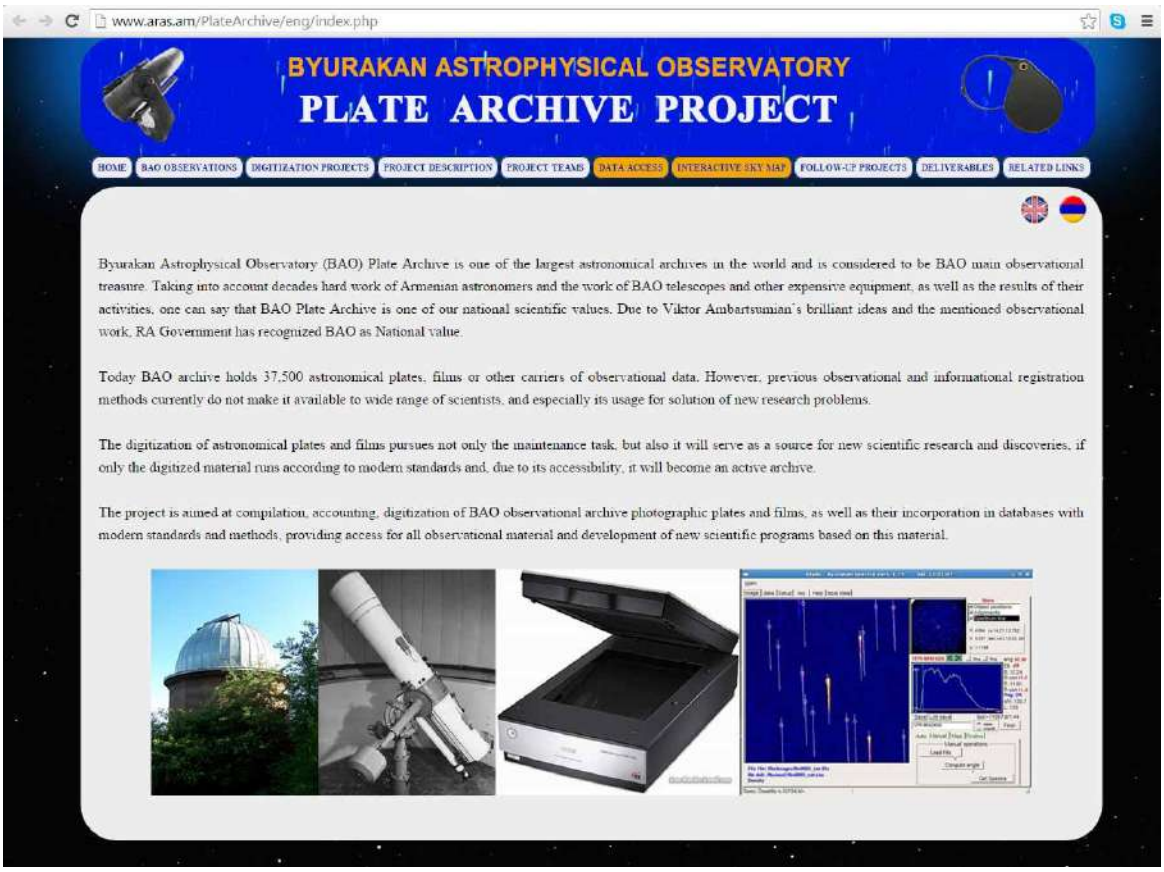

Figure 2. BAO Plate Archive Project webpage.

stars; Gigoyan & Mickaelian (2012)). All spectra were put in a standard format, so that automatic reduction was possible (Figure 3). 101 FBS blue stellar objects were published and a number of planetary nebulae, white dwarfs, hot subdwarfs and HBB stars have been revealed (Sinamyan & Mickaelian, 2009).

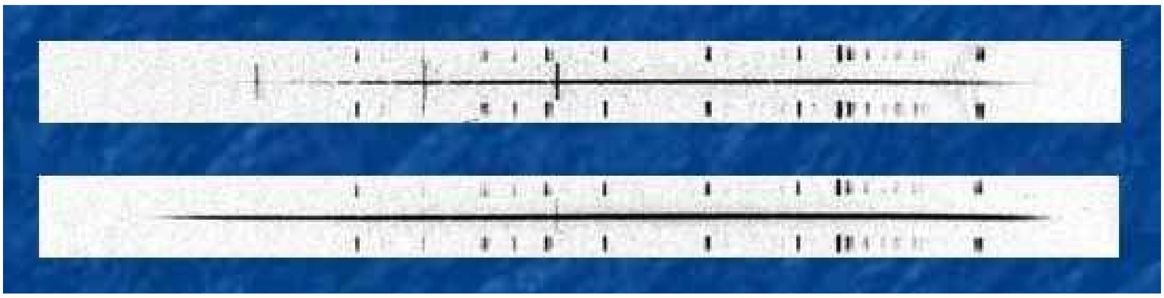

Figure 3. Standard format of FBS spectra with 650×21 pix sizes images for automatic reduction.

Another project was the study of long-term variability of ON 231, which appeared in the Coma field, where photographic chains for discovery of flare stars were carried out. In total 189 plates with a total number of more than 1200 exposures in 1969-1976 with the Byurakan 21" and 40" Schmidt telescopes were obtained. This was a valuable material for study of ON231 long-term variability (Figure 4; Erastova (2004)).

Having digitized plates and modern digital observational data, a number of efficient research projects have become possible, such as data discovery, spectral analysis, SED building and fitting, modelling, variability studies, cross-matching, etc. Some examples are variability studies (Samus & Antipin, 2012), Cross-matching of Astronomical Catalogs (Malkov, 2012), Search for Asteroids and Exoplanets using VO tools (Sarkissian et al., 2012).

Our science projects are aimed at discoveries of new interesting objects searching definite types

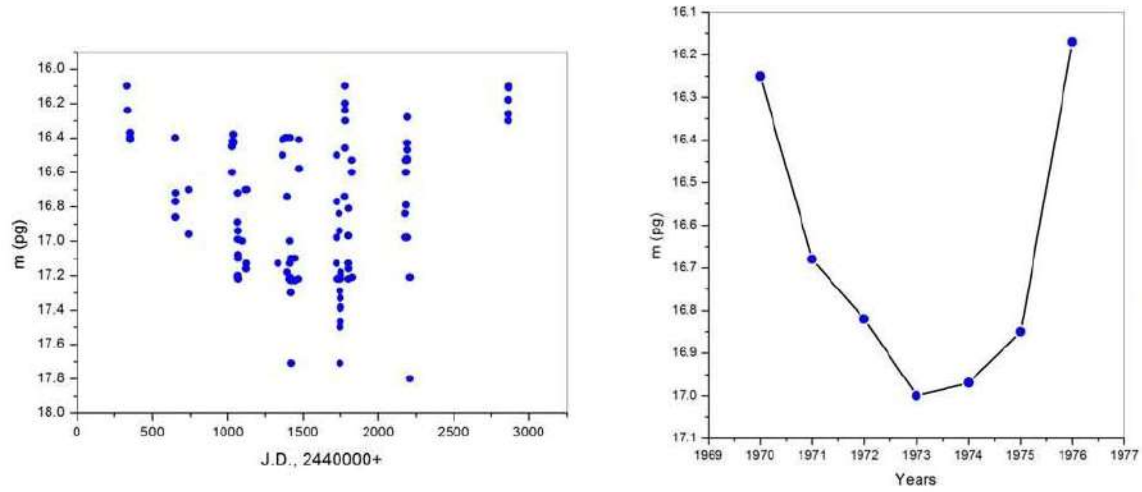

Figure 4. Photometric measurements and variability study of the blazar ON 231 observed in the Coma field.

of low-dispersion spectra in the DFBS, by optical identifications of non-optical sources (X-ray, IR, radio) also using the DFBS and DSS/SDSS, by using cross-correlations of large catalogs and selection of objects by definite criteria, etc.

5. Summary

BAO Plate Archive is one of the most important astronomical databases. A project of its digitization and creation of the electronic database is active. At present the main part of the project, the scanning of the plates has produced more than 30,000 digital images of roughly 200 MB files (each image). All they have been stored and double copies are available.

BAO Electronic Database will give access to observing data by various parameters, as shown in Table 2, so that it will fit many requirements for future studies.

Table 2. BAO Electronic Database structure and access modes.

BAO Electronic Database	
Dates / Julian dates	Targets / coordinates
Telescope	Sky area
Observing modes/methods	Surface
Instrument	Scale
Receiver	Spatial resolution
Emulsion	Spectral range
Filters	Spectral resolution
Seeing	Limiting magnitude
Project name	Number of nights
Project PI	Number of exposures
Observers	Links

BAO Plate Archive Project will lead to preservation of BAO valuable observational material obtained during 1947-1991. However, our goal is not only to create a passive archive of scanned plates and films, but also to make use of especially those fields, where more studies are possible. Proper motion and variability studies are most important, as time domain material is contained in historical plates. Such possibilities based on DFBS were shown by Mickaelian et al. (2006a); DFBS as a unique database for proper motion, variability studies, and object classification. New variable stars discovered on digitized plates of Moscow collection was reported by Sokolovsky et al. (2014).

There are a number of further **possible research projects** that will be conducted having the plates digitized:

- Correction of ephemerides of known asteroids and search for new asteroids (ex. Thuillot et al. (2007); Berthier et al. (2009); Mickaelian et al. (2019b))
- Discovery and study of variable stars (ex. Mickaelian et al. (2011); Nesci et al. (2009))
- Revealing high proper motion stars (ex. Mickaelian & Sinamyan (2010))
- Study of variability of known blazars and discovery of new blazars
- Revealing Novae and Supernovae progenitors (Nesci et al. (2009))
- Discovery of new QSOs
- Discovery of new white dwarfs (ex. Sinamyan & Mickaelian (2011))
- Discovery of new late-type stars (ex. Gigoyan et al. (2010, 2019))
- Discovery of optical sources of gamma-ray bursts
- Optical identifications of X-ray, IR and radio sources (ex. Mickaelian & Sargsyan (2004); Mickaelian & Gigoyan (2006); Mickaelian et al. (2006b); Hovhannisyan et al. (2009)).

References

Berthier J., Sarkissian A., Mickaelian A. M., Thuillot W., 2009, "European Planetary Science Congress 2009, held 14-18 September in Potsdam, Germany, p. 526

Erastova L. K., 2004, A&AT, 23, 209

Gigoyan K. S., Mickaelian A. M., 2012, MNRAS, 419, 3346

Gigoyan K. S., Sinamyan P. K., Engels D., Mickaelian A. M., 2010, Astrophysics, 53, 123

Gigoyan K. S., Kostandyan G. R., Gigoyan K. K., Zamkotsian F., Sarkissian A., 2019, Astrophysics, 62, 573

Hovhannisyan L. R., Mickaelian A. M., Weedman D., et al. 2009, AJ, 251, 138

Hudec R., 2014, in Proc. Astroplate-2014 Conf., Eds. L. Mišková & S. Vítek. Prague, p. 1

Kazantseva L., 2014, in Proc. Astroplate-2014 Conf., Eds. L. Mišková & S. Vítek. Prague, p. 13

Knyazyan A. V., Astsatryan H. V., Mickaelian A. M., 2016, Astronomical Surveys and Big Data, Eds. A. M. Mickaelian, A. Lawrence and T. Yu. Magakian. ASP Conf. Series, 505, 236

Malkov O. Y., 2012, in Proc. Conf. "50 years of Cosmic Era: Real and Virtual Studies of the Sky". Yerevan, NAS RA, p. 48

Markarian B. E., Lipovetsky V. A., Stepanian J. A., et al. 1989, Comm. SAO, 62, 5

Massaro E., Mickaelian A. M., Nesci R., Weedman D., (Eds.) 2008, The Digitized First Byurakan Survey, ARACNE Editrice, Rome, 78p.

Mickaelian A. M., 2006, Rom. Astron. J., 16S, 23

Mickaelian A. M., 2007, Highlights of Astronomy, 14, 594

Mickaelian A. M., 2008, AJ, 136, 946

Mickaelian A. M., 2012, in Proc. Conf. "50 years of Cosmic Era: Real and Virtual Studies of the Sky". Yerevan, NAS RA. , p. 29

Mickaelian A. M., 2014a, in Proc. Astroplate-2014 Conf., Eds. L. Mišková & S. Vítek. Prague, p. 109

Mickaelian A. M., 2014b, in Proc. IAU S304: Multiwavelength AGN Surveys and Studies. Vol. 304, p. 1

Mickaelian A. M., Gigoyan K. S., 2006, A&A, 455, 765

Mickaelian A. M., Sargsyan L. A., 2004, Astrophysics, 47, 213

Mickaelian A. M., Sinamyan P. K., 2010, MNRAS, 407, 681

Mickaelian A. M., Malkov O. Y., Samus N. N., (Eds.) 2012, Proc. Conf. 50 years of Cosmic Era: Real and Virtual Studies of the Sky. NAS RA, 251 p., Yerevan

Mickaelian A. M., Hagen H.-J., Sargsyan L. A., Mikayelyan G. A., 2005, Catalog No. VI/116 at CDS, Strasbourg

Mickaelian A. M., Nesci R., Cirimele G., et al. 2008, Proc. ESAC Workshop on Astronomical Spectroscopy and Virtual Observatory, Madrid, ESA, p. 29

Mickaelian A. M., Sargsyan L. A., Mikayelyan G. A., 2010, Proc. of Science, 30

Mickaelian A. M., Mikayelyan G. A., Sinamyan P. K., 2011, MNRAS, 415, 1061

Mickaelian A. M., Sargsyan L. A., Mikayelyan G. A., et al. 2006a, Heron Press Sci. Ser., p. 82

Mickaelian A. M., Hovhannisyan L. R., Engels D., et al. 2006b, A&A, 449, 425

Mickaelian A. M., Gigoyan K. S., Nesci R., Rossi C., 2006c, Mem.S.A.It., 77, 1159

Mickaelian A. M., Nesci R., Rossi C., et al. 2007a, A&A, 464, 1177

Mickaelian A. M., Sargsyan L. A., Nesci R., et al. 2007b, Highlights of Astronomy, 14

Mickaelian A. M., Astsatryan H. V., Sahakyan V. G., et al. 2009a, Proc. CSIT-2009, p. 420

Mickaelian A. M., Kochiashvili N., Astsatryan H. V., et al. 2009b, Proc. CSIT-2009, p. 424

Mickaelian A. M., Sargsyan L. A., Astsatryan H. V., et al. 2009c, Data Science Journal, 8, 152

Mickaelian A. M., Sargsyan L. A., Gigoyan K. S., et al. 2009d, Rom. Astron. J., 185, 249

Mickaelian A. M., Astsatryan H. V., Knyazyan A. V., et al. 2016a, in Astronomical Surveys and Big Data. Eds. A. M. Mickaelian, A. Lawrence & T. Yu. Magakian. ASP Conf. Ser., V. 505, p. 16

Mickaelian A. M., Abrahamyan H. V., Andreasyan H. R., et al. 2016b, in Astronomical Surveys and Big Data. Eds. A. M. Mickaelian, A. Lawrence & T. Yu. Magakian. ASP Conf. Ser., V. 505, p. 262

Mickaelian A. M., Sargsyan L. A., Mikayelyan G. A., Erastova L. K., Gigoyan K. S., Sinamyan P. K., Hovhannisyan L. R., 2019a, ASP Conf. Ser., V. 520, p. 105

Mickaelian A. M., Sarkissian A., Berthier J., Meftah M., Thuillot W., Vachier F., 2019b, Icarus, 330, 5

Nesci R., Mickaelian A. M., Rossi C., 2009, ATel, 2338, 1

Nesci R., Bagaglia M., Nucciarelli G., 2014a, in Proc. Astroplate-2014 Conf., Eds. L. Mišková & S. Vítek. Prague, p. 75

Nesci R., Gaudenzi S., Rossi C., Pezzotti C., Gigoyan K., Mauron N., 2014b, in Proc. Astroplate-2014 Conf., Eds. L. Mišková & S. Vítek. Prague, p. 91

Osborn W., 2014, in Proc. Astroplate-2014 Conf., Eds. L. Mišková & S. Vítek. Prague, p. 15

Samus N. N., Antipin S., 2012, in Proc. Conf. "50 years of Cosmic Era: Real and Virtual Studies of the Sky". Yerevan, NAS RA, p. 39

Sarkissian A., Arzoumanian E., Mickaelian A. M., et al. 2012, in Proc. Conf. "50 years of Cosmic Era: Real and Virtual Studies of the Sky". Yerevan, NAS RA, p. 56

Sinamyan P. K., Mickaelian A. M., 2009, Astrophysics, 52, 76

Sinamyan P. K., Mickaelian A. M., 2011, Astrophysics, 54, 403

Sokolovsky K. V., Antipin S. V., Zubareva A. M., et al. 2014, ARep, 58, 319

Stepanian J. A., 2005, RMxAA, 41, 155

Stupka J., Benesova E., 2014, in Proc. Astroplate-2014 Conf., Eds. L. Mišková & S. Vítek. Prague, p. 31

Thuillot W., Berthier J., Sarkissian A., et al. 2007, Highlights of Astronomy, 14, 616

Tsvetkov M., Tsvetkova K., 2012, in Proc. IAU S285: New Horizons in Time-Domain Astronomy. Cambridge Univ. Press, p. 417

Véron-Cetty M.-P., Véron P., 2010, A&A, 518, 10

Communications of BAO, Vol. 67, Issue 2, 2020, pp.302-310

Evolving the VO: from interoperable data collections to an integrated system of services for data-intensive science

Fabio Pasian[*], Marco Molinaro[†] and Giuliano Taffoni[‡]

INAF – Osservatorio Astronomico di Trieste, Trieste, Italy

Abstract

The Virtual Observatory (VO) represents a successful international enterprise providing interoperability of data collections, thus allowing the possibility of multi-frequency and multi-messenger research. The Big Data era, that astrophysics has stepped into, is forcing scientists to perform data-intensive research. This new concept requires an evolution of the VO concept to provide additional services, in order to transform the VO: from sets of interoperable data to an integrated system of services capable of supporting data-intensive science.

Keywords: *Virtual Observatory, big data, data-intensive research, science platforms, open science clouds*

1. Introduction: the Virtual Observatory

1.1. The VO

The Virtual Observatory (VO) is the vision that astronomical datasets and other resources should work as a seamless whole. The original ambition of the VO was linking all of the main activities of astronomers into a coherent "circular" framework: from publications (with their associated data, tables and figures) to new observing proposals, from observatory info (meteo, calibrations, raw data) to analysis (data processing software, catalogues, data products) from comparison with theory and models, back to publications. Although extremely successful, the VO achieved results only partially fitting the above-described original ambition.

The VO aims at maximising scientific results out of archival research, by providing data of the highest quality achievable to all scientists and interested individuals; and also achieving a new type of science, crossing not only the boundaries of nations, but also those of wavelength, messenger, instrument specificities. In this way, science is not enabled just for power users, but the full research community is expected to have meaningful access to all data.

The mechanism governing the VO is most easily described by analogy with the World Wide Web: the information (and specifically data, in the VO case) is expected to appear seamlessly at the user's desk. And just as in the case of the WWW, the VO is not a fixed system, but rather a way of doing things.

The VO is made possible by the standardisation of data and metadata, by the standardisation of data exchange methods, and by the use of a registry, a repository of resources (entities, standards, data collections, services, ...), their mutual relationships and actionable interfaces.

The VO was probably the first environment to anticipate in practice the eventual implementation of the so-called FAIR principles Wilkinson et al. (2016): data and services provided are Findable, Accessible, Interoperable and Re-usable.

[*]fabio.pasian@inaf.it, IVOA Exec member, former IVOA Chair, Corresponding author
[†]marco.molinaro.inaf.it, IVOA Data Access Layer (DAL) WG Chair
[‡]giuliano.taffoni@inaf.it, IVOA Grid and Web Services (GWS) WG Chair

DOI: 10.52526/25792776-2020.67.2-302

1.2. The IVOA

Since 2002, many projects and data centres worldwide have been working towards the goal of implementing an increasingly effective VO. The International Virtual Observatory Alliance (IVOA) is the organisation that debates and agrees the technical standards that are needed to make the VO possible. It also acts as a focus for VO aspirations, a framework for discussing and sharing VO ideas and technology, and body for promoting and publicising the VO. Participation in the IVOA includes VO initiatives in 19 countries (plus The Netherlands and Thailand interested in joining), 1 super-national institution (the European Space Agency), and 1 international collaboration (the European VO initiative).

The aims of the IVOA standards are:

- interrogate multiple data centres in a seamless and transparent way;
- new powerful analysis and visualisation tools within that system;
- a standard framework for data centres to publish and deliver services using their data.

Lots of successful work has been done. But it is to noted that IVOA standards have always been driven by data resource interoperability. A limited amount of work has been therefore done on processing/analysis services (and therefore a limited number of services is available in that area).

For an overview of VO and IVOA activities, see e.g. the collection of papers edited some years ago by Hanisch (2015).

2. The VO and Big Data

With the increasing size of data sets in the "Big Data" era, to move data around the network becomes heavy and cumbersome.

To explain and visualise the problem, let's consider as an example the classification of star spectra in globular clusters. The user (see Figure 1) finds two VO-compliant archives containing digitised objective prism plates and spectra, respectively. The archives do not provide what is needed (i.e. catalogues of classified stars), but data retrieval services only. The user thus needs to download images and spectra (with delays caused by the network) and perform the processing at his/her own premises.

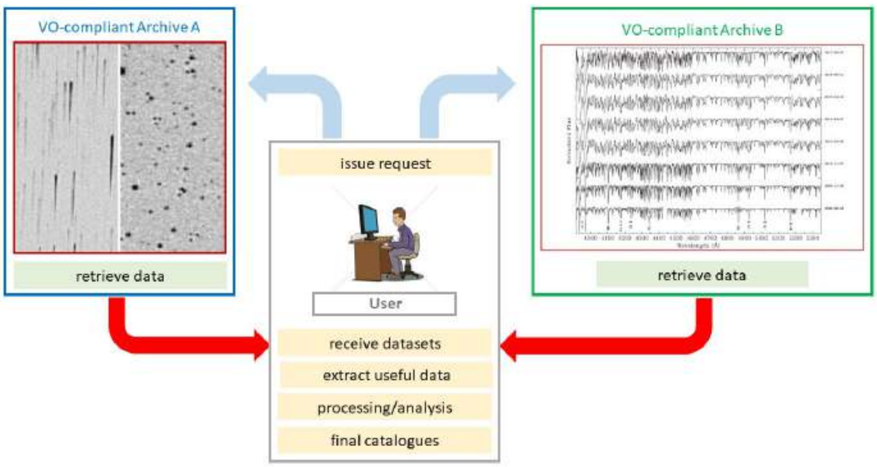

Figure 1. Classification of star spectra: Data Centres provide retrieval services only (explanation in the text). Yellow boxes indicate user actions and code, green boxes server-side actions.

How can this situation be improved? The provision of increased services (involving some level of computing) at the Data Centres would help a lot.

The need for a tighter connection between data and computing facilities has been brought forward for more than a decade. This was initially referred to the connection between the VO and Grid computing by Pasian et al. (2007), and to data mining in the VO context by Pasian et al. (2012). This new paradigm has gained momentum in the IVOA in the past 5 years as *"bring processing to the data"*. This topic was included in 2016 by the IVOA Science Priorities Committee (after discussion) among the top priorities for the VO. But the IVOA is a "joint venture" of separate national VO initiatives with no budget of its own, and since each initiative has its own set of priorities and funded activities, progress in this direction has been limited.

But recently, the importance of providing data processing and analysis services as part of archival activities has gained momentum. It is therefore foreseen that "bringing processing near the data" will be increasingly common. Of course, computing services applied to archived data can occur in a number of different ways.

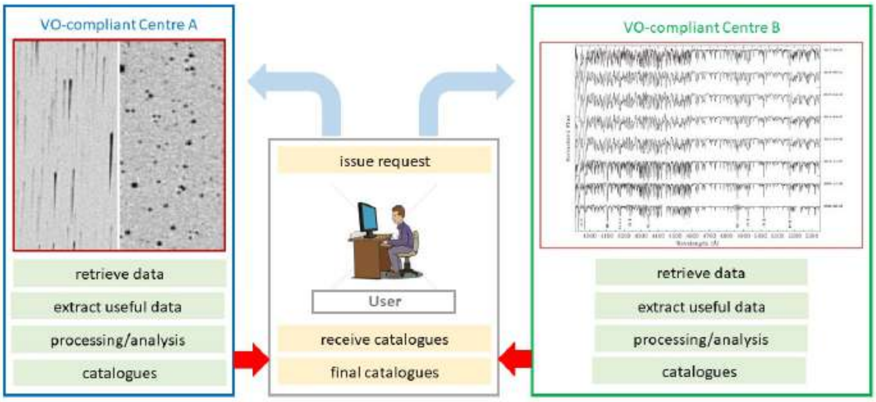

Figure 2. Classification of star spectra: Data Centres provide complete computing and classification services (explanation in the text). Yellow boxes indicate user actions and code, green boxes server-side actions.

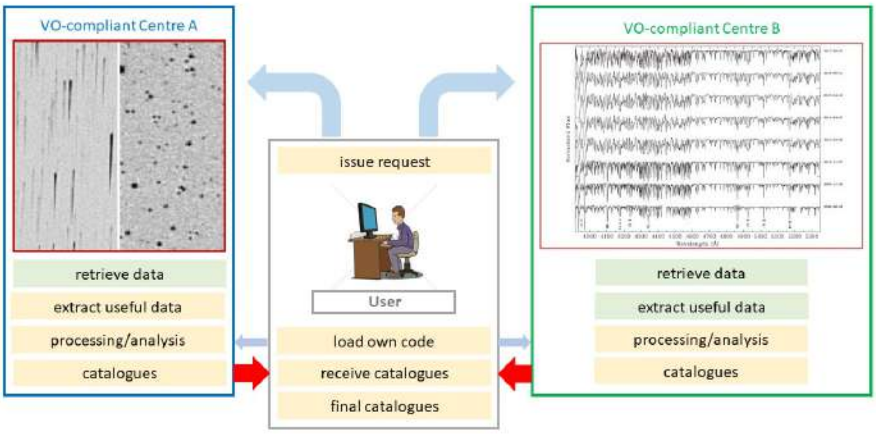

Figure 3. Classification of star spectra: Data Centres provide the running of user-provided code as a service (explanation in the text). Yellow boxes indicate user actions and code, green boxes server-side actions.

Proceeding with the example proposed above (classification of star spectra), new sets of services can be provided by Data Centres (Figure 2). E.g. cut-out of spectra in spectral images (e.g. using SODA, the IVOA standard Server-side Operations for Data Access web service capability that can act upon the data files, performing various kinds of operations: filtering/subsection, transformations, pixel operations, and applying functions to the data); and, in increasing order of computing complexity: optimal extraction of spectra, classification of spectra, preparation of catalogues of classified spectra. Only final results (catalogues) need to be sent back through the network. This case, in which users can run available services at the remote site can be described in Cloud terms as Software-as-a-Service (SaaS).

But Data Centres could also provide as a service the running of user-provided code (Figure 3). E.g. for the extraction of spectra or classification of spectra (e.g. the user could try new algorithms for this purpose). Also in this case only final results (catalogues) need to be sent back through the network; but this solution allows processing to be performed directly by users (and not on their behalf). In Cloud terms, this mechanism can be described as Infrastructure-as-a-Service or Platform-as-a-Service (IaaS/PaaS). While maybe better for the remote users, this mechanism implies a more complex handling of Authorisation&Accounting for a Data Centre. The increased complexity of the Autentication&Authorization&Accounting affects only marginally the technical implementations, but rather the policy for the usage of computing resources offered by an institution to external users for their own research. This implies a revolution in the approach of Data Centres and institutions on the way resources are consumed and new ways to report to funding agencies: a global agreement could be found in the framework of an Open Science Cloud (as discussed in the next sections).

3. Extending the VO paradigm

3.1. Concepts

The requirements of the Astronomy community (especially access to archives and the VO, processing of data, "bring computing to the data") call for an expansion of the standard concept of the VO. A tighter integration (or at least interoperability) of data and computing resources is needed.

The key point is that Data Centres, ideally linked within an International Open Science Cloud, are to provide to all of their users (following a VO-aware approach) the following resources:

1) archived dataset collections;
2) an amount of computing power;
3) user storage.

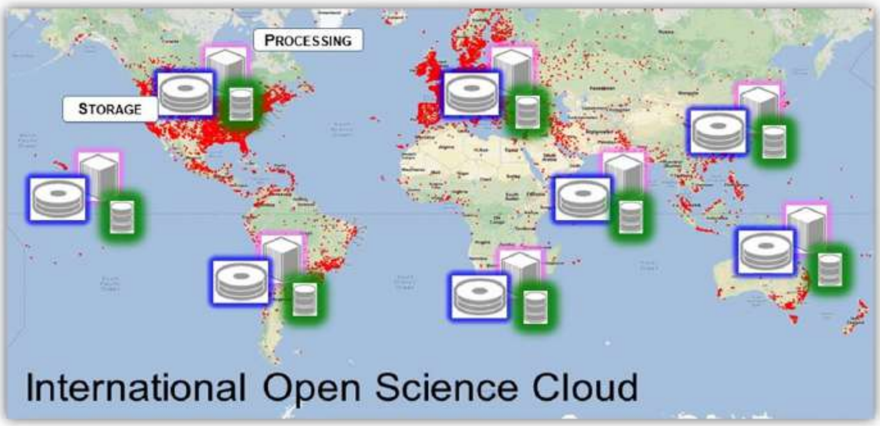

Figure 4. The concept of International Open Science Cloud. Each Data Centre provides the archived dataset collections, an amount of computing power, and user storage: all the Data Centres are made interoperable through federation of Open Science Clouds (viewgraph shown by David Schade, CADC, at the UN/Italy Open Universe Workshop, Vienna, 22 Nov 2017).

Building an International Open Science Cloud (Figure 4) is a vision shared by many colleagues all over the world, e.g. the Astrocloud initiative set up by VO-China, described by Cui et al. (2017). It is furthermore to be noted that the EGI (and now EOSC) in Europe and CANFAR Compute-Canada clouds have a similar approach and have worked on interoperability / federation of clouds (through a collaboration between INAF-OATs and CADC), as discussed in Bertocco et al. (2018) and Bertocco et al. (2020).

An International Open Science Cloud scenario allows to encompass different needs (Figure 5):

- Large collaborations project-oriented data centres offer access to instrument specific data (e.g. SKA, LSST). They build their own data and computing on top of dedicated infrastructure or Private or Hybrid Clouds (IaaS).
- Multi-purpose Data Centres: to manage small archival needs: surveys, key projects, thematic data resource aggregations, multiple projects, etc.
- Individual scientists.
- Citizen Science and Education / Public Outreach.

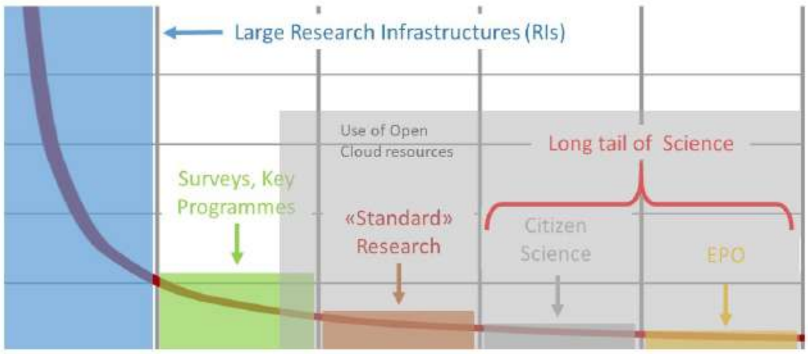

Figure 5. Usage of computing and data resources by different classes of users: in grey, the area where Open Science Clouds prove to be most useful.

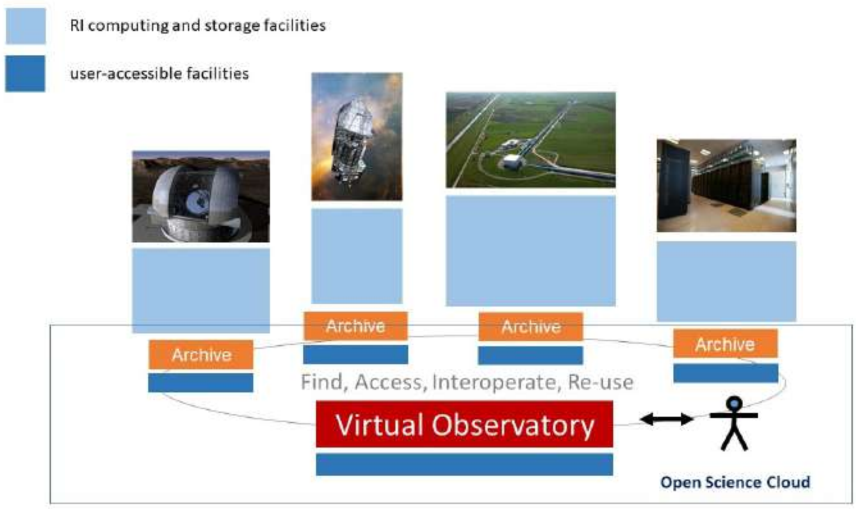

Figure 6. Open Science Cloud from the users' point of view (explanation in the text).

Figure 6 depicts the situation from the users' point of view. The observational Research Infrastructures (ground-based, space-borne, multi-messenger, including models and theory data providers) have their own infrastructure and store their data in their own archives. Additionally, personal space and some computing resource is provided to users, who can combine their own resources with what is available within an Open Science Cloud. The Virtual Observatory needs to be embedded in such a cloud, since it is the key to provide FAIR access (through community-accepted standards) to all available data and computing services.

3.2. Technical feasibility

Most of the technical tools needed for this switch in paradigm are already available. Data centres should offer computing and storage capabilities to process data. Where? Computing resources must be close to data: the advent of 100 Gbps networks (a speed comparable with the access speed of magnetic disks) promotes the concept of network proximity (the concept of "data lakes" with "computing islands"). Data providers may offer the possibility to process data using Web Apps within a SaaS framework. Additionally, astronomers should be able to deploy their own code in a PaaS mode: the Science Platforms approach.

A Science Platform (SP) is an environment designed to offer users a smoother experience when interacting with data and computing resources. A SP implements SaaS and PaaS capabilities to allow the most "elastic" use of the resources and of the data. A SP provides services to search data and software, process data with software (reduction, analysis, visualisation, etc.), access to computing resources, access to storage resources.

This point is worth expanding. SPs actually fill a gap in the services provided by Open Science Clouds, that currently offer only IaaS, while public/commercial Clouds often offer PaaS as well: in such environments, building SPs would probably be simplified by the additional services provided.

Deeply embedded with the SP concept is the mechanism of containers, which allow the practical implementation of moving the code to data. It involves encapsulating or packaging up software code and all its dependencies so that it can run uniformly and consistently on any infrastructure. Containers are a portable, lightweight, efficient and easy to maintain solution to offer software: they are at the basis of scientific experiment reproducibility; containers, just as data, should be annotated in order to make them FAIR and associated to scientific data (such connectors allow users to check their reciprocal compatibility).

Among the current technical tools allowing the use of containers, one may mention Docker (for micro servicing, default standard, isolation, etc.) and Singularity (for advanced environments, HPC, HTC), and the so-called Orchestrators (e.g. Kubernates).

Popular terms connected to container technology are the following.

- *Registry* "hosts" containers and allows to easily maintain and deploy on infrastructures (this Registry refers to containers, and is of course *different* from the VO Registry).
- *Marketplace* provides the tools necessary for the communities to share their science products in a harmonised way respecting the FAIR principles.
- *Annotations* (metadata), *versioning* and *DOI* allow precise citation of the used software on dataset. The use of keywords allows to filter and organise the content.

3.3. Steps ahead and challenges

An important step ahead could be the definition of AaaS as a new framework for analysis. Analytics-as-a-Service (AaaS) provides subscription-based data analytics software and procedures through the cloud. AaaS uses data mining, predictive analytics and AI to effectively reveal trends and insights from existing data sets. Data Centres (maybe large project data centres) may look to AaaS as a specific service to explore and analyse their data offering it as a WEB applications (please note that "WEB" does not mean "graphical browser"). AaaS implies access to high end computing resources (HPC, GPUs etc). For details, look out for Taffoni (2021), in preparation.

The main challenges to be tackled are listed in the following.

- The identification of software tools and packages for data processing and/or the deployment of custom workflows to the platform.
- How to take advantage of HPC and HTC computing infrastructures that require batch processing to execute analysis.

- Tools, software, computing and storage resources should be findable, accessible and sharable transparently.
- Authentication, Authorisation and Accounting: Data Centres want to know who is using their infrastructure and why!
- The identification of API and protocols to build intelligent data lakes capable of distributing data among different cloud Data Centres and offering services for SPs in order to couple software, computing, and data.

4. The role of IVOA

The IVOA, as the organisation defining the VO standards, has the key role to play in the evolution of the VO and the extension of its paradigm. The main items to tackle are the following.

1) The current IVOA standards provide protocols for data discovery and access.
2) The IVOA shall identify metadata to describe software: a software "data-model".
3) The IVOA shall identify technologies to build software marketplaces based on "common" standards.
4) The IVOA should discuss, build and promote policies and trust to implement a "data lake with computing islands" (providing services consuming resources requires important policy decisions by each data centre).
5) The IVOA shall investigate a way to let public data to remain fully accessible, "unharmed" by Authentication&Authorisation policy concerns. Up to now, VO-compliant data centres have provided free and public access to data (usually by means of anonymous access). Additional services may imply a set of different requirements, therefore it must be possible to enforce A&A&A (Authentication-Authorisation-Accounting) e.g. for complex services and user processing, while keeping at the same time anonymous access, e.g. for read-only access and no processing, EPO, citizen science, simple services requiring computing.

A promising step made by IVOA to cope with these needs is the fact that the IVOA Technical Coordination Group (TCG) has included the update to A&A&A technologies, the software "data-model" and a discussion on Science Platforms in the 2020 IVOA Technical Roadmap.

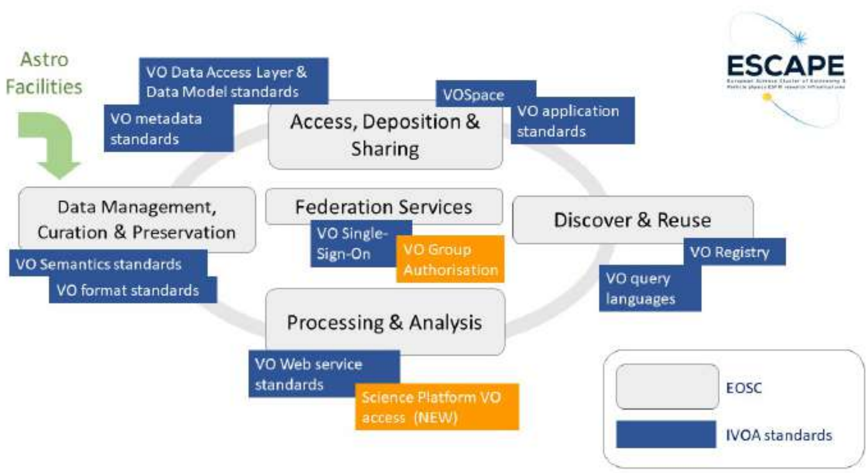

Figure 7. Integration of astronomy VO data and services into the European Open Science Cloud (EOSC).

As an example of practical work being carried out, the ESCAPE project (funded by the European Union within its Horizon 2020 programme) can be mentioned. The developments relevant to this discussion are carried out within its VO (Virtual Observatory) and ESAP (ESFRI Science Analysis Platforms) work-packages, and are shown in Figure 7. In the figure, the tools and mechanisms provided by EOSC cloud to perform a set of operations are marked in grey. The blue boxes represent existing VO standards, which need to be interfaced with the EOSC tools; the orange boxes define the need for new VO standards, that need to be defined.

The definition of a software "data-model" (item 2 above) could be performed in connection with the already advanced work provided by ASCL. It is worth noting that ESCAPE (within its OSSR, Open Software and Services Repository work-package) is also tackling code description with respect to the data formats it can consume.

The above example shows that new IVOA standards are needed to support the extensions.

- Besides VO Authentication (handled through the IVOA Single Sign-On standard), to use resources Authorisation is needed as well (at the level of group authorisation). This is being discussed within IVOA GWS WG since October 2016, and the approval of an IVOA standard is expected soon.
- VO-compliant access to Science Platforms. This is a new concept, being worked upon within ESCAPE project; a new set of standards will be proposed to the IVOA.

5. Conclusions

Recently the importance of providing data processing and analysis services as part of archival activities, and the concept of an International Open Science Cloud, have received increasing interest.

- In early 2019, among the 294 "APC" (Activities, Projects, and State of the Profession Considerations) white papers submitted by astronomers to the Astro2020 Decadal Survey on Astronomy and Astrophysics organized by the US National Academy of Sciences, one by Desai et al. (2020) is particularly relevant to this discussion. The white paper advocates for the adequate funding of data centers to develop and operate "science platforms", which will provide storage and computing resources for the astronomical community to run analyses near the data; these platforms should be furthermore connected among each other to enable cross-center analysis and processing.
- The idea of building a multi-disciplinary Global Open Science Cloud (GOSC) was initiated during the CODATA 2019 Beijing conference. A Global Open Science Cloud Workshop has been organised for 3-4 November 2020 with the participation of representatives of international initiatives, research communities and public digital infrastructure providers. The IVOA will be represented by its current Chair.

In this framework, it is essential for the Virtual Observatory to evolve its concept in order to allow data-intensive research in the Big Data era.

From the technical point of view, there no obstacles: the Cloud paradigm offers a good set of solutions. The main issue of allowing the various clouds to operate together (i.e. federation) has been successfully experimented in a number of cases.

However, for this new evolution of the VO to be accepted and become operational, there are a number of policy implications, and decisions to be taken:

- all Data Centres are to provide, besides access to archive data, personal user storage and computing resources (here there are also some local technical decisions to be made);
- the VO community needs to adapt and evolve the IVOA standards to support this new paradigm: an agreement on the new technical standards to be defined needs to be found;
- the international astronomical community needs to move coherently in this direction: and here the lead of governing bodies to push these policy decisions forward is necessary.

Acknowledgements

The authors wish to thank the colleagues who shared their visions and points of view on Open Science Clouds (in particular David Schade and Chenzhou Cui), and the whole team at INAF-OATs working on VO and computing. The European Science Cluster of Astronomy Particle Physics ESFRI Research Infrastructures (ESCAPE) project is funded by the European Union's Horizon 2020 research and innovation programme under Grant Agreement no. 824064.

References

Bertocco S., Dowler P., Gaudet S., et al. 2018, Astronomy and Computing, 24, 36

Bertocco S., Major B., Dowler P., et al. 2020, in Astronomical Data Analysis Software and Systems XXVII. Astronomical Society of the Pacific, p. 327

Cui C., Yu C., Xiao J., et al. 2017, in Astronomical Data Analysis Software and Systems XXV. Astronomical Society of the Pacific, p. 553

Desai V., Allen M., Arviset C., et al. 2020, Bulletin of the AAS, 51

Hanisch R. J., 2015, Astronomy and Computing, 11, 73

Pasian F., Taffoni G., Vuerli C., 2007, Highlights of Astronomy, 14, 601

Pasian F., Brescia M., Longo G., 2012, in Science - Image in Action. World Scientific Publishing Co. Pte. Ltd., p. 230

Taffoni G., 2021, in Astronomical Data Analysis Software and Systems XXX. Astronomical Society of the Pacific, pp invited, in preparation

Wilkinson M. D., Dumontier M., Aalbersgberg I. J., et al. 2016, Scientific Data, 3

FSR19 and FSR25 confirmed as two new faint and metal-rich globular clusters in the galactic bulge

C. Obasi*[1], M. Gómez†[1], D. Minniti‡[1,2], and J. Alonso-García[3]

[1]Depto. de Ciencias Físicas, Facultad de Ciencias Exactas, Universidad Andres Bello, Av. Fernandez Concha 700, Las Condes, Santiago, Chile.,
[2]Vatican Observatory, V00120 Vatican City State, Italy.,
[3]Centro de Astronomía (CITEVA), Universidad de Antofagasta., Av. Angamos 601, Antofagasta, Chile.

Abstract

We combined the near-IR photometry from the VISTA Variables in the Vía Láctea extended Survey (VVVX) with Gaia EDR3 catalog to study some properties of FSR19 and FSR25. These are confirmed to be low luminosity metal-rich bulge globular clusters (Obasi et al. 2020). The proper motions (PM) remain unchanged and the Color magnitude diagrams (CMD) are consistent with what we previously reported and the red giant branches are narrower than the field.

Keywords: *Galaxy: bulge - globular clusters: general - Red-clump stars, MK formation and evolution, Star clusters*

1. Introduction

GCs are powerful probes in our understanding of the galactic evolution, each confirmation of a new GC in the Milky Way is a treasure as they are key tracers of the field stellar populations, and provide valuable evidence for the formation of the Galaxy. Those found in the Galactic bulge in particular, may probably be among the oldest objects in the Galaxy (e.g., Barbuy et al., 2016). Bica et al. (2019) presented a catalog of star clusters, Associations and Candidates in the Milky Way which contains over 10000 star clusters, including many new low-luminosity candidates discovered by the VVV Survey (e.g., Camargo, 2018, Minniti et al., 2017b), these have significantly increased the bulge GC sample. While many of these have already been confirmed or discarded by follow up studies (e.g., Gran et al., 2019, Palma et al., 2019, Piatti, 2018), it is clear that the bulge GC census is incomplete (Ivanov et al., 2005, Minniti et al., 2017a). In our first paper (Obasi et al., 2020, submitted) hereafter known as paper I, we demonstrated that both FSR19 and FSR25 are genuine low luminosity bulge globular clusters by combining clean photometry data from VVVX, 2MASS and Gaia DR2. We measured distances (D)=7.3± 0.4 and 7.6±0.4, integrated luminosities M_{Ks}(FSR19)=-7.72 and M_{KS}(FSR25)=-7.31 core-radii=2.76 pc and 1.92 pc, tidal radii=5.31 and 6.85 pc for both FSR19 and FSR25. Also, metallicilty [Fe/H]=-0.50 dex and -0.55 dex and ages of 11 Gyr were estimated. These measurements are in agreement with other studies (Buckner & Froebrich, 2013, Froebrich et al., 2007, Kharchenko et al., 2013, 2016). These two objects are located in an interesting complex dark nabulae (FSR19 next to Barnard 268, and FSR25 next to Barnard 276). Figure 1 shows that this is a complicated region in terms of extinction, we have checked different extinction maps (Schlafly & Finkbeiner, 2011, Schlegel et al., 1998) and found that they are not located in any particular region of low extinction, so they can not be confused with extinction window. In this paper we used the Gaia EDR3 and VVVX catalogs to reexamine some of the clusters properties such as CMD, differential reddening and PM

In section 2 we describes the data, differential reddening and CMD of the field stars as well as the PM selected samples. and finally summarize our conclusions in section 3.

*c.obasi@uandresbello.edu, Corresponding author
†matiasgomez@unab.cl
‡vvvdante@gmail.com

DOI: 10.52526/25792776-2020.67.2-311

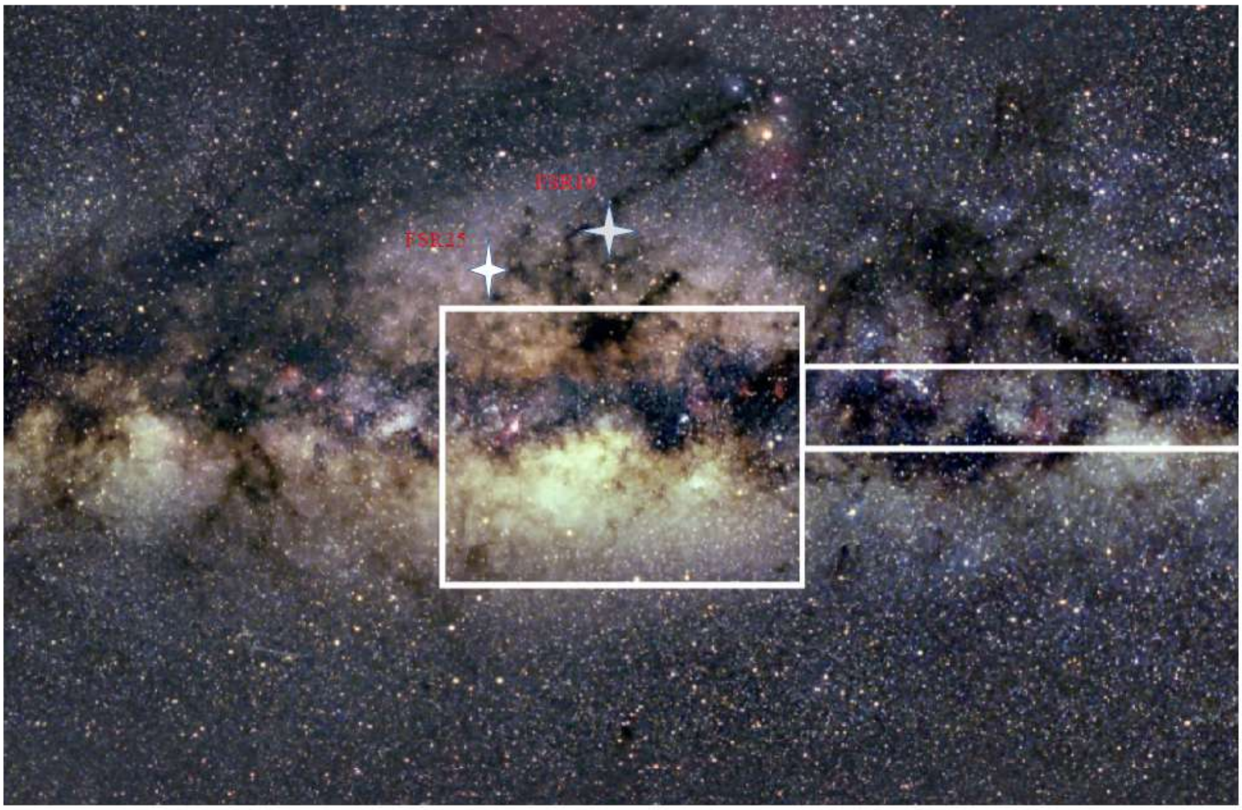

Figure 1. This shows the complex region where the clusters are located in terms of extinction, The white rectangle is the region covered by the VVV, the approximate positions of the clusters are shown. The image was adapted from (Mellinger, 2009)

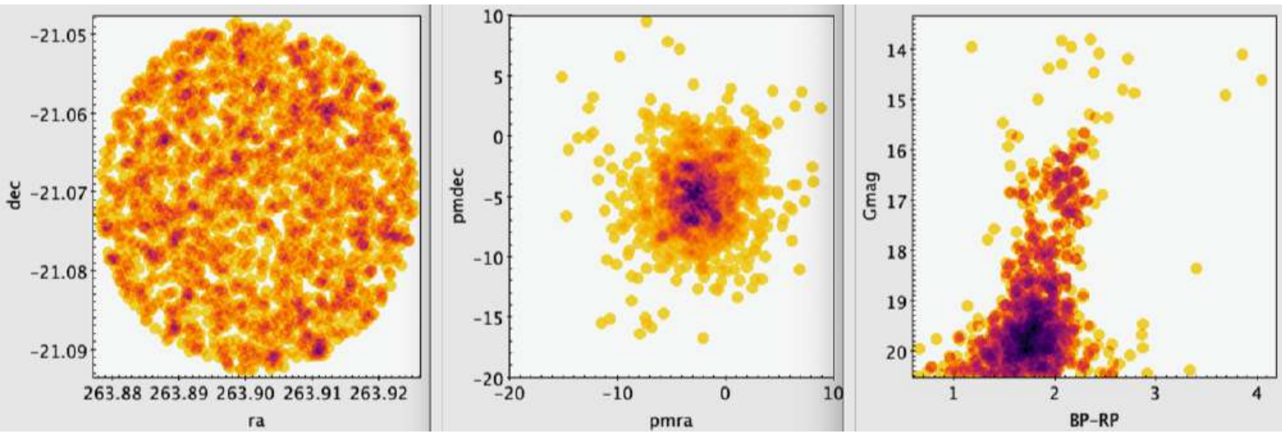

Figure 2. The central 3 arcmin region of the cluster FSR19 from Gaia EDR3, Gaia star density map (left), the vector PM diagram (middle) and CMD of both field and cluster stars (right)

2. Gaia EDR3 and VVVX Data

The major challenge in probing the galactic bulge with photometric surveys is the non-uniform reddening toward our Galactic centre (Schlafly & Finkbeiner, 2011) this probably had been mitigated through the extinction maps derived from the VVV (Alonso-García et al., 2017, 2018, Gonzalez et al., 2012), to minimize any systematics, we have used the combination of near-IR VVVX and the recently released Gaia EDR3 to build our clean sample. Gaia EDR3 contains the apparent brightness in G magnitude for over 1.8×10^9 sources which are brighter than 21 mag, and for 1.5×10^9 sources, passbands G_{BP} covering 330-680 nm and G_{RP} covering 630-1050 nm, which are not available in DR1 and DR2. (Gaia Collaboration et al., 2020). The data have been processed by the Gaia Data Processing and Analysis Consortium (DPAC).

The VVVX Survey (Minniti, 2018) maps the Galactic bulge and southern disk in the near-IR with the VIRCAM (VISTA InfraRed CAMera) at the 4.1 m wide-field Visible and Infrared Survey Telescope for Astronomy (Emerson & Sutherland, 2010)(VISTA) at ESO Paranal Observatory (Chile). In the Galactic bulge, the VVVX Survey covers about 1700 sqdeg., using the J (1.25 μm), H (1.64 μm), and K_s (2.14 μm) near-IR passbands.

2.1. Physical parameters of FSR19 and FSR25

By combining the Gaia EDR3 with VVVX catalog, we selected the central 3 arcmin region of the clusters. We plotted the Gaia star density map showing the differential reddening in the RA and Dec for both FSR19 and FSR25 as shown in figures 2 and 3 (left) showing the improved systematics and accurancy in the Gaia EDR3. The middle plot shows the vector PM diagrams of FSR19 and FSR25 centred at $PMRA$=-3.5 masyr^{-1}; $PMDE$= -5.0 mas yr^{-1} for FSR19, and $PMRA$= -4.0 mas yr^{-1}; $PMDE$=-2.0 mas yr^{-1} which is consistent with paperI though of a better quality. In the right we plotted the CMD of the field and clusters members. Figure 4 shows the PM selected CMD for both FSR19 and FSR25. From this plot it evident that the red giant branches are narrower than the field as reported in paper I.

3. Summary

Using the improved data from Gaia EDR3, we examined some of the properties of FSR19 and FSR25 and compared the results to paperI. We established that the PM centred at $PMRA$=-3.5 masyr^{-1}; $PMDE$= -5.0 mas yr^{-1} for FSR19, and $PMRA$= -4.0 mas yr^{-1}; $PMDE$=-2.0 mas yr^{-1} remains unchanged, the CMD is consistent in all cases. It is clear that the red giant branches of the clusters are narrower than the field as first reported in paper I.

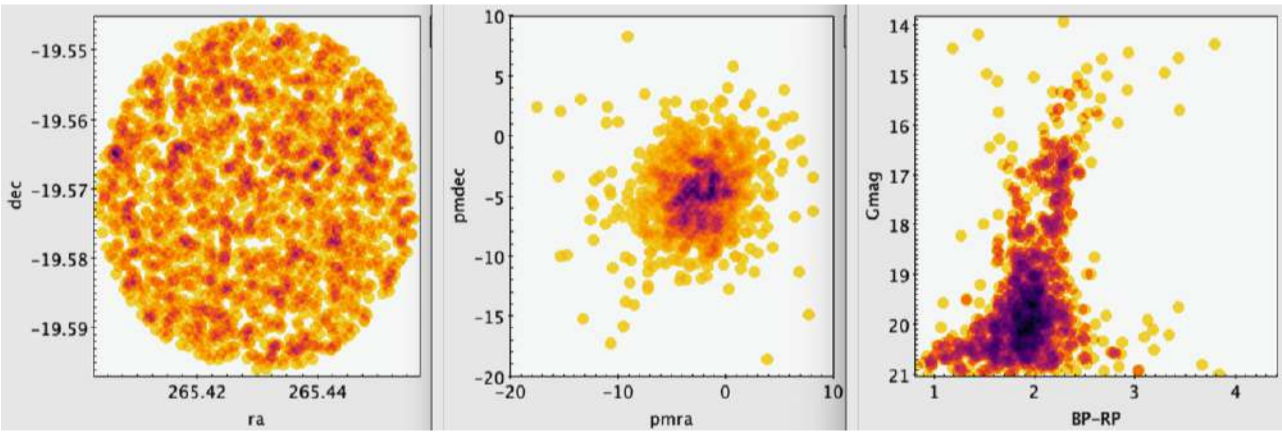

Figure 3. Shows the central 3 arcmin region of the cluster FSR25 from Gaia EDR3, Gaia star density map (left), the vector PM diagram (middle) and CMD of both field and cluster stars (right)

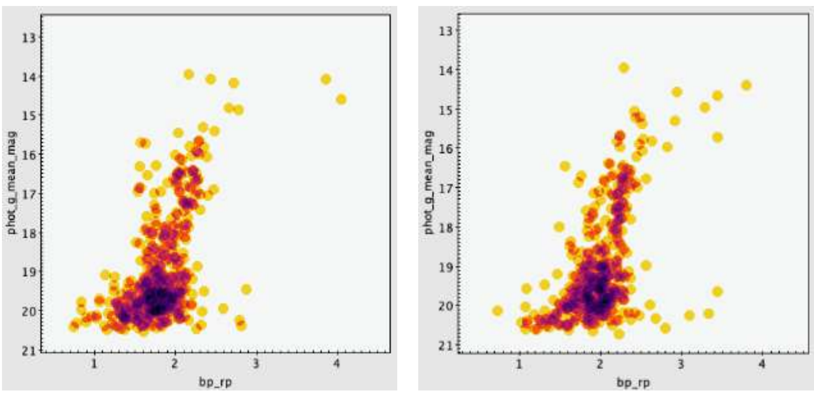

(a) (b)

Figure 4. PM selected CMDs for both clusters. (a) CMD of G vs BP-RP showns the narrow red giant branch of FSR19 . (b) CMD of G vs BP-RP showns the narrow red giant branch of FSR25.

References

Alonso-García J., et al., 2017, ApJ, 849, L13

Alonso-García J., et al., 2018, AJ, 619, A4

Barbuy B., et al., 2016, A&A, 591, A53

Bica E., Pavani D., Bonatto C., Lima E., 2019, yCAT, 515

Buckner A. S., Froebrich D., 2013, MNRAS, 436, 1465

Camargo D., 2018, ApJ, 860, L27

Emerson J., Sutherland W., 2010, MSNGR, 139, 2

Froebrich D., Scholz A., Raftery C., 2007, MNRAS, 374, 399

Gaia Collaboration B., et al., 2020, arXiv preprint arXiv:2012.01533

Gonzalez O., et al., 2012, A&A, 543, A13

Gran F., et al., 2019, A&A, 628, A45

Ivanov V. D., Kurtev R., Borissova J., 2005, A&A, 442, 195

Kharchenko N., et al., 2013, A&A, 558, A53

Kharchenko N., et al., 2016, A&A, 585, A101

Mellinger A., 2009, Publications of the Astronomical Society of the Pacific, 121, 1180

Minniti D., 2018, in , The Vatican Observatory, Castel Gandolfo: 80th Anniversary Celebration. Springer, pp 63–71

Minniti D., et al., 2017a, ApJ, 838, L14

Minniti D., et al., 2017b, ApJ, 849, L24

Palma T., et al., 2019, MNRAS, 487, 3140

Piatti A. E., 2018, MNRAS, 477, 2164

Schlafly E. F., Finkbeiner D. P., 2011, AJ, 737, 103

Schlegel D. J., Finkbeiner D. P., Davis M., 1998, ApJ, 500, 525

Communications of BAO, Vol. 67, Issue 2, 2020, pp. 316-322

The Armenian Virtual Observatory (ArVO)

A. M. Mickaelian*[1], H. V. Astsatryan[2], A. V. Knyazyan[2], G. A. Mikayelyan[1], Gh. Gevorgyan[2], D. S. Baghdasaryan[1], and H. V. Abrahamyan[1]

[1]Byurakan Astrophysical Observatory (BAO)
[2]Institute of Informatics and Automation Problems (IIAP)

Abstract

The Astrophysical Virtual Observatories (AVOs) have been created in a number of countries using their available databases and current observing material as a collection of interoperating data archives and software tools to form a research environment in which complex research programs can be conducted. Among all these data, a large spectroscopic database for all objects is especially useful. The Armenian Virtual Observatory (ArVO) has being created to utilize the Digitized First Byurakan Survey (DFBS) as an appropriate spectroscopic database. ArVO is a project of the Byurakan Astrophysical Observatory (BAO) aimed at construction of a modern system for data archiving, extraction, acquisition, reduction, use and publication. ArVO is based on DFBS and is the Armenian contribution to the International Virtual Observatories Alliance (IVOA). One of the ArVO's main tasks is to create and utilize a global Spectroscopic Virtual Observatory, which will combine data from DFBS and other low-dispersion spectroscopic databases, as well as provide the first understanding on the nature of any object up to $B=18^m$. In frame of ArVO, BAO collaborates with the Institute of Informatics and Automation Problems (IIAP) of the Armenian National Academy of Sciences to develop software for ArVO corresponding to the IVOA standards. Beside the DFBS, ArVO is being complemented by the Digitized Second Byurakan Survey (SBS) database, the Byurakan photographic archive, and BAO 2.6m and 1m Schmidt telescope observations, and will be a part of IVOA.

1. Introduction

The **Armenian Virtual Observatory (ArVO**, www.aras.am/Arvo/arvo.htm) was created 10 years ago, in 2005, when after the accomplishment of the **Digitized First Byurakan Survey (DFBS**, www.aras.am/Dfbs/dfbs.html) we had enough resources to run a VO project and contribute in the **International Virtual Observatory Alliance (IVOA**, www.ivoa.net). ArVO is a project of Byurakan Astrophysical Observatory (BAO) aimed at construction of a modern system for data archiving, extraction, acquisition, reduction, use and publication. ArVO technical and research projects include Global Spectroscopic Database, which is being built based on DFBS. Quick optical identification of radio, IR or X-ray sources will be possible by plotting their positions in the DFBS or other spectroscopic plate and matching all available data. Accomplishment of new projects by combining data is so important that the International Council of Scientific Unions (ICSU) recently created **World Data System (WDS**, www.icsu-wds.org/) for unifying data coming from all science areas, and BAO has also joined it due to DFBS and ArVO projects.

*aregmick@yahoo.com, Corresponding author

DOI: 10.52526/25792776-2020.67.2-316

Virtual Observatory (VO) is a collection of interoperating data archives and software tools which utilize the Internet to form a scientific research environment in which astronomical research programs can be conducted. In the same way as a real observatory consists of telescopes, each with a collection of unique astronomical instruments, VO consists of a collection of data centres each with unique collection of astronomical data, software systems and processing capabilities. The main goal is to allow transparent and distributed access to data available worldwide. This allows scientists to discover, access, analyze, and combine space and laboratory data from heterogeneous data collections in a user-friendly manner.

Virtual Observatories have been created in a number of countries since 2000, and IVOA was created in 2002 as a coordinating body to develop and agree the vital interoperability standards upon which the VO implementations are constructed. So far, countries with most developed astronomy have VO projects and Armenia is among these 19 ones (in addition 2 European projects, Euro-VO and ESA, are IVOA members). ArVO was accepted in IVOA in 2005 and is one of its projects until now.

Figure 1. The International Virtual Observatory Alliance (IVOA)

IVOA software is aimed at data discovery (Aladin, Astroscope, VOExplorer, Datascope), spectral analysis (VOSpec, SPLAT, EURO-3D, Specview), data visualization and reduction (VOPlot, Topcat, VisIVO, STILTS), spectral energy distribution (SED) construction and fitting (VOSED, Yafit, easy-z, GOSSIP), etc.

The development of ArVO project includes Armenian astronomical archives and present telescope data preservation, cross-correlations of direct images and low-dispersion spectra, creation of joint low-dispersion spectral database (DFBS/DSBS/HQS/HES/Case) and a number of other technical and scientific projects.

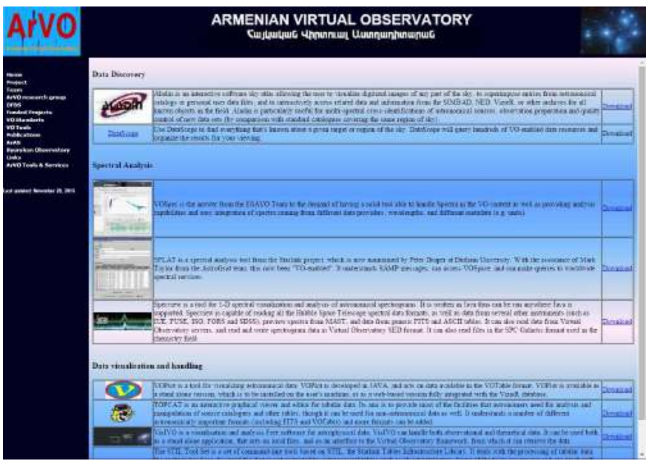

Figure 2. ArVO webpage

2. ArVO projects and developments

Beside DFBS, some other projects are active in frame of ArVO:

- Digitized Second Byurakan Survey (DSBS, started in 2003),
- Digitization and automated MIDAS reduction of FBS Blue Stellar Objects (BSOs) 2.6m slit spectra (Sinamyan & Mickaelian, 2009),
- Digitization of photometric chain observations in Coma field (started in 2004),
- Optical identification of IR sources in Boötes field of Spitzer Space Telescope (SST; 2005, the first science project using DFBS/ArVO) (Hovhannisyan et al., 2009),
- Optical identifications of X-ray, IR and radio sources.

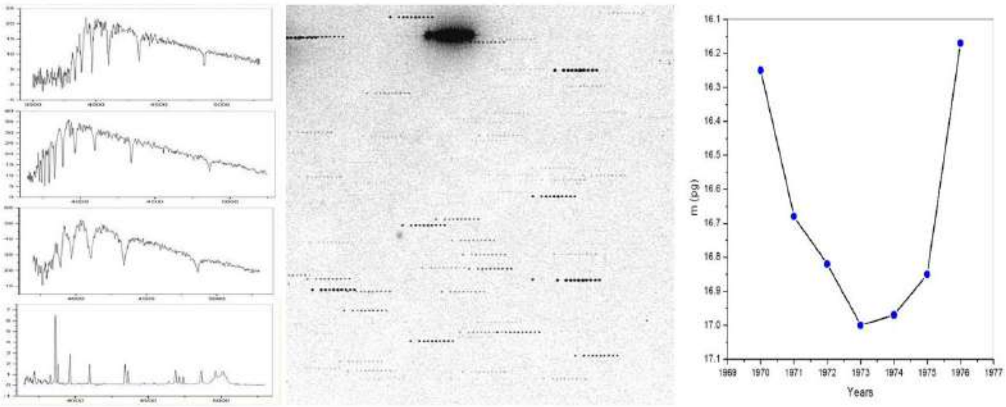

Figure 3. ArVO projects Spectroscopic study of FBS Blue Stellar Objects (BSOs) and Variability of ON 231

Most advanced ArVO project was the **Search for asteroids in DFBS** jointly with IMCEE (Observatoire de Paris, France) colleagues (Berthier et al., 2009, Thuillot et al., 2007), for which VO software Aladin and SkyBote are being used. Bright ($< 15^m$-16^m) asteroids observed in DFBS are being studied, which are divided into "fast" and "slow" ones depending on their motion during the typical DFBS plate exposure time (20 min), more or less than 3". All asteroid spectra are being extracted after they are found by means of SkyBote. Sample spectra are being modeled similar to Solar spectra. Using these spectra and by means of comparisons with other catalogues, new candidate asteroids are being searched. Spectra analysis of asteroid spectra is being accomplished aimed at obtaining definite physical parameters.

Since 2008, ArVO also is a **collaboration between BAO and NAS RA Institute of Informatics and Automation Problems (IIAP)**. In frame of this collaboration, a number of joint astrophysical computational projects have been accomplished, including DFBS database and analysis, cross-correlations, etc. *Dr.* Hrachya Astsatryan from IIAP is ArVO Technical Manager and Aram Knyazyan defended his PhD thesis on ArVO software development and utilization. Two ISTC grants (A-1451 and A-1606) were won. ArVO also collaborates with Euro-VO, VO-France and some other VO projects.

3. ArVO Tools and Services

In frame of this collaboration, ArVO Tools & Services have been developed: **DFBS archive, ArVO Data Discovery tool, Catalogue cross-matching service**, and **DFBS spectra extraction service** (the latter one still being under development):

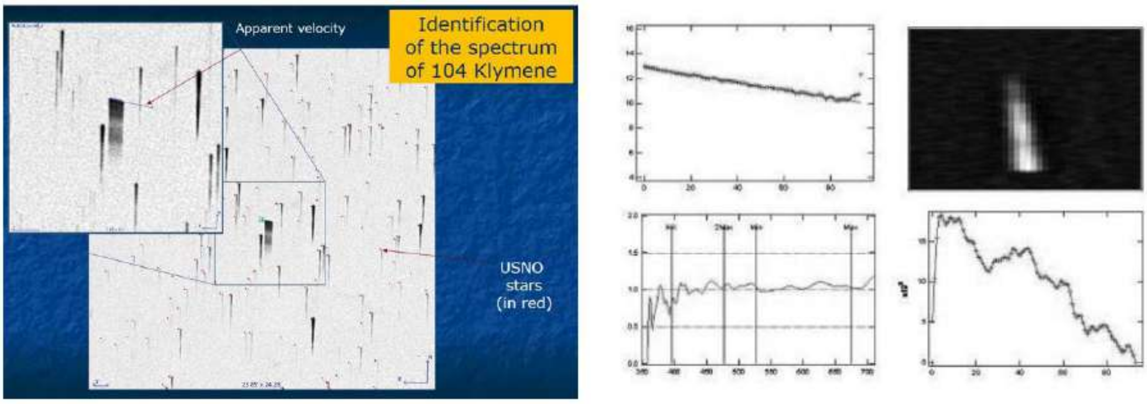

Figure 4. ArVO research projects: search for asteroids in DFBS by means of SkyBote sowtfare and the software EXATODS – Extraction and Analysis TOol of DFBS Spectra

1) DFBS archive page gives access to all DFBS data, view the plates and spectra of their sources. More about DFBS archive you can read here (http://byurakan.phys.uniroma1.it/).

2) ArVO Data Discovery tool gives possibility to access to all available data on it, which is dynamically updating by astronomers and developers (http://arvo.sci.am).

3) Catalogue cross-matching service includes a new cross-correlation program, which is doing the correlation of uploaded or available on server catalogues using as correlation radius for each pair of sources their RMS average error multiplied by some input constant. You can upload your own catalogues, run the service and download the resulting list. The new program is more accurate than the classic cross-correlation methods (http://arvo.sci.am/crosscorrelation/crosscor.html).

4) Spectra Extraction service will include a tool which extracts astronomical spectra catalogs from uploaded fits files (http://arvo.sci.am/extraction/index.html).

In 2015, **BAO Plate Archive Project** was conducted, which will significantly complement ArVO data. It is planned that all BAO observational material will be digitized, a full database will be created and BAO observations interactive sky map will be built. The project is also aimed at utilization of the digitized data for further science projects.

4. Meetings and Schools

ArVO has organized individual sessions at the largest ever meeting held in Armenia, Joint European and National Astronomical Meeting (JENAM-2007), Computer Science and Information Technologies (CSIT-2009) Conference (jointly with IIAP) and other symposia and workshops. A Conference of Young Scientists of CIS Countries *"50 years of Cosmic Era: Real and Virtual Studies of the Sky"* was held in November 2011. An international symposium *"Astronomical Surveys and Big Data"* (https://bao.am/meetings/meetings/ASBD) dedicated to 50th anniversary of Markarian Survey and 10th anniversary of ArVO was held on Oct 5-8, 2015 in Byurakan, Armenia. We intended to combine astronomers and computer scientists with heavy involvement of astronomical surveys, catalogs, archives, databases and VOs. IVOA and national VO project leaders took part.

In 2020, two international events were organized related to Data Science. The International Symposium *"Astronomical Surveys and Big Data 2"* (ASBD-2) was held on Sep 14-18, 2020 (https://www.bao.am//meetings/meetings/ASBD2/). Because of COVID-19 pandemic, this year the summer school was held online. This was the 2nd such meeting organized by the Byurakan Astrophysical Observatory (BAO); the 1st one was in 2015 with participation of astronomers and computer scientists. This time, also astronomers and computer scientists participated, in total 91 participants from

24 countries. During the meeting, large astronomical surveys were reviewed and discussed, a tribute was given to Markarian and other important surveys, the future of astronomical research by joint efforts of astronomers and computer scientists were discussed. 12 invited and 30 contributed talks were given and 11 posters were presented.

The Topics of the Symposium were the following:

- Historical surveys; Byurakan surveys for active galaxies (Markarian, Arakelian, Kazarian) and others
- Surveys for exoplanets; Surveys for stars and nebulae
- Extragalactic and cosmological surveys
- Digitization of astronomical data
- Astronomical Catalogues, Archives and Databases
- Cross-identifications between surveys and discovery of new objects
- Future large-area surveys
- Big Data in Astronomy; Data Science
- Computational Astrophysics, Astrostatistics and Astroinformatics
- Virtual Observatories

Among the invited speakers of the symposium, there were Areg Mickaelian (Director of BAO), Fabio Pasian (Italy), Markus Demleitner (Germany), Oleg Malkov (Russia), co-founder of Astroinformatics Ashish Mahabal (USA), Chair of the International Virtual Observatory Alliance (IVOA) Chenzhou Cui (China), Alain Sarkissian (France) and others.

The 7$^{\text{th}}$ Byurakan International Summer School (7BISS) for Young Astronomers on *"Astronomy and data Science"* was held on Sep 7-11. 2020 (https://www.bao.am//meetings/meetings/SS2020/index.html). Because of COVID-19 pandemic, this year the summer school was held online. 50 young astronomers and 12 lecturers from 21 countries participated in 7BISS. Moreover, an opportunity was created for the public sector to take part in the school as listeners. In the framework of the school, participants had 15 lectures and 11 practical tutorial sessions on *Astronomical Surveys, Digitization of astronomical data, Astronomical Catalogues, Databases and Archives, Astrostatistics and Astroinformatics, Big Data in Astronomy and Virtual Observatory tools.* Among the famous lecturers were IAU Vice-President Ajit Kembhavi (India), co-founder of Astroinformatics Ashish Mahabal (USA), Chair of International Virtual Observatory Alliance (IVOA) Chenzhou Cui, Fabio Pasian (Italy), Markus Demleitner (Germany), Oleg Malkov (Russia) and others. All the presentations are available online: https://www.bao.am//meetings/meetings/SS2020/programme.html. The Byurakan Summer School once again proved the importance of Astronomy in the development of Data science and e-Science.

5. ArVO collaborations

ArVO Project Manager Areg Mickaelian has several times attended **IVOA Interoperability meetings, ADASS meetings** and **WDS Forums**, and regularly participates in IVOA teleconferences organized several times each year. ArVO young team members have attended and presented contributions in Euro-VO, NVO other meetings and schools. VO subject was always present at Byurakan International Summer Schools (BISS) and Byurakan Summer Schools (BSS) for YSU students series since 2005, where a number of outstanding foreign lecturers have taught.

ArVO funded projects include several ANSEF grants (PS-450, PS-702 and PS 2968) and CRDF grant ARP1-2849-YE-06 in 2007-2010 *"Digitized First Byurakan Survey and Armenian Virtual Observatory"*, as well as the above mentioned ISTC grants in collaboration with IIAP ISTC A-1451

"Development of Scientific Computing Grid on the Base of Armcluster for South Caucasian Region" and ISTC A-1606 *"Development of Armenian-Georgian Grid Infrastructure and applications in the fields of high energy physics, astrophysics and quantum physics"*. Others were COST Action TD1403 *Big Data Era in Sky and Earth Observation* (BigSkyEarth) in 2015-2019, *BAO Plate Archive Digitization and e-Database* in 2015-2018 and is *BAO Plate Archive e-Database and Scientific Usage* in 2020-2021.

In frame of **ArVO and GAVO collaboration in 2017-2019** (MES-BMBF: project *"Building a high-performance research environment through German and Armenian Astrophysical Virtual Observatories"*), more than 30 visits were accomplished between Armenia and Germany (BAO and ARI Heidelberg). Areg Mickaelian, Aram Knyazyan, Daniel Baghdasaryan, Hrachya Astsatryan, Gor Mikayelyan, and Hayk Abrahamyan participated in the project, as well as some other young scientists attended workshops organized in frame of the projects. German scientists visited to Armenia to lecture at the workshops and training schools. Joachim Wambsganss, Markus Demleitner and Hendrik Heinl participated from GAVO. The collaboration products included the DFBS classification and SIAP/SSAP services for DFBS.

Other collaborations were with **OV-France / OV-Paris** projects with participation of Philippe Prugniel, Alain Sarkissian, Jerome Berthier, William Thuillot and Pierre Le Sidaner. It included the creation of the DFBS database, SIAP/SSAP services and search and verification of asteroids ephemeris. The **Armenian-Italian collaboration** was with the Universita Napoli Federico II. *Prof.* Giuseppe Longo led the Italian team.

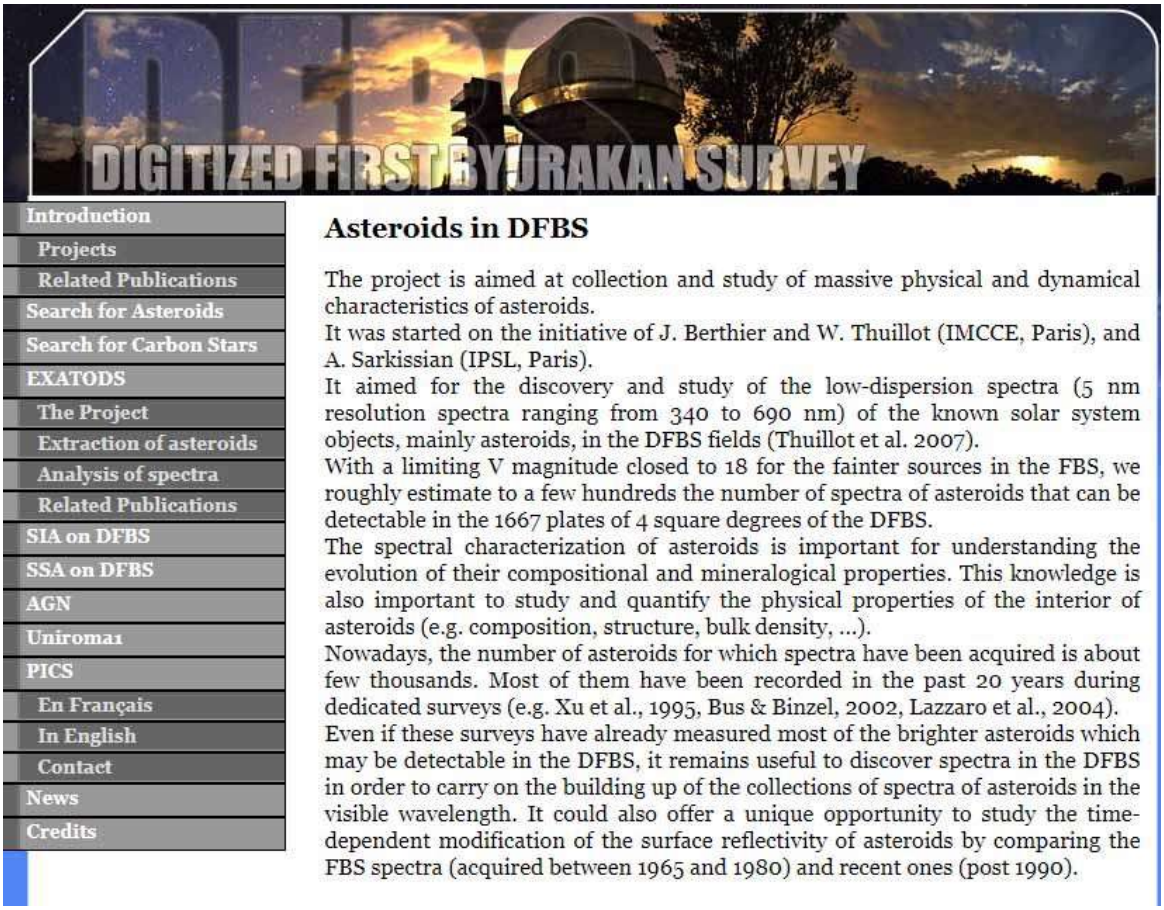

Figure 5. ArVO-VO-France collaboration webpage

References

Abrahamyan H. V., Mickaelian A. M., Knyazyan A. V., Harutyunyan G. S., 2012, CIS Young Scientists Conference, p. 223

Abrahamyan H. V., Mickaelian A. M., Knyazyan A. V., 2015, A&C, 10, 99, VizieR Online Data Catalog yCat.2338, 2015

Abrahamyan H. V., Mickaelian A. M., Paronyan G. M., Mikayelyan G. A., Gyulzadyan M. V., 2018, A&C, 25, 176

Astsatryan H. V., Knyazyan A. V., Mickaelian A. M., Sargsyan L. A., 2010, Fifth Intern. Conf. on Parallel Computing and Control Problems (PACO'2010), Moscow, Russia, PCCP book, p. 109

Astsatryan H. V., Knyazyan A. V., Mickaelian A. M., 2016, ASP Conference Series, 505, 220

Berthier J., Sarkissian A., Mickaelian A., Thuillot W., 2009, European Planetary Science Congress, EPSC2009, 4, 526

Demleitner M., Mickaelian A., Mikayelyan G., Knyazyan A., Baghdasaryan D., 2019, GAVO

Gevorgyan G., Knyazyan A. V., Astsatryan H. V., Mickaelian A. M., Mikayelyan G. A., 2020, A&C, in press

Hovhannisyan L. R., Weedman D. W., Mickaelian A. M., 2009, AJ, 138, 251

Knyazyan A. V., Mickaelian A. M., Astsatryan H. V., 2011, Int. J. "Information Theories and Appl.", 18, 243

Knyazyan A. V., Astsatryan H. V., Mickaelian A. M., 2016, ASP Conference Series, 505, 236

Knyazyan A. V., Astsatryan H. V., Mickaelian A. M., 2017, A&C, 19, 23

Mickaelian A. M., 2007, Highlights of Astronomy, 14, 594

Mickaelian A. M., 2009, Romanian Astron. J., 16S, 23

Mickaelian A. M., 2012, Proc. Conf. Young Scientists of CIS Countries "50 years of Cosmic Era: Real and Virtual Studies of the Sky", held 21-25 Nov 2011, Yerevan, Armenia, Eds.: A.M. Mickaelian, O.Yu. Malkov, N.N. Samus, Yerevan, NAS RA, pp 29–38

Mickaelian A. M., Astsatryan H. V., 2015, Proc. of Conference: Relation of Astronomy to Other Sciences, Culture and Society, NAS RA, p. 188

Mickaelian A. M., Sargsyan L. A., Mikayelyan G. A., et al 2006a, Heron Press Science Series, pp 82–92

Mickaelian A. M., Gigoyan K. S., Nesci R., Rossi C., 2006b, MemSAIt, 77, 1159

Mickaelian A. M., Sargsyan L. A., Nesci R., et al 2007a, Highlights of Astronomy, 14

Mickaelian A. M., Nesci R., Rossi C., et al 2007b, A&A, 464, 1177

Mickaelian A. M., Nesci R., Cirimele G., et al 2008a, Proc. ESAC Workshop on Astronomical Spectroscopy and Virtual Observatory, held in ESAC, Villafranca del Castillo, Spain, 21-23 March 2007, ESA, pp 29–32

Mickaelian A. M., Sargsyan L. A., Gigoyan K. S., et al 2008b, Romanian Astron. J., 18S, 249

Mickaelian A. M., Astsatryan H. V., Sahakyan V. G., et al 2009a, Proc. CSIT-2009 meeting, pp 420–423

Mickaelian A. M., Kochiashvili N., Astsatryan H. V., et al 2009b, Proc. CSIT-2009 meeting, pp 424–427

Mickaelian A. M., Sargsyan L. A., Astsatryan H. V., et al 2009c, Data Science Journal, 8, 152

Mickaelian A. M., Sargsyan L. A., Nesci R., et al 2010, ASP Conference Series, 434: Astronomical Data Analysis Software and Systems XIX, 325

Mickaelian A. M., Malkov O. Y., Samus N. N., (Eds.) 2012, 50 years of Cosmic Era: Real and Virtual Studies of the Sky, Proc. Conference of Young Scientists of CIS Countries, NAS RA, 251 p., Yerevan

Mickaelian A. M., Astsatryan H. V., Magakian T. Y., et al 2016a, Armenian-Iranian Astronomical Workshop, NAS RA, p. 62

Mickaelian A. M., Astsatryan H. V., Knyazyan A. V., et al 2016b, ASP Conference Series, 505, 16

Mickaelian A. M., Astsatryan H. V., Knyazyan A. V., Mikayelyan G. A., 2017, BAOJP, 2, 8

Mickaelian A. M., Sarkissian A., Berthier J., Meftah M., Thuillot W., Vachier F., 2019, Icarus, 330, 5

Sarkissian A., Arzoumanian E., Mickaelian A. M., et al 2012, Proc. Conf. Young Scientists of CIS Countries "50 years of Cosmic Era: Real and Virtual Studies of the Sky", held 21-25 Nov 2011, Yerevan, Armenia, Eds.: A.M. Mickaelian, O.Yu. Malkov, N.N. Samus, Yerevan, NAS RA, pp 56–64

Sinamyan P. K., Mickaelian A. M., 2009, Astrophysics, 52, 76

Thuillot W., Berthier J., Sarkissian A., et al 2007, Highlights of Astronomy, 14, 616

Communications of BAO, Vol. 67, Issue 2, 2020, pp. 323-328

Resurrecting DFBS into the Virtual Observatory

Markus Demleitner*[1], Aram Knyazyan[2], Daniel Baghdasaryan[2], Gor Mikayelyan[2], and Areg Mickaelian[2]

[1]Universität Heidelberg, Zentrum für Astronomie, Mönchhofstr. 12-14, 69221 Heidelberg, Germany
[2]Byurakan Astrophysical Observatory, Byurakan, Armenia

Abstract

The Digitised First Byurakan Survey has digitised and processed about 1900 photographic plates from the objective prism surveys conducted in Byurakan by Benjamin Markarian and collaborators in the 1960ies and 1970ies. After digitization, a custom web service was built and operated first in Rome, then in Trieste. However, as astronomical data systems and standards evolved, it became desirable to update the data and build standards-compliant, Virtual Observatory services from it.

This contribution reports on the challenges encountered during this migration, the solutions we chose, and the lessons to be learned. It also discusses the use of the resulting services.

Keywords: *Virtual Observatories, Spectroscopy, Surveys, Astronomy Databases*

1. Introduction

The first Byurakan survey was an objective-prism survey of the sky north of $-15°$ and farther than $15°$ from the Galactic plane, performed between 1965 and 1980 by Benjamin Markarian and his team. This important resource was digitised in the early 2000s in the DFBS project (Mickaelian et al., 2007), which yielded a set of scanned plates and low-resolution spectra for about 20 million objects extracted from them. The spatial distribution of these data products is shown in Fig. 1.

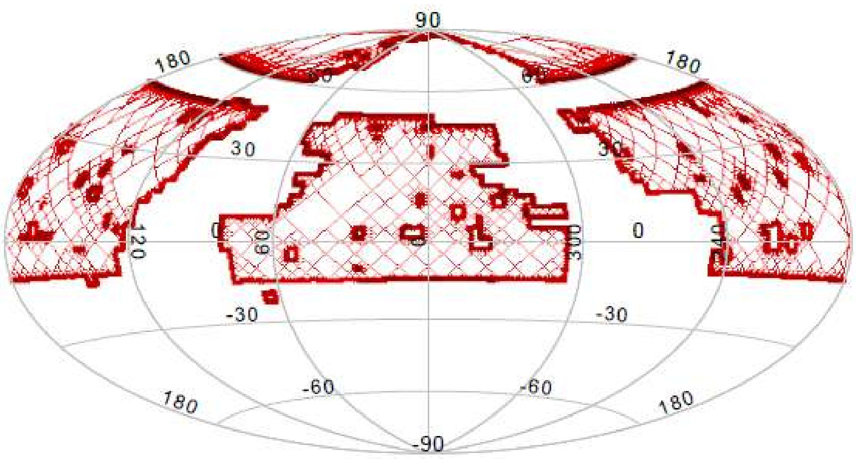

Figure 1. Spatial coverage of the scanned plates from the first Byurakan Survey; this figure was generated by plotting the result of `SELECT SUM(MOC(coverage)) FROM dfbs.plates` on the GAVO TAP service though a TOPCAT sky plot area control. The conspicuous gap around 50 degrees of declination is because the plates in that zone were used with the second Byurakan survey.

*msdemlei@ari.uni-heidelberg.de, Corresponding author

DOI: 10.52526/25792776-2020.67.2-323

When the programme reported on here was started in 2017, the results of this effort were available on an aging, unmaintained machine in Rome, accessible only through a browser interface, with spectra given in text form. It was clear that a migration of this valuable data towards standard discovery and usage patterns was highly desirable.

The reminder of this paper discusses what challenges had to be overcome in order to perform this migration in sect. 2 and goes on to describe the services now available through Virtual Observatory protocols in sect. 3. It concludes with some proposals on how the utility of the data could further be improved and a set of lessons that can be derived from our experience.

2. Migration Challenges

The first problem to be overcome was that the server that published the results of the digitisation project was running without maintenance, and the persons who had set it up had left the hosting institution. In particular, none of the project partners had any access to the machine's mass storage any more.

Hence, we started the migration with data obtained through web crawling; this concerned both the plate images and the spectra, which amounted to about 20 million little text files.

Expectably, the result was highly incomplete data, riddled with truncated files when the connections were interrupted during the transfer. Still, it was enough to set up a prototype service by writing two resource descriptors for the DaCHS publication package (Demleitner et al., 2014). The resulting resource directories are available under version control, one each for the plates[1] and for the spectra[2]. Of course, their current form is rather different from the early prototypes, but the basic structure has remained stable.

The important next step was to obtain access to the file system of the old publishing machine. This was eventually established through the help of Trieste Observatory, who managed to transfer the machine from Rome and save its mass storage to a modern virtual machine, which keeps running the legacy web interface for the time being; by today's standards, the raw data volumes are relatively modest (about 300 GB plate scans and 17 GB extracted spectra).

In this way, we could safely transmit the collected data through rsync.

The plates had expectably been stored in FITS format; however, the FITS headers were lacking important information, such as the observation date or the emulsion used. More seriously, their astrometric calibration was in the now severely outdated format of the Digitised Sky Survey (Lasker et al., 2008).

To remedy the first deficiency, we obtained the additional metadata from a TAP-accessible version of the Wide Field Plate Database[3] (Tsvetkova & Tsvetkov, 2006) and used this to add FITS headers in the Tuvikene convention for scanned photographic plates[4].

Repairing the second deficiency was harder. It appears that no analytic method of transforming from DSS calibration to modern WCS-SIP (Calabretta & Greisen, 2002, Shupe et al., 2005) that preserves the plate corrections has been worked out. Hence, we ended up creating the WCS-SIP headers numerically by computing a mesh of grid points (in practice, we used one per 200 pixels on each axis) and using astrometry.net's `fit-wcs` utility to compute the header (Lang et al., 2010). The implementation is found in the `compute_WCS` method in `addstandardheaders.py` in the DFBS RD repository mentioned above.

The extracted spectra were delivered to us in the form of an otherwise undocumented dump of a MySQL database that, for instance, still contained a large table of logs of the extraction procedures. The actual spectra turned out to be in per-plate tables using a custom array serialisation. That understood, it was straightforward to serialise all spectra into a single PostgreSQL table, with the flux values ending up in an array-valued column. Since the original extraction already has constant spectral bins, the spectral axis is added as a constant through a database view.

[1] https://svn.ari.uni-heidelberg.de/svn/gavo/hdinputs/dfbs
[2] https://svn.ari.uni-heidelberg.de/svn/gavo/hdinputs/dfbsspec
[3] ivo://org.gavo.dc/wfpdb/q/cone
[4] https://www.plate-archive.org/applause/project/fits-header-for-photoplates/.

In addition to the technical migration issues, there were also minor curational problems. One that deserves mentioning because it baffled us for a while although the original extraction team must already have noticed it is that the survey staff, presumably inadvertently, assigned some plate identifiers twice, namely 326, 449, and 966. This was a problem for us because spectra metadata like the emulsion used or the observation date is established through the plate identifier alone. Fortunately, in these three cases, the fields imaged are far apart, and so a certain identification of the source plate of a spectrum can be effected through a combination of plate number and position. It later turned out that of the affected plates, only the first one, FBS 0326, first epoch, were scanned, so that the duplication has not impacted data previously available.

3. Services After Migration

The result of our efforts is a set of standard services registered in the Virtual Observatory, available through both the data centers of the German Astrophysical Virtual Observatory GAVO and the Armenian Virtual Observatory ArVO. In this section, we will discuss these services and present usage scenarios.

Figure 2. DFBS spectra discovery in Aladin. See the text for how to reproduce the figure.

3.1. Spectra for Simple Clients

In the VO, the family of "S-protocols" (where the "S" stands for "Simple") gives straightforward, HTTP-based interfaces for the most common discovery tasks. In the case of spectra, this is the Simple Spectral Access Protocol SSAP (Tody et al., 2012).

We therefore publish the extracted spectra through SSAP[5]. A simple usage scenario employs the Aladin client (Bonnarel et al., 2000), in which one would point it to a location in the DFBS' coverage (M51, say), then look for "Byurakan" in Aladin's discovery tree and select one of the two DFBS services. In the resulting pop-up dialogue, check "in view" and then then click the Load button. Figure 2 illustrates the density of spectra in DFBS.

The spectra discovered in this way can be sent to TOPCAT, Splat, or some other table-processing application via the SAMP desktop messaging protocol for visualisation or analysis.

3.2. Datalink for Spectra

In a data collection like the DFBS extracted spectra, being able to inspect the provenance – in this case, the appearance of the objective prism spectra on the plates – is particularly important, because unusal spectral features may simply be due to plate defects or, in particular in crowded regions, spectral blends. Our services offer access to this provenance using the IVOA's Datalink protocol

[5] ivo://org.gavo.dc/dfbsspec/q/getssa and ivo://arvo/dfbsspec/q/getssa.

(Dowler et al., 2015). Datalink lets operators associate service calls to rows in query results, with a well-defined format of the results of these service calls.

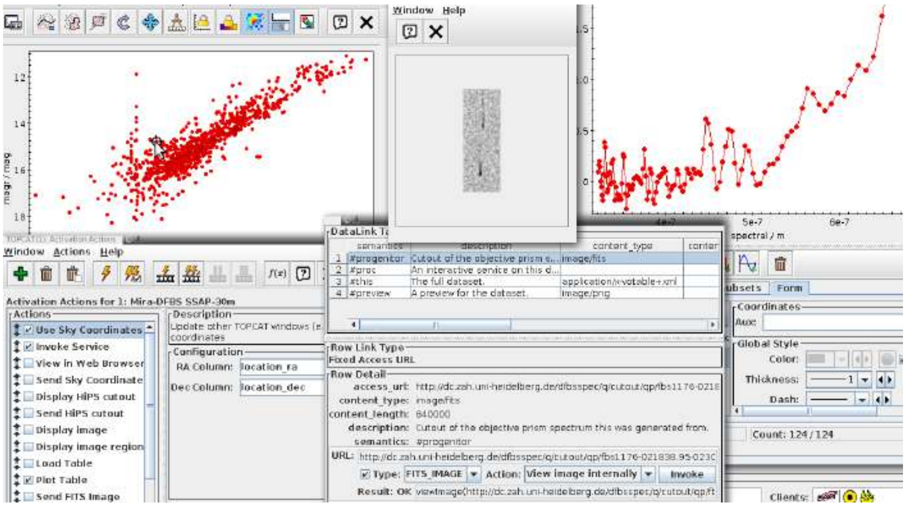

Figure 3. Accessing a cutout for a DFBS spectrum through Datalink with TOPCAT

To see how this works, start the TOPCAT VO client (Taylor, 2005). In this case, SSAP access is through the "Spectral Query" item in the VO menu. In the resulting dialogue, again look for "Byurakan" and choose one of the DFBS services. To reproduce Fig. 3, run a query on a 0.5 degrees vicinity of Mira. For this example, you could plot the result by, say, the magb versus the magr columns.

To view the spectra, in Views/Activation Action, check "Plot Table"; thanks to the metadata associated with the SSAP response, the activation action is already properly pre-configured. TOPCAT will now open a plot of the corresponding spectrum if you click on a point in the mag/mag plot.

If you additionally check "Invoke Service", another window will come up after selecting a point in the plot; this shows the extra Datalinks, among which there is one with a semantics of "#progenitor". Clicking "Invoke" will show the image; it could again be sent and displayed in Aladin using SAMP.

3.3. Bulk Spectra Processing Using TAP

For low-resolution spectra, the information content of a single dataset is limited. Their true power comes from bulk analysis of many spectra at a time.

To facilitate that without having to download a large number of spectra to local storage, the

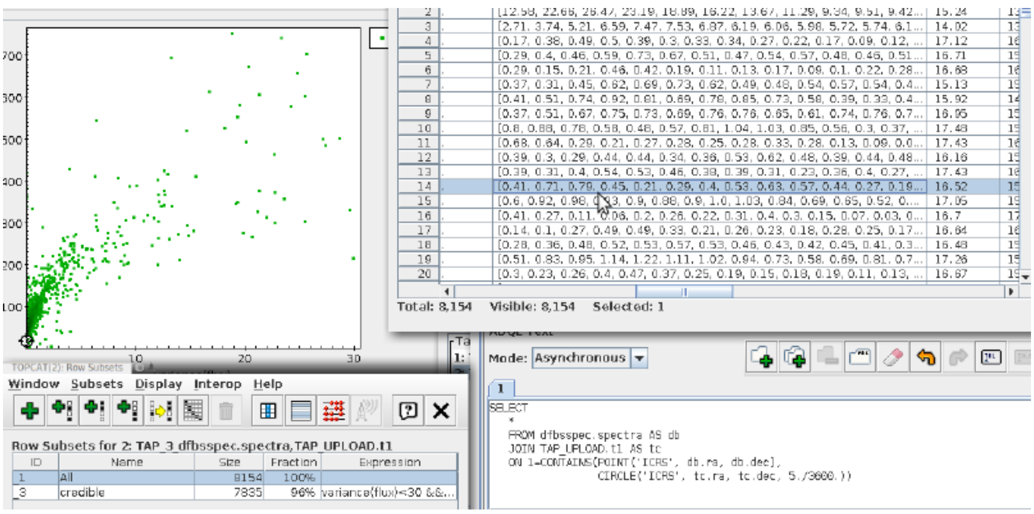

Figure 4. A sample bulk analysis of spectra of Seyfert galaxies in TOPCAT.

Byurakan spectra are also available through TAP services[6]. TAP, the IVOA's Table Access Protocol (Dowler et al., 2015), is a powerful means of performing selection and (to some extent) computation tasks in relational databases under the control of remote users. A full scenario involving outlier analysis has been written in the context of the project reported on here and is available as Demleitner et al. (2019).

A quick illustration of the power of the approach could be an overview of the spectral properties of known Seyfert galaxies as in Fig. 4.

To reproduce this, in TOPCAT, open the TAP window. To obtain a list of Seyfert galaxies, look for Simbad's TAP service and click "Use Service". On Simbad, run a query like

```
SELECT main_id, ra, dec
FROM basic
WHERE otype='Sy2'
  AND dec>-15
```

(the constraint on the declination reflects the DFBS' coverage).

This table can now be matched against the DFBS; to do that, in the TAP window, go back to the service selection tab and look for Byurakan. Select either of the ArVO or GAVO services, click "Use Service" again and locate the DFBS spectra table in the table browser. Select the table dfbsspec.spectra.

With this preparation, TOPCAT can generate an ADQL query performing a join between the local Simbad result and the remote spectra table by clicking on the "Examples" button and choosing Upload/Upload Join. The resulting query could be further edited, but it will work as generated by TOPCAT. Since the upload is relatively large, choose "async" mode before sending off the query.

The result of the query has the spectra DFBS has for the positions given by Simbad for the Seyfert galaxies as arrays in the flux column. A natural analysis might plot `sum(flux)` against `variance(flux)` (these expressions can be entered in the plot fields).

A few very noisy spectra will disturb the plot; to filter them out, create a subset through Views/Row Subsets, using `variance(flux)<30 && sum(flux)>0`. Objects standing out in the resulting plot can then be investigated using the techniques discussed above.

4. Further Work

The data as published could be made even more useful by addressing some open issues.

For one, the DFBS used a number of emulsions, which obviously will influence the shape of the spectra in ways relevant for, for instance, classification tasks. There are 31 different emulsions – most of which are rather similar, though – given in the database. Characterising them better would make global analysis more robust. Taking this endeavour further, a reliable flux calibration might be attempted, potentially using Gaia's RP/BP spectra when these become available; conversely, such a flux calibration might be used to characterise the emulsions, which would be a useful resource with a view to working with scanned plates in general.

For robust classification, estimates of the flux errors would be highly desirable. There are several conceivable paths towards providing such estimates, but all of them require resources beyond the means of our rather modest project. A side benefit of such an endeavour would be that the negative or excessively large fluxes that the extraction pipeline occasionally produced – they are what required the subsetting in the TAP example above – might be remedied.

5. Conclusions

Conclusions projects planning on larger-scale data publications could draw from our experiences include:

[6] `ivo://org.gavo.dc/tap`, `ivo://arvo/tap`

- Avoid proprietary, stand-alone proprietary solutions: They do not age well. Yes, this includes custom-made web pages.
- If you really cannot avoid proprietary code, try to co-locate it with established data centers that will (hopefully) maintain and migrate it as technology evolves.
- Make sure you keep contact with staff operating the machines that publish the data physically; you should always retain an option to access the file system the published data resides on.
- As people leave, make sure there is documentation on the files, tables, and procedures and, probably even more importantly, that someone staying knows where this documentation is.
- Plan upgrades to your data products' metadata and data formats as the relevant standards and practices progress.

Acknowledgements

This work was supported by a joint German-Armenian programme, BMBF FKZ 01DK17055, and the e-inf-astro project, BMBF FKZ 05A17VH2. This work would not have been possible without the help of Marco Molinaro of Trieste Observatory. We thank François Bonnarel for helping us out with the DSS polynomials, which otherwise were hard to locate.

References

Bonnarel F., et al., 2000, Astronomy and Astrophysics Supplement, 143, 33

Calabretta M. R., Greisen E. W., 2002, A&A, 395, 1077

Demleitner M., Neves M. C., Rothmaier F., Wambsganss J., 2014, Astronomy and Computing, 7, 27

Demleitner M. aand Mickaelian A., Knyazyan A., Baghdasaryan D., Mikayelyan G., 2019, Outlier Analysis in Low-Resolution Spectra: DFBS and Beyond, VO Tutorial, doi:10.21938/MxUvKseqU˙gxCwyGocudlg, http://www.g-vo.org/tutorials/dfbs.pdf

Dowler P., Bonnarel F., Michel L., Demleitner M., 2015, IVOA DataLink Version 1.0, IVOA Recommendation 17 June 2015 (arXiv:1509.06152), doi:10.5479/ADS/bib/2015ivoa.spec.0617D

Lang D., Hogg D. W., Mierle K., Blanton M., Roweis S., 2010, AJ, 139, 1782

Lasker B. M., et al., 2008, AJ, 136, 735

Mickaelian A. M., et al., 2007, A&A, 464, 1177

Shupe D. L., Moshir M., Li J., Makovoz D., Narron R., Hook R. N., 2005, in Shopbell P., Britton M., Ebert R., eds, Astronomical Society of the Pacific Conference Series Vol. 347, Astronomical Data Analysis Software and Systems XIV. p. 491

Taylor M. B., 2005, in Shopbell P., Britton M., Ebert R., eds, Astronomical Society of the Pacific Conference Series Vol. 347, Astronomical Data Analysis Software and Systems XIV. p. 29

Tody D., et al., 2012, Simple Spectral Access Protocol Version 1.1, IVOA Recommendation 10 February 2012 (arXiv:1203.5725), doi:10.5479/ADS/bib/2012ivoa.spec.0210T

Tsvetkova K. P., Tsvetkov M. K., 2006, in Tsvetkov M., Golev V., Murtagh F., Molina R., eds, Virtual Observatory: Plate Content Digitization, Archive Mining and Image Sequence Processing. pp 45–53

Asteroid Detection using Machine Learning Algorithm

L.V.R. Chaitanya Prasad[1], T. Anjali Shivani Reddy*[1], and Bhuvaneshwari Kashi[2]

[1]Sreenidhi Institute of Science and Technology, Dept of Electronics and Communications, Telengana, India
[2]CVR College Of Engineering,Dept Of Electronics and Communications, Telengana, India

Abstract

My paper starts from the question many of us wonder 'What if an Asteroid hit Earth? The answer depends on how big an asteroid is in terms of dimension- Let's say an asteroid of baseball ground hits earth, which can completely erase a city. Most of the asteroids are detected by Satellites, Probes and telescopes with large aperture length. Mostly large Telescopes from earth are used for tracking main belt asteroid but what if it gets out of sight from researchers or Scientists; it might take away peoples life. In this paper, I introduced machine learning to detect the asteroid with more than 60 percent of efficiency. The famous Scientist Stephen Hawking wrote in his last book that 'Asteroids are great threatened to the planets'. Machine learning being a one of the best predictive method without explicitly giving any external command. In this paper, I attempt to introduce new machine learning algorithm in the replacement of Astrometrica software with Pan-Starr Telescope real-time Fits file data which is located in Hawaii, USA.

Keywords: *asteroid, astrometrica software, PAN-STAR telescope. machine learning*

1. Introduction to Asteroids

Asteroids are smaller moving objects in space. Every year around thousands of asteroids is entering into earth's orbit apart from meteoroids and comets but only 10-20 we can actually noted. Because many of them evaporate into small particles before reaching the earth. There are different classification of asteroids are done based on composition and their belt orbit- C,S,M based on composition and dark c, bright S, bright M based on their orbit. Some asteroids are found to be in NEO as long as they don't overlap with earth's orbit, we are safe. Most popularly we heard main belt asteroid between planet Mars and Jupiter which has greater probability of entering into earth's atmosphere.

Asteroid impact is one of the reasons for dinosaurs' extinction. They is a theory suggest that a mountain sized asteroid entered into earth atmosphere because of high speed, there was terrible impact on the organisms living on earth. Today in modern world, if an asteroid is detected after danger zone, we still cannot destroy asteroid using any available techniques – for instance if one want to use kinetic method to destroy, it is actually just multiplying own problems or trying with laser might be apt for reasonable size of asteroid but it might not work for huge size asteroid like planetoids. Craters in moon and earth are created by asteroid but if falls in a busy city, and then there will be huge loss to mankind. There are many technologies in use for destruction of these deadly Asteroids but most of the technology must be implemented in space, which is indeed difficult to deal with it. Detecting at first place will be good choice rather than destroying them after reaching the danger zone.

2. Asteroid Detection-current techniques

There are many Satellites and probes in space using a far better image processing to detect asteroid in space. Now a day's people are coming up with the nana satellite and innovative ideas for detection.

*anjalishivani99@gmail.com, Corresponding author

DOI: 10.52526/25792776-2020.67.2-329

Telescopes with large aperture size play prominent role in asteroid detection producing thousands of Fits file. A specific software are used in detecting asteroids from sets.

From my own experience, I got to use one such data in All Indian Asteroid Search Campaign where data is given from international telescope (pan-star) to Researchers, Scientists and common people to discover the asteroid using Astrometrica software by blinking the images the asteroid can be manually detected using brightness and Gaussian curve .

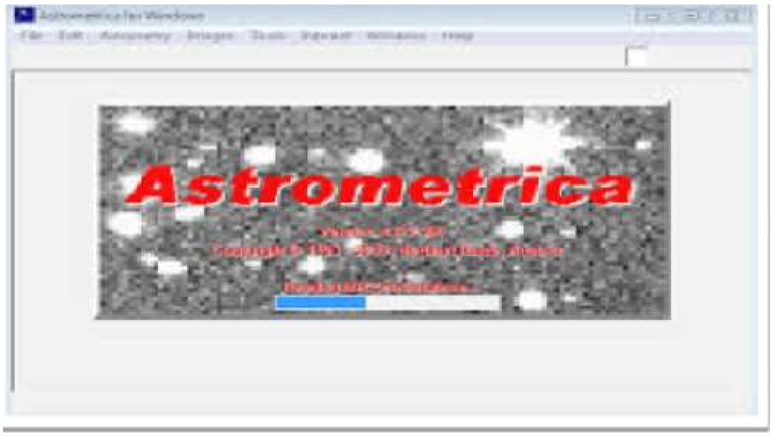

Figure 1. Astrometrica Software

.

Fits files are accessed from IAISC Website and each set consists of four fits files. These are reduced in size to perform blink operation.

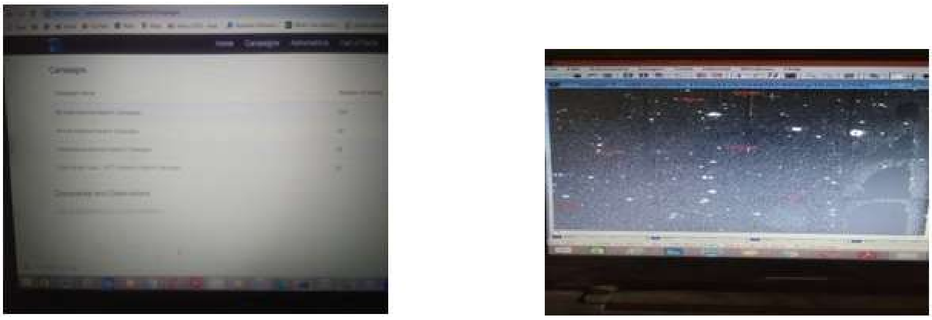

Figure 2. Left panel: Fits file download; right panel: Features of Astronomica

.

Fits files are accessed from IAISC Website and each set consists of four fits files. These are reduced in size to perform blink operation. Using blinking the images the pattern is predicted and named and report is generated as shown. The data can be reduced into required size and converted into pixels from inbuilt feature of software or using python. Reduced data takes any 9 stars as reference from 200 to 400 catalog stars as shown.

3. Replacement of Convenient method of detection with machine learning

Always there may not be possibility of recognizing the asteroid with human eye but machine learning with good test code can actually ease the detection with more efficiency.

Machine learning can be implemented with many software like R, JavaScript but I choose Python with pandas, nunpy,matpy libraries with one more important astronomical library 'astropy' to work on fits file. Anaconda with python 3.7.1 version jupyter notebook i will be further working to obtain the same result as Astrometrica report. Installation pip and following libraries are done in jupyter notebook. Data reduction is performed using numpy and reduced data is displaced by matpy as shown

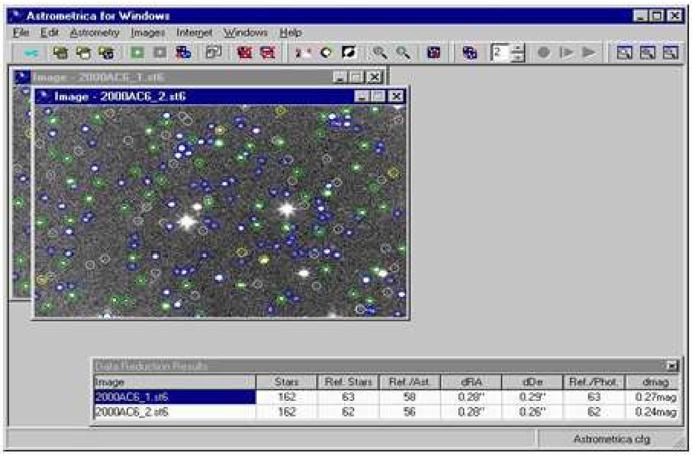

Figure 3.
.

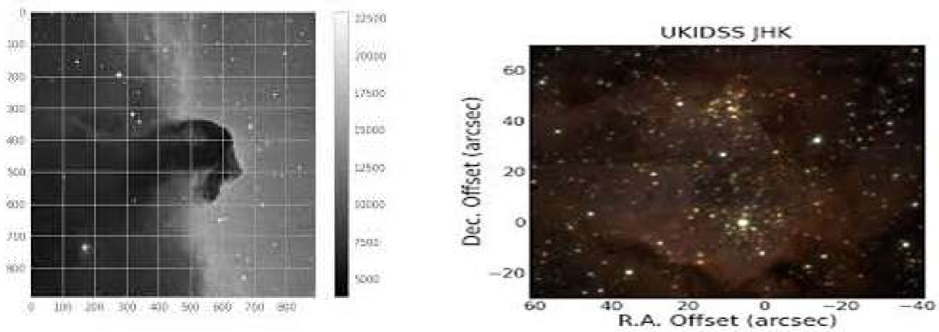

Figure 4.
.

4. Detection of Asteroid and stars

Stars and Asteroids are detected as point source rejecting the fussy type sources using photometry libraries in python. For instance, I used DAO star Finder Algorithm to write the object coordinate system and flux and using numpy the data can be stored in word document.

5. Machine learning Algorithm Implementation

The data with same flux are considered and using machine learning, they are points which form linear equation at least with three data points out of four are named as asteroid. Here a new machine learning algorithm is used to form linear equation based on test data with various cases.

6. Results and Conclusion

Output is verified from overlapping predicted values to original values in graph form as shown.

Here I used 500 data sets to recheck with the prediction and two real time data to verify the asteriods, which it is taking minitues to give predict the asteriods where as in Astrometrica software it takes days and months to detect asteriods. Machine learning technique is indeed useful for this application This paper mostly concentrated on different approach of detecting asteroid including the magnitude classification and convolution method in detail. I conclude that convolution method has high efficiency.

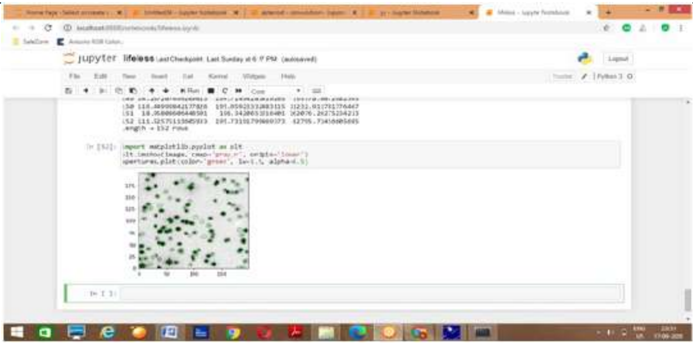

Figure 5.

.

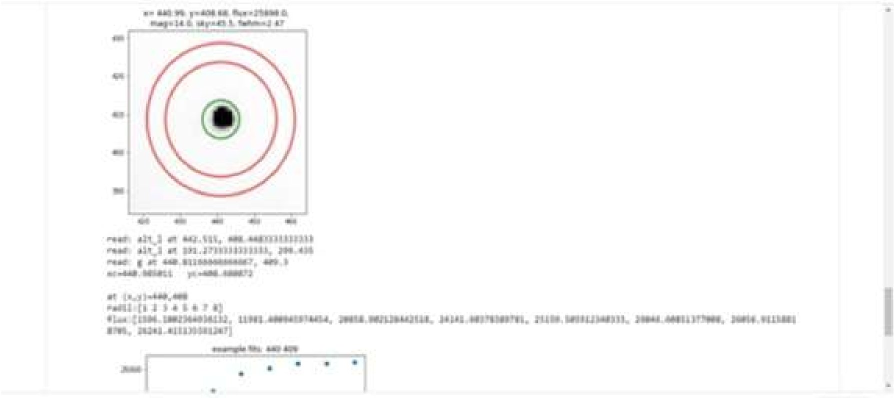

Figure 6.

.

7. Future Scope

One can easily implement this method of prediction with knowledge of python and libraries. Though it requires too much of test data, On positive note: There are many websites data are available like zoo universe. Even one can approach by contacting any receiving telescope ground station

I think more efficiency can be increased by taking Gaussian curve into consideration and latency can be reduced. I am continuing my work further. I will be coming up more efficient algorithm.

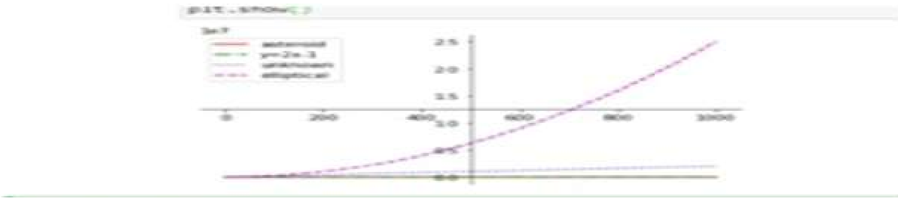

Figure 7.

.

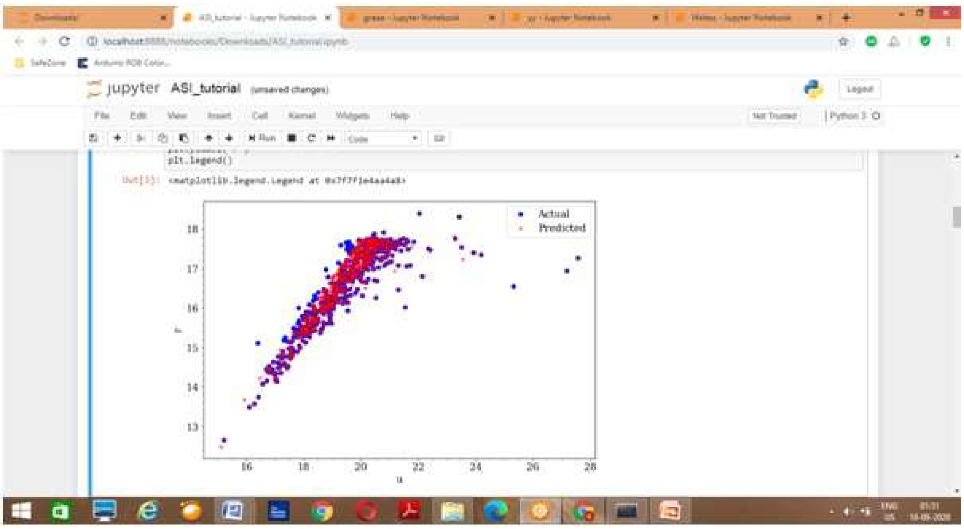

Figure 8.

.

References

1. Asteroid. NASA – Jet Propulsion Laboratory. Retrieved 13 September 2010.

2. Frequently Asked Questions (FAQs) – What Are Asteroids And Comets? CNEOS. Archived from the original on 9 September 2010. Retrieved 13 September 2010.

3. What is the difference between an asteroid and a comet?Cool Cosmos. Infrared Processing and Analysis Center. Retrieved 13 August 2016.

4. Jump up to Rubin, Alan E.; Grossman, Jeffrey N. (January 2010). "Meteorite and meteoroid: new comprehensive definitions". Meteoritic and Planetary Science. 45 (1): 114–122. Bib code: 2010MPS...45..114R. doi:10.1111/j.1945-5100.2009.01009.x.

5. Atkinson, Nancy (2 June 2015). What is the difference between asteroids and meteorites?. Universe Today. Retrieved 13 August 2016.

6. Britt, Robert Roy (4 February 2005). Closest Flyby of Large Asteroid to be Naked-Eye Visible. SPACE.com.

7. Jump up to: Latest Published Data". International Astronomical Union Minor Planet Center. Retrieved 11 March 2020.

8. United Nations General Assembly proclaims 30 June as International Asteroid Day. United Nations Office for Outer Space Affairs (Press release). 7 December 2016. UNIS/OS/478.

9. International cooperation in the peaceful uses of outer space. United Nations. Rapporteur: Awale Ali Kullane. 25 October 2016. Retrieved 6 December 2016.

Communications of BAO, Vol. 67, Issue 2, 2020, pp. 335-337

Infrared study of IRAS 18316-0602 star-forming region

Andreasyan D.[*], Azatyan N, Nikoghosyan E., Harutyunian H., and Baghdasaryan D.

Byurakan Astrophysical Observatory, Aragatsotn region, Byurakan vil., Armenia

Abstract

We present the results of the investigation of ISM and the young stellar population in the IRAS 18316-0602 star-forming region which is referred to as UC HII (G25.65+1.05). Single temperature modified blackbody model shows that values of N(H_2) hydrogen column density and T_d dust temperature are in ranges $2\text{-}7 \times 10^{23}\,\text{cm}^{-2}$ and 12 - 30 K, respectively. The analysis of infrared photometric data allowed to reveal about 50 young stellar objects in the G25.65+1.05 UC HII region.

Keywords: *stars: pre-main sequence – infrared: stars – radiative transfer – ISM: hydrogen column density, dust temperature*

1. Introduction

IRAS 18316-0602 (also known as G25.65+1.05 UC HII region) is associated with an irregular compact radio source, first identified at 3.6 cm by Kurtz et al. (1994). The radio peak is coincident with an unresolved infrared (IR) source, identified as a young B1V star with large K band excess (Zavagno et al., 2002). Based on the CO observations, Shepherd & Churchwell (1996) detected an energetic bipolar outflow centred on the radio source. It is also closely associated with NH_3 emission (Molinari et al., 1996) and strong CH_3OH (Szymczak et al., 2000) and H_2O maser (Kurtz & Hofner, 2005) emissions. The distance to the source is an open question. Molecular line observations in most cases argue in favor of the near kinematic distance ∼3.17 kpc (Molinari et al., 1996). In contrast, HI self-absorption toward the source suggests a far kinematic distance of 12.5 kpc (Green & McClure-Griffiths, 2011).

IR study of the star-forming region in G25.65+1.05 was carried out in two main directions: determination of ISM physical parameters (hydrogen column density (N(H_2)) and dust temperature (T_d), as well as the identification of the young stellar population in this region.

2. Method

To obtain the physical parameters like N(H_2) and T_d, the thermal emission from cold dust lying in the *Herschel* FIR optically thin bands (160–500 μm) can be used (Battersby et al., 2011, Hildebrand, 1983). For this task, Level 2.5 processed *Herschel* images were used. The initial processing of the images was carried out with HIPE software. To obtain the N(H_2) and T_d, we used the modified single-temperature blackbody fitting which was subsequently carried out on a pixel-by-pixel basis using the following formula:

$$S_\nu = B_\nu(\nu, T_d)\Omega(1 - e^{-\tau(\nu)}), \tag{1}$$

with

$$\tau(\nu) = \mu_{H_2} m_H k_\nu N(H_2), \tag{2}$$

where ν is the frequency, $S_\nu(\nu)$ is the observed flux density, $B_\nu(\nu, T_d)$ is the Planck function, T_d is the dust temperature, Ω is the solid angle in steradians from where the flux is obtained, $\tau(\nu)$ is the optical

[*]derenik@bao.sci.am, Corresponding author

DOI: 10.52526/25792776-2020.67.2-335

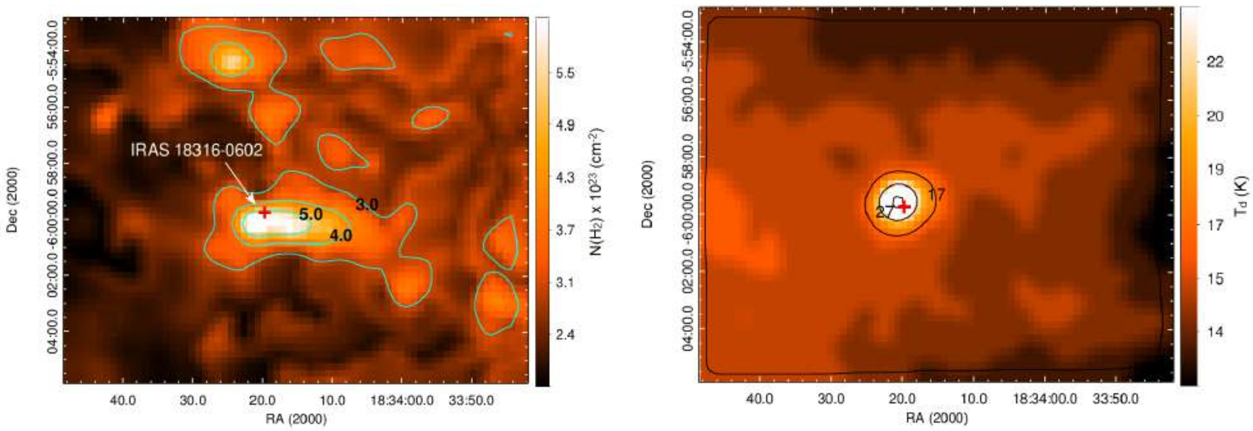

Figure 1. Maps of N(H_2) (left panel) and T_d (right panel) of the region surrounding G25.65+1.05 UC HII object. On the N(H_2) map, the isodenses corresponding to the values of $3.0\times10^{23}\,cm^{-2}$, $4.0\times10^{23}\,cm^{-2}$, and $5.0\times10^{23}\,cm^{-2}$ are shown. On the T_d map, isotherms corresponding to the values of 17 K and 27 K are shown. The positions of IRAS 18316-0602 are marked by crosses.

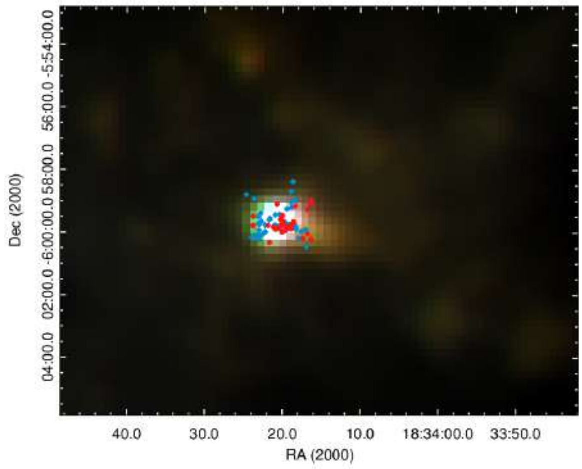

Figure 2. Distribution of YSOs in the region on *Herschel* 500 μm image. Class I and Class II objects are indicated by filled red and blue circles, respectively.

depth, μ_{H_2} is the mean molecular weight (adopted as 2.8 here), m_H is the mass of hydrogen, k_ν is the dust opacity, and $N(H_2)$ is the hydrogen column density. For opacity, we adopted a functional form of $k_\nu = 0.1(\nu/1000\,GHz)^\beta\,cm^2g^{-1}$, with $\beta = 2$ (Hildebrand, 1983). For each pixel, equation (1) was fitted using the four data points (160, 250, 350, and 500 μm) keeping T_d and N(H_2) as free parameters.

For the search, identification, and classification of the young stellar population of the UC HII region, we used their NIR (UKIDSS), MIR (*Spitzer*, WISE), and FIR (*Herschel*) photometric data. When selecting potential members of the cluster from stars located in the direction of the molecular cloud, we proceeded from the assumption that the overwhelming majority of the members of the considered star-forming region are young stellar objects (YSO). According to the star formation theory, the IR excess of YSOs is caused by a circumstellar disk and gas-dust envelope, which are known as the main characteristics of YSOs (Hartmann, 2009, Lada & Lada, 2003). Therefore, according to the IR excess, it is possible to carry out the selection of Class I and Class II evolutionary stage YSOs. One of the most powerful tools for identifying YSO candidates via IR excess is their location on color-color (c-c) diagrams. The choice of colors depends on the available data.

3. Results and Conclusion

The $N(H_2)$ and T_d of the wider region surrounding G25.65+1.05 UC HII region are shown in Figure 1. We can see that the column density distribution has three, well distinguished concentrations. In general, within UC HII region the column density varies from $\sim 3.0 \times 10^{23}$ to $7.0 \times 10^{23}\,\mathrm{cm}^{-2}$, which corresponds to the values of $N(H_2)$ in other UC HII regions (Churchwell et al., 2010). The T_d distribution has spherical symmetry. It decreases from the center to the periphery, from 30 K to 15 K. The maxima of both density and temperature coincide with the position of the IRAS source.

The search, identification, and classification of the young stellar population of the molecular cloud using their NIR, MIR, and FIR photometric data was based on one of the main properties of young stars, namely the IR excess due to the presence of circumstellar disks and envelopes. In total, relative to the stellar objects' position in the c-c diagrams, we managed to identify 69 YSOs with different evolutionary stages (Class I and II). The YSOs are located directly in the vicinity of IRAS 18316-0602, forming a young stellar cluster.

The results obtained undoubtedly create a prerequisite for further detailed studies of this star-forming region.

Acknowledgements

The authors are grateful to the organizers for holding the International Symposium "Astronomical Surveys and Big Data 2" and for publishing the paper.

References

Battersby C., et al., 2011, , 535, A128

Churchwell E., Sievers A., Thum C., 2010, A&A, 513, A9

Green J. A., McClure-Griffiths N. M., 2011, MNRAS, 417, 2500

Hartmann L., 2009, Astrophysics and Space Science Proceedings, 13, 23

Hildebrand R. H., 1983, QJRAS, 24, 267

Kurtz S., Hofner P., 2005, AJ, 130, 711

Kurtz S., Churchwell E., Wood D. O. S., 1994, ApJS, 91, 659

Lada C. J., Lada E. A., 2003, ARA&A, 41, 57

Molinari S., Brand J., Cesaroni R., Palla F., 1996, A&A, 308, 573

Shepherd D. S., Churchwell E., 1996, ApJ, 472, 225

Szymczak M., Hrynek G., Kus A. J., 2000, A&AS, 143, 269

Zavagno A., Deharveng L., Nadeau D., Caplan J., 2002, A&A, 394, 225

Runaway stars in Vel OB1 association

N. Azatyan*[1], L. Kaper[2], D. Guo[2], and E. Nikoghosyan[1]

[1]Byurakan Astrophysical Observatory, 0213, Aragatsotn prov., Armenia
[2]Astronomical Institute "Anton Pannekoek" and Center for High-Energy Astrophysics, University of Amsterdam, Kruislaan 4003, 1098 SJ Amsterdam, The Netherlands

Abstract

We present the origins of two runaway stars in the Vel OB1 association using *Gaia* proper motions and parallaxes. Proper motions and parallaxes show that mentioned two runaways came out from Vel OB1 association: one of them, namely CD-41 4637 is the result of dynamical interaction in its host cluster and Vela X-1 high-mass X-ray binary became a runaway after supernova explosion.

Keywords: *stars: early type stars – stars: binary stars – Open clusters and associations: Vel OB1 – stars: mass loss – individual: Vela X-1, CD-41 4637*

1. Introduction

The two most popular scenarios to explain the existence of runaway stars and their high velocity are: (1) the supernova of the companion star in a massive binary (Blaauw, 1961) and (2) the dynamical ejection from a young cluster in the early stages of evolution (Poveda et al., 1967).

Vel OB1 is one of the largest OB associations known at a distance of 1.5-1.9 kpc (Bassino et al., 1982, Humphreys, 1978, Sahu, 1992). Humphreys (1978) derived angular extent of Vel OB1 (l=262° to 268°, b=-2.°7 to +1.°4) and 17 probable members. Reed (2000) extant the size of the association (l=255° to 275°, b=-5° to +5°) and the probable members of Vel OB1 up to 70 stars.

Vela X-1 (also V*GPVel, HD77581 and HIP44368) high-mass X-ray binary (HMXB) is a short-period (8.96 d; Forman et al., 1973) and low-eccentricity (e≈0.09; Bildsten et al., 1997) eclipsing binary system composed of a blue supergiant star (B0.5 Ia; Hiltner et al., 1972) of mass of $\approx 24\,M_\odot$ and a neutron star of mass of $\approx 1.9\,M_\odot$ (the most massive neutron star known to date; Koenigsberger et al., 2012). The distance is estimated of 2.4 kpc from the *Gaia* second data release (DR2) (Bailer-Jones et al., 2018).

CD-41 4637 is massive star binary with one unresolved companion and spectral type of the brightest component is O6 Ib(f)(n) (Aldoretta et al., 2015). The distance estimate by *Gaia* DR2 is 2.89 kpc (Bailer-Jones et al., 2018).

The identification of the "parent" OB association of a runaway is important because it provides unique constraints on its evolution. The purpose of this study is to understand from which part of the Vel OB1 association the stars were kicked out and what was the reason.

2. Results and Discussions

We used the proper motions and positions of *Gaia* DR2 (Gaia Collaboration et al., 2018) for runaways and all individual members of Vel OB1 association to trace back in time to determine the location of the closest encounter and the time that has passed since that event: the kinematic age. Figure 1 shows the small part of Vel OB1 association in Equatorial coordinates, the current location of Vela X-1 and CD-41 4637 runaway stars and their possible origins.

*nayazatyan@bao.sci.am, Corresponding author

DOI: 10.52526/25792776-2020.67.2-338

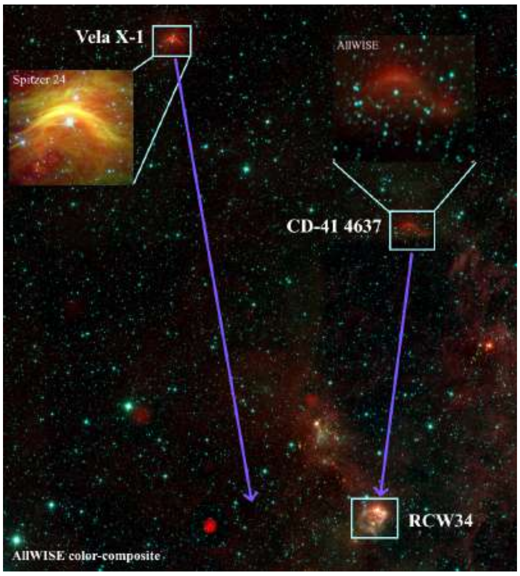

Figure 1. AllWISE color-composite image of Vel OB1 association, the current location of Vela X-1 and CD-41 4637 runaway stars and their possible origins in Equatorial coordinates.

Constructed path of Vela X-1 HMXB over 5 Myr did not provide any information about its parent star cluster although the binary system was kicked out Vel OB1 less than 3 Myr ago (van Rensbergen et al., 1996). The search for the origin of Vela X-1 runaway must be continued further.

Constructed path of CD-41 4637 over 5 Myr shows that CD-41 4637 is supposed to have come out of the RCW 34 HII region 2 Myr ago. Since the age of the RCW 34 HII region is also estimated to be 2 Myr (Bik et al., 2010), then one can supposed there was a dynamic interaction between the members of HII region and in the result CD-41 4637 left the birthplace.

3. Conclusions

Using the proper motions and positions of *Gaia* DR2 (Gaia Collaboration et al., 2018) for Vela X-1 and CD-41 4637 runaway stars and members of Vel OB1 association, we trace back in time to determine their origin. Constructed path of Vela X-1 HMXB confirmed that the binary system was kicked out from Vel OB1 less than 3 Myr ago although the search for the origin of Vela X-1 runaway must be continued further. According to the constructed path of CD-41 4637, we assume that it have came out of the RCW 34 HII region 2 Myr ago after dynamic interaction between the members of HII region.

Acknowledgements

The authors thanks to the organizers for the opportunity to take a part in International conference 'Astronomical Surveys and Big Data 2'

References

Aldoretta E. J., et al., 2015, AJ, 149, 26

Bailer-Jones C. A. L., Rybizki J., Fouesneau M., Mantelet G., Andrae R., 2018, AJ, 156, 58

Bassino L. P., Dessaunet V. H., Muzzio J. C., Waldhausen S., 1982, MNRAS, 201, 885

Bik A., et al., 2010, ApJ, 713, 883

Bildsten L., et al., 1997, ApJS, 113, 367

Blaauw A., 1961, BAN, 15, 265

Forman W., Jones C., Tananbaum H., Gursky H., Kellogg E., Giacconi R., 1973, ApJ, 182, L103

Gaia Collaboration et al., 2018, A&A, 616, A1

Heydari-Malayeri M., 1988, A&A, 202, 240

Hiltner W. A., Werner J., Osmer P., 1972, ApJ, 175, L19

Humphreys R. M., 1978, ApJS, 38, 309

Koenigsberger G., Moreno E., Harrington D. M., 2012, A&A, 539, A84

Poveda A., Ruiz J., Allen C., 1967, Boletin de los Observatorios Tonantzintla y Tacubaya, 4, 86

Reed B. C., 2000, AJ, 119, 1855

Sahu M. S., 1992, PhD thesis, Kapteyn Institute, Postbus 800 9700 AV Groningen, The Netherlands

van Rensbergen W., Vanbeveren D., De Loore C., 1996, A&A, 305, 825

Communications of BAO, Vol. 67, Issue 2, 2020, pp. 341-343

Detailed Studies of Radiogalaxy Mrk1032

Hakopian S.A.*[1], Dodonov S.N.†[2], and Andreasyan R.R.‡[1]

[1]V.Ambartsumian Byurakan Astrophysical Observatory (BAO), Armenia
[2]SpecialAstrophysical Observatory(SAO), Russia

Abstract

The first results of the observations of Mrk1032, conducted with the 6-m telescope of SAO Russia, are given. It is shown, in particular, that a large complex of HII-regions, revealed by the integral−field spetroscopy, is the main source of UV radiation in the galaxy.

Keywords: *3D−spectroscopy: Hα-emission: HII−regions: − objects: Mrk1032.*

1. Introduction

The first publication on the object Mrk1032 (PGC008924) appeared as the manifestation of it as a "UV−excess" galaxy through the conducting of the First Byurakan Survey, FBS, (Markarian et al., 1979). The object of about 16m(pg) apparent magnitude and 9"x7" size received survey classification ds3e:. It was noted, herewith, that the west component of an interacting pare was implied, which denoted A on Fig.1 with the image from DSS. The only available optical spectrum of Mrk1032 has been obtained through the follow-up spectroscopy with 70−cm telescope, which showed emission in Balmer Hα, and two forbidden lines of ionized nitrogen at λ6584 and sulfur at λ6731 (Denisiuk & Lipovetskii, 1984).The very first observations of Mrk1032 conducted with RATAN radiotelescope (Sanamian & Kandalian, 1968) revealed radioemission. Further observations (Maehara et al., 1985) and publications confirmed that the "UV-excess" Mrk1032 is a radiogalaxy too.This became the basis for attributing to the galaxy the AGN nature of presumably Sy2 type.

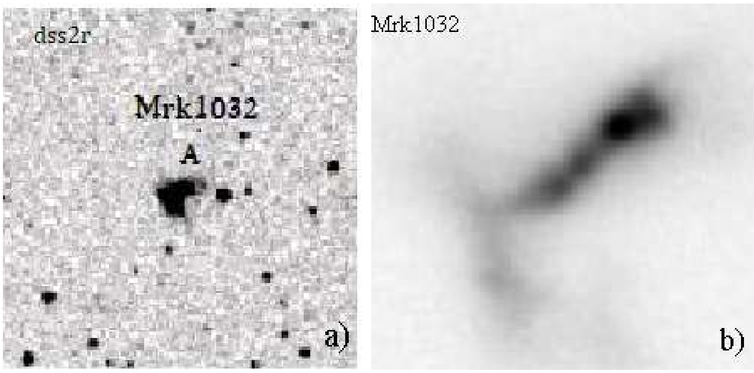

Figure 1. Image of Mrk1032: a) from DSS2r, b) from PANSTARRS red.

.

Due to the "high degree of UV-excess (H)" the object was included in the KISO survey catalog (Takase & Miyauchi-Isobe, 1984) too, with morphological classification "Pair of interacting galaxy (Pi)". Cross-identifications between different surveys show sources associated with the object in GALEX, 2MASSXJ, IRAS, GAIA, NVSS and other surveys, from ultraviolet to radio. An image from the PanSTARRS survey, shown in Fig.1b, is the most detailed for now.

*susannahakopian@yahoo.com, Corresponding author
†dodo@sao.ru
‡randrasy@bao.sci.am

DOI: 10.52526/25792776-2020.67.2-341

2. Results of integral-field spectroscopy of Mrk1032

Aimed at detailed investigations of the galaxy we have undertaken its observations with the 6−m telescope of SAO of Russia using the MPFSpectrograph (http://www.sao.ru/hq/lsfvo/index.html). Some results from the provided integral-field spectroscopy are presented below. Fig.2 contains: main information on the mode of observations, field of view as smoothed pixels of intensities summarized over the whole registered spectral range and the spectrum obtained in the pixel, where an intensity in Balmer Hα line, I(Hα)max, has peak value. What is evident from the profiles of the most intense lines present in the spectrum, namely Hα and the forbidden doublets of nitrogen [NII]6548,6584 and sulfur [SII]6717,6731, is that the processes ongoing in Mrk1032 are not of AGN nature, but have a starburst activity. In correspondence to our scheme of activity classification (Hakopian, 2013) the object is of star−forming type galaxy in nebular phase (SfGneb).

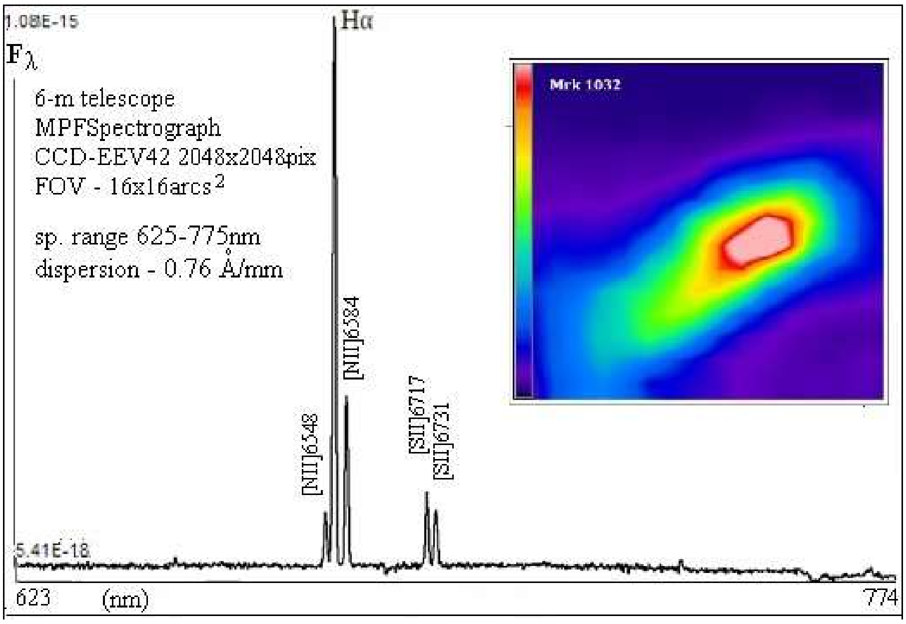

Figure 2. General data on the mode of observations, FOV and the spectrum in the pixel I(Hα)max.

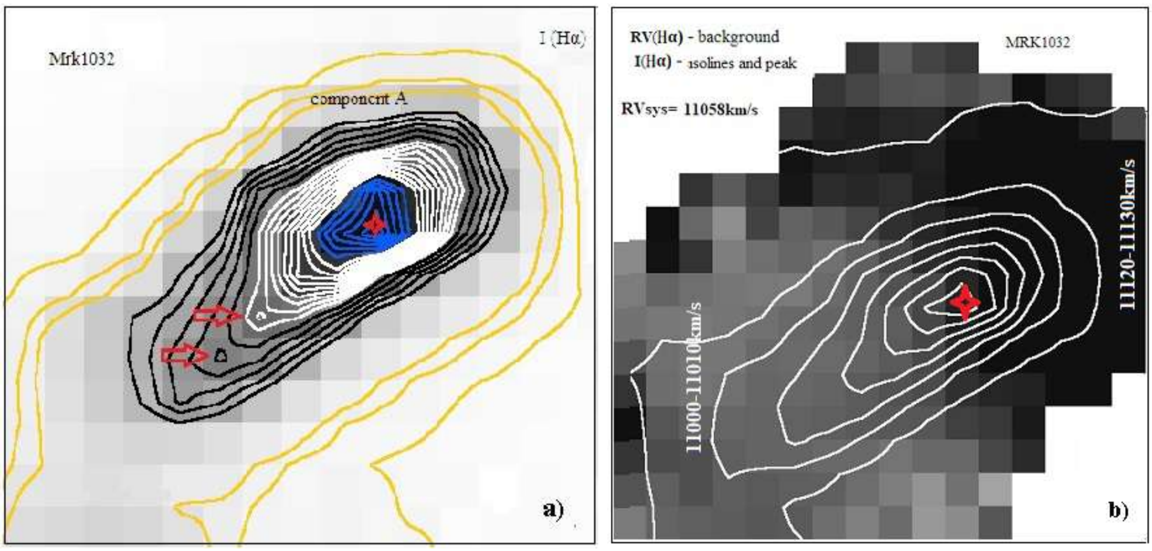

Figure 3. a)Hα−intensity distribution over the entire FOV; b)Hα radial velocities across the main part of the FOV with some numerical data.

Surface distribution of Hα−emission, first of all, allowed to reveal HII−regions of a galaxy directly connected to star−formation processes. Fig.3 illustrates the observed for Mkn1032 FOV as a gray scaled background with superimposed isolines, both reflecting Hα − line intensities. Two small HII−regions with centers indicated by arrows, and a large HII−zone with the peak intensity pixel I(Hα)max marked by a cross, are differentiated. On the whole their locations repeat positions of condensations, which are visually differentiated from the given on Fig.1b image. Herewith, upon removal from the peak I(Hα)max the shapes and different gradients of the isolines, as seen on Fig.3a, indicate that the large HII−zone is not monosyllabic. The same conclusion is drawn from the analysis of the velocity field.

Fig.3b gives distribution of radial velocities RV(Hα) as background gradations with superimposed Hα − isolines.The values of systemic velocity, obtained for the cross marked pixel of peak Hα-intensity and the values averaged over two border areas are also given. A sharp transition from the smaller values of RV(Hα) to the larger ones is visually seen on this map due to changing in the background gradations reflecting them. Passing through the marked peak its trajectory divides the HII−zone into two parts and evidences the presence of at least a double structure aligned along the line of sight.

3. Conclusions

These are the first results from our observations of Mrk1032, still incomplete, but giving answers to the two remaining open questions.

First, the object is not a galaxy of Sy2 type, which follows from the spectral line profiles. According to our classification scheme, this is a star-forming galaxy in the nebular phase, SfGneb.

Second, that the eastern tail of the object is too diffuse and has not enough dense structural features to be considered as a separate component. The distribution over the whole field of the galaxy in the continuum, having only one peak, confirms it.

Thus, the Mrk1032 is not doubled, not interacting, but a galaxy of irregular morphology. A large complex of HII-regions in its west part, originally designated A, is the main source of its UV radiation.

References

Denisiuk E. K., Lipovetskii V. A., 1984, Astrofizika, 20, 525D

Hakopian S. A., 2013, arXiv:1403.0127,

Maehara H., Inoue M., Takase B., et al. 1985, PASJ, 37, 451M

Markarian B. E., Lipovetskii V. A., Stepanian D. A., 1979, Astrofizika, 13, 397M

Sanamian V. A., Kandalian R. A., 1968, Astrofizika, 4, 129A

Takase B., Miyauchi-Isobe N., 1984, AnTok, 192, 595T

Multiple asteroid systems from the UkrVO digitized photographic plates

Kazantseva L*[1] and Shatokhina S†[2]

[1]Taras Shevchenko National University of Kyiv, Ukraine, Kyiv, Ukraine
[2]Main Astronomical Observatory of the NAS of Ukraine, Kyiv, Ukraine

Abstract

Several catalogs of various celestial objects were compiled based on the processing of Ukrainian VO archives and observatories in Kitab (Uzbekistan) and Baldone (Latvia). We analyzed the catalogs of asteroid positions and B-magnitudes obtained from the processing of digitized photographic plates and selected from them asteroids, which are known as multiple. Positional observations cover the period 1973-1993 and may be useful for a more detailed study of the dynamics of these systems. The obtained photometric characteristics of asteroids will be useful for studying changes in brightness.

Keywords: *Double asteroids, positional catalog, digitized photographic observations*

1. Introduction

The first observations indicating the possible presence of satellites in asteroids were obtained in 1977 (visual observation of stellar occultation of minor planet 6 Hebe) and 1978 (photometric light curve observation of asteroid 532 Herculina). But in the absence of other observational evidence, the existence of multiple asteroids and asteroids with satellites remained likely until space missions. Since then, the search for asteroid multiplicity by various methods (Hubble Space Telescope, observations with ground-based telescopes, radar, etc.) has begun.

As of October 2020, 416 such celestial bodies are already known (Johnston (2018)). 42 of them were detected from ground-based observations, 97 from space-based surveys, 49 by radar, 227 from the analysis of photometric curves. These are 400 double systems, 15 triple. Also recently, this group of objects includes a sextuple system of Pluto. In total, these small bodies have 435 satellites. According to the types of orbits, they are divided into near-Earth (78), main-belt asteroids (187), those that cross the orbit of Mars (31), the Trojan asteroids of Jupiter (6), and trans-Neptune (114). Also, among them, there is 1 object with rings and 1 object with signs of a double comet.

But the main feature of this extremely interesting new group of celestial bodies is that they are still insufficiently studied. According to the type and level of confirmation, only 48 of them are currently available for observation, 27 already have certain parameters, 126 are considered confirmed, and 215 are still probable.

Therefore, any new observational data on these objects is very important extensive work on the processing of photographic plates, obtained in 1969-1995, was carried out by MAO NASU (Vavilova et al. (2012)) in cooperation with the observatories participating in the Northern Sky Survey (FON) project.

*kazantsevaliliya1@gmail.com, Corresponding author
†svetash@mao.kiev.ua

DOI: 10.52526/25792776-2020.67.2-344

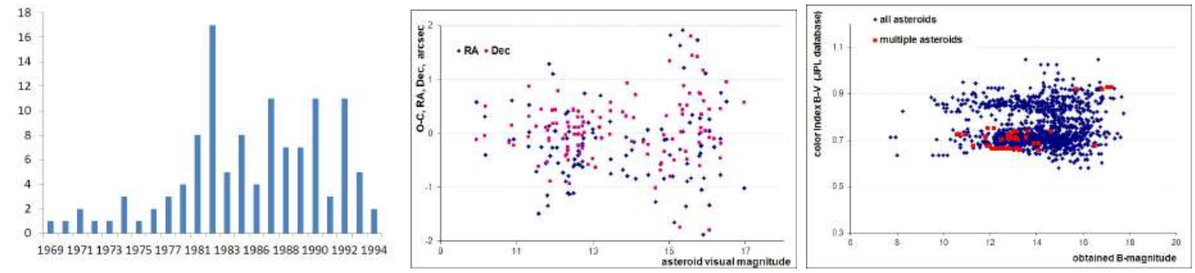

Figure 1. Distributions of selected multiple asteroids by observation time (left), by coordinate differences O-C (in the middle) and B-magnitudes in comparison with all identified asteroids from FON-Kyiv part of the project

2. Main results

Several catalogs of coordinates and B-magnitudes for more than 32 million stars and galaxies have been created based on the processing of Kyiv and Kitab digitized observations of the FON project (Andruk et al. (2016), Andruk et al. (2017), Yuldoshev et al. (2018), Yuldoshev et al. (2019)). Becides, a few catalogs of coordinates and B-magnitudes of asteroids and comets were compiled based on these data (Shatokhina et al. (2018b), Shatokhina et al. (2018a),Shatokhina et al. (2019)). A preliminary catalog of asteroid positions and magnitudes was compiled based on digitized observations of the open star clusters in UBVR color bands obtained at the Baldone observatory (Latvia) in 1967-1995 (Eglitis et al. (2019)).

The coordinates determined in the Tycho-2 reference system, and the B-magnitudes are obtained in the system of photoelectric standards. Digitization of photographic plates was carried out using $Epson^{TM}$ and $Microtek^{TM}$ commercial scanners, with scanning mode - 1200 dpi, linear image size 30x30 cm or 13000x13000px.

We have analyzed 5020 positions of asteroids on digitized observations of the Kyiv and Kitab parts of the FON project and 1872 previous positions in UBVR spectral bands on digitized observations in Baldone. As a result, 119 positions were selected for 69 asteroids, which are multiple asteroid systems or asteroids with companions according to the databases (http://cbat.eps.harvard.edu/minorsats, http://www.johnstonsarchive.net/astro/asteroidmoons). Most of them belong to the main belt asteroids, three of them belong to the Jupiter Trojans family, 4 are Mars crossers and 1 are near- Earth object. According to these data, positions were obtained from observations of the period 1969-1994. The all positions were compared with the JPL ephemeris and the O-C differences calculated, shown in Fig. 1. The figure also shows the obtained B-magnitudes of multiple asteroids depending on their color indices in comparison with all identified asteroids from the FON-Kiev part of the project. Both bright asteroids and faint ones were selected. Given that the average positional accuracy of determining coordinates and B-values for bright $11-13^m$ is twice better than for faint $11-16^m$ asteroids (Shatokhina et al. (2018a)), this may be essential for determining some kinematic and photometric characteristics these asteroids.

3. Conclusion

From catalogs of asteroid positions and magnitudes based on the processing of digitized photographic observations of the FON project and the Baldone archive we selected and analyzed 119 positions and magnitudes of multiple asteroid systems. Considering that this group of multiple asteroids has not been sufficiently studied, any of their positional observations can be useful for studying the dynamics of their systems. And the magnitudes obtained simultaneously with their coordinates can be used to construct and analyze the light curves and other photometric characteristics of these asteroids.

References

Andruk V. M., Pakuliak L. K., Golovnia V. V., et al. 2016, Kinem. Phys. Cel. Bodies, 32, 260

Andruk V. M., Pakuliak L. K., Golovnia V. V., et al. 2017, VizieR Online Data Catalog, p. I/342

Eglitis I., Yizhakevych O., Shatokhina S., et al. 2019, Odessa Astron. Publ., 32, 189

Johnston W., 2018, NASA Planetary Data System,

Shatokhina S. V., Relke H., Yuldoshev Q., et al. 2018a, Odessa Astron. Publ., 31, 235

Shatokhina S. V., Kazantseva L. V., Yizhakevych O. M., et al. 2018b, Kinem. Phys. Cel. Bodies, 34, 270

Shatokhina S. V., Kazantseva L. V., Yizhakevych O. M., et al. 2019, VizieR Online Data Catalog (other), 0030, J/other/KFNT/34

Vavilova I. B., Pakulyak L. K., Shlyapnikov A. A., et al. 2012, Kinem. Phys. Cel. Bodies, 28, 85

Yuldoshev Q. X., Ehgamberdiev S. A., Muminov M. M., et al. 2018, VizieR Online Data Catalog, p. I/346

Yuldoshev Q., Protsyuk Y., Relke H., et al. 2019, Astron. Nachr., 340, 494

Stellar spectra analysis of giant stars: ARCTURUS

Maria Rah*[1,2]

[1]National Astronomical Observatories and Key Laboratory of Computational Astrophysics, Chinese Academy of Sciences, 20A Datun Rd., Chaoyang District, Beijing 100101, China
[2]Research Institute for Astronomy and Astrophysics of Maragha, Iran

Abstract

In this study, we analyzed the evolved red giant ARCTURUS using high-resolution spectroscopy that was taken by HARPS. The other names of this star is α Boo – Arcturus – HR 5340 – HD 124897 – HIP 69673. This evolved ($\log g = 1.66$ dex) star shows low metallicity nature ([Fe/H] = -0.52) which could be employed to study the chemical evolution of the early universe.

Keywords: *stars: abundances—stars: atmospheres—stars*

1. Introduction

The fourth brightest star in the Northern Hemisphere Arcturus will die as a white dwarf. This constellation Boötes member has a stellar mass of $1.08\,M_{\odot}$, luminosity in about $\sim 170\,L_{\odot}$, and age of 7.1 Gyr (Mardini et al., 2019a,b, Masda et al., 2019, Taani et al., 2019b,c). Astronomers believe that Arcturus show high enhancements in the α elements (e.g., C, O, Ne, Mg, Si) relative to iron ([α/Fe] $> +0.4$ dex). This peculiarity in Arcturus atmospheric chemical abundances suggests that it could be a direct descendant of the Population III stars. Therefore, detailed chemical abundances analysis of this astrophysical interesting object might help to constraint it origin (Abdusalam et al., 2020, Mardini. et al., 2019c, Mardini et al., 2020, Placco et al., 2020, Taani et al., 2019a, 2020).

2. Analysis and some results

Firstly, we downloaded the archived spectrum HARPS. This spectrum has very high resolution (R= 40,000), signal-to-noise ratio (S/N = 600 at 4500 Å), and wide wavelength coverage (λ = 4100-6000 Å). Taking advantage of this spectrum, we derived the basic stellar parameters: effective temperature (Teff= 4286 ± 30), surface gravity ($\log g = 1.66 \pm 0.05$) and metallicity ([Fe/H]= -0.52 ± 0.04) using ATLAS_SYNTHE software. In the second step, we have modeled our target star for which you can find the comparison of the final model with the observational flux in Figure 1.

We then have plotted the H_{α} line for the models which are different just in one basic stellar parameter, to show the modifications of the models in terms of these changes. As you can see in Figure 2, we have shown the modifications of metallicity versus the temperature in three models, and the effects of temperature and the gravity on the depth of lines.

In the next steps, we plan to provide an accurate atmospheric abundance for 17 light elements; from Oxygen to Zinc. We expect that ARCTURUS atmospheric chemical composition should be consistent with its kinematics (thick-disk star). Collectively, this study tries to improve our understanding of ARCTURUS atmospheric chemical composition that is more important as a differential analysis scale. These parameters and the chemical abundances are typical for the study of the nature and structure of our Galaxy; having accurate stellar parameters and chemical composition of red giant stars, provide useful information about the astrophysical condition that lead to the born of these stars.

*mariarah.astro@gmail.com

DOI: 10.52526/25792776-2020.67.2-347

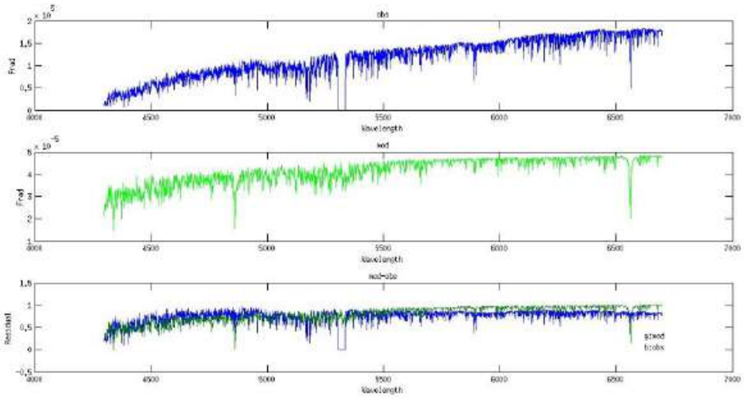

Figure 1. The Comparison of the final model with the observational flux

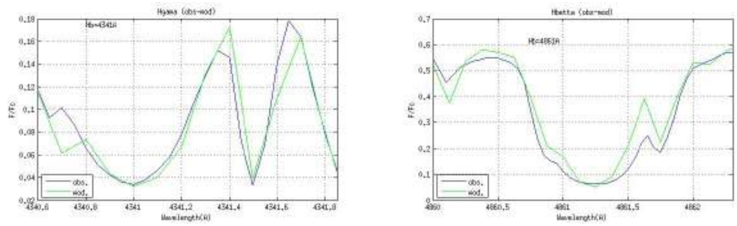

Figure 2. An illustrative example of the effect of modifying metallicity and temperature. These effects can be seen by the depth of lines.

References

Abdusalam K., Ablimit I., Hashim P., Lü G. L., Mardini M. K., Wang Z. J., 2020, Astrophys. J., 902, 125

Mardini M. K., et al., 2019a, The Astrophysical Journal, 875, 89

Mardini M. K., Placco V. M., Taani A., Li H., Zhao G., 2019b, The Astrophysical Journal, 882, 27

Mardini. M. K., Ershiadat N., Al-Wardat M. A., Taani A. A., Özdemi S., Al-Naimiy H., Khasawneh A., 2019c, in Journal of Physics Conference Series. p. 012024 (arXiv:1904.09608), doi:10.1088/1742-6596/1258/1/012024

Mardini M. K., et al., 2020, arXiv e-prints, p. arXiv:2009.12142

Masda S. G., Docobo J. A., Hussein A. M., Mardini M. K., Al-Ameryeen H. A., Campo P. P., Khan A. R., Pathan J. M., 2019, Astrophysical Bulletin, 74, 464

Placco V. M., Santucci R. M., Yuan Z., Mardini M. K., Holmbeck E. M., Wang 2020, Astrophys. J., 897, 78

Taani A., Karino S., Song L., Al-Wardat M., Khasawneh A., Mardini M. K., 2019a, Research in Astronomy and Astrophysics, 19, 012

Taani A., Abushattal A., Mardini M. K., 2019b, Astronomische Nachrichten, 340, 847

Taani A., Karino S., Song L., Mardini M., Al-Wardat M., Abushattal A., Khasawneh A., Al-Naimiy H., 2019c, in Journal of Physics Conference Series. p. 012029, doi:10.1088/1742-6596/1258/1/012029

Taani A., Khasawneh A., Mardini M., Abushattal A., Al-Wardat M., 2020, arXiv e-prints, p. arXiv:2002.03011

Communications of BAO, Vol. 67, Issue 2, 2020, pp.349-350

The Early-phase Distribution of the Milky Way Using K-giant Stars From LAMOST DR5

Ali Taani *

Physics Department, Faculty of Science, Al-Balqa Applied University,Jordan

Abstract

With the advent of large astronomical surveys, the need of identification of the most interesting astrophysical object is required. In this work we focus on extracting red giant metal-poor stars from the LAMOST DR5. We then query the 5-D space coordinates from the *Gaia* DR2 to investigate their energy-action space. This sample will be used for studying the chemical and dynamical evolution of the early galactic phase. Also, identifying stars with kinematical similarities would enable us to trace the galactic assembly.

Keywords: Galaxy: halo– stars: kinematics and dynamics–galaxies: structure

1. large data surveys

The next wave of astronomical surveys will substantially increase the number of observed stars in the Milky Way (Mardini et al., 2019b, Mardini. et al., 2019c, Masda et al., 2019, Taani et al., 2019a,b,c, 2020). Part of the challenge is how to efficiently select the most exciting targets for spectroscopic to follow-up, especially when dealing with photometric surveys, where all the information on physical parameters and chemistry of stars is encoded in their observed colors. The immediate future involve (i) identification of low-metallicity star candidates from photometry and low/medium resolution spectroscopy, (ii) high-resolution spectroscopic follow-up to determine detailed chemical abundance patterns, (iii) compare observations with results from theoretical and computational models, and v) computationally tracing the kinematic history and orbital evolution of these stars with Gaia data (Abdusalam et al., 2020, Mardini et al., 2019a, Mardini et al., 2020, Placco et al., 2020).

Large data surveys usually provide low-resolution ($R \simeq 400$) spectra that can be used to examine the strength of the CaII K line and thus obtain a first estimate of the metal content of the star. However, some surveys provided mixture resolution (low and medium-resolution). The Large Sky Area Multi-Object Fiber Spectroscopic Telescope (LAMOST) survey is a example of such surveys. In its all phases (pilot survey + six years surveys) provided spectra for 8,966,416 stars.

The HK survey and the Hamburg/ESO (HES) survey are other surveys of this low-resolution surveys, that were prolific sources of metal-poor stars. The HK-II survey aimed at identifying the metal-poor red giant cool stars that may have been missed in the original analysis due to the temperature bias against cool stars. It allowed to raise the efficiency of the HK survey to detect metal-poor stars from 11 to 32 %.

Application of mathematical clustering algorithms to the space of orbital energies and other suitable dynamical parameters will result in stars being grouped based on the similarity of their orbits around the Galaxy. Identification of dynamically tagged groups in large catalogs of very metal-poor will provide another means to identify their likely progenitor environments.

We applied some sophisticated cuts on the fifth data release of the Large Sky Area Multi-Object Fibre Spectroscopic Telescope (LAMOST DR5) to efficiently select, astrophysically important, K-giants stars. We queried in about 2000 stars. Further, we crossed-match the LAMOST K-giant sample

*ali.taani@bau.edu.jo

DOI: 10.52526/25792776-2020.67.2-349

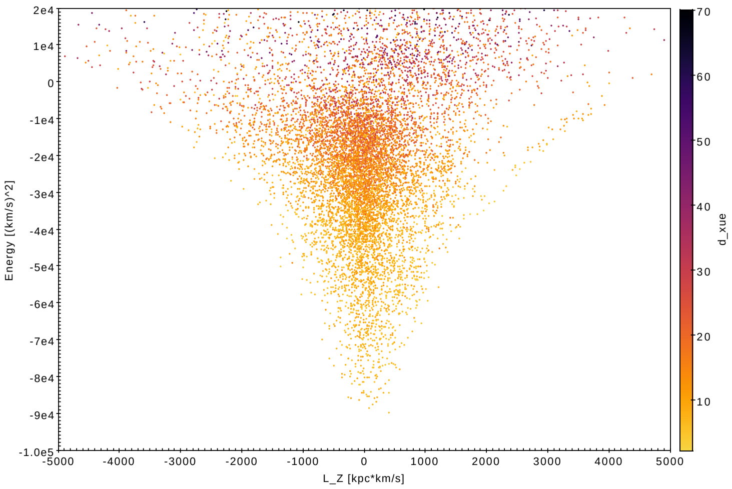

Figure 1. The distribution of K-giant stars (2000) adopted from LAMOST DR5 in the energy-action space. Color-coded by their spectroscopic metallicities [Fe/H].

with the second Gaia data release to query full 6 dimensional phase-space coordinates. Actions and total orbital energy were calculated with galpy using the 'MW- Potential2014' potential (see Figure 1).

2. Future Recommendation/work

In future work we will identify potential dynamical groups in our sample. These groups are crucial for the study of the galactic assembly. We expect to determine the role of K-giant stars as tracers of the dynamical evolution of the Milky Way.

Acknowledgements

This work has made use of data from the European Space Agency (ESA) mission *Gaia* (https://www.cosmos.esa.int/gaia), processed by the *Gaia* Data Processing and Analysis Consortium (DPAC, https://www.cosmos.esa.int/web/gaia/dpac/consortium). Funding for the DPAC has been provided by national institutions, in particular the institutions participating in the *Gaia* Multilateral Agreement.

References

Abdusalam K., Ablimit I., Hashim P., Lü G. L., Mardini M. K., Wang Z. J., 2020, Astrophys. J., 902, 125

Mardini M. K., et al., 2019a, The Astrophysical Journal, 875, 89

Mardini M. K., Placco V. M., Taani A., Li H., Zhao G., 2019b, The Astrophysical Journal, 882, 27

Mardini. M. K., Ershiadat N., Al-Wardat M. A., Taani A. A., Özdemi S., Al-Naimiy H., Khasawneh A., 2019c, in Journal of Physics Conference Series. p. 012024 (arXiv:1904.09608), doi:10.1088/1742-6596/1258/1/012024

Mardini M. K., et al., 2020, arXiv e-prints, p. arXiv:2009.12142

Masda S. G., Docobo J. A., Hussein A. M., Mardini M. K., Al-Ameryeen H. A., Campo P. P., Khan A. R., Pathan J. M., 2019, Astrophysical Bulletin, 74, 464

Placco V. M., Santucci R. M., Yuan Z., Mardini M. K., Holmbeck E. M., Wang 2020, Astrophys. J., 897, 78

Taani A., Karino S., Song L., Al-Wardat M., Khasawneh A., Mardini M. K., 2019a, Research in Astronomy and Astrophysics, 19, 012

Taani A., Abushattal A., Mardini M. K., 2019b, Astronomische Nachrichten, 340, 847

Taani A., Karino S., Song L., Mardini M., Al-Wardat M., Abushattal A., Khasawneh A., Al-Naimiy H., 2019c, in Journal of Physics Conference Series. p. 012029, doi:10.1088/1742-6596/1258/1/012029

Taani A., Khasawneh A., Mardini M., Abushattal A., Al-Wardat M., 2020, arXiv e-prints, p. arXiv:2002.03011

From Evolved Stars to the Formation and Evolution of NGC 6822

Sima Taefi Aghdam*[1], Elham Saremi[1], and Atefeh Javadi[2,1]

[1]School ofAstronomy, Institute for Research in Fundamental Sciences (IPM), P. O. Box. 19395-5531, Tehran, Iran
[2]Department of Physics, Sharif University of Technology, P. O. Box 11365-9161, Tehran, Iran

Abstract

NGC 6822, an isolated dwarf irregular galaxy (dIrr), due to close distance, apparent isolation, and easy observation, has been always selected as a desired candidate for studying star formation and galactic evolution, without the strong gravitational influences of other systems. To derive the SFH of NGC 6822, the method mentioned by Javadi et al. (2011) is used which is based on theoretical models coupled with color-magnitude diagrams (CMDs) by using directly the long period variable (LPV) stars which are mostly asymptotic giant branch (AGB) stars at their very late stage of evolution, as well as more massive red super-giant (RSG) stars according to their significant role to study the star formation rate (SFR). To calculate the SFH in the bar of the galaxy, we use more than 600 LPV stars from different catalogs of variable stars that two of the most important are Whitelock et al. (2013) and Letarte et al. (2002) that they reported the main part of the LPVs and the Carbon stars, respectively, Patrick et al. (2015) announced the RSG stars. Understanding the star formation history of NGC 6822 plays an important role in comparing the galaxy history evolution with other nearby dwarf galaxies as well as studying the nature of the evolving population of galaxies which were detected in deep redshift surveys.

Keywords: *stars: variables: AGB; stars: carbon; galaxies: distances and redshifts; galaxies: individual: NGC 6822; (galaxies:) Local Group: Dwarf Irregular; infrared: stars*

1. Introduction

In the recent decade, attention to dwarf galaxies has been increased as a special tool to understand the galaxy evolution of the different morphological types of dwarf galaxies. NGC 6822, due to close distance to us and apparent isolation, has been always selected as a desired candidate for studying star formation and galactic evolution, without the strong gravitational influences of other systems (Battinelli et al., 2006). AGB stars are helpful tracers for the properties of a galaxy. They illustrate the old- and intermediate–age population (between 1 and several Gyr), whose period is mainly between 100 up to 1500 days (Goldman et al. 2019). Understanding the star formation history (SFH) of NGC 6822 plays an important role in comparing the NGC 6822 history evolution with other nearby dwarf galaxies (Saremi et al., 2019, 2020).

2. Data

The confirmed long period variable (LPV) stars, red super-giant (RSG) candidates, and Carbon stars (C-type), expected to be LPVs, are selected from a number of published catalogs. In 2002, Letarte et al. used the CN–TiO technique and they found 904 C-type stars that 539 stars are in the galaxy bar. Kacharov et al. (2011) and Sibbons et al. (2015), by studying the spectral type, classified some of the AGB stars that many of them were common with C-stars confirmed by Letarte et al. (2002). Whitelock et al. (2013) selected 3 overlapping fields of a bar of NGC 6822 for monitoring in

*aylin.t.aghdam@gmail.com

DOI: 10.52526/25792776-2020.67.2-351

3.5 years, thus they identified 61 Mira LPVs and some long amplitude variable (LAV) stars. Battinelli & Demers (2011) used an area in the eastern spheroid of NGC 6822 and they reported some of cyclic and semi-regular variables in this galaxy; twenty of variables are located within the optical bar of galaxy which are often common with Whitelock Group data. The RSG stars in the NGC 6822 are identified by Massey et al. (2011) and Patrick et al. (2015) with spectroscopically confirmation.

3. Method

In this section, we use the method mentioned by (Javadi et al., 2011) that is based on initial mass function (IMF), introduced by Kroupa (2001), coupled with color-magnitude diagram (CMD) of galaxy by using directly the LPV stars. In this method, fitting of the theoretical isochrones are used, since it allows us to obtain stellar ages and star formation rate (SFR) which they are in preferable agreement with the observational data. There are some steps to study the SFH which are the individual mass, age (look-back time, t), and pulsation duration of the LPV stars must be determined. Meanwhile, the most desirable models to satisfy our purpose are those theoretical models from the Padova group (Marigo et al., 2017). Investigating the SFR and the used method were explained thoroughly in Hamedani Golshan et al. (2017), Hashemi et al. (2017), Javadi et al. (2011, 2017, 011b), Rezaei Kh et al. (2014), Saremi et al. (2017, 2019, 2020).

4. Discussion and On-going Work

The SFH of NGC 6822 will be presented by using LPV stars as a tracer of the SFH of the galaxy. Figure 1, left panel, shows the CMD which is over-plotted isochrones by Marigo et al. (2017) with a distance modulus of 23.51 ± 0.051 mag and interstellar extinction of $A_V = 0.77$ (Whitelock et al., 2013), and also Z = 0.0007 based on the result of Fusco et al. (2014), who is reported in a range of $0.0001 < Z < 0.01$.

We have calculated the mass of detected stars for 3 metallicities by using IMF mentioned by Kroupa (2001) which is shown in figure 1, right panel. It is understood that most of the stars whose mass investigated in a range of $log\,(M/M_\odot) = -0.1$ to 0.5, are $log\,(t) = 10.2$ to $8.4yr$. These stars are detected as LPV, LAV, extreme-AGB (x-AGB), C- and S-type stars.

In the following, we are going to report the SFH of the galaxy for various metallicities and discuss about the role of stellar feedback and its effect on SFR of the isolated galaxy, NGC 6822.

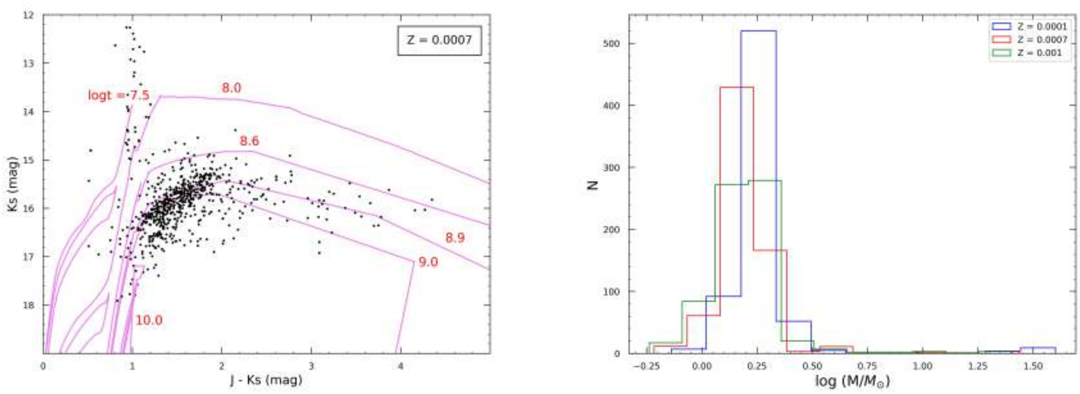

Figure 1. Left panel: overplotted CMD with isochrones at Z = 0.0007. Right panel: calculated mass of detected stars with theoretical isochrones in 3 different metallicities

.

References

Battinelli P., Demers S., 2011, A & A, 525, A69

Battinelli P., Demers S., Kunkel W., et al. 2006, A & A, 451, 99

Fusco F., Buonanno R., Hidalgo S. L., et al. 2014, A & A, 572, A26

Goldman S. R., Boyer M. L., McQuinn K. B. W., et al. 2019, ApJ, 877, 49

Hamedani Golshan R., Javadi A., van Loon J. T., et al. 2017, MNRAS, 466, 1764

Hashemi S. A., Javadi A., van Loon J. T., et al. 2017, MmSAI, 88, 436

Hashemi S. A., Javadi A., van Loon J. T., 2018, MNRAS, 483, 4751

Hashemi S. A., Javadi A., van Loon J. T., et al. 2019, IAUS, 344, 77

Javadi A., van Loon J. T., Mirtorabi M. T., 2011, MNRAS, 414, 3394

Javadi A., van Loon J. T., Khosroshahi H. G., et al. 2017, MNRAS, 464, 2103

Javadi A., van Loon J. T., Mirtorabi M. T., 2011b, ASPC, 445, 497

Kacharov N., Rejkuba M., Cioni M.-R. L., 2011, A & A, 537, A108

Kroupa P., 2001, MNRAS, 322, 231

Letarte B., Demers S., Battinelli P., et al. 2002, Astron. J., 123, 832

Marigo P., Girardi L., Bressan A., et al. 2017, ApJ, 835, 77

Massey P., Olsen K. A. G., Hodge P. W., et al. 2011, Astron. J., 141, 28

Patrick L., Evans C. J., Davies B., et al. 2015, ApJ, 803, 14

Rezaei Kh S., Javadi A., Khosroshahi H., et al. 2014, MNRAS, 445, 2214

Saremi E., Javadi A., van Loon J. T., et al. 2017, J. Phys. Conf. Ser, 869, 012068

Saremi E., Javadi A., van Loon J. T., et al. 2019, IAUS, 344, 125

Saremi E., Javadi A., van Loon J. T., et al. 2020, ApJ, 894, 135

Sibbons L. F., Ryan S. G., Napiwotzki R., et al. 2015, A & A, 574, A102

Whitelock P., Menzies J., Feast M., et al. 2013, MNRAS, 428, 2216

Communications of BAO, Vol. 67, Issue 2, 2020, pp. 354-358

Deep Convolutional Neural Networks models for the binary morphological classification of SDSS-galaxies

Vasylenko M.[*1,2], Dobrycheva D.[†1], Khramtsov V.[‡3], and Vavilova I.[§1]

[1]Main Astronomical Observatory the National Academy of Sciences of Ukraine, Kyiv, Ukraine
[2]Institute of Physics of the National Academy of Sciences of Ukraine, Kyiv, Ukraine
[3]Institute of Astronomy, V. N. Karazin Kharkiv National University, Kharkiv, Ukraine

Abstract

We present the deep learning approach for the determination of morphological types of galaxies. We demonstrate the method's performance with the redshift-limited ($z < 0.1$) training sample of 6 163 galaxies from the SDSS DR9. We exploited the deep convolutional neural network classifiers such as InceptionV3, DenseNet121, and MobileNetV2 to process images of SDSS-galaxies (100x100 pixels, 25 arcsec in each axis in size) using g, r, i filters as $R - G - B$ channels to create images. We provided the data augmentation (horizontal and vertical flips, random shifts on ± 10 pixels, and rotations) randomly applied to the set of images during learning, which helped increase the classifier's generalization ability. Also, two different loss functions, MAE and Lovasz-Softmax, were applied to each classifier. The target sample galaxies were classified into two morphological types (late and early) trained on the images of galaxies from the sample. It turned out that the deep convolutional neural networks InceptionV3 and DenseNet121 with MAE-loss function show the best result attaining 93.3% accuracy.

Keywords: *Galaxies, galaxy morphology, machine learning methods*

1. Introduction

The morphological classification of galaxies is one of the critical elements in studying the evolution of the Universe for astrophysics and observational cosmology. The most accurate method of classifying galaxies used so far by astronomers is visual classification. In 1654, Giovanni Battista Hodierna published the work "On the taxonomy of the world of comets and magnificent objects in the sky", in which one of the parts was devoted to the classification of nebulae into three classes: "Luminosae", "Nebulosae" and "Occultae" (Fodera-Serio et al. (1985)). A century later, Charles Messier compiled a larger list of nebulae, star clusters, and galaxies without classifying them. After confirming that some nebulae are "outer" galaxies, Edwin Hubble proposed his famous morphological classification of galaxies into three classes: elliptical, spiral, and irregular (Hubble (1926)). This classification is still used with many refinements made by Gerard Henri de Vaucouleurs and other scientists. However, a main drawback of visual classification (human labeling) is an involvement of many labor from highly qualified specialists or, in some cases, amateur astronomers (for example, the Galaxy Zoo project[1]). Current or future galaxy surveys such as SDSS (Blanton et al., 2017, Eisenstein et al., 2011), LSST (Ivezić et al., 2017), DES (Dark Energy Survey Collaboration et al., 2016), KiDS (de Jong et al., 2017), etc. can detect hundreds of millions of galaxies that cannot be manually classified. This increases interest in the alternative approach in artificial intelligence, such as various recently developed machine learning methods for automated morphological classification of galaxies in optical, radio, and other

*vasmax@mao.kiev.ua, Corresponding author
†daria@mao.kiev.ua
‡vld.khramtsov@gmail.com
§irivav@mao.kiev.ua
[1]http://data.galaxyzoo.org

DOI: 10.52526/25792776-2020.67.2-354

spectral ranges. There is probably not a day without an article about machine learning techniques for different astrophysical tasks.

In previous our research with traditional machine learning methods, we have discovered relationships between the photometric parameters of galaxies and their morphological types, which give the opportunity to classify galaxies without preliminary visual inspection (Dobrycheva & Melnyk, 2012, Dobrycheva et al., 2015, Melnyk et al., 2012). As a result, we conducted ternary and binary morphological classification of the low-redshift SDSS galaxies. We demonstrated (Dobrycheva et al., 2017, 2018, Vasylenko et al., 2019, Vavilova et al., 2020) that the Random Forest (RF) and Support Vector Machine (SVM) with Scikit-learn machine learning in Python provide the highest accuracy for the binary galaxy morphological classification: 96.4% correctly classified (96.1% early E and 96.9% late L types) and 95.5% correctly classified (96.7% early E and 92.8% late L types), respectively. We had a good experience with such methods as the decision-tree-based classifiers likely CatBoost for searching new gravitationally lensed quasars (Khramtsov et al., 2019b), generative adversarial networks (GAN) for restoring the Zone of Avoidance (Vavilova et al., 2018), machine-learning regression techniques (linear, polynomial, k-nearest neighbors, gradient boosting, and artificial neural network regression) for inference of moduli distances to galaxies (Elyiv et al., 2020), Xception Convolutional Neural Network (CNN) model to classify morphological galaxy inner features (**?**).

It allowed us to reveal problem points of methods, to build the prediction model, and to surely apply the supervised learning technique as deep convolutional neural networks for the automated morphological galaxy classification, which will be described in this article.

2. Sample

Target sample. We emphasize that, unlike most other authors, we paid attention to the visual cleaning of the dataset (see details (Dobrycheva, 2013)). Our target dataset contains of N = 316 031[2] SDSS-galaxies from DR9 (Ahn et al., 2012) with unknown morphological types at redshift $z < 0.1$ with the absolute stellar magnitudes $-24^m < M_r < -13^m$ limits $m_r < 17.7$ by visual stellar magnitude in r-band to avoid typical statistical errors in spectroscopic flux.

Training sample. Any supervised machine learning method (SMLM) needs a representative training sample because SMLM is searching for a relationship between input and output data. The accuracy of SMLM strictly depends on the training sample's quality. Our first step before applying the machine learning methods was to compose a training sample (Fig.1)

With this aim, we made visual binary morphological classification of 6 163 galaxies ($\sim 2\,\%$ of the target sample), which were randomly selected at different redshifts and with different luminosity: early type galaxies E – from ellipticals to lenticulars ($N = 4\,147$); late type galaxies L – from $S0a - Sdm$ to irregular Im/BCG galaxies ($N = 2\,016$) in slightly modified de Vaucouleurs classification.

Parameters for Deep Learning (DL) methods. We processed the SDSS-galaxy's images that are 100x100 pixels, or 25 arcsec in each axis in size. We used g, r, i filters with SDSS as $R - G - B$ channels to create images.

3. Methods and Results

We analyzed the classification quality of different Deep Convolutional Neural Networks models for the binary morphological classification of galaxies (spiral and elliptical) to reveal their problems. The non-triviality and relevance of this task is that for the training of models, we use a relatively small sample of images (6 163 images of SDSS-galaxies), which imposes restrictions on the assessment of the quality of models and their further operation. This challenge provoked us to use several well-known techniques: image augmentation (horizontal and vertical flips, random shifts on ±10 pixels, and rotations within 180 degrees), splitting training data into training and test samples. As the neural network models, we used InceptionV3, DenseNet121, and MobileNetV2. To train the models, we divided the input sample of 6 163 objects into two parts: $\sim 90\,\%$ (5 545 images) as a training and

[2]http://leda.univ-lyon1.fr/fG.cgi?n=hlstatistics&a=htab&z=d&sql= iref=52204

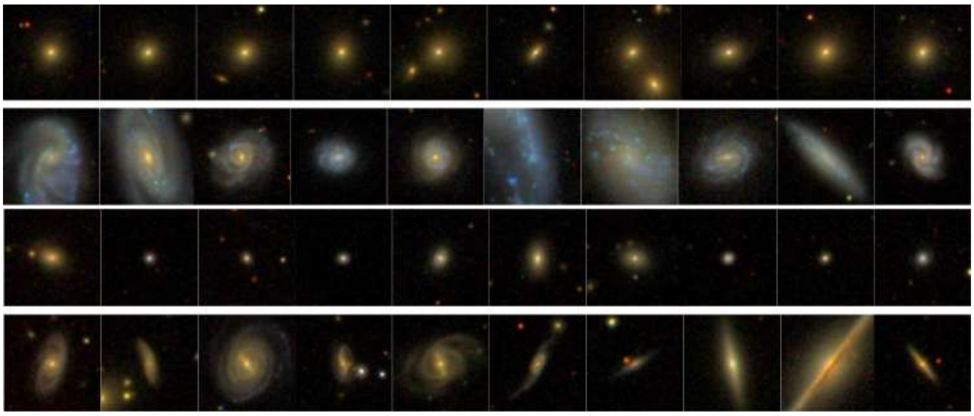

Figure 1. (Top figure) Representative galaxy sample with rival probabilities; top row: Ellipticals with DL, Spirals with SVM; bottom row: Ellipticals with SVM, Spirals with DL. (Bottom figure) Representative galaxy sample with reliable DL classification; top row: Ellipticals; bottom row: Spirals (Khramtsov et al., 2019a)

$\sim 10\,\%$ (618 images) as a validation. However, to better control the models' generalizing capabilities, we conducted a 5-fold cross-validation, in which a sample of 5 545 images were divided into 5 parts. We drove five exercises of each of the models on 4/5 of all 5 545 images (4 436 images) and tested on 1/5 of all 5 545 images (1 109 images), where different test samples were used during each training. As a result, we obtained five implementations trained on different subsets of 5 545 images for each of the models. The resulting classification algorithm for each model is the averaged one of the predicted classes by all five implementations.

We showed that the highest accuracy in the validation sample was attained with InceptionV3 ($> 92.0\,\%$) and DenseNet model ($> 93.0\,\%$), where the accuracy depends on the loss function. Table 1 shows that Mean Absolute Error (MAE) is the best for the InceptionV3 and DenseNet models as a loss function. One can see that, in this case, the accuracy of the test and training samples is practically coincided, and we can say that our models are not overfitted. We also tried to develop an unsupervised learning neural network representing each image as only a few dozen numbers. We hoped that galaxies of different types would be in different areas of the created space, but this method was not implemented with such high classification accuracy as the conventional Deep Convolutional Neural Networks.

DenseNet121. This neural network's feature is that each layer is connected to each subsequent layer, which allows to learn deeper and more accurate models. Before transmission, the features are not summed but combined into one tensor (channel-wise concatenation). Also, the number of parameters of this network is much smaller than that of networks with the same accuracy, which increases the classifier's accuracy on small data sets relative to other networks (Huang et al. (2017)).

InceptionV3. The fundamental difference from other networks lies in several features. Neighboring pixels are often correlated so you can reduce the dimension before the convolution without losing information, so the 5x5 convolution is replaced by two consecutive non-linearly connected 3x3, which in turn are collapsed into a vector $1\mathrm{x}n$. Besides, a hybrid scheme is used, namely, the pool operation is applied to half of the parameters and the convolution to the other. This operation will compress the previous layer without reducing the number of features, some convolutions will be processed with half the resolution but with fewer features. The network will learn to share, which requires maintaining the resolution, and for which the pool is enough. Also, this network feature is that the last layers become wider after reducing the dimension, which allows the network to increase the effectiveness of training in the place where training is the most effective (Szegedy et al. (2015)).

MobileNetV2. The peculiarity of this network is that it does not use max pooling-layers. Instead, it uses a convolution with a coke equal to two. Hyperparameters for MobileNet are the width factor and the depth factor. The width factor is responsible for the number of channels in each layer, and the depth factor is responsible for the size of the tensors fed to the input. Varying these parameters, we choose the optimal network size and image processing depth to optimize the ratio of execution

Table 1. Accuracy of the classification depending on the type of neural network and loss function

Model	**Loss function**	**Accuracy on the validation sample (618 images)**	**Accuracy of 5-fold cross-validation on the training sample (6 163 images)**	**Accuracy on the training sample (6 163 images)**
InceptionV3	MAE	93.3 %	94.2 %	94.3 %
InceptionV3	$Lovasz-Softmax$	92.2 %	93.9 %	94.2 %
MobileNetV2	MAE	89.7 %	89.9 %	89.2 %
MobileNetV2	$Lovasz-Softmax$	89.9 %	90.4 %	90.8 %
DenseNet121	MAE	93.3 %	94.2 %	94.3 %
DenseNet121	$Lovasz-Softmax$	93.0 %	94.1 %	94.0 %

time, resources spent, and the classifier's obtained accuracy (Howard et al. (2017)).

Loss function determines the model's ability to predict and quantifies the difference between the calculated and true values for a data sample. This function is used to maximize the quality of the classifier by minimizing the value of this function. We have anticipated that our model may contain emissions (damaged images). By this reason we chosen the mean absolute error (MAE) as one of the variants of the loss function. We remind that MAE is the sum of the absolute differences between our target and predicted values. It copes well with the averaging of results and is less sensitive to emissions. Its disadvantage is that this function's gradient remains constant even for its small values and it does not differentiate at zero. Additionally, we used the Lovasz-Softmax loss function, which showed good results for classifying segmented images (Berman et al. (2018)).

4. Conclusion

In this way, we determined the data classification algorithm, the model training strategy, and the models themselves that should be used to attain the highest accuracy. Also, for other models (DenseNet, Inception), we used several other image pre-processing methods (image shift by several pixels, logarithm of pixel intensity, etc.), which improve the resulting accuracy. With a given dataset, we also used the state-of-art deep neural networks such as CapsNet, InceptionResNetV2, VGG16, and VGG19, but they don't give a good result.

We conclude that Convolutional neural networks InceptionV3 and DenseNet121 with the MAE-loss function show the best result providing 93.3% accuracy for the binary morphological classification of the low-redshift SDSS-galaxies based on their images.

Acknowledgements

This work was conducted in the frame of the budgetary program "Support for the development of priority fields of scientific research" (CPCEL 6541230) and the Youth Scientific Project (2019-2020, Dobrycheva D.V., Vasylenko M.Yu.) of the National Academy of Sciences of Ukraine.

HyperLeda (Makarov et al., 2014) and SDSS-IV (Blanton et al., 2017) were helpful to our research. This study has also used the NASA/IPAC Extragalactic Database (NED), which is operated by the Jet Propulsion Laboratory, California Institute of Technology, under contract with the National Aeronautics and Space Administration.

References

Ahn C. P., Alexandroff R., Allende Prieto C., et al. 2012, ApJS, 203, 21

Berman M., Triki A. R., Blaschko M. B., 2018, arXiv e-prints, p. 1705.08790v2

Blanton M. R., Bershady M. A., Abolfathi B., et al. 2017, AJ, 154, 28

Dark Energy Survey Collaboration Abbott T., Abdalla F. B., Aleksić J., et al. 2016, MNRAS, 460, 1270

Dobrycheva D. V., 2013, Odessa Astron. Publ., 26, 187

Dobrycheva D., Melnyk O., 2012, Advances in Astronomy and Space Physics, 2, 42

Dobrycheva D. V., Melnyk O. V., Vavilova I. B., et al. 2015, Astrophysics, 58, 168

Dobrycheva D. V., Vavilova I. B., Melnyk O. V., et al. 2017, arXiv:1712.08955,

Dobrycheva D. V., Vavilova I. B., Melnyk O. V., et al. 2018, Kin.Phys.Cel.Bod., 34, 290

Eisenstein D. J., Weinberg D. H., Agol E., Aihara H., et al. 2011, AJ, 142, 72

Elyiv A. A., Melnyk O. V., Vavilova I. B., et al. 2020, A&A, 635, A124

Fodera-Serio G., Indorato L., Nastasi P., 1985, Journal for the History of Astronomy, 16, 1

Howard A. G., Zhu M., Chen B., Kalenichenko D., et al. 2017, arXiv e-prints, p. 1704.04861v1

Huang G., Liu Z., et al. 2017, arXiv e-prints, p. 1608.06993v5

Hubble E. P., 1926, ApJ, 64, 321

Ivezić Ž., Connolly A. J., Jurić M., 2017, in Brescia M., Djorgovski S. G., Feigelson E. D., Longo G., Cavuoti S., eds, Vol. 325, Astroinformatics. pp 93–102 (arXiv:1612.04772), doi:10.1017/S1743921316013156

Khramtsov V., Dobrycheva D. V., Vasylenko M. Y., et al. 2019a, Odessa Astron. Publ., 32, 21

Khramtsov V., Sergeyev A., Spiniello C., et al. 2019b, A&A, 632, A56

Makarov D., Prugniel P., Terekhova N., Courtois H., Vauglin I., 2014, A&A, 570, A13

Melnyk O. V., Dobrycheva D. V., Vavilova I. B., 2012, Astrophysics, 55, 293

Szegedy C., Vanhoucke V., Ioffe S., Shlens J., Wojna Z., et al. 2015, arXiv e-prints, p. 1512.00567v3

Vasylenko M. Y., Dobrycheva D. V., Vavilova I. B., et al. 2019, Odessa Astron. Publ., 32, 46

Vavilova I. B., Elyiv A. A., Vasylenko M. Y., 2018, Rus.Rad.Phys.Rad.Astr., 23, 244

Vavilova I., Dobrycheva D., Vasylenko M., et al. 2020, Multiwavelength Extragalactic Surveys: Examples of Data Mining. Elsevier, doi:10.1016/B978-0-12-819154-5.00028-X

de Jong J. T. A., Verdoes Kleijn G. A., Erben T., et al. 2017, A&A, 604, A134

In memory of a colleague !

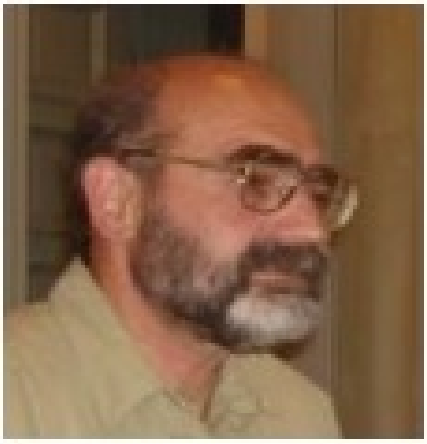

Artur S. Amirkhanian, age 73, passed away suddenly on Saturday, December 19, 2020, at his home in Byurakan Astrophysical Observatory as a result of acute cardiovascular failure. Artur was the Head of the laboratory of small telescopes, and also an employee of the Department of Astrochemistry, Astrobiology and Exoplanets in the Byurakan Astrophysical Observatory. He lived the life of a conscientious and honest worker, a respected citizen of his country.

Artur Amirkhanian was born on July 20, 1947 in the city of Port Arthur, People's Republic of China (in those years - a joint naval base of the USSR and PRC), in the family of a military doctor. While in a secondary school (Baku city), Artur also gladly participated in the school astronomy club, where he built his first telescope-reflector (of 18 cm). With this telescope, he carried out quite skillful observations of the planets. Since 1975, having studied at the Yerevan State University in physics and astrophysics (1969-1973), and having served in the army for 2 years, he began working by profession at the Byurakan Astrophysical Observatory, dealing with the operation of the new Byurakan 2.6-meter telescope, and did a lot in preparing it for the first light. Actually, Artur have a never-ending love for astronomy and incessant need to talk about his research, in general, and about methods he used, in particular. In practical work, Artur was appreciated for his business qualities, assertiveness and ability to achieve set goals. For example, Artur was the first in the BAO to obtain the spectra one of a faintest at that time magnitude galaxy with a 2.6 m telescope, using a 3-stage electro-optical converter tube (built independently from spare parts in 1978 !) And V.A. Ambartsumyan's remark on such a message: "Oh, new prospects are opening up for us." One may remember also the visit of E.M. Lifshitz at the BAO in 1979, when Artur showed the guest the 2.6 m telescope and asked him about the nonzero neutrino mass. Artur could very quickly set up a very complex electronic-optical system, was distinguished by phenomenal memory and knowledge in almost all areas of technics and technologies. His ability to calculate the benefits from the use of any new telescopic system with any electronic amplifier, often on fingers, could be envied by many design departments! In 1988 A. Amirkhanian defended his Ph.D. thesis "Methods and results of studies of compact groups of galaxies" on spectrophotometry of galaxies in compact clusters. It should be emphasized that Artur was a unique specialist in the field of astro-instrumentation in general, and in the preparation of these very complex systems for operation, in particular !

The memory of him will forever remain in our hearts. A. Amirkhanian was buried in the village cemetery, in the Byurakan.